Geometrical Problems In Computer Vision.

Thesis submitted in accordance
with the requirements of the
University of Liverpool
for the degree of
Doctor in Philosophy

by

Gordon James Fletcher.

November 1996.

Fig. XCI.

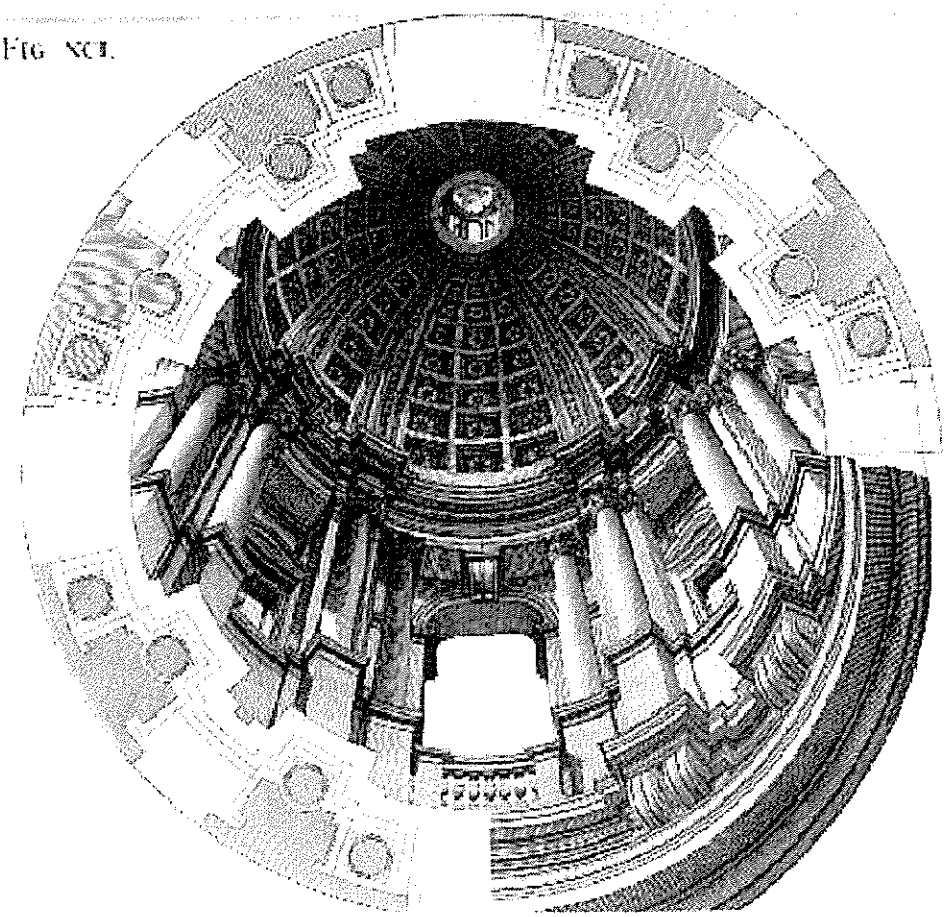

Fig. XC.

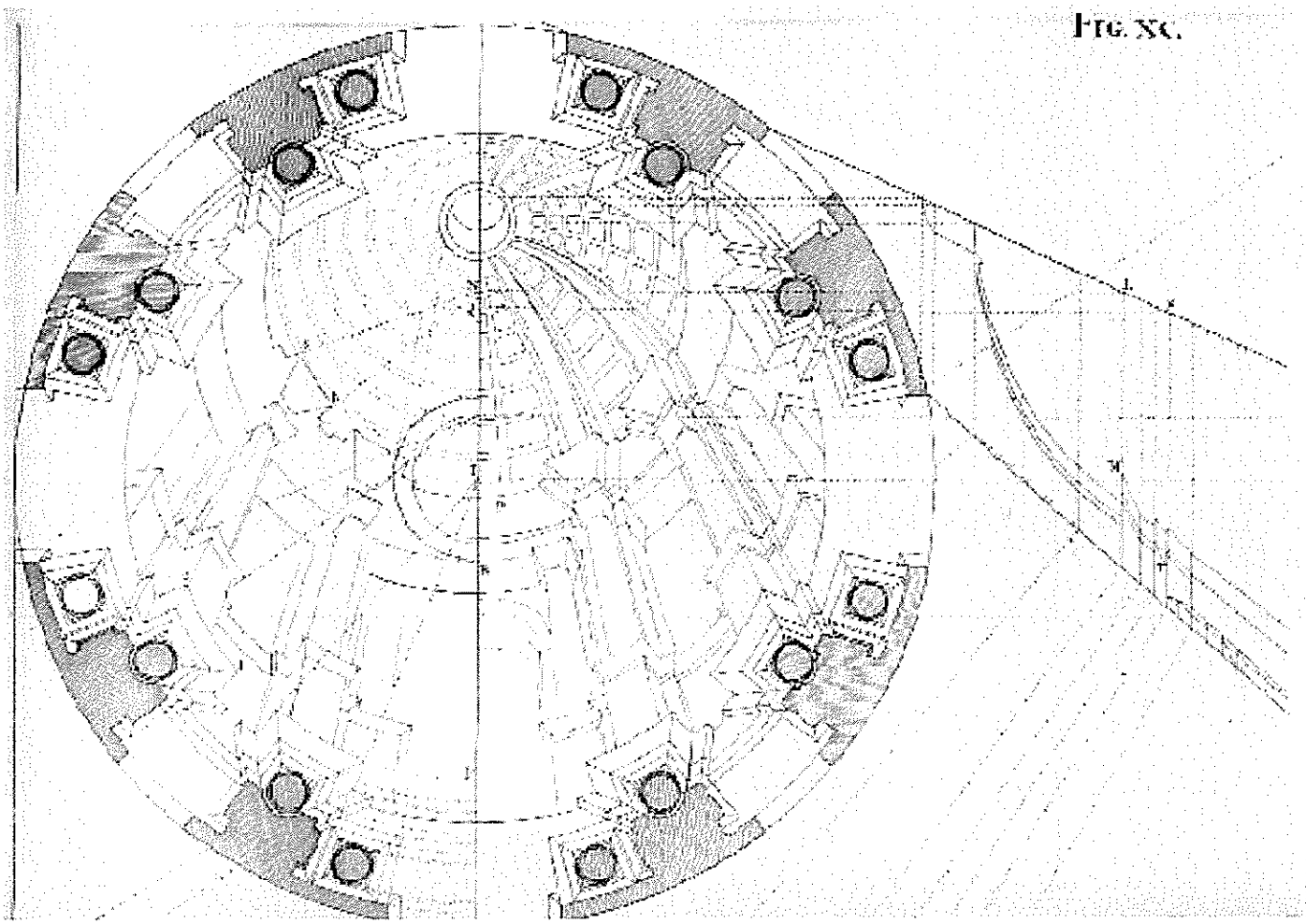

Geometrical Problems In Computer Vision

Gordon James Fletcher

Abstract

In this thesis we consider three geometrical problems in Computer Vision. The main tools we use are from differential geometry and singularity theory.

We consider general one parameter families of monocular central projections of a surface. In particular the generic stable singularity that occurs on the profile, the cusp, is tracked and information concerning the geometry of the surface is determined. We provide formulae for reconstructing the depth, Gauss and Mean curvatures from *tracking cusps*. A mathematical analysis of the geometrical and topological configurations of the critical sets, cusp curves and profiles is performed. We track cusps on special surface classes; a surface of revolution, ruled surface and canal surface, and find that global information can be derived.

The frontier of a curved surface is examined and the problem of surface *construction* is introduced. Here we seek to establish the necessary and sufficient conditions on the camera motion and profiles for the reconstruction of a doubly covered surface with boundary. We find that our construction maps have corank 1 along a curve, and we examine the resulting singularites by working at the jet level of our map.

The conjugate curve congruence $\mathcal{C}_\alpha$ is introduced in the last chapter as a one parameter family of curve congruences on the surface that contains both the asymptotic and principal curve congruence. We analyse the family of discriminants and the zeros of $\mathcal{C}_\alpha$. The family of spherical images is found to be connected to a cubic form defined on the surface, and these are connected to the geodesic inflections of the critical set of some parallel projection.

Acknowledgements

I would like to thank my supervisor Peter Giblin for his enthusiasm, excellent supervision, and for reading this work. Many mathematicians patiently endured my persistent questioning and in particular Bill Bruce, Farid Tari, Neil Kirk and Richard Morris made significant contributions towards my understanding of the mathematics. Many of the pictures within were created with the excellent Liverpool Surface Modelling Package.

This thesis could not have been completed without the financial help of the EPSRC funding body and the Department of Social Security. I would like to thank the University of Liverpool and the Department of Pure Mathematics for providing financial contributions towards a conference visit.

For their friendship and fun, I owe thanks to Chris, Anna, Ken, Steve, Clare and James.

Thanks to Janet for her support, and for making me laugh.

FOR MY PARENTS

Contents

Introduction

In interpreting the world around us, the human visual system uses many sophisticated techniques and takes advantage of a wide range of visual cues. It is certainly the case that one of the most constraining, and perhaps useful visual cues to solid shape, is the outline or silhouette of an object. In computer vision we seek to model this mathematically via projections and the differential geometry of surfaces.

This thesis contains essentially three main topics of investigation; tracking the cusps of smooth profiles of a surface, the frontier of a surface, and the conjugate curve congruence. The link between them is that they all seek to provide geometrical models and solutions for situations in computer vision. Another common thread is that many of the techniques used utilise a Singularity Theory approach. Results made in recent decades in this area, have helped to make powerful assertions concerning generic geometry and ultimately computer vision.

In Chapter 1 we provide a review of the literature concerning the topics in this thesis, and describe the context and relevance of this work. Standard results from differential geometry that are often used in this work are provided in this chapter. The 'Monge form' of a surface is introduced where the surface is given parametrised as the graph of a function, and the second fundamental form defined, allowing us to introduce the notion of surface curvature. By extending the asymptotic directions along the parabolic curve of a smooth surface we create a ruled surface, this is proven to be developable. Extending the flecnodal directions along the flecnodal curve gives the so called flecnodal scroll. These two ruled surfaces are significant when considering the bifurcation of singularites of the projection of surfaces, and are used in later chapters.

Let M be a smooth surface in $\mathbf{R}^3$. For a direction $\mathbf{w}$ the orthogonal projection of M to a plane perpendicular to $\mathbf{w}$ has a critical set Σ and the image of Σ is the profile. In the case of perspective projection we consider our projection through

the point $\mathbf{c}$. For a generic surface we expect the cone of rays with vertex $\mathbf{c}$ to be tangent to M along a curve, which is the critical set. The intersection of this cone with a unit sphere centre $\mathbf{c}$ is the profile. Chapter 2 provides the basic definitions and setup for geometrical problems in computer vision. We examine parallel and perspective projection and provide some standard results concerning the critical set and profile of a projection. There is a rather involved section that is devoted to proving Koenderink's result connecting the Gauss curvature with the curvature of the profile, and seeing how this result in parallel projection is the limit of the perspective result. If we now consider a one parameter family of perspective projections, with camera centres $\mathbf{c}(t)$, of M this results in a one parameter family of critical sets on the surface, and a family of profile curves. It is possible to 'spread out' the family of critical sets in the time direction forming the so called Spatio-Temporal surface $\widetilde{M}$. The main use for $\widetilde{M}$ is for when the critical sets form an envelope, in which case the projection $\widetilde{M} \rightarrow M$ has a fold. At the end of the chapter we use some technical results to find a generic classification of critical sets, subject to an equivalence described in the main text.

It is possible to view the projection of smooth surfaces as maps from the plane to the plane. The generic singularities we expect are the fold and cusp, i.e. the map germ is equivalent to $x, y \mapsto x^2, y$, $x, y \mapsto x^2, y^2$ respectively. In fact when projecting a hyperbolic region of surface we expect the profile to have isolated singularities, or cusps. These are stable under viewer motion, and we thus 'track' cusps in a one parameter family of central projections. Chapter 3 provides the more mathematical results that are used when tracking cusps under perspective projection and arbitrary viewer motion, and introduces the locus of cusps. The points on the surface that generate cusps form the 'cusp generator curve' and the interplay between this and the critical sets is investigated. We are particularly interested in the singular instances of the cusp locus, and these are found and related to the underlying geometry. The final section provides some results using the method of *versal unfoldings*. These provide typical pictures, in some sense, of the profiles.

Chapter 4 provides those results that are more of a computer vision nature. One of the main results is that since the cusps are visible features the Gauss curvature K and Mean curvature H may be found from tracking cusps. In fact the formulae

$$K = -\frac{(\mathbf{p}_t.\mathbf{n})^4}{[\mathbf{p}, \mathbf{c}_t, \mathbf{p}_t]^2}$$

$$H = \frac{\mathbf{p}_t.\mathbf{n}}{2[\mathbf{p}, \mathbf{c}_t, \mathbf{p}_t]^2} \left(\mathbf{c}_{tt}.\mathbf{n}\ \mathbf{p}_t.\mathbf{n} - \mathbf{c}_t.\mathbf{n}\ \mathbf{p}_{tt}.\mathbf{n} - 2\mathbf{p}.\mathbf{c}_t\ (\mathbf{p}_t.\mathbf{n})^2 \right).$$

use lower derivatives (an important fact when considering any implementation) than other reconstruction formulae in the literature. We also find that these formulae for the curvatures are independent of spatio-temporal parametrisation. This means that when parametrising the surface by using the family of critical sets as one half of the coordinate grid, we are free to take any other family of transverse curves to form a parametrisation on M, and this will not affect the formulae for K or H. The next section is concerned with the question of whether tracking cusps provides a constraint on the motion of the camera. We prove that this is not the case. Some examples are provided illustrating the methods that one might adopt in a physical implementation. These examples increase in sophistication and we are able to make some analysis of the stability of the depth and curvature formulae under error. This stability is found to be good, even under relatively large noise. The final section reproves results of an earlier paper on tracking cusps in the restricted case of parallel projection and circular motion.

In Chapter 5 we consider tracking cusps on special surface classes. The classes are, surfaces of revolution, canal surfaces (formed as the envelope of spheres of constant radius along a spacecurve) and ruled surfaces. For instance it is proven that cusps on profiles of surfaces of revolution are generated in pairs by points on the same parallel circle. This constraint combined with knowledge of the geometry of such surfaces allows us to reconstruct the axis of revolution, and finally the whole surface. In fact we find that the geometrical structure of these classes are sufficiently constrained so as to allow global reconstruction, where the theory of the previous chapter only promised local information. For a generic surface by tracking cusps we can reconstruct the cusp generator curve C on the surface, the tangent plane, and the second fundamental form along C. For any one of the above surface classes we can reconstruct C as usual but now we find that with knowledge of the geometry a *whole curve* through points of C can in fact be recovered. For each surface class we examine the theoretical results and then devise some synthetic examples.

A large area of theoretical and practical research in computer vision is the area of surface reconstruction from profiles. By taking a known camera motion giving a one parameter family of profiles it has been shown that it is possible to recover the surface. Chapter 6 introduces the notion of surface *construction*. This is an abstraction of the idea of surface *reconstruction*. In the case of surface reconstruction it is generic for the critical sets to locally form an envelope on the

underlying smooth surface. This envelope separates (locally at least) the visible (i.e. the part covered by the family of critical sets) from invisible region. In effect what we reconstruct is a smooth surface with a boundary, and the boundary is the envelope of critical sets, called the frontier. Now we ask, conversely, precisely what properties of the profile curves and camera motion guarantee that the reconstructed surface is a smooth surface with boundary? This leads us to surface construction where we take essentially arbitrary curves and use these as profiles and a camera motion, and using the standard techniques construct a surface. We seek to find the exact conditions on these profiles and camera motion for the critical sets to construct a surface with boundary, that will form the frontier for the motion. We describe how the construction map can be viewed as map from the plane to three space and is in fact found to be rank one along a curve. We work at the jet level and use results of Mond to calculate the conditions for singularities of the construction map. Working in the double point space we find that we construct cusp edges and cuspidal cross caps, clearly showing that there are constraints missing on the profiles curves and camera motion that are needed to construct a genuine frontier.

Chapter 7 introduces a one parameter family of binary differential equations (BDEs) that we call the Conjugate Curve Congruence $\mathcal{C}_\alpha$. Given a smooth surface M we can take all directions in all tangent planes that make a fixed angle α with their conjugate direction. This is $\mathcal{C}_\alpha$. We apply results of Bruce and Tari to obtain topological pictures and we investigate the discriminant curves and zeros of the BDEs. The family of spherical images is described, and the relation with the critical set of the projection of a surface is elucidated. A new characterisation of the sub parabolic lines and flecnodal curves of a surface is found. The chapter finishes with some speculative work concerning the umbilical cords of a surface and their global impact.

The illustration at the front, and the quotations within this work are from the treatise of one of the most influential perspective theorists of the 17th century: *"Rules and Examples of Perspective proper for painters and architect, etc in English and Latin: containing a most easie and expeditious method to delineate in perspective all designs relating to architecture, after a new manner, wholly free from the confusion of occult lines; by that master thereof Andrea Pozzo, Soc. Jes."* Andrea Pozzo was a Jesuit brother who earned considerable fame for his monumental perspective creations that harmonised high spiritual art with linear perspective.

Pozzo is particularly well known for the illusory cupola on the church of

St.Ignatius in Rome. When St.Ignatius was first opened to the public it was still incomplete, and a shortage of funds rendered the completion unlikely. An over ambitious plan for a cupola, only a little smaller than St.Peter's, caused a dilemma since this would have been the only way to honour the Saint who had founded the Society of Jesus. The solution provided us with a glorious illusion, and Brother Pozzo with the opportunity to apply his consummate technique, which finally led to a commission to decorate the whole church. Pozzo was not without his critics, and when they accused him of misuse of the baroque style by resting the columns of his 'cupola' on simple brackets, he said wryly: "If my brackets give way and columns start to fall to the ground, you will easily find some painters among my friends to remake them and remake them better" [JD].

Chapter 1

Introductory Results.

> This being of much the more general use, and, when rightly understood, renders the difficulties of the circular or irregular surfaces, easy and familiar. *Preface* [Poz]

1.1 Background Literature.

For the main topics in this thesis we now present a short discussion on related work, and its relevance to the research in the subsequent chapters.

1.1.1 Projections and Profiles.

In later chapters we will consider 'tracking' singular points of profiles. These objects have a venerable history in the mathematics of Singularity Theory and have more recently been studied with a view towards Computer Vision. Whitney [Wh] showed that the fold and the cusp are the stable singularities of maps from the plane to the plane. The projection of a surface on to a plane (which could be local coordinates of an image sphere) can be considered as a map from the plane to the plane. Consider the surface given as the graph of a function, so we have the map

$$\begin{aligned} \mathbf{R}^2, 0 &\rightarrow \mathbf{R}^3, 0 \\ (x, y) &\mapsto (x, y, h(x, y)). \end{aligned}$$

We then project the surface orthogonally on to a plane (which we call the image plane) perpendicular to (0,1,0) (the view direction), the projection map is π;

$$\pi(x, y, h(x, y)) = (x, h(x, y)).$$

The composite of these two maps is the map f which is sometimes called the visual mapping

$$f(x, y) = (x, h(x, y)).$$

Whitney's result shows that generically the projection of a surface is either locally smooth or has a cusp. For a cusp it can be shown that the view direction is along an asymptotic direction to the surface.

Koenderink and van Doorn [KvD76] considered 'local events' and showed that the visual mapping can be a lips/beaks map or a swallowtail map. Such phenomena are only generic in a one parameter family of projections, or one parameter family of surfaces.

Gaffney [G] classified all orthogonal projections of a generic surface in $\mathbf{R}^3$. The classification process was carried out with Maria Ruas. Gaffney gives the germ of the mapping in each case, the name of the mapping (e.g. swallowtail) and the condition for such a singularity to arise. The list includes the fold, cusp, lips/beaks, swallowtail together with the codimension two singularities of gull, goose and butterfly. Lips/beaks singularities arise when the view direction is an asymptotic direction at a parabolic point. The view direction lies in the cylinder axis [K]. A swallowtail singularity arises when the view direction has four points of contact. The view direction then lies in the flecnodal scroll [K]. The list is also presented in Arnold [A] Chapter 12 and Kergosien [Ke].

Rieger studied the singularities of the projections of surfaces on to planes in his thesis [R88] and extends the classification to the case of 1-parameter families of surfaces [R87]. More recently Rieger [R92] classified the perspective projection of generic surfaces of revolution from any centre of projection up to diffeomorphism of the profile.

1.1.2 Recovery of Surface Shape from Profiles.

The reconstruction of smooth surfaces from smooth profiles under a known viewer motion has received much attention in the Computer Vision research field. See for example [CB], [BB], [GW], [KD], [SW], [VF] and [Z]. The first real attempt

to extract useful reconstruction information from singular profiles was [GS]. This paper dealt with the special case of circular motion and parallel projection. In Chapter 4 we discuss the general case of reconstructing surfaces from tracking the singular profile points under a known viewer motion, and the formulae we present are reduced to the case of [GS].

Some of the material from Chapters 4 and 5 has appeared in [CFG, CFG2] and [FG]. For general perspective motion one should consult [CFG] and [CFG2]. In these papers and Chapter 4 below formulae for the Gauss and Mean curvature are presented and the simplifications compared to [CB] are noted. There is a discussion on the possibility of tracking cusps in order to provide a motion constraint, but this is found to be impossible. By restricting the class of observed surfaces one can make more powerful statements, and this is the subject of [FG]. Here we can make global assertions where previously [CFG, CFG2] promised only local information. We find that by simply tracking the cusps under known viewer motion we can reconstruct a characteristic curve of that surface and hence as the cusp sweeps over the surface we reconstruct the whole surface.

1.1.3 Recovery of Structure and Motion from Profiles.

Structure and motion from the images of point features has attracted considerable attention and a large number of algorithms exist to recover both the spatial configuration of the points and the motion compatible with the views. Structure and motion from the outline of curved surfaces, on the other hand, has been thought to be more difficult because of the *aperture problem*, i.e. it is not possible to get the correspondence of points between two images since the profiles at different times correspond to *different* critical sets on the surface.

For a smooth arbitrary curved surface an important image feature is the profile or apparent contour. This is the projection of the locus of points on the surface which separates the visible from the occluded parts. Each different viewpoint will generate a different critical set or contour generator with the critical sets 'slipping' over the visible surface under viewer motion. The *frontier* is the envelope of critical sets showing the boundary, at least locally, of the visible region swept out under viewer motion.

As above, under *known* viewer motion, the deformation of profiles can be used to recover surface geometry (structure) [CB], [BB], [GW], [KD], [SW], [VF] and [Z]. This requires a spatio-temporal parametrisation of the image-curve motion.

The *epipolar* parametrisation is most naturally suited to the recovery of surface curvature, cf [CB]. In reconstruction techniques such as [CB] the frontier is viewed more as a nuisance since it is one instance of the failure of the epipolar parametrisation. In fact the frontier can provide a constraint on the viewer motion and it is this that interests those involved in the area of 'Structure and Motion'. Frontier points are sometimes referred to in the literature as *epipolar tangency points.* The epipole is the instantaneous direction of the camera motion and the epipolar plane is spanned by the epipole and the view direction. An epipolar tangency occurs when the epipolar plane is the tangent plane. This characterisation of the frontier is described elsewhere in this thesis.

Rieger [R86] considered circular motion, showing how to infer the axis of rotation when the rotation is perpendicular to the view direction, by finding corresponding points on two profiles. The restriction of circular motion was further explored in [GPR] which generalised [R86]. In this the authors consider the surface rotating about an unknown axis and viewed by orthogonal projection to a fixed image plane. Porrill and Pollard in [PP] consider corresponding points on profiles in much the same way as Rieger, in the context of epipolar tangencies. This was primarily concerned with stereo calibration from space curves and they noted that the intersection of two profiles from two distinct viewpoints generated a real point visible in both images. Carlsson [C] exploited frontier type constraints in the analysis of the visual motion of space curves.

Recent papers have tried to generalise to arbitrary viewer motion (not just circular motion) and general perspective projection of smooth surfaces. Joshi et al [JAP] discussed a method of recovering structure and motion from perspective images acquired by a calibrated trinocular camera rig. The authors of [ACG95] sought to determine the epipolar geometry for infinitesimal and discrete motions. The technique is iterative and requires an initial guess for the epipole or for the essential matrix. The iteration over some high dimensional manifold aims to minimise so called residuals which arise as either angles between epipolar planes in the discrete case, or normal velocities in the continuous case. The residuals are a measure of how good the guess is for the epipole and rotation, but no formal results are given for the uniqueness of any minima in the search space.

Novel techniques have been used recently in [VKP] where viewpoint invariant representations of curves such as bitangents, inflections, parallel tangents are used to match discrete frontier points. Velocity cues of the tangents are also utilised to provide constraints on the matching. The paper deals with scaled orthographic projection and this is necessary for the method.

It is constructive to examine in more detail the differences and similarities between [ACG95, ACG96] and [VKP]. On closer inspection it seems that passing from parallel projection [VKP] to perspective projection [ACG95] gives the same measure for finding the epipole. In [VKP] they draw parallel lines in the image plane tangent in the two images to fix a guess for the epipole. For orthographic projection the epipolar geometry consists of parallel lines. In actual fact bitangents and inflections are used in [VKP]. The analogous case in [ACG96] is fixing a point on the image sphere for the epipole. Consider the discrete case with two time steps where we would have to fix an epipole at each time, giving four degrees of freedom. Drawing great circles through the proposed epipole tangent to the profiles gives the frontier points, just as drawing parallel lines tangent to plane profiles in the parallel case, gives the frontier points.

Thus we immediately see that in the parallel projection case the search space is considerably reduced. Specifying epipolar geometry for parallel projection is one degree of freedom per view, since we only have to specify the direction of a set of parallel lines. For perspective we need two degrees per view since the epipole is a point on the sphere.

The residuals described in [ACG96] are angles between epipolar planes. These are planes that are members of a pencil containing the epipole direction. If we imagine the camera receding to infinity these planes become parallel and the epipolar great circles on the image sphere become parallel epipolar lines on the image plane. Moreover the angle between the planes become distances between the lines. This is what is measured in [VKP]. Thus we see that the criterion for judging the accuracy of the estimate of the epipolar geometry is the same in the two papers. The method at arriving at that estimate is different though.

The method in [VKP] is novel in the sense that they pick a bitangent point b on a profile and search through time to find its occurrence again (a little thought shows that this is generic), where b is now a discrete frontier point for those two camera positions. In other words the tangent plane at b is the epipolar plane for the two camera positions. The key is to exploit invariancy with parallel tangents that result in only considering orthogonal projection. These parallel tangents to bitangents or inflections provide a 'signature' with which we can recognise future appearances of this point in the image. This search is made more efficient by use of an 'indexing' data structure such as a hash table or tree.

The disadvantage of this method is that it does not easily generalise to perspective projection. The invariancy described is dependent on orthogonal pro-

jection.

Chapter 6 introduces the concept of surface *construction*, as opposed to surface reconstruction. Here we seek to find the precise conditions on the profiles and camera motion for us to reconstruct a smooth part of a surface bounded by the frontier. We choose arbitrary curves $\mathbf{p}(s,t)$ and camera motion $\mathbf{c}(t)$ subject to some limited constraint and construct a new surface. We find that the constraints used in all the previous papers on the frontier are in fact incomplete. Incomplete in the sense that imposing them is not sufficient to construct a smooth surface with boundary. Some early results of this chapter appear in [FG2].

1.1.4 The Conjugate Curve Congruence.

Consider all directions in all tangent planes to a smooth surface in $\mathbf{R}^3$ making a fixed angle α with their conjugate direction. 'Conjugate' in this sense is with respect to the second fundamental form. This is the curve congruence $\mathcal{C}_\alpha$.

It is perhaps initially surprising that the Conjugate Curve Congruence $\mathcal{C}_\alpha$ is not a classical object found in late nineteenth century textbooks on differential geometry. It is certainly the case that the notion of conjugacy was well known to Darboux and before. On further reflection though the concepts that arise when studying $\mathcal{C}_\alpha$ are not in general 'classical'; concepts such as 'cusps of Gauss', 'subparabolic curves', 'flecnodal curves' etc. were not common geometrical objects to the late nineteenth or early twentieth century geometers, and may perhaps explain the lack of interest in such an object as $\mathcal{C}_\alpha$. Also the methods used in this thesis utilise a singularity theory approach to families of BDEs that provide a sophisticated tool for analysing the integral curves of $\mathcal{C}_\alpha$. These methods were of course unavailable until recently, though we should note Darboux's great achievement at the turn of the century of providing us with the lines of curvature at a generic umbilic.

There is some discussion in Eisenhart [E, 129] and Goursat [GO, 512] on 'conjugate networks' or 'conjugate systems'. These are a two parameter family of curves on the surface with the property that at a point the tangents are conjugate. There is no mention though of conjugate networks with equal angle. In [E, 129] and [K, 244] the 'characteristic directions' are defined as 'those conjugated directions that subtend the smallest angle among all possible conjugated pairs'. Of course for an hyperbolic patch the characteristic directions are asymptotic.

This is perhaps the nearest one gets to $\mathcal{C}_\alpha$ in the literature.

A problem related to $\mathcal{C}_\alpha$ and described in Chapter 7 is when the critical set or contour generator of a parallel projection has a geodesic inflection. There has been a huge interest in the computer vision literature concerning the critical sets of projections of smooth surfaces (which also appear as the shadow boundary in shape from shading problems [KD]), but the question of geodesic inflections of the critical set has been neglected. We note that the projection to a view plane of a geodesic inflection is not visible.

1.2 Surface Geometry.

In this section we give the basic definitions and results from differential geometry that are used in the rest of the thesis. These are found in [ON] or most other books on differential geometry.

1.1 Definition: *A surface given by*

$$f(x,y) = (x, y, h(x,y))$$

is said to be given as the graph of a function as $z = h(x,y)$. This is the Monge form of the surface. We usually take $h_x(0,0) = h_y(0,0) = 0$ so that the tangent plane at the origin is coincident with the xy plane.

We will need to calculate the second fundamental form II of a surface. Here we calculate the matrix of II for a surface M given as the graph of a function, as we will mostly have the surface in this form. O'Neill [ON] gives the method for a general parametrised surface.

1.2 Lemma: *Let the surface M be given as a graph of a function $z = h(x,y)$ and the normal $(-h_x, -h_y, 1)$ be in the direction $\mathbf{w}$. Choose a tangent direction $\mathbf{u}$ to the surface M. Then II is calculated with reference to $\mathbf{u}$ and another tangent direction given by $\mathbf{v} = \mathbf{w} \wedge \mathbf{u}$. Then the matrix B of the second fundamental form is given by*

$$B = \begin{pmatrix} a & b \\ b & c \end{pmatrix}$$

where

$$a = \frac{\mathbf{u}H\mathbf{u}^T}{\|\mathbf{w}\|\|\mathbf{u}\|^2} \quad b = \frac{\mathbf{u}H\mathbf{v}^T}{\|\mathbf{w}\|\|\mathbf{u}\|\|\mathbf{v}\|} \quad c = \frac{\mathbf{v}H\mathbf{v}^T}{\|\mathbf{w}\|\|\mathbf{v}\|^2}$$

and

$$H = \begin{pmatrix} h_{xx} & h_{xy} & 0 \\ h_{xy} & h_{yy} & 0 \\ 0 & 0 & 0 \end{pmatrix}.$$

Proof: Let there be coordinate axes ξ, η and ζ in directions $\mathbf{u}$, $\mathbf{v}$ and $\mathbf{w}$ respectively. The surface M is given locally as the graph of a function

$$z = h(x,y) = xh_x + yh_y + \frac{(x^2 h_{xx} + 2xyh_{xy} + y^2 h_{yy})}{2} + \cdots. \tag{1.1}$$

Thus (x,y,z) coordinates in $\mathbf{R}^3$ becomes (ξ,η,ζ) coordinates where

$$\zeta = \frac{a\xi^2 + 2b\xi\eta + c\eta^2}{2} + \cdots \tag{1.2}$$

We can write ξ, η, ζ in terms of x, y, z

$$\begin{aligned} \xi &= (x,y,z).\frac{(u_1,u_2,u_3)}{\|\mathbf{u}\|} \\ \eta &= (x,y,z).\frac{(v_1,v_2,v_3)}{\|\mathbf{v}\|} \\ \zeta &= (x,y,z).\frac{(-h_x,-h_y,1)}{(1+h_x^2+h_y^2)^{1/2}} \end{aligned}$$

where $(1+h_x^2+h_y^2)^{1/2} = \|\mathbf{w}\|$. In matrix form this is

$$\begin{pmatrix} \xi \\ \eta \\ \zeta \end{pmatrix} = \begin{pmatrix} \frac{u_1}{\|\mathbf{u}\|} & \frac{u_2}{\|\mathbf{u}\|} & \frac{u_3}{\|u\|} \\ \frac{v_1}{\|\mathbf{v}\|} & \frac{v_2}{\|\mathbf{v}\|} & \frac{v_3}{\|v\|} \\ \frac{-h_x}{(1+h_x^2+h_y^2)^{1/2}} & \frac{-h_y}{(1+h_x^2+h_y^2)^{1/2}} & \frac{1}{(1+h_x^2+h_y^2)^{1/2}} \end{pmatrix} \begin{pmatrix} x \\ y \\ z \end{pmatrix}.$$

Using (1.1) we substitute for x, y, z from above. Equating coefficients of ξ^2, $\xi\eta$ and η^2, making a substitution for ζ from (1.2) where necessary, yields a, b,nd c respectively and hence obtain II. We obtain

$$\begin{aligned} a &= \frac{h_{xx}u_1^2 + 2h_{xy}u_1u_2 + h_{yy}u_2^2}{(1+h_x^2+h_y^2)^{1/2}\|\mathbf{u}\|^2}, \\ b &= \frac{h_{xx}u_1v_1 + h_{xy}(u_1v_2 + v_1u_2) + h_{yy}u_2v_2}{(1+h_x^2+h_y^2)^{1/2}\|\mathbf{u}\|\|\mathbf{v}\|}, \\ c &= \frac{h_{xx}v_1^2 + 2h_{xy}v_1v_2 + h_{yy}v_2^2}{(1+h_x^2+h_y^2)^{1/2}\|\mathbf{v}\|^2}. \end{aligned}$$

□

The second fundamental form at p of M is denoted $II(u,v)$ where u and v lie in the tangent plane to M at p. The matrix of the second fundamental form will be denoted by B, as stated above. Hence

$$II(u,v) = uBv^T.$$

The second fundamental form is very useful as it contains the information about the surface up to second order, for example, the Gauss curvature, mean curvature, principal curvatures and principal directions may all be obtained from II. We make this more precise, and give two equivalent definitions.

1.3 Definition: *The normal curvature k of M at p in the tangent direction u is the curvature of the curve formed by the intersection of the surface and the plane spanned by the normal to M at p and u.*

Note: It is a fact that the normal curvature of M at p in the direction u is obtained from the second fundamental form

$$k = II(u,u) = uBu^T.$$

1.4 Definition: *The maximum and minimum values of the normal curvature of M at p are the principal curvatures k_1 and k_2. The directions in which these extreme values occur are called the principal directions of M at p. These directions are mutually perpendicular. The principal curvatures are the eigenvalues of B and the principal directions are the corresponding eigenvectors.*

1.5 Remark: *A point p on M is an umbilic if $k_1 = k_2$, that is all the normal sections of M have the same curvature. At such points all the directions are principal. Umbilics are divided into three classes: star, monstar and lemon, [BF]. The final chapter will make use of this distinction.*

We now come to the concept of *conjugacy* which is essential for the work in Chapter 7 and some other viewpoints presented there.

1.6 Definition: *The tangent directions u and v are conjugate directions iff*

$$II(u,v) = 0.$$

An asymptotic direction is self conjugate i.e.

$$II(u,u) = 0.$$

Remark: Whereas a tangent vector to M at p has two point contact with the surface ([BG] give a definition of contact) an asymptotic direction has three point contact with the surface at p. The notion of contact is used later in this thesis, (1.23).

The Gauss curvature of a surface is a measure of the intrinsic surface curvature at some point p.

1.7 Definition: *The Gauss curvature K of M at p is given by the determinant of B.*

1.8 Lemma: *The Gauss curvature K of M at p is the product of the principal curvatures of M at p, that is,*

$$K = k_1 k_2.$$

Proof: The principal curvatures are eigen values of B. □

The sign of the Gauss curvature classifies surface points into three distinct types.

1.9 Definition: *A point p on M is classified as*

(1) An elliptic point if $K > 0$ at p;
(2) A hyperbolic point if $K < 0$ at p;
(3) A parabolic point if $K = 0$ at p.

The number of asymptotic directions at p on M depends on the Gauss curvature of M at p.

1.10 Lemma: *The surface M at p has*

(1) No asymptotic directions if $K > 0$ at p;
(2) Two asymptotic directions if $K < 0$ at p;
(3) One asymptotic direction if $K = 0$ at p.

Proof: The asymptotic directions are given as root directions of $uBu^T = 0$. □

Remark: If a surface contains a straight line then the line will be an asymptotic direction to the surface at points on the line. At a parabolic point on the surface every direction is a conjugate direction to the asymptotic direction, This is equivalent to saying that if two directions are conjugate at a parabolic point one of them is the asymptotic direction.

1.11 Definition: *A* **flecnode** *is a point on the surface where an asymptotic direction possesses an extra point of contact (i.e. four points of contact). The* **flecnodal curve** *is the locus of such points.*

Note on 1.11: at a flecnodal point the flecnodal line doesn't pierce the surface, whereas an ordinary (three-point contact) asymptotic line pierces the surface. In the image one sees a 'swallowtail' singularity on the profile [K, p.448]. We expect for a generic surface the flecnodal points to occur in curves. Indeed they come in two 'flavours' depending on which of the asymptotic directions has four points of contact.

For a point p on a surface M the Gauss map assigns a point Q on the unit sphere whose radius vector is parallel to the outward normal vector to the surface at p. More formally:

1.12 Definition *For a surface M in $\mathbf{R}^3$ the Gauss map $G : M \to S^2$ sends each point p on M with unit normal vector (g_1, g_2, g_3) to the point (g_1, g_2, g_3) on the unit sphere.*

The Gauss map fails to be a local diffeomorphism at p on M if and only if p is a parabolic point on M. At such points the Gauss map is locally, almost always, a fold map [BGM].

1.2.1 Curves on Surfaces

Consider a curve γ on a surface M in $\mathbf{R}^3$. Let T be the tangent to the curve, S be the surface normal and V be $S \wedge T$.

1.13 Definition: *For a curve γ parametrised by arc length the connection matrix for the T, V, S frame is*

$$\begin{pmatrix} T' \\ V' \\ S' \end{pmatrix} = \begin{pmatrix} 0 & g & k \\ -g & 0 & t \\ -k & -t & 0 \end{pmatrix} \begin{pmatrix} T \\ V \\ S \end{pmatrix}$$

where k is the normal curvature, g is the geodesic curvature and t is the geodesic torsion.

1.2.2 Ruled Surfaces

In this thesis we will require the following definitions and simple results.

1.14 Definition: *A ruled surface is formed by taking a spacecurve $\gamma(u)$ and a curve on the unit sphere $\delta(u)$, and the parametrisation is*

$$\mathbf{r}(u,v) = \gamma(u) + v\delta(u).$$

1.15 Definition: *The* **flecnodal scroll** *(FS) is the ruled surface formed by taking the flecnodal curve as a base curve, and the rulings as the asymptotic directions with four–point contact.*

We now turn our attention to another ruled surface.

1.16 Definition: *The* **cylinder axis developable** *(CAD) is the ruled surface formed by taking the parabolic line on the surface as the generating curve, and the asymptotic directions as the ruling.*

Note on 1.16:

1. Whilst it is perhaps acceptable to call a hyperbolic point 'saddle like' and an elliptic point 'bowl like', a generic parabolic point is unlike a cylinder. A cylinder is developable with *every* point parabolic. In general the intersection of a generic surface at a generic parabolic point with its tangent plane is a cusp and not a line. Thus the cuspidal tangent should take the place of the 'cylinder axis'.

2. We follow Koenderink [K, p.453] and assume that the singularities of the CAD for a generic surface are curves in space. We prove below that the CAD is a developable and so expect these to be cusp edges and swallowtail points. We conclude that for a single camera motion it is not generic for it to pass through the singular points of the CAD.

3. We consider our surfaces free from flat umbilics. These points, where both principal curvatures vanish, are non generic for a single generic surface. Flat points are generic in families, or on special classes, e.g. minimal surfaces.

1.17 Definition: *A ruled surface M is* **developable** *if and only if M is the envelope of a one parameter family of planes.*

A cascade of Lemmas leads us to the important result that the CAD is a developable surface.

1.18 Lemma: *The ruled surface given in parametric form by the equation,*

$$r(u,v) = \gamma(u) + v\delta(u)$$

is developable if and only if,

$$[\gamma', \delta, \delta'] \equiv 0.$$

Proof: [WE, p.137] □

1.19 Lemma: *M is a developable ruled surface iff M has the same tangent plane at all points of a ruling.*

Proof: If M is an envelope of a family of planes S_t say, then the tangent plane to the envelope at a point p is the plane S_t itself.

Now $\gamma' + v\delta'$ and δ span the tangent plane, so $(\gamma' + v\delta') \times \delta$, for a fixed t, is independent of v. Therefore $\delta' \times \delta$ is parallel to $\gamma' \times \delta$. This implies $[\gamma, \delta, \delta'] = 0$. □

1.20 Lemma: *If we let $\gamma(t)$ denote the parabolic curve parametrised on the surface M, and $\delta(t)$ be the direction of the asymptotic rays on the parabolic curve then providing $\delta(t)$ is not parallel to $\gamma'(t)$ then $\delta'(t)$ lies in the plane of $\delta(t)$ and $\gamma'(t)$.*

Proof: Let $\Gamma(u,t)$ be a local parametrisation of the surface M, with $\Gamma(0,t) = \gamma(t)$, $\Gamma_u(0,t) = \delta(t)$, and $\Gamma_t(0,t) = \gamma'(t)$.

Then we have $\Gamma_{ut}(0,t) = \delta'(t)$. At $u = 0$ the Gaussian curvature is,

$$\begin{aligned} K &= (\Gamma_{uu}.\mathbf{n})(\Gamma_{tt}.\mathbf{n}) - (\Gamma_{ut}.\mathbf{n})^2 \\ &= -(\Gamma_{ut}.\mathbf{n})^2 \end{aligned}$$

since $\Gamma_{uu}.\mathbf{n} = 0$ because $\delta(t)$ is an asymptotic direction. On the parabolic line, $K = 0$, so Γ_{ut} lies in the plane of $\delta(t)$ and $\gamma'(t)$. □

1.21 Lemma: *The cylinder-axis developable is a developable ruled surface.*

Proof: Lemma 1.20 proves that for the cylinder-axis developable it is true that $[\gamma', \delta, \delta'] \equiv 0$. Thus by Lemma 1.18 we see that the surface is indeed developable. □

Note on 1.21: the result of the previous lemma would have been obvious to the ancients. It was (and perhaps still is) a well known result that upon taking the envelope of tangent planes along a smooth curve on the surface, the characteristics (rulings) of the resulting developable will be in conjugate directions to the tangent to the curve [E, p.126]. Thus if we take the envelope of tangent planes to the parabolic curve we find that the generators are the unique asymptotic direction, since every direction is conjugate to this one.

1.3 Other Useful Results

In this thesis we will often parametrise curves and surfaces that are given by explicit functions and thus use the Implicit Function Theorem. This theorem appears in most texts on real analysis.

1.22 Theorem:

Let $f : \mathbf{R}^{n+q}, (a, b) \to \mathbf{R}^q$ be a smooth map, defined on a neighbourhood of $(a, b) \in \mathbf{R}^n \times \mathbf{R}^q = \mathbf{R}^{n+q}$, with $f(a, b) = c$. Write $(x_1, \ldots x_n, y_1, \ldots y_q)$ for coordinates in $\mathbf{R}^{n+q}$ and consider the $q \times q$ matrix

$$\begin{pmatrix} \frac{\partial f_1}{\partial y_1} & \cdots & \frac{\partial f_1}{\partial y_q} \\ \vdots & & \vdots \\ \frac{\partial f_q}{\partial y_1} & \cdots & \frac{\partial f_q}{\partial y_q} \end{pmatrix}.$$

If this matrix is nonsingular at (a, b) then there exist neighbourhoods A of a in $\mathbf{R}^n$, B of b in $\mathbf{R}^q$ such that for all x in A there is a unique point $g(x)$ in B with $f(x, g(x)) = c$. Furthermore the map $x \mapsto g(x)$ is smooth.

Proof: [BG, p.58]. □

Given two plane curves there is an associated order of contact between them at any points of the two curves. If the curves cross transversely at a point p we say they have 1-point contact. If the curves have a common tangent line at p they have $\geq$ 2-point contact and so on. This idea is expressed for a curve in $\mathbf{R}^n$ by the following definition [BG, p.17].

1.23 Definition: *Let $\gamma : I \to \mathbf{R}^n$ be a regular curve, where $\gamma = (\gamma_1, \ldots, \gamma_n)$, and*

$$F^{-1}(0) = \{x \in \mathbf{R}^n : F(x) = 0\}.$$

Then γ and F^{-1} have k-fold contact for $t = t_0$ provided the function g defined by

$$g(t) = F(\gamma_1(t), \ldots, \gamma_n(t)) = F(\gamma(t))$$

satisfies

$$g(t_0) = g'(t_0) = \ldots = g^{k-1}(t_0) = 0$$

and

$$g^k(t_0) \neq 0.$$

Here superscripts denote differentiation.

When considering a curve or surface given by the zero set of a map we will generally assume that zero is a regular value of the map ([BG, p.56]).

1.24 Definition: *Let $f : \mathbf{R}^m \to \mathbf{R}^p$ be smooth with $m \geq p$. A point x of $\mathbf{R}^m$ is called a regular point of f and f is called a submersion at x, provided $Df(x)$ has rank p. A regular value of f is a point $c \in \mathbf{R}^p$ such that every x in the domain of f with $f(x) = c$ is a regular point.*

Finally we will need to find tangent planes to surfaces and tangent lines to curves.

1.25 Proposition: *Let $f : \mathbf{R}^{n+q}, v \to \mathbf{R}^q, c$ be a smooth map where c is a regular value of f. In the neighbourhood V of v, $M = f^{-1}(c)$ is a parametrised n-manifold. The tangent space to M at v is equal to*

$$\{x_v : x \in KernelDf(v)\}.$$

The tangent space passes through v and is parallel to the linear subspace kernel $Df(v)$ of $\mathbf{R}^{n+q}$.

Proof: [BG, p.68]. □

Chapter 2

Critical Sets and Profiles.

'Tis therefore absolutely necessary, that you employ yourself for some time in Drawing; till you can readily describe the Plan of any Upright, and from thence project the Section or Profile.
Advice To Beginners [Poz]

2.1 Introduction

In this chapter we aim to give a comprehensive introduction to the main types of projections used in this thesis and the geometric and topological structure of the critical sets and profiles that arise from projections of surfaces. In the literature the critical set is sometimes called 'contour generator' or the 'rim', see Figure 2.1. The profile is sometimes called the 'apparent contour' or 'silhouette'.

The early sections of this chapter contain relatively well known results concerning the critical sets and profiles, and later results introduce the 'Spatio-Temporal surface' which we use to provide a more technical analysis of the critical sets and to introduce the frontier.

2.2 Basic Definitions

We describe the essential differences between perspective and parallel projection. The definitions of the critical set and profile are given by, for example, Giblin and Weiss [GW], Koenderink and van Doorn [KvD91] for orthogonal projection,

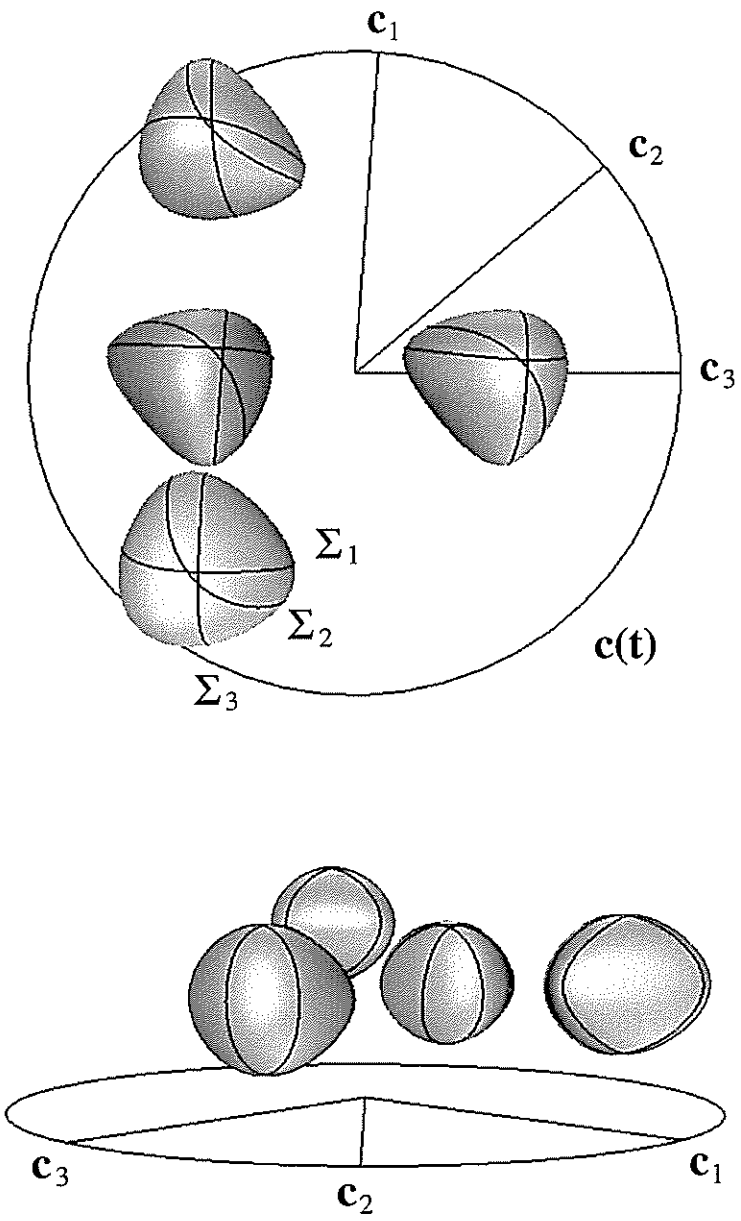

Figure 2.1: Two diagrams of a scene containing four (virtual) blobs. The camera motion $\mathbf{c}(t)$ is circular and the critical sets Σ_i for the three different view points $\mathbf{c}_i$ are shown.

Cipolla [CI] for perspective projection onto a sphere and Vaillant and Faugeras [VF] for perspective projection onto a plane.

2.2.1 Orthogonal Projection

Orthogonal (or parallel) projection is projection onto a plane perpendicular to a vector called the view direction. If the view direction is w and the image plane is spanned by the perpendicular unit vectors u and v the projection is given by

$$\begin{aligned} \pi_1 : \mathbf{R}^3 &\rightarrow \mathbf{R}^2 \\ (x,y,z) &\rightarrow ((x,y,z).u, (x,y,z).v). \end{aligned}$$

The size of the projection of a surface is unchanged if the surface is moved parallel to the view direction.

2.1 Definition: *Given a smooth surface M and a view direction w, with an image plane perpendicular to w, the* **critical set** Σ *in direction w consists of points p on M such that the tangent plane contains the view direction or, equivalently, the surface normal at p is perpendicular to w. The projection of Σ onto the image plane gives the* **profile**.

We now prove the important result that the surface normal on the critical set is parallel to the normal to the profile in the case when the image plane is perpendicular to the view direction. It is straightforward to generalise to perspective projection.

2.2 Lemma: *For parallel projection the normal to the surface is parallel to the profile normal.*

Proof: Suppose the profile $\mathbf{p}(s)$ is smooth (we can generalise to the case of a singular profile and use limiting tangents). Let $\mathbf{w}$ be the fixed view direction and $\mathbf{r}(s)$ the critical set. There is then a depth $\lambda(s)$ such that,

$$\mathbf{r}(s) = \mathbf{p}(s) + \lambda(s)\mathbf{w}. \tag{2.1}$$

Let $\mathbf{n}(s)$ be the surface normal along the critical set and so we have the identity $\mathbf{n}(s).\mathbf{w} = 0$. Differentiating (2.1) by s and dotting with $\mathbf{n}$ we get $\mathbf{r}_s.\mathbf{n} = \mathbf{p}_s.\mathbf{n} + \lambda_s\mathbf{w}.\mathbf{n} = \mathbf{p}_s.\mathbf{n}$, and so $\mathbf{p}_s.\mathbf{n} = 0$. Thus the plane spanned by $\mathbf{p}_s$ and $\mathbf{w}$ (which are always independent) is orthogonal to $\mathbf{n}$ i.e. the normal to the profile $\mathbf{w} \wedge \mathbf{p}_s$ is parallel to the normal to the surface $\mathbf{n}$. □

2.2.2 Perspective Projection

Perspective projection (or polar projection) is projection from a finite point, called the centre of projection, onto a sphere or a plane. With perspective projection the size of the projection of a surface is dependent on the positioning of the surface relative to the centre of projection. There is a choice of projection, onto a plane or a sphere. Perspective projection onto a plane involves the choice of an optical axis which is perpendicular to the plane and passes through the centre of projection. There is a diffeomorphism between a hemisphere and a tangent plane to the hemisphere [RY, Lemma 2.2.4].

2.3 Definition *Given a smooth surface M and a centre of projection C, the* **critical set** Σ *consists of points p on M where the tangent plane to M at p passes through C. On a sphere with centre C the* **profile** *is the intersection of the lines from C to p on Σ with the sphere. In the plane the* **profile** *is the intersection of the lines from C to p on Σ with the plane. The perpendicular distance from C to the plane is called the focal length.*

2.2.3 Notation.

We use $\mathbf{r}$ for the parametrisation of a smooth surface M and $\mathbf{c}(t)$ for the locus of centres of a one parameter family of central projections not intersecting M. If $\mathbf{r}(s,t)$ is a point on the critical set for some t then we can find a view direction $\mathbf{p}(s,t)$ and a non-zero depth $\lambda(s,t)$ such that,

$$\mathbf{r}(s,t) = \mathbf{c}(t) + \lambda(s,t)\mathbf{p}(s,t). \tag{2.2}$$

See Figure 2.2. Note that it is not necessarily the case that $\mathbf{r}(s,t)$ is a non-singular parametrisation of M, and in fact Chapter 6 is concerned with precisely this.

2.2.4 Epipolar Parametrisation

The above section describes the setup for a spatio-temporal parametrisation of the surface M. By this we mean a parametrisation of the surface via the critical sets Σ_t. Obviously this fails to be a smooth parametrisation if the critical sets form an envelope or are singular. Assume that they do form a smooth

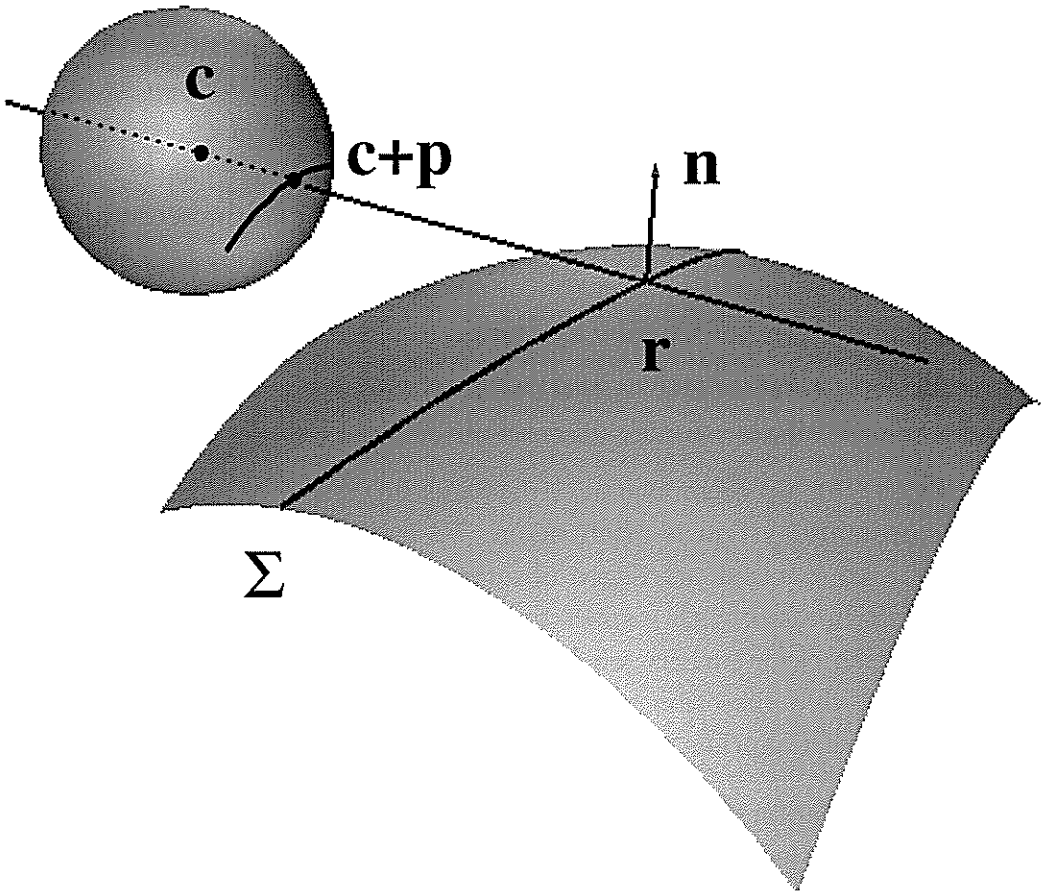

Figure 2.2: Perspective projection: the critical set Σ with a typical point $\mathbf{r}$, the image sphere with centre $\mathbf{c}$ and the corresponding profile point $\mathbf{c}+\mathbf{p}$. Thus $\mathbf{p}$ is the unit vector joining the centre $\mathbf{c}$ to the profile point. Also $\mathbf{n}$ is normal to the surface at $\mathbf{r}$.

parametrisation of M, and the critical sets 'slip' over the surface allowing us to use time as a local parameter.

Thus the critical sets Σ_t, form one set of parametrising curves on M. What are the constant-s curves? These are essentially arbitrary since there is no obvious connection between points on Σ_{t_0} and Σ_{t_1}, just as there is no 'matching' between profiles in the image.

One natural parametrisation is the **epipolar parametrisation** (e.g. [CB]) where the direction $\mathbf{r}_t$ is taken to be in the view direction at that point. Recall that the view direction lies in the tangent plane since the point lies in the critical set. The direction $\mathbf{r}_s$ is the tangent to Σ. One consequence of this parametrisation is that $\mathbf{r}_s$ and $\mathbf{r}_t$ are conjugate with respect to the second fundamental form (see Proposition 2.5 part 6).

2.3 Rotated Coordinates.

In setting up a geometrical problem in computer vision a preferred basis or coordinate system is often taken. We call this the *world system* and denote it $\boldsymbol{W}$. An external privileged observer can make measurements of directions and points in space with respect to $\boldsymbol{W}$. For example a parametrised surface may be given as $\mathbf{r}(u, v)$ where we understand the three-vector $\mathbf{r}$ is with respect to $\boldsymbol{W}$. Also a view direction $\mathbf{p}$, which is a geometrical vector connecting one point in space with another, can be given in terms of $\boldsymbol{W}$.

In Chapters 3, 4, 5, and 6 we will be considering a one-parameter family of central projections. At each projection centre an observer will be able to measure rays with respect to an internal basis that is related to $\boldsymbol{W}$ via a translation and rotation. An observer no longer has the facility to take measurements with respect to $\boldsymbol{W}$. If our projection centres are $\mathbf{c}(t)$ then the internal basis at time t is related to $\boldsymbol{W}$ by a rotation $\boldsymbol{R}(t)$.

2.4 Lemma: *If a direction* $\mathbf{p}$ *is measured in the rotated frame* $\mathbf{RW}$ *with coordinates* $(\alpha_1, \alpha_2, \alpha_3)$ *then there exists a vector* $\mathbf{q}$ *such that* $\mathbf{p} = \boldsymbol{R}\mathbf{q}$ *and* $\mathbf{q}$ *has coordinates* $(\alpha_1, \alpha_2, \alpha_3)$ *with respect to the basis* $\mathbf{W}$.

Proof: Let the basis vectors for $\boldsymbol{W}$ be w_1, w_2 and w_3, then the rotated basis

$\mathbf{RW}$ has basis vectors $\mathbf{R}w_1, \mathbf{R}w_2, \mathbf{R}w_3$. We then have,

$$\begin{aligned} \mathbf{p} &= \alpha_1 \boldsymbol{R} w_1 + \alpha_2 \boldsymbol{R} w_2 + \alpha_3 \boldsymbol{R} w_3 \\ &= \boldsymbol{R}(\alpha_1 w_1 + \alpha_2 w_2 + \alpha_3 w_3) \\ &= \boldsymbol{R}\mathbf{q} \end{aligned}$$

hence the result. □

Notes on the Lemma:

1. As an observer at $\mathbf{c}(t)$ the *only* measurement we have of a ray $\mathbf{p}$ is the triple of numbers $(\alpha_1, \alpha_2, \alpha_3)$.

2. If the rotation $\boldsymbol{R}$ is known then by creating the vector $\mathbf{q}$ (as above) in $\boldsymbol{W}$ we can rotate to get $\mathbf{p}$, which is the true direction of the observed vector.

3. Often we will take measurements at many different times and we are then presented with the problem of how to uniformly represent these measurements when the world basis is unknown. Given some basis $\overline{\boldsymbol{W}}$ related to $\boldsymbol{W}$ by a rotation $\boldsymbol{R}_0$, $\boldsymbol{W} = \mathbf{R}_0 \overline{\boldsymbol{W}}$, then using some measured coordinates $(\alpha_1, \alpha_2, \alpha_3)$ we can draw the vectors with respect to the basis $\overline{\boldsymbol{W}}$. Thus we take a measurement of a vector $\mathbf{p}$ at time t in the camera basis giving a triple $(\alpha_1, \alpha_2, \alpha_3)$, then given a fixed basis $\overline{\boldsymbol{W}}$ we create the vector $\overline{\mathbf{q}}$ in this basis whose coordinates are $(\alpha_1, \alpha_2, \alpha_3)$. We now have $\mathbf{p} = \boldsymbol{R}_0 \boldsymbol{R}(t) \overline{\mathbf{q}}$.

In much of the following work we use $\mathbf{p}$ coordinates. These are world coordinates that are written with respect to W. In any practical application in computer vision one would have to use $\mathbf{q}$ coordinates where these are rotated with respect to the $\mathbf{p}$ coordinates. In the following work we refer to $\mathbf{p}$ and $\mathbf{q}$ coordinates for brevity. As shown above the $\mathbf{p}$ and $\mathbf{q}$ coordinates are related by

$$\mathbf{p} = \mathbf{R}(t)\mathbf{q}.$$

There is then a unique vector $\boldsymbol{\Omega}(t)$ such that,

$$\mathbf{p}_t = \mathbf{R}_t \mathbf{q} + \mathbf{R}\mathbf{q}_t = \boldsymbol{\Omega} \times \mathbf{R}\mathbf{q} + \mathbf{R}\mathbf{q}_t.$$

See [KK, p.290] for a derivation of this, and [CB] for its use in computer vision.

2.4 Properties of the Critical Set and Profile

The following proposition gives several properties of critical sets and profiles for a surface M in the case of orthogonal projection. A complete proof can be found in [RY, p.18], the first four properties can be found in [GW], Property 5 is stated by [BT]. Property 6 is given by Koenderink in [K84].

2.5 Proposition: *Given a smooth surface M and a view direction w:*

1. *The critical set is smooth at p unless p is a parabolic point and the view direction is the asymptotic direction at p.*
2. *The profile arising from a point p on the critical set is smooth unless the view direction is an asymptotic direction.*
3. *When the critical set is smooth at p the tangent direction to Σ is parallel to the view plane if and only if the view direction is a principal direction at p.*
4. *When the profile is smooth the tangent to the profile is always in the tangent plane to the surface at p.*
5. *The surface normal at p is parallel to the normal to the profile at the image of p.*
6. *The view direction and the tangent to the critical set Σ are in conjugate directions with respect to the second fundamental form at p.*

□

The results of the previous Proposition also hold in the case of perspective projection, where the term view direction is replaced by ray direction, which is the vector from the centre of projection to the point on the surface. Properties 3,4,5 and 6 are shown by Blake and Cipolla in [BC89]. The analogous results of Properties 1 and 2 of the previous Proposition are given below and proofs can be found in [RY, p.20].

2.6 Proposition: *For perspective projection of a smooth surface M from a centre of projection C;*

- *The critical set is smooth at p unless p is a parabolic point and the direction C_p is the asymptotic direction at p.*
- *The profile arising from p on the critical set, is smooth unless C_p is in an asymptotic direction.*

□

2.5 Koenderink's Formula for the Gauss Curvature

The motivation behind the work in this section was to examine in what way parallel projection is a natural limit of perspective projection. We examine how the Koenderink formula for Gauss curvature ($K = \frac{\kappa^p \kappa^t}{\lambda}$), changes as we pass to this limit. The reduction is instructive in that it brings out some of the differences between perspective projection and parallel projection.

Subsection 2.5.1 derives the parallel projection equivalent for the Koenderink formula for Gauss curvature. Subsection 2.5.2 details a derivation for perspective projection, and lays some groundwork for future calculations. The lemmas appear at the end of the section to preserve the flow of the work. An expression for the curvature of the profile from parallel projection is given in Subsection 2.5.3, and a similar formula for perspective projection, in Subsection 2.5.4. Subsection 2.5.5 describes how we revise the Koenderink formula and take a limit.

2.5.1 Gauss Curvature From Parallel Projection

Consider our surface patch passing through the origin with the tangent plane at the origin coincident with the x, y plane. In Monge-Taylor form $z = \frac{1}{2}(ax^2 + 2bxy + cy^2) + \cdots$ We take the x axis as the view direction, and project onto a plane parallel to the y, z plane. We denote the normal curvature in the view direction as κ^t, and the Gauss curvature K. Thus it is easily seen that,

$$\kappa^t = a \tag{2.3}$$

$$K = ac - b^2. \tag{2.4}$$

We denote the critical set of the projection mapping as Σ, and in this situation it is defined by $z_x = 0$. Using the Monge form this condition becomes, $ax + by + \cdots =$

0, or $x = \frac{-b}{a}y + \cdots$. Higher terms are indicated by $\cdots$.

We wish to find the curvature of the profile. The profile is simply the projection of the critical set onto our image-plane. If $\pi(x, y, z) = (y, z)$, then we are concerned with the profile curve $\pi(\Sigma)$. The profile is written $(y, \frac{1}{2}(ax^2 + 2bxy + cy^2) + \cdots)$, and if we substitute $x = \frac{-b}{a}y + \cdots$ we arrive at the formula for $\pi(\Sigma)$,

$$\left(y\ , \frac{1}{2}\left(\frac{ac - b^2}{a}\right) y^2 + \cdots \right).$$

This is a planar curve and the curvature of the profile is the coefficient, $\frac{ac-b^2}{a}$. We call the curvature of the profile κ^p. Thus it is easily seen from above that,

$$K = \kappa^p \kappa^t.$$

This is the formula for Gauss curvature in the case of parallel projection.

2.5.2 Gauss Curvature from Perspective Projection

Recall the notation of Subsection 2.2.3 where $\mathbf{r}$ is our surface point, $\mathbf{c}$ is the projection centre, λ is the depth, and $\mathbf{p}$ is the unit vector, so that

$$\mathbf{r} = \mathbf{c} + \lambda \mathbf{p}.$$

We wish to find expressions for the curvature of the profile, κ^p and the normal curvature in the view direction, κ^t. The curvature of the profile is understood in this case to mean the geodesic curvature of the profile on the image sphere. In the following we let $\mathbf{n}$ be the normal to the surface and by Proposition 2.5 part 5 is the profile normal. Using common formulae, e.g. [ON, p.230] and the proof of Lemma 2.7 below, we can write,

$$\kappa^p = \frac{\mathbf{p}_{ss}.\mathbf{n}}{\|\mathbf{p}_s\|^2}.$$

By Lemma 2.7 below this is related to κ^s, the normal curvature of the surface in the tangent direction to the critical set, by

$$\kappa^p = \frac{\lambda \kappa^s}{\sin^2 \theta}$$

where θ is the angle between the view-direction $\mathbf{p}$ and the tangent $\mathbf{r}_s$ to the critical set. As usual λ is the depth.

By Lemma 2.8 below we can write the Gauss curvature as,

$$K = \frac{\det \begin{bmatrix} \mathbf{r}_{ss}.\mathbf{n} & \mathbf{r}_{st}.\mathbf{n} \\ \mathbf{r}_{ts}.\mathbf{n} & \mathbf{r}_{tt}.\mathbf{n} \end{bmatrix}}{\det \begin{bmatrix} \mathbf{r}_s.\mathbf{r}_s & \mathbf{r}_s.\mathbf{r}_t \\ \mathbf{r}_t.\mathbf{r}_s & \mathbf{r}_t.\mathbf{r}_t \end{bmatrix}}.$$

In the epipolar parametrisation (Subsection 2.2.4 and [CB]) where $\mathbf{r}_t$ is taken to be the view direction, and $\mathbf{r}_s$ is the tangent to the critical set, this becomes

$$K = \frac{\det \begin{bmatrix} \kappa^s & 0 \\ 0 & \|\mathbf{r}_t\|^2\kappa^t \end{bmatrix}}{\det \begin{bmatrix} 1 & \cos\theta\|\mathbf{r}_t\| \\ \cos\theta\|\mathbf{r}_t\| & \|\mathbf{r}_t\|^2 \end{bmatrix}}.$$

We have $\mathbf{r}_{tt}.\mathbf{n} = \|\mathbf{r}_t\|^2\kappa^t$, by Lemma 2.9 below. Also note that off-diagonal entries are zero since $\mathbf{r}_s$ and $\mathbf{r}_t$ are in conjugate directions, since in the epipolar parametrisation $\mathbf{r}_t$ is along the view direction and $\mathbf{r}_s$ is the tangent to the critical set. Also we can safely parametrise the critical sets by arclength (i.e.$\|\mathbf{r}_s\| = 1$), but it is not necessarily the case that $\|\mathbf{r}_t\| = 1$. Thus,

$$K = \frac{\kappa^s\kappa^t}{\sin^2\theta} \tag{2.5}$$

$$= \frac{\kappa^p\kappa^t}{\lambda} \tag{2.6}$$

with the last equality from Lemma 2.7 below. This is the Koenderink formula for Gauss curvature, $K = \frac{\kappa^p\kappa^t}{\lambda}$ for perspective projection.

2.7 Lemma: *If κ^p is the curvature of the profile, κ^s the normal curvature of the surface in the direction tangent to the critical set, $\mathbf{n}$ the surface normal and θ is the angle between the view direction and the tangent to the critical set then,*

$$\kappa^p = \frac{\lambda\kappa^s}{\sin^2\theta}.$$

Proof: Let $\mathbf{p}(s)$ be the profile on the image sphere parametrised by s. If σ is arclength we can write $\mathbf{p}_s.\mathbf{p}_s = (\sigma_s)^2$. If $\mathbf{T}$ is the unit tangent to the profile, g the geodesic curvature, and k the normal curvature, then $\mathbf{T}_\sigma = g\mathbf{n} + k\mathbf{p}$. Thus $\mathbf{T}_s = \mathbf{T}_\sigma\sigma_s = (g\mathbf{n}+k\mathbf{p})\|\mathbf{p}_s\|$. So, $\mathbf{p}_s = \mathbf{T}\|\mathbf{p}_s\|$ and, $\mathbf{p}_{ss} = (g\mathbf{n}+k\mathbf{p})\|\mathbf{p}_s\|^2+\mathbf{T}\frac{d\|\mathbf{p}_s\|}{ds}$. We have an expression for κ^p,

$$\kappa^p = \frac{\mathbf{p}_{ss}.\mathbf{n}}{\|\mathbf{p}_s\|^2}.$$

By definition the normal curvature of the critical set Σ is $\kappa^s = \mathbf{r}_{ss}.\mathbf{n}$. Using $\mathbf{r} = \mathbf{c} + \lambda\mathbf{p}$, we can write,

$$\kappa^s = \lambda g \|\mathbf{p}_s\|^2.$$

Observing that $\sin^2\theta = \|\mathbf{p} \wedge \mathbf{r}_s\|^2$, and $\|\mathbf{p}\| = \|\mathbf{r}_s\| = 1$, we get the result. □

2.8 Lemma:

$$K = \frac{det\begin{bmatrix} \mathbf{r}_{ss}.\mathbf{n} & \mathbf{r}_{st}.\mathbf{n} \\ \mathbf{r}_{ts}.\mathbf{n} & \mathbf{r}_{tt}.\mathbf{n} \end{bmatrix}}{det\begin{bmatrix} \mathbf{r}_s.\mathbf{r}_s & \mathbf{r}_s.\mathbf{r}_t \\ \mathbf{r}_t.\mathbf{r}_s & \mathbf{r}_t.\mathbf{r}_t \end{bmatrix}}.$$

Proof: In this proof we use the *shape operator* S that is a linear map on the tangent space given by $S(v) = -\nabla_v n$ where n is the unit surface normal and ∇_v is the directional derivative along v. We can write S operating on the basis vectors in the following way.

$$S(\mathbf{r}_s) = \alpha\mathbf{r}_s + \beta\mathbf{r}_t$$
$$S(\mathbf{r}_t) = \delta\mathbf{r}_s + \gamma\mathbf{r}_t.$$

Then $\alpha, \beta, \delta, \gamma$ define the shape operator with respect to this basis. In matrix notation we can write,

$$\begin{bmatrix} S(\mathbf{r}_s).\mathbf{r}_s & S(\mathbf{r}_s).\mathbf{r}_t \\ S(\mathbf{r}_t).\mathbf{r}_s & S(\mathbf{r}_t).\mathbf{r}_t \end{bmatrix} = \begin{bmatrix} \alpha & \beta \\ \delta & \gamma \end{bmatrix} \begin{bmatrix} \mathbf{r}_s.\mathbf{r}_s & \mathbf{r}_s.\mathbf{r}_t \\ \mathbf{r}_t.\mathbf{r}_s & \mathbf{r}_t.\mathbf{r}_t \end{bmatrix}.$$

We take determinants, and hence result. □

The following result is true for the epipolar parametrisation where $\mathbf{r}_t$ is along the view direction $\mathbf{p}$.

2.9 Lemma: *For the epipolar parametrisation*

$$\kappa^t = \frac{\mathbf{r}_{tt}.\mathbf{n}}{\|\mathbf{r}_t\|^2}.$$

Proof: Let $\mathbf{r}(t)$ be the curve $\mathbf{r}(s_0, t)$. We are considering the epipolar parametrisation so $\mathbf{r}_t$ is parallel to $\mathbf{p}$, and the normal to $\mathbf{r}(t)$ is $\mathbf{p}_s$ and the surface normal is $\mathbf{n}$.

If σ is arclength we can write $\mathbf{r}(t).\mathbf{r}(t) = (\sigma_t)^2$. Let $\mathbf{T}$ be the unit tangent to $\mathbf{r}(t)$ and $\mathbf{T}_\sigma = g\mathbf{p}_s + \kappa^t\mathbf{n}$, then

$$\mathbf{T}_t = \mathbf{T}_\sigma\sigma_t = (g\mathbf{p}_s + \kappa^t\mathbf{n})\|\mathbf{r}(t)\|.$$

We have $\mathbf{r}_t = \mathbf{T}\|\mathbf{r}_t\|$ and

$$\mathbf{r}_{tt} = (g\mathbf{p}_s + \kappa^t\mathbf{n})\|\mathbf{r}(t)\|^2 + \mathbf{T}\frac{d\|\mathbf{r}_t\|}{dt}$$

and dotting with $\mathbf{n}$ gives the required result. □

2.5.3 Geodesic Curvature of Profile from Parallel Projection

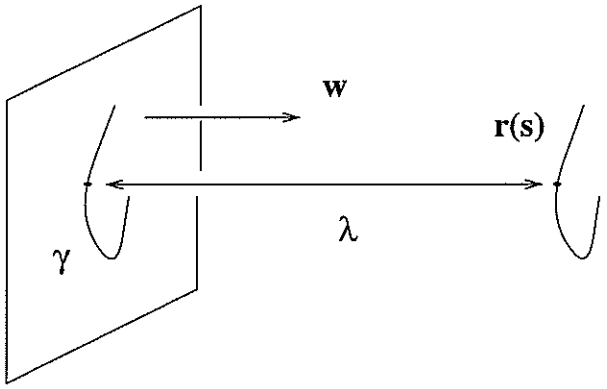

We consider $\mathbf{r}(s)$ to be the critical set of some surface with normal $\mathbf{n}$ for some fixed time, under the parallel projection with kernel $\mathbf{w}$. There is a non zero λ such that $\mathbf{r} = \gamma + \lambda\mathbf{w}$. Now $\gamma(s)$ is not necessarily unit speed, so letting μ be arclength and $\mathbf{T}$ be the unit tangent we write,

$$\frac{d\mathbf{T}}{ds} = \frac{d\mathbf{T}}{d\mu}\frac{d\mu}{ds} = (\kappa^p\mathbf{n} + k\mathbf{w})\left\|\frac{d\gamma(s)}{ds}\right\|.$$

The geodesic curvature is κ^p and k the normal curvature. In fact the geodesic curvature of this curve is equal to its curvature in the sense of a plane-curve. It is less cumbersome to write $\mathbf{T}_s = (\kappa^p\mathbf{n} + k\mathbf{w})\|\gamma_s\|$, where sub-scripts denote differentiation. We can derive the formula for κ^p,

$$\begin{aligned}
& \gamma_s = \mathbf{T}\|\gamma_s\| \\
\Rightarrow\ & \gamma_{ss} = \mathbf{T}_s\|\gamma_s\| + \mathbf{T}\frac{d}{ds}\|\gamma_s\| \\
\Rightarrow\ & \gamma_{ss}.\mathbf{n} = \kappa^p\|\gamma_s\|^2 \\
\Rightarrow\ & \kappa^p = \frac{\gamma_{ss}.\mathbf{n}}{\|\gamma_s\|^2}.
\end{aligned}$$

Now using the fact that $\mathbf{r} = \gamma + \lambda \mathbf{w}$, we can calculate the following derivatives,

$$\begin{aligned} \mathbf{r}_s &= \gamma_s + \lambda_s \mathbf{w} \\ \mathbf{r}_s.\gamma_s &= \gamma_s.\gamma_s + \lambda \mathbf{w}.\gamma_s \\ \mathbf{r}_{ss} &= \gamma_{ss} + \lambda_{ss} \mathbf{w} \\ \mathbf{r}_{ss}.\mathbf{n} &= \gamma_{ss}.\mathbf{n}, \end{aligned}$$

and so

$$\kappa^p = \frac{\mathbf{r}_{ss}.\mathbf{n}}{\mathbf{r}_s.\gamma_s}. \tag{2.7}$$

This is then the (geodesic) curvature of the profile for the case of parallel projection in terms of $\mathbf{r}(s)$ and the projected curve. Now a similar formula is derived for the perspective case, and we see how they are related.

2.5.4 Geodesic Curvature of Profile From Perspective Projection

We now wish to consider the perspective projection of a space-curve, $\mathbf{r}(s)$ onto an image sphere of radius σ, centred at the point $\rho\mathbf{c}$. What we plan to do is to take the image sphere passing through the origin and then let the centre of the sphere recede to infinity and simultaneously let the radius increase so that the sphere remains through the origin. In the limit we expect the projection to behave like parallel projection to a plane at the origin.

A formula for the geodesic curvature[1] of the profile is derived.

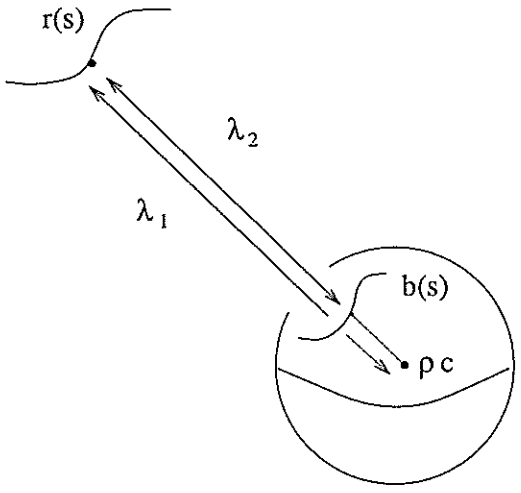

[1]This is now indicated $\kappa^p(\sigma)$, to show the dependence on the image sphere radius.

The profile is denoted $\mathbf{b}(s)$, and is not necessarily parametrised by arclength. If we let μ be arclength of the curve $\mathbf{b}$, then $\mathbf{T}_\mu = \kappa^p(\sigma)\mathbf{n} + k\mathbf{p}$. $\mathbf{p}$ is the unit normal pointing outwards from the centre of the sphere, and k is the normal curvature of the space-curve, $\mathbf{b}(s)$. $\mathbf{T}$ is the unit tangent vector to the profile, $\lambda_1(s)$ is the depth from the centre of the sphere to the point $\mathbf{r}(s)$, and $\lambda_2(s)$ is the depth from $\mathbf{r}(s)$ to the image $\mathbf{b}(s)$. $\kappa^p(\sigma)$ is the geodesic curvature of this curve as a space-curve on the surface of the sphere, radius σ. We can derive an expression for $\kappa^p(\sigma)$ in a similar way to the parallel projection case. Thus,

$$\kappa^p(\sigma) = \frac{\mathbf{b}_{ss}.\mathbf{n}}{\|\mathbf{b}_s\|^2}.$$

We can now use the fact that $\mathbf{b} = \rho\mathbf{c} + \sigma\mathbf{p}$. By differentiating this we get, $\kappa^p(\sigma) = \frac{\mathbf{p}_{ss}.\mathbf{n}}{\sigma\|\mathbf{p}_s\|^2}$. By observing that $\mathbf{r} = \rho\mathbf{c} + \lambda_2\mathbf{p}$, we reach the final form for the curvature of the profile,

$$\kappa^p(\sigma) = \frac{\mathbf{r}_{ss}.\mathbf{n}}{\mathbf{r}_s.\mathbf{b}_s}. \tag{2.8}$$

This is remarkably similar to the formula for the parallel projection case (2.7). If we let $\sigma = \rho\|\mathbf{c}\|$ then the image sphere passes through the origin. Now we let ρ tend to infinity (keeping $\mathbf{c}$ fixed) which simultaneously moves the image sphere away from the origin but increases the radius so that it still passes through the origin. In the limit $\mathbf{b}(s) \to \gamma(s)$, and $\kappa^p(\sigma) \to \kappa^p$. In other words the (geodesic) curvature of the curve on the image sphere equals the (geodesic) curvature of the planar curve, in the limit as we let the radius of the image sphere tend to infinity (in a controlled way).

2.5.5 Gauss Curvature In The Limit

This section will derive a slightly altered Koenderink formula for the Gauss curvature. We are now considering the case when the image sphere is centred at $\rho\mathbf{c}$, and has radius σ, where $\sigma = \rho\|\mathbf{c}\|$, so that it passes through the origin, for all ρ.

From the last section it was shown that

$$\kappa^p(\sigma) = \frac{\mathbf{r}_{ss}.\mathbf{n}}{\mathbf{r}_s.\mathbf{b}_s}.$$

If we assume that $\|\mathbf{r}_s\| = 1$, then the normal curvature of the critical set is written, $\kappa^s = \mathbf{r}_{ss}.\mathbf{n}$, and we have the simple connection,

$$\kappa^p(\sigma) = \frac{\kappa^s}{\mathbf{r}_s.\mathbf{b}_s}.$$

Referring back to Subsection 2.5.2 on Gauss curvature from perspective projection we know, $K = \frac{\kappa^s \kappa^t}{\sin^2\theta}$ (2.5). This makes no reference to the projected curve since κ^s and κ^t are the normal curvatures *on the surface*, of the critical set and view direction respectively. It is therefore a good place to start the new calculation. We know κ^s and substitute to get, $K = \frac{(\mathbf{r}_s.\mathbf{b}_s)\kappa^p(\sigma)\kappa^t}{\sin^2\theta}$. Using $\mathbf{r} = \rho\mathbf{c} + \lambda_1\mathbf{p}$ and $\mathbf{b} = \rho\mathbf{c} + \sigma\mathbf{p}$, we can substitute for $\mathbf{r}_s$ and $\mathbf{b}_s$. Thus $K = \frac{\lambda_1\sigma\|\mathbf{p}_s\|\kappa^p(\sigma)\kappa^t}{\sin^2\theta}$. By writing $\sin^2\theta = \|\mathbf{p} \wedge \mathbf{r}_s\|^2$ we can make more substitutions to get,

$$K(\sigma) = \frac{\sigma\kappa^p(\sigma)\kappa^t}{\lambda_1}.$$

This is the slightly revised Koenderink formula for the Gauss curvature for perspective projection on a image sphere radius σ. We next use the relationship, $\lambda_1 = \lambda_2 + \sigma$ to get,

$$K(\sigma) = \kappa^p(\sigma)\kappa^t - \frac{\lambda_2\kappa^p(\sigma)\kappa^t}{\lambda_1}.$$

Now by letting $\rho \to \infty$ we see the right hand term vanishes since, $\frac{\lambda_1}{\lambda_2} \to 0$ as $\rho \to \infty$. In the left hand term, κ^t is unchanged since it does not depend on ρ, but it has already been shown that $\kappa^p(\sigma) \to \kappa^p$. So we might write the suggestive formula $K(\sigma) \to \kappa^p\kappa^t$, which says that the Koenderink formula makes sense as we pass from perspective to parallel projection, in the (special) limit.

2.6 The Spatio–Temporal Surface

When considering families of curves in the plane or on a smooth surface, it is often natural to 'lift' them into a new extended space where they form a surface [BG]. The inverse operation is the projection of the surface back to a family of curves. More concretely, we wish to lift our family of critical sets on M that have resulted from some camera motion $\mathbf{c}(t)$, to form a new surface called the *Spatio–Temporal surface*, $\widetilde{M}$.

2.10 Definition: *Given a smooth surface M parametrised $\mathbf{r}(u,v)$ with normal $\mathbf{n}(u,v)$ and a camera motion $\mathbf{c}(t)$, then the spatio-temporal surface in (u,v,t) space is given by,*

$$(\mathbf{r}(u,v) - \mathbf{c}(t)).\mathbf{n}(u,v) = 0$$

2.11 Notes on the definition.

- Level-t sets are the critical sets at time t in the u, v plane. Therefore the spatio–temporal surface can be viewed as the critical sets 'stacked up' in (u, v, t) space.
- The projection $\pi_t(u, v, t) = (u, v)$ projects $\widetilde{M}$ on to the parameter space of M (essentially M itself). Restricting π_t to $\widetilde{M}$ gives us a map from the plane to the plane which (generically) may be a diffeomorphism, fold or cusp.
- In the case when $\widetilde{M}$ is not diffeomorphic to M the critical sets form an envelope, the **frontier**, on M (see Definition 2.15).

It is the third note above that reveals the usefulness of the spatio–temporal surface. It provides a natural setting for studying the envelope of critical sets.

It is of interest to ask when the spatio–temporal surface is singular, and the following two results addresses this.

2.12 Lemma: *If the surface M is described locally at a point $\mathbf{r}$ by the equation $z = h(u, v)$, then we may parametrise $\widetilde{M}$ by,*

- *u and t provided the view direction is not a principal direction.*
- *v and t provided the view direction is not asymptotic.*
- *u and v provided $\mathbf{r}$ is not a frontier point*

Proof: We can set up the surface in Monge form $(u, v, h(u, v))$ (Definition 1.1) with the camera passing through the point $(\lambda, 0, 0)$ at time zero. The differential of the map $(\mathbf{r} - \mathbf{c}).\mathbf{n}$, whose zero set is the spatio temporal surface, is

$$[\lambda h_{uu},\ \lambda h_{uv},\ -c_3'(t)]$$

Recall (Lemma 3.1) that $h_{uu} = 0$ is the condition for the view direction to be asymptotic, and in addition $h_{uv} = 0$ gives a parabolic point. It is then straightforward to invoke the implicit function theorem to derive the result. □

2.13 Proposition: *Given a smooth surface M, a camera motion $\mathbf{c}(t)$ not passing through M and the corresponding spatio–temporal surface $\widetilde{M}$, then the following are equivalent.*

1. *The spatio–temporal surface is singular at (u,v,t).*

2. *The view direction is asymptotic at a parabolic point* $\mathbf{r}(u,v)$ *and the point is on the frontier, see Definition 2.15 i.e.* $\mathbf{c}_t(t).\mathbf{n}(u,v) = 0$.

3. *The camera motion is tangent to the Cylinder Axis Developable at* $\mathbf{c}(t)$. *(See the proof of the following corollary.)*

Proof: $1 \Leftrightarrow 2$

We can examine $\widetilde{M}$ locally at the origin by taking our original surface M in Monge form (Definition 1.1), and $\mathbf{c}(t) = (c_1(t), c_2(t), c_3(t))$ with $\mathbf{c}(0) = (\lambda, 0, 0)$ and non-zero λ. The equation for $\widetilde{M}$ is,

$$h_u(c_1 - u) + h_v(c_2 - v) + h - c_3 = 0.$$

The Jacobian at $(u,v,t) = (0,0,0)$ is then $[\lambda h_{uu}, \lambda h_{uv}, -c_3']$, where $\mathbf{c}(0) = (\lambda, 0, 0)$. This is zero precisely when the view direction is asymptotic ($h_{uu} = 0$), the origin is parabolic (additionally $h_{uv} = 0$) and the point is on the frontier ($c_3' = 0$). This is the condition for $\mathbf{c}_t.\mathbf{n} = 0$ the frontier, by Definition 2.15.

$2 \Leftrightarrow 3$

By the first part of the proof we see that for $\widetilde{M}$ to be singular the camera must necessarily lie in the cylinder–axis developable (CAD). We consider our surface in Monge form with the parabolic curve passing through the origin and the asymptotic direction at the origin coincident with the u–axis. Since the CAD is developable the tangent plane is constant along any ruling. Thus the tangent plane to the CAD at the point $\mathbf{c}(0) = (\lambda, 0, 0)$ is coincident with the u, v plane. Also the tangent plane to the CAD at the point on the surface is equal to the tangent plane to the surface since it is spanned by the tangent to the parabolic curve and the asymptotic direction. Therefore the condition that the camera motion is tangential to the CAD is equivalent to the condition $c_3' = 0$. Which is the condition for a frontier. □

2.14 Corollary: *For a single camera motion it is generic for the spatio–temporal surface to be smooth.*

Sketch Proof: The CAD is not in general smooth but it is stratified into smooth manifolds abd of dimension 2. Therefore a 1-dimensional curve $\mathbf{c}(t)$ will generically be transverse to the CAD, hnece missing the singular set. □

2.7 The Frontier.

We remain in the situation of considering the critical sets that arise from a one parameter family of projections parametrised by t. We saw in the last section that the critical sets can be 'stacked up' in time to produce the spatio-temporal surface $\widetilde{M}$. In [CB] the authors are concerned with when the critical sets form a local parametrisation of the surface M, so that surface reconstruction can be performed (1.1.2). In this section we concern ourselves with precisely the situation when the critical sets do not foliate M. The following definition introduces the condition for a *frontier* in terms of the camera velocity $\mathbf{c}_t(t)$ and surface normal $\mathbf{n}(t)$.

2.15 Definition: *If our smooth parametrised surface is* $\mathbf{r}(u,v)$ *and the camera motion is* $\mathbf{c}(t)$ *then the* **frontier** *is the curve on the surface defined by the following two equations,*

$$\begin{aligned}(\mathbf{r}(u,v)-\mathbf{c}(t)).\mathbf{n}(u,v) &= 0\\ \mathbf{c}_t(t).\mathbf{n}(u,v) &= 0.\end{aligned}$$

Frontier points are sometimes called **epipolar tangency points**. *A* **collision point** *is a point on the frontier for which in addition the vector* $\mathbf{c}_t(t)$ *is parallel to the view direction* $\mathbf{p}$. *(See (2.2.3) for a review of* $\mathbf{p}$ *and* $\mathbf{c}$*.)*

Notes:

- This characterisation $\mathbf{c}_t.\mathbf{n}=0$ is very geometrical and says that a frontier point occurs when the camera trajectory is tangent to a tangent plane of the surface. If $\mathbf{c}$ passes through a tangent plane then the point is on the critical set, but if it is tangent to the tangent plane then it is also a frontier point. Figure 2.3 illustrates this.
- In a later section we prove that another characterisation of the frontier is that the critical sets form an envelope (Lemma 2.22).
- The direction $\mathbf{c}_t$ is sometimes called the **epipolar direction** and the **epipolar plane** is spanned by the view direction to the surface, and the epipolar direction. Frontier points are those points where the epipolar plane is a tangent plane.

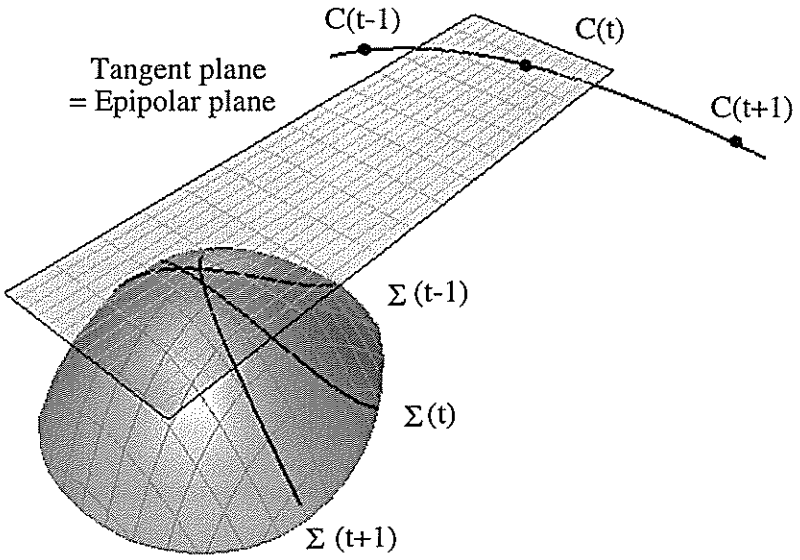

Figure 2.3: Illustration of a frontier point with three camera positions **c** and three critical sets Σ shown.

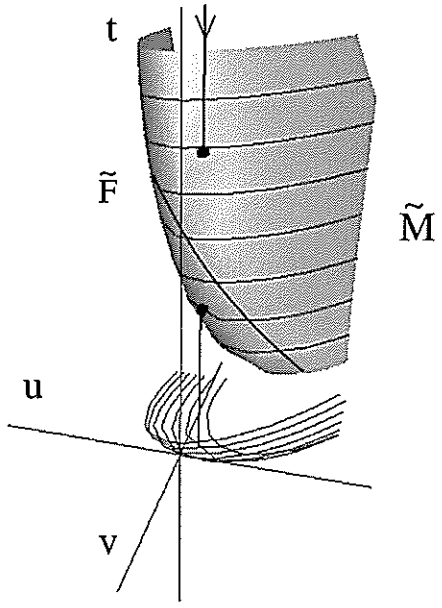

Figure 2.4: Lifted frontier shown for an example spatio-temporal surface.

- The frontier forms the boundary (locally at least) between the region visible from some point on $\mathbf{c}(t)$ and invisible for all points.

The **lifted frontier** (see Figure 2.4) denoted $\widetilde{F}$ is the critical set of the projection $\pi_t(u,v,t) = (u,v)$. The projection of this curve in the (u,v) plane is the frontier on M. Parametrising $\widetilde{M}$ and restricting π_t to $\widetilde{M}$ we have a map from the plane to the plane. Maps of this type are well studied and we expect either a fold or cusp singularity. We wish to answer the question; when is F a cusp, i.e. when is the projection map a cusp map? First we find the conditions for $\widetilde{F}$ to be singular, and then implement the recognition criterion found in [LU, p.38], which is reproduced as Definition 2.18 below.

2.16 Lemma: *If $\mathbf{r}(u,v)$ is a smooth parametrisation of M, $\mathbf{c}(t)$ a smooth camera motion and $\mathbf{n}$ the normal to M, then $\widetilde{F}$ is singular at p if either p is a parabolic point and the view line is asymptotic, or $\mathbf{c}_{tt}.\mathbf{n} = 0$ and p is a collision point.*

Proof: Let $\pi_t(u,v,t)$ be the projection map on the first two coordinates from $\widetilde{M}$ to the parameter space of M. Let $\Sigma(\pi_t)$ be the critical set of π_t which is $\widetilde{F}$. Then $\Sigma(\pi_t)$ is given by two conditions in the three variables (u,v,t),

$$\begin{aligned} \mathbf{c}_t.\mathbf{n} &= 0 \\ (\mathbf{r}-\mathbf{c}).\mathbf{n} &= 0. \end{aligned}$$

The differential of $\mathbf{c}_t.\mathbf{n}$ is $[\ \mathbf{c}_t.\mathbf{n}_u\ \mathbf{c}_t.\mathbf{n}_v\ \mathbf{c}_{tt}.\mathbf{n}\ ]$, and the differential of $(\mathbf{r}-\mathbf{c}).\mathbf{n}$ is $[(\mathbf{r}-\mathbf{c}).\mathbf{n}_u\ (\mathbf{r}-\mathbf{c}).\mathbf{n}_v\ -\mathbf{c}_t.\mathbf{n}]$, since $\frac{\partial}{\partial u}((\mathbf{r}-\mathbf{c}).\mathbf{n}) = \mathbf{r}_u.\mathbf{n} + (\mathbf{r}-\mathbf{c}).\mathbf{n}_u = (\mathbf{r}-\mathbf{c}).\mathbf{n}_u$ and $\mathbf{n}$ is the surface normal. Similarly for $\frac{\partial}{\partial v}$. So the tangent to $\widetilde{F}$ lies in the kernel of both. Since $\mathbf{c}_t.\mathbf{n} = 0$ we examine 2×2 minors of the following matrix,

$$\begin{bmatrix} \mathbf{c}_t.\mathbf{n}_u & \mathbf{c}_t.\mathbf{n}_v & \mathbf{c}_{tt}.\mathbf{n} \\ (\mathbf{r}-\mathbf{c}).\mathbf{n}_u & (\mathbf{r}-\mathbf{c}).\mathbf{n}_v & 0 \end{bmatrix} \tag{2.9}$$

These are

$$\begin{aligned} \mathbf{c}_t.\mathbf{n}_u(\mathbf{r}-\mathbf{c}).\mathbf{n}_v - \mathbf{c}_t.\mathbf{n}_v(\mathbf{r}-\mathbf{c}).\mathbf{n}_u &= 0 \\ \mathbf{c}_{tt}.\mathbf{n}(\mathbf{r}-\mathbf{c}).\mathbf{n}_u &= 0 \\ \mathbf{c}_{tt}.\mathbf{n}(\mathbf{r}-\mathbf{c}).\mathbf{n}_v &= 0. \end{aligned}$$

If $\mathbf{c}_{tt}.\mathbf{n} \neq 0$ then we must have $(\mathbf{r}-\mathbf{c}).\mathbf{n}_u = (\mathbf{r}-\mathbf{c}).\mathbf{n}_v = 0$. Now $(\mathbf{r}-\mathbf{c})$ is the view direction, and the only way for it to be conjugate to both the linearly

independent directions $\mathbf{r}_u$ and $\mathbf{r}_v$ is if the view line is asymptotic at a parabolic point.

If $\mathbf{c}_{tt}.\mathbf{n} = 0$ we must have $\mathbf{c}_t.\mathbf{n}_u(\mathbf{r}-\mathbf{c}).\mathbf{n}_v - \mathbf{c}_t.\mathbf{n}_v(\mathbf{r}-\mathbf{c}).\mathbf{n}_u = 0$. Now let $\mathbf{r}_v$ be the tangent to the critical set. The parametrisation $\mathbf{r}$ is essentially arbitrary so we allow ourselves this, and we know that the critical set is smooth since the previous case dealt with the singular critical set. Therefore $(\mathbf{r}-\mathbf{c}).\mathbf{n}_v = 0$ since this just says that the view direction $\mathbf{p}$ (recall notation of 2.2.3) is conjugate to $\mathbf{r}_v$ the tangent to the critical set. We therefore must also have $\mathbf{c}_t.\mathbf{n}_v = 0$. That is $\mathbf{c}_t$ is conjugate to $\mathbf{r}_v$ (since $\mathbf{c}_t$ lies in the tangent plane), and since $\mathbf{r}_v$ has a unique conjugate we must conclude that $\mathbf{c}_t$ and $\mathbf{p}$ are parallel giving rise to a collision point. This concludes the proof. □

Note: The conditions given above for a singular $\widetilde{F}$ are non generic for a single camera motion. The first condition says that we have a parabolic point on the frontier with the view line asymptotic. Recall from Proposition 2.13 that this is the condition for the spatio-temporal surface to be singular. More geometrically the camera is tangent to the CAD. This is not a generic occurrence.

For the second condition we require two conditions to hold on the frontier, namely $\mathbf{c}_{tt}.\mathbf{n} = 0$ and a collision point. Since $\widetilde{F}$ is a curve we do not expect two conditions to hold simultaneously, and we assume for the remainder of the thesis that $\widetilde{F}$ is smooth.

2.17 Lemma: *Provided the lifted frontier $\widetilde{F}$ is smooth (see Lemma 2.16), then its tangent is parallel to the t-axis if and only if $\mathbf{c}_{tt}.\mathbf{n} = 0$.*

Proof: The proof of this lemma closely follows the first part of the proof of Lemma 2.16. Following from equation 2.9 the tangent to $\widetilde{F}$ is parallel to the t-axis if and only if,

$$\begin{bmatrix} \mathbf{c}_t.\mathbf{n}_u & \mathbf{c}_t.\mathbf{n}_v & \mathbf{c}_{tt}.\mathbf{n} \\ \mathbf{r}-\mathbf{c}.\mathbf{n}_u & \mathbf{r}-\mathbf{c}.\mathbf{n}_v & -\mathbf{c}_t.\mathbf{n} \end{bmatrix} \begin{bmatrix} 0 \\ 0 \\ 1 \end{bmatrix} = \begin{bmatrix} 0 \\ 0 \end{bmatrix}$$

Since $\mathbf{c}_t.\mathbf{n} = 0$ we have the result. □

We can use the previous lemma to establish when the projection has a cusp singularity. We reproduce the recognition criterion for a fold and cusp from [LU, p.38] below.

2.18 Definition: *Let $\phi(t) = (t, \gamma(t))$ be a C^2-parametrisation of a nonsingular fold of f such that $\phi(0) = p$ where p is a singular point of f.*

1. *p is a* **fold point** *of f if $\frac{d}{dt}(f \circ \phi)(0) \neq 0$*
2. *p is a* **cusp point** *of f if $\frac{d}{dt}(f \circ \phi)(0) = 0$ but $\frac{d^2}{dt^2}(f \circ \phi)(0) \neq 0$.*

2.19 Lemma: *If $\mathbf{c}_t.\mathbf{n} = \mathbf{c}_{tt}.\mathbf{n} = 0$ but $\mathbf{c}_{ttt}.\mathbf{n} \neq 0$ then the projection from $\widetilde{M}$ to M will be a cusp singularity and no worse (hence the frontier has a cusp).*

Proof: Assume that $\mathbf{c}_t.\mathbf{n} = \mathbf{c}_{tt}.\mathbf{n} = 0$ at $t = 0$ and $(u, v) = (0, 0)$. In the Monge-Taylor form we write the camera motion as,

$$\mathbf{c}(t) = (\lambda + c_{11}t + \cdots, c_{21}t + \cdots, c_{33}t^3 + \cdots)$$

and the surface as $(u, v, h(u, v))$ where,

$$h(u, v) = \frac{1}{2}(b_1u^2 + 2b_2uv + b_3v^2) + \cdots.$$

Now since $\mathbf{c}_t.\mathbf{n} = \mathbf{c}_{tt}.\mathbf{n} = 0$ at $u = v = t = 0$ we can use the previous lemma to say that the tangent to $\widetilde{F}$ (at the cusp point) is parallel to the t-axis. We may therefore write $\widetilde{F}$ locally as,

$$(u, v, t) = (\alpha t^2 + \cdots, \beta t^2 + \cdots, t)$$

Recall from the note following Lemma 2.16 that we assume $\widetilde{F}$ is smooth and so can parametrise in this way. By the criterion in Lu; F is worse than a cusp if and only if $\alpha = 0$ and $\beta = 0$. Therefore using Monge form,

$$\begin{aligned} \mathbf{c}_t.\mathbf{n} = 0 \quad \Leftrightarrow \quad & -(c_{11} + \cdots)(b_1\alpha + b_2\beta)t^2 \\ & -(c_{21} + \cdots)(b_2\alpha + b_3\beta)t^2 + 3c_{33}t^2 + O(t^3) = 0. \end{aligned}$$

Now since $c_{33} \neq 0$ (since $\mathbf{c}_{ttt}.\mathbf{n} \neq 0$) we can not have $\alpha = 0$ and $\beta = 0$, and we conclude that the map is no worse than a cusp. □

2.7.1 Structure of the Critical Sets.

We now turn our attention to the pattern of critical set on M at a frontier point. Can we classify their geometric form up to a suitable equivalence ? This section is almost entirely based on the work of Dufour and his paper [DU].

Dufour is concerned with a (one parameter) "family of plane curves". This he represents by the diagram,

$$\begin{array}{ccccc} & & f & & \gamma & \\ \mathbf{R} & \leftarrow & U & \rightarrow & \mathbf{R}^2 \end{array}$$

where U is open in $\mathbf{R}^2$ and f and γ are smooth. Two families $\mathbf{R} \overset{f}{\leftarrow} \mathbf{R}^2 \overset{\gamma}{\rightarrow} \mathbf{R}^2$ and $\mathbf{R} \overset{f'}{\leftarrow} \mathbf{R}^2 \overset{\gamma'}{\rightarrow} \mathbf{R}^2$ are "equivalent" if there is a commutative diagram

$$\begin{array}{ccccccc} & & f & & \gamma & & \\ & \mathbf{R} & \leftarrow & \mathbf{R}^2 & \rightarrow & \mathbf{R}^2 & \\ \lambda & \downarrow & & \downarrow & H & \downarrow & K \\ & \mathbf{R} & \leftarrow & \mathbf{R}^2 & \rightarrow & \mathbf{R}^2 & \\ & & f' & & \gamma' & & \end{array}$$

where λ, H, K are diffeomorphisms. He then derives a generic classification for the families.

We consider the situation in [DU] with our spatio-temporal surface $\widetilde{M}$ foliated by the lifted critical sets and then projected in the standard way onto our surface M. We define the lifted critical sets as level sets of a function $f(u, v, t) = t$, and the projection γ as $\gamma(u, v, t) = (u, v)$. We then wish to consider the situations arising when we project the f-curves under the map γ,

$$\begin{array}{ccccc} & & f & & \gamma & \\ \mathbf{R} & \leftarrow & \widetilde{M} & \rightarrow & M \end{array}$$

We now reproduce from Dufour recognition criteria for the generic behaviour of these families,

1. Diffeomorphism: γ regular; f regular.
2. Singular: γ regular; f Morse.
3. Fold: γ admits a fold; (γ, f) is regular and f restricted to the critical set of γ is regular.
4. Parabolic point on fold: γ admits a fold; (γ, f) is regular and f restricted to the critical set of γ is Morse.
5. Whitney Umbrella: γ admits a fold; (γ, f) admits a Whitney Umbrella with its double point line transverse to $\mathbf{R}^2 \times 0$ in $\mathbf{R}^2 \times \mathbf{R}$. Note that this does not occur in our family.

6. Cusp type: γ admits a cusp and (γ, f) is regular.

A succession of lemmas provides the hypotheses for these standard forms.

2.20 Lemma: *Assume the point* $\mathbf{r}$ *on* M *is not a frontier point and the view direction is not asymptotic. Then,*

- γ *is regular,*
- f *is regular.*

Proof: Parametrise $\widetilde{M}$ by v and t. The map f is then $f : (v,t) \to t$ since $\widetilde{\Sigma}_t$ are t-level sets. The map γ is $\gamma|\widetilde{M} : (v,t) \to (u(v,t), v)$.

Note that f is regular, and

$$d\gamma = \begin{bmatrix} \frac{\partial u}{\partial v} & \frac{\partial u}{\partial t} \\ 1 & 0 \end{bmatrix}$$

So γ fails to be regular iff $\frac{\partial u}{\partial t} = 0$.

Recalling the notation introduced in (2.2.3) we have

$$(\mathbf{r} - \mathbf{c}).\mathbf{n} = 0 \Rightarrow \lambda \mathbf{p}.\mathbf{n}_u \frac{\partial u}{\partial t} - \mathbf{c}_t.\mathbf{n} = 0,$$

so $\frac{\partial u}{\partial t} = 0 \Rightarrow \mathbf{c}_t.\mathbf{n} = 0$. But $\mathbf{c}_t.\mathbf{n} \neq 0$ thus $\frac{\partial u}{\partial t} \neq 0$ and γ is regular. □

For the following result we assume that the singularity of the visual mapping is no worse than a lips/beaks. It can be worse than a lips/beaks if we are viewing a cusp of Gauss on a parabolic curve along an asymptotic direction. This is called a 'Gulls' singularity [BG85].

2.21 Lemma: *Suppose the point* $\mathbf{r}$ *is parabolic but not on the frontier, the view direction is asymptotic and the singularity of the visual mapping is no worse than a lips/beaks then,*

- γ *regular,*
- f *is Morse.*

Proof: Parametrise $\widetilde{M}$ by u and v. The map γ is then $\gamma : u, v \to u, v$ which is regular. The map f is $f : (u, v) \to t(u, v)$. Let the camera motion be $\mathbf{c}(t) = (\lambda + c_1(t), c_2(t), c_3(t))$ with $c_1(0) = c_2(0) = c_3(0) = 0$, then $\widetilde{M}$ is given by the equation

$$(u - \lambda - c_1)h_u + (v - c_2)h_v - (h - c_3) = 0$$

i.e.

$$h_u(u - \lambda) + h_v v - h = c_1 h_u + c_2 h_v - c_3. \tag{2.10}$$

If $t = t(u, v)$ then we wish to evaluate first and second derivatives of t. Differentiate (2.10) with respect to u and using a dash to indicate derivatives with respect to t we find,

$$\begin{aligned} h_{uu}(u - \lambda) + h_u + h_{uv}v - h_u &= c_1' \frac{\partial t}{\partial u} h_u + c_1 h_{uu} \\ &\quad + c_2' \frac{\partial t}{\partial u} h_v + c_2 h_{uv} - c_3' \frac{\partial t}{\partial u} \end{aligned}$$

and evaluating at $u = v = 0$ gives $\lambda h_{uu} = c_3' \frac{\partial t}{\partial u}$ and $\lambda h_{uv} = c_3' \frac{\partial t}{\partial v}$ when we differentiate with respect to v.

Now $c_3'(0) \neq 0$ since we are not at a frontier point, so f is singular since the point is parabolic and the view direction asymptotic, making $h_{uu} = h_{uv} = 0$.

We now calculate the second derivatives,

$$\begin{aligned} h_{uuu}(u - \lambda) + 2h_{uu} + h_{uuv}v - h_{uu} &= c_1'' \left(\frac{\partial t}{\partial u}\right)^2 h_u + c_1' \frac{\partial^2 t}{\partial u^2} h_u + c_1' \frac{\partial t}{\partial u} h_{uu} \\ &\quad + c_1' \frac{\partial t}{\partial u} h_{uu} + c_1 h_{uuu} \\ &\quad + c_2'' \left(\frac{\partial t}{\partial u}\right)^2 h_v + c_2' \frac{\partial^2 t}{\partial u^2} h_v + c_2' \frac{\partial t}{\partial u} h_{uv} \\ &\quad + c_2' \frac{\partial t}{\partial u} h_{uv} + c_2 h_{uuv} \\ &\quad - c_3'' \left(\frac{\partial t}{\partial u}\right)^2 - c_3' \frac{\partial^2 t}{\partial u^2} \end{aligned}$$

and evaluate at $u = v = 0$. In this way we can form the Hessian matrix of second derivatives,

$$d(df)_0 = -\lambda \begin{bmatrix} h_{uuu} & h_{uuv} \\ h_{uuv} & h_{uvv} \end{bmatrix}$$

Thus f is Morse if $h_{uu} = h_{uv} = 0$ and $h_{uuu}h_{uvv} \neq h_{uuv}^2$. This is true by hypothesis since $\mathbf{r}$ is a parabolic point along an asymptotic direction ($h_{uu} = h_{uv} = 0$) and not a 'Gulls' singularity ($h_{uuu}h_{uvv} \neq h_{uuv}^2$). □

2.22 Lemma: *Let* $\mathbf{r}$ *be a frontier point with* $\mathbf{c}_{tt}.\mathbf{n} \neq 0$ *and not parabolic or a collision point (2.15) or the view direction asymptotic then,*

- γ *admits a fold at* u.
- (γ, f) *is regular.*
- $f|_{\Sigma\gamma}$ *is regular.*

Proof: Frontier points are contained in $\Sigma(\gamma)$ and are precisely the fold points.

We parametrise $\widetilde{M}$ by v and t, then $\gamma : v, t \to u(v,t), v$ and $f : v, t \to t$ and the map (γ, f) is $v, t \to u(v,t), v, t$, which is regular.

Let the lifted frontier be parametrised by v, which is possible since γ is not a cusp map, then,

$$\begin{array}{ccccc} & & \widetilde{F} & & f \\ v & \to & v, t(v) & \to & t(v) \end{array}$$

Let $u = u_1 v + u_2 v^2 + \cdots$ and $t = t_1 v + t_2 v^2 + \cdots$ parametrise $\widetilde{F}$ on $\widetilde{M}$; we examine our surface in Monge form. Our object is to prove $t_1 = 0$, which shows that $f|_{\Sigma\gamma}$ is regular. We have the following equations,

$$\begin{aligned} h &= \frac{1}{2}(b_1 u^2 + 2b_2 uv + b_3 v^2) + \cdots \\ h_u &= b_1 u + b_2 v + \cdots \\ h_v &= b_2 u + b_3 v + \cdots \end{aligned}$$

Our camera motion is given by,

$$\mathbf{c}(t) = (\lambda + c_{11}t + c_{12}t^2 + \cdots, c_{21}t + \cdots, c_{32}t + \cdots).$$

The condition for points to be frontier points is that $\mathbf{c}_t.\mathbf{n} = 0$. Thus our curve, $(u_1 v + u_2 v^2 + \cdots, v, t_1 v + t_2 v^2 + \cdots)$ must satisfy this, i.e.,

$$\begin{aligned} -(c_{11} + 2c_{12}t_1 v + 2c_{12}t_2 v^2 + \cdots)(b_1 v + b_2 u_1 v + b_2 u_2 v^2 + \cdots) \\ -(c_{21} + 2c_{22}t_1 v + 2c_{22}t_2 v^2 + \cdots)(b_2 v + b_3 u_1 v + b_3 u_2 v^2 + \cdots) \\ +2c_{32}t_1 v + 2c_{32}t_2 v^2 + O(v^3) = 0 \end{aligned}$$

We now equate coefficients of v in the above to get,

$$-c_{11}b_1 - c_{11}b_2 u_1 - c_{21}b_2 - c_{21}b_3 u_1 + 2c_{32}t_1 = 0.$$

We also demand that our curve satisfies the equation to lie on $\widetilde{M}$, $(\mathbf{r}-\mathbf{c}).\mathbf{n}=0$, giving,

$$\begin{aligned}-(v-\lambda-c_{11}t_1v-c_{11}t_2v^2)(b_1v+b_2v_1v+b_2v_2v^2)\\ -(v_1v+v_2v^2-c_{21}t_1v)(b_2v+b_3v_1v+b_3v_2v^2)\\ +\frac{1}{2}(b_1v^2+2b_2v_1v^2+b_3v_1^2v^2)-c_{32}t_1^2v^2+O(v^3)=0\end{aligned}$$

Equating coefficients of y we find,

$$u_1=\frac{-b_1}{b_2},$$

and thus,

$$t_1=\frac{c_{21}}{2c_{32}b_2^2}(b_2^2-b_1b_3).$$

This can not be zero since the point is neither parabolic nor collision. □

2.23 Lemma: *If the point u is a parabolic point on the frontier or a collision point ($c_{21}\neq 0$) and the view direction is not asymptotic, then,*

- *γ admits a fold,*
- *(γ,f) is regular,*
- *$f|_{\Sigma\gamma}$ is Morse.*

Proof: The proof is very similar to the previous proof. □

2.24 Lemma: *Let u be a point for which $\mathbf{c}_t.\mathbf{n}=\mathbf{c}_{tt}.\mathbf{n}=0$ and $\mathbf{c}_{ttt}.\mathbf{n}\neq 0$ and the view direction not asymptotic, then,*

- *γ admits a cusp at u,*
- *(γ,f) is regular at u.*

Proof: The hypotheses imply that γ cusps by (2.19). We can parametrise $\widetilde{M}$ by v and t thus, $(\gamma,f):v,t\rightarrow u(v,t),v,t$ is regular.

□

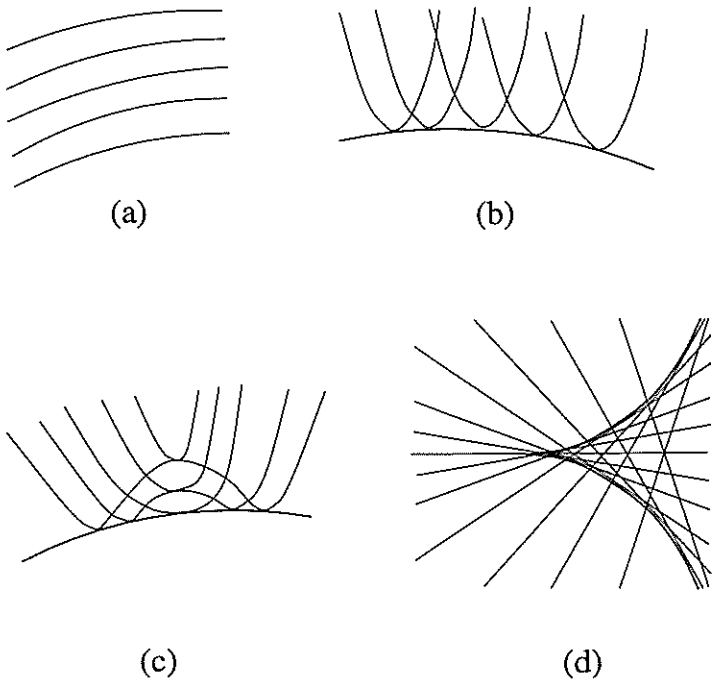

Figure 2.5: Classification of Critical Sets at the frontier. Models from Dufour. (a) Away from frontier. (b) The frontier. (c) Parabolic point on the frontier. (d) Cusp of the frontier.

We are now in a position to use the local models (up to equivalence) detailed in [DU]. Pictures are by far the most helpful models as shown in Figure 2.5. Figure 2.5(a) is the configuration corresponding to Lemma 2.20 where we are away from the frontier and the projection from $\widetilde{M}$ to M is a diffeomorphism. The local model up to equivalence is $y \overset{f}{\leftarrow}(x,y) \overset{\gamma}{\rightarrow}(x,y)$.

Figure 2.5(b) is the configuration corresponding to Lemma 2.22 and shows the critical sets making an envelope along the frontier away from a parabolic point. The local model up to equivalence is $x + y \overset{f}{\leftarrow}(x,y) \overset{\gamma}{\rightarrow}(x,y^2)$.

Figure 2.5(c) is the configuration corresponding to Lemma 2.23 and shows critical sets at a parabolic point on the frontier. The local model up to equivalence is $x^2 + y \overset{f}{\leftarrow}(x,y) \overset{\gamma}{\rightarrow}(x,y^2)$.

Figure 2.5(d) is the configuration corresponding to Lemma 2.24 and is the case for when the locus of camera centres has extra contact with the tangent plane and the frontier cusps. The local model up to equivalence is $y + g(x, xy + y^3) \overset{f}{\leftarrow}(x,y) \overset{\gamma}{\rightarrow}(x, xy + y^3)$.

Chapter 3

Tracking Cusps: Mathematical Aspects

It may sometimes happen that the Visual may be so direct
as to render the Profile too close and narrow.
The Ionick Pedestal, and the way to shun another difficulty [Poz]

3.1 Introduction

We consider a one parameter family of central projections of a surface onto an image sphere. We are particularly interested in the family of critical sets Σ_t (sometimes called contour generators) of this visual mapping and its image, see Figure 2.2. Locally maps from a surface to the sphere behave as maps from the plane to the plane. We therefore expect two types of stable singularities, the fold and cusp (e.g.[LU, p.33]). The image of a fold is called the profile and the image of the cusp is a cusp on the profile or a contour ending in the opaque surface case. It can easily be shown (e.g.[K, p.439] and Proposition 2.5) that the profile (also known as the apparent contour or silhouette) is singular if and only if the view direction is coincident with an asymptotic direction of the surface at the point being viewed. See Figure 3.1 and Figure 3.2. Of course this will only occur if we view a hyperbolic patch of surface.

Due to the stability of the singularities small changes in viewer position will result in small changes in the position of the cusp in the image. We consider the locus of these cusp points in the standard image sphere. The standard image sphere is obtained by taking the image spheres at different times and identifying

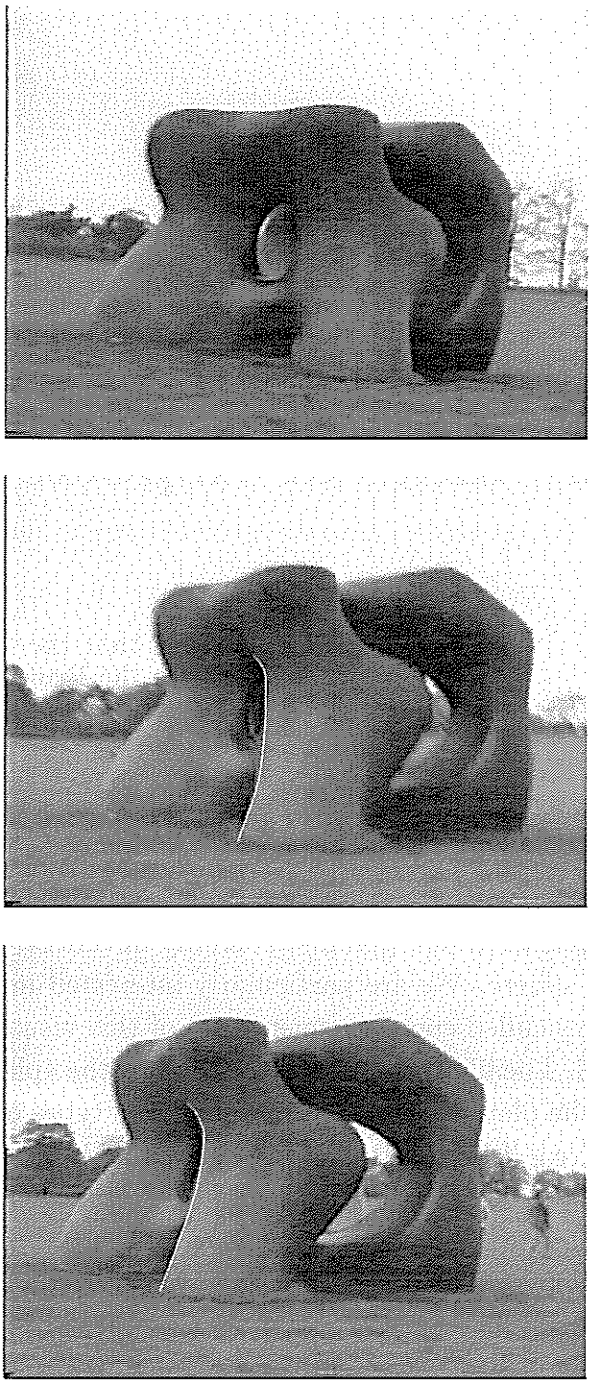

Figure 3.1: Sequence of real images with the lower two showing a moving contour ending (or partially occluded cusp). Thanks to Dr.R.Cipolla for this video sequence from the Yorkshire Sculpture Park.

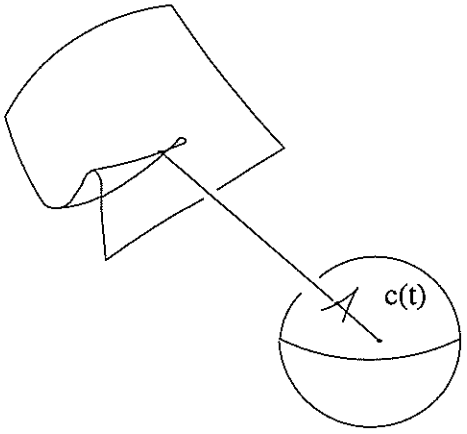

Figure 3.2: A schematic showing the projection of the critical set of a smooth surface on to the image sphere, giving a singular curve.

the points by translation to the unit sphere at the origin. This is called the $\mathbf{p}$ coordinates. In this work we also consider the situation when the image-spheres are all rotating with respect to the world frame. This we denote by $\mathbf{q}$ coordinates, see Subsection 2.2.3.

Thus for some surface and some camera motion we have a curve on the sphere that is called the cusp locus C. We can also view the locus of cusps as a curve on the surface by simply tracing along the view direction from the image sphere. These give the points on the surface that *generate* the cusps in the image with respect to this camera motion. Since the cusp points lie on critical sets for different times the locus of cusps can also be lifted on to the spatio-temporal surface. The cusp generator curve on the surface is called L, and on the spatio-temporal surface $\tilde{L}$.

In this chapter we present a detailed investigation of the locus of cusps.

3.2 The Locus Of Cusps

3.2.1 The Spatio-Temporal surface

In this subsection we examine the lifted cusp generator curve $\tilde{L}$. The principal result describes the singular instances of $\tilde{L}$. The spatio temporal surface also

provides a useful tool for examining the cusp locus in the vicinity of a frontier point. Recall (Lemma 2.22) that the fold of $\widetilde{M}$ in projecting to M is the frontier curve. The critical set of this fold is the lifted frontier $\widetilde{F}$.

We consider our camera $\mathbf{c}(t)$ to be moving through an area of space occupied by the *asymptotic ray complex* (ARC) of our surface M. This consists of the two parameter family of lines got by extending all asymptotic directions out from all the hyperbolic and parabolic points on the surface. Therefore as $\mathbf{c}$ moves through the ARC we find ourselves sitting on some asymptotic direction and hence observing a cusp in the image. The nature of the critical sets and cusp locus depends on the position of $\mathbf{c}$ with respect to the 'boundaries' of the ARC. In characterising these boundaries we beat the bush of auxiliary ruled surfaces and scare out the exotic sounding flecnodal scroll (FS) and cylinder axis developable (CAD). Recall Subsection 1.2.2 for an introduction to these.

In many of the proofs below we represent our surface in Monge-Taylor form (recall 1.1). We also make use of a 'standard' (without losing generality) camera motion, where the centre of our image sphere is taken to lie at the position $\mathbf{c}(t) = (c_1(t), c_2(t), c_3(t))$. We also demand that the image sphere passes through the point $(\lambda, 0, 0)$ at time zero. i.e.. $\mathbf{c}(0) = (\lambda, 0, 0)$.

The following elementary lemma relates common geometric situations with this particular form of local coordinates.

3.1 Lemma: *If our surface M is given in Monge-Taylor form with height function $h(x, y)$ and we take the camera motion $\mathbf{c}(t) = (c_1(t), c_2(t), c_3(t))$ with $\mathbf{c}(0) = (\lambda, 0, 0)$ then the following results hold.*

- *The condition $h_{xx} = 0$ is equivalent to our view direction at $t = 0$ (the x-axis) being an asymptotic direction. Then the cusp generator curve passes through $(0, 0, 0)$.*
- *If $h_{xx}(0, 0) = 0$ then the origin is a parabolic point if and only if $h_{xy}(0, 0) = 0$.*
- *If $h_{xx}(0, 0) = 0$ and $h_{xxx} = 0$ then we call this a Swallowtail point [K, p.448], and the view direction has an extra point of contact.*
- *The frontier is a curve on the surface given by the set of points satisfying $\mathbf{c}_t.\mathbf{n} = 0$, namely the envelope of critical sets. In the situation above the origin is a frontier point if and only if $c_3'(0) = 0$.*

- *The special case of a frontier when the camera motion is instantaneously towards the corresponding point of surface is called a Collision point (2.15) and is given by* $c_2'(0) = c_3'(0) = 0$.

□

The following definition of the map F and the subsequent proposition will describe the lifted cusp generator curve $\widetilde{L}$ as the zeroes of the map F on $\widetilde{M}$.

3.2 Definition: *We define the mapping* $F : \mathbf{R}^3 \to \mathbf{R}^2$ *as*

$$F(x,y,t) = \begin{pmatrix} h_x(c_1 - x) + h_y(c_2 - y) + h - c_3, \\ h_{xx}(c_1 - x)^2 + 2h_{xy}(c_1 - x)(c_2 - y) + h_{yy}(c_2 - y)^2 \end{pmatrix} \quad (3.1)$$

where h_x, h_y, h_{xx}, h_{xy} *and* h_{yy} *are evaluated at* (x, y).

3.3 Proposition: *The locus of cusps* $\widetilde{L}$, *is given by the equation* $\widetilde{L} = F^{-1}(0)$.

Proof: In this proof we represent our surface in Monge form.

It is well known that a line has three point contact with a surface at a point p if and only if it is an asymptotic direction at p. It is this characterisation that is the most useful, and will be used in this proof. We want the view direction (the line joining $\mathbf{c}(t)$ and the surface point $(x, y, h(x, y))$) at time t, to have three point contact with the surface. Taking the following line parametrised by μ

$$(1 - \mu)(x, y, h) + \mu(c_1, c_2, c_3)$$

we compose it with the equation of the surface $z - h(x, y) = 0$ and evaluate first and second derivatives at $\mu = 0$. The vanishing of these two derivatives will determine the locus of cusp points on $\widetilde{M}$. The mapping F above, incorporates these equations so that $F^{-1}(0)$ describes the cusp locus. □

Therefore it can be seen that $F^{-1}(0)$ is the intersection of two surfaces, one of which is the spatio-temporal surface.

The principal results of this section concern the singular cases of $\widetilde{L}$. Before we embark on this we first require some results concerning the differential geometry of some special ruled surfaces, and the interplay between these and the camera motion. Recall the results of Subsection 1.2.2.

We now find the condition for the camera motion to be tangent to the FS.

3.4 Proposition: *Let our surface M be given in Monge form with the standard camera motion $\mathbf{c}(t) = (c_1, c_2, c_3)$ and $\mathbf{c}(0) = (\lambda, 0, 0)$, then provided the origin is not parabolic and the view line has no more than four points of contact, the conditions (evaluated at $x = y = t = 0$)*

$$\begin{aligned} h_{xx}(0) = h_{xxx}(0) &= 0, \\ c_3'(2h_{xy} - \lambda d_2) - 2c_2'\lambda h_{xy}^2 &= 0 \end{aligned}$$

are equivalent to the camera motion being tangential to the flecnodal scroll of the surface at the origin.

Proof: We examine the surface in Monge form with the flecnodal curve passing through the origin, and the asymptotic direction at the origin along the x-axis. The camera at time zero is positioned at $(\lambda, 0, 0)$. We now wish to find the tangent plane to the flecnodal scroll at the point $(\lambda, 0, 0)$ and determine when the camera motion is tangential to it. We write the surface as $(x, y, h(x, y))$ where,

$$h(x, y) = \frac{1}{2}(2b_1xy + b_2y^2) + \frac{1}{6}(3d_2x^2y + 3d_3xy^2 + d_4y^3) + \frac{1}{24}(e_1x^4 + \cdots$$

It is straightforward to calculate the first, second and third derivatives.

The flecnodal curve $\gamma(y)$, is written as an expansion and p is an unknown coefficient.

$$\gamma(y) = (py + \cdots, y, h(py + \cdots, y)).$$

The situation when we could not parametrise γ by y is when γ is tangent to the x-axis. This case has been excluded since then the flecnodal curve is tangent and not transverse to the asymptotic direction, which according to [K, p.296] corresponds to five points of contact. Let $\delta(y)$ be the direction of the asymptotic rays having four-point contact with the surface. We have,

$$\delta(y) = (1, qy + \cdots, ry + \cdots)$$

for some constants q and r. Note that we have only included linear terms, since it is these that determine the tangent plane. Thus the flecnodal scroll is given in the usual form for a ruled surface by the equation $\gamma(y) + u\delta(y)$. Now consider fixing y and moving along the direction $\delta(y)$. We substitute the line in $z = h(x, y)$ and find the condition for four-point contact.

$$h(py + \cdots, y) + u(ry + \cdots) = h(py + \cdots u, y + u(qy + \cdots))$$

Taking the first three derivatives with respect to u and evaluating at $u = 0$, we get the following equations,

$$\begin{aligned} ry + \cdots &= h_x(py + \cdots, y) + (qy + \cdots)h_y(py + \cdots, y) \\ 0 &= h_{xx} + 2(qy + \cdots)h_{xy} + (qy + \cdots)^2 h_{yy} \\ 0 &= h_{xxx} + 3(qy + \cdots)h_{xxy} + 3(qy + \cdots)^2 h_{xyy} + (qy + \cdots)^3 h_{yyy} \end{aligned}$$

Evaluating the coefficient of y in each case we can find expressions for the coefficients, p, q and r.

$$p = \frac{3qd_2}{e_1}, \; q = \frac{-d_2}{2b_1}, \; r = b_1$$

The tangent plane to the ruled surface $\gamma(y) + u\delta(y)$ is spanned by $\gamma'(y) + u\delta'(y)$ and $\delta(y)$. Evaluating at $y = 0$ and $u = \lambda$, we find that the tangent plane is spanned by

$$(1, 0, 0) \text{ and } (p, 1 + \lambda q, \lambda r)$$

The normal to this plane is,

$$(0, -\lambda r, 1 + \lambda q)$$

So the camera motion is tangential to this plane if and only if,

$$\frac{1}{2b_1}\left[c_3'(2b_1 - \lambda d_2) - 2c_2'\lambda b_1^2\right] = 0$$

□

The following proposition is the principal result of this subsection and connects the FS, CAD and cusp locus $\widetilde{L}$.

3.5 Proposition: *$\widetilde{L}$ is singular if and only if either of the following two conditions hold.*

- *The camera motion is tangent to the cylinder-axis developable.*
- *The camera motion is tangent to the flecnodal scroll.*

Proof: To examine the singularities of this curve at the origin we evaluate the Jacobian matrix of the mapping F (equation 3.1), at $x = y = t = 0$, which is

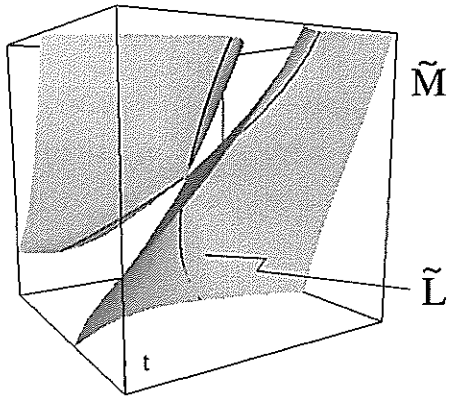

Figure 3.3: A singular spatio temporal surface produced from some example surface and camera motion.

shown below [1].

$$\begin{bmatrix} 0 & \lambda h_{xy}(0) & -c_3' \\ \lambda^2 h_{xxx}(0) & \lambda^2 h_{xxy}(0) - 2\lambda h_{xy}(0) & 2\lambda h_{xy}(0) c_2' \end{bmatrix} \tag{3.2}$$

By examining the vanishing of the two-by-two minors of this matrix we can determine the conditions for the curve to be singular. The three conditions are,

$$h_{xxx} h_{xy} = 0$$
$$c_3' h_{xxx} = 0$$
$$\lambda c_3' h_{xxy} + 2\lambda h_{xy}^2 c_2' - 2 h_{xy} c_3' = 0$$

Consider first $h_{xxx} = 0$ then the first two equations above are zero and then by Proposition 3.4 we see that the third equation implies that the camera is tangent to the FS. If $h_{xxx} \neq 0$ then we must have $h_{xy} = c_3' = 0$ and by Proposition 2.13 we have the camera tangent to the CAD. □

Figure 3.3 shows an example of a singular $\widetilde{M}$ and the lifted cusp locus $\widetilde{L}$.

We are also interested in when the line of cusps can be parametrised, and by what parameter.

3.6 Lemma: *$\widetilde{L}$ can be parametrised by time unless we are viewing a swallow-tail or parabolic point.*

[1] It is not always stated but the reader must remember that we are always considering the view direction to be an asymptotic direction at $t = 0$, giving $h_{xx}(0) = 0$, so that the profile is singular.

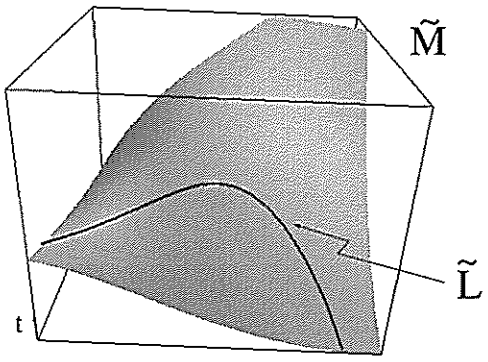

Figure 3.4: The vertical axis (with respect to the page) is time and horizontal slices of $\widetilde{M}$ are the lifted critical sets. Here we see that at a swallowtail point $\tilde{L}$ is tangent to $\tilde{\Sigma}$. Nearby critical sets intersect in either zero or two points.

Proof: Our main tool is the implicit function theorem, which we use by examining minors of (3.2). To enable the parametrising of $\tilde{L}$ by time we require the non-vanishing of the matrix,

$$\begin{bmatrix} 0 & \lambda h_{xy}(0) \\ \lambda^2 h_{xxx}(0) & \lambda^2 h_{xxy}(0) - 2\lambda h_{xy}(0) \end{bmatrix}$$

Recall Lemma 3.1 for the conditions for a swallowtail and parabolic point in this setup, and hence result. □

This is an intuitive result since it says that in these two cases we can not locally parametrise $\tilde{L}$ by the critical sets, see Figure 3.4 for an example illustration. In the light of the above lemma there are two cases of interest, parabolic points and swallowtail points.

1. If we consider the standard setup with $\mathbf{c}(0) = (\lambda, 0, 0)$ and the view direction at $t = 0$ the x-axis, then if p is parabolic then the curve $\tilde{L}$ can be parametrised locally at (p, t) by x provided p is not on the frontier and the singularity is not a gulls or worse.

2. If p is a flecnodal point then we can parametrise by x provided the camera velocity is not tangential to the FS.

These results were achieved in a very similar way to the proof of Lemma 3.6,

by first substituting $h_{xy} = 0$ (parabolic point) in (3.2) and then $h_{xxx} = 0$ (swallowtail point) in (3.2).

3.2.2 The Surface

We now project $\widetilde{L}$ onto the surface M and ask when the locus of cusps is singular on M. Projecting from $\widetilde{M}$ to M is achieved by the map π, where $\pi(x, y, t) = (x, y)$. Thus it is easily seen that if the locus of cusps is singular in $\widetilde{M}$ then the curve in M inherits that singularity. Figure 3.5 shows the cusp generator curve on a surface.

3.7 Lemma: *Suppose $\widetilde{L}$ is smooth, then L is singular iff the point of M is a collision point (2.15).*

Proof: Clearly this will happen when the tangent to $\widetilde{L}$ is vertical with respect to the xy plane. Then the projection will cusp. In the language of differential topology we have the kernel of $dF(0, 0, 0)$ contained in the kernel of π. Calculations reveal that this is the case when,

$$c_3' = h_{xy}c_2' = 0.$$

Thus if the curve in $\widetilde{M}$ is smooth the only condition that will create a singular curve on M is if the point is a collision point. □

It is often useful in calculations to parametrise L by time. Figure 3.7 gives the cases when the lifted cusp generator curve $\widetilde{L}$ can be parametrised by time, but we now wish to know when L is tangent to Σ_t, in which case L can not be parametrised by time. This is shown in the lemma below.

3.8 Lemma: *Assume L is non singular (see Proposition 3.7 and Lemma 3.5), and Σ_t is non singular. Then L is tangent to Σ_t if and only if the point is a swallowtail point or a frontier point.*

Proof: Consider our surface in the usual Monge form, with the x-axis as the view direction at $t = 0$ and L passing through the origin. Then we have $h_{xx}(0) = 0$ and Σ_0 is tangent to the x-axis. Also $h_{xy} \neq 0$ since Σ_0 is smooth. We

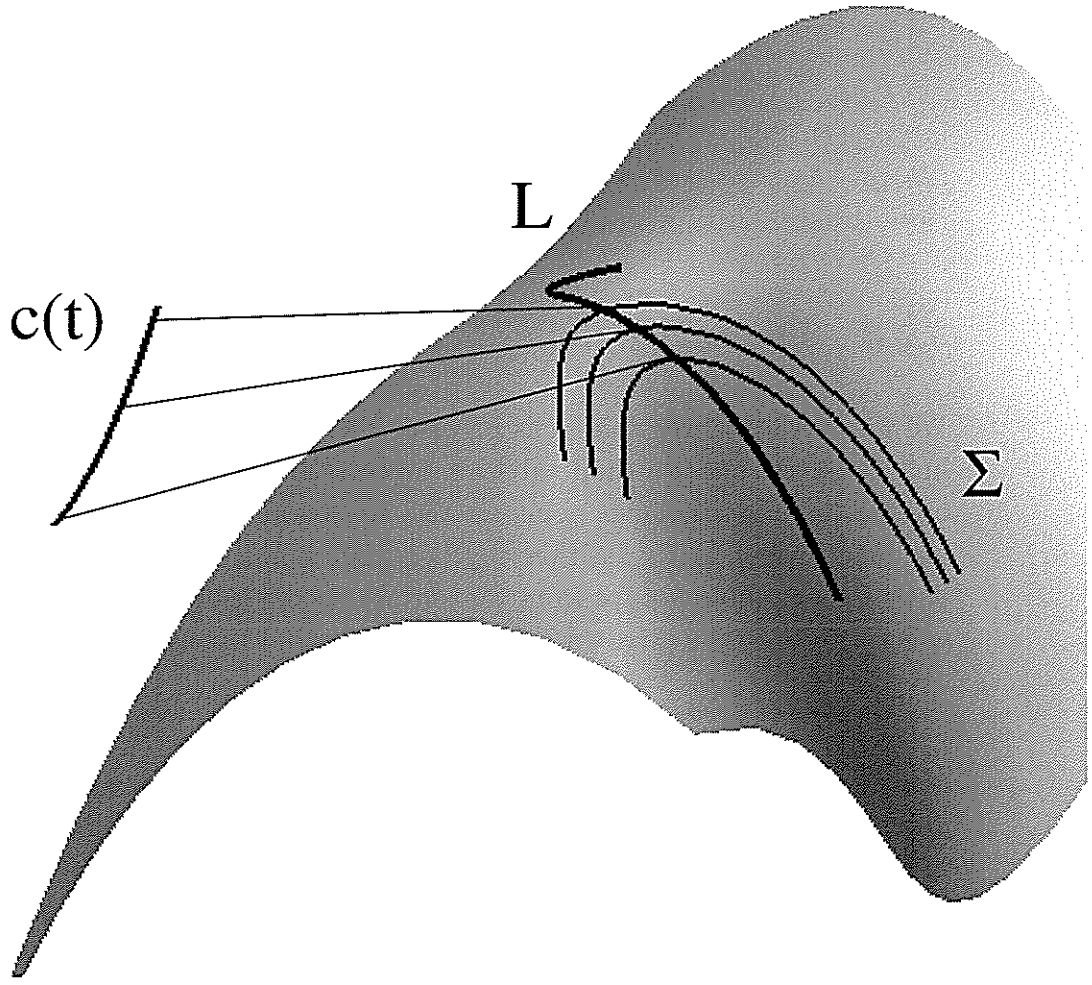

Figure 3.5: The simplest case, where **c** avoids the CAD and the flecnodal scroll: the cusp generator curve is nonsingular and transverse to the critical sets Σ. Also the cusp locus in the image sphere (not shown) is nonsingular.

project $\widetilde{L}$ onto the xy plane. We find the tangent to $\widetilde{L}$ by examining the kernel of dF (3.1), the matrix,

$$\begin{bmatrix} 0 & \lambda h_{xy} & -c_3' \\ \lambda^2 h_{xxx} & \lambda^2 h_{xxy} - 2\lambda h_{xy} & 2\lambda h_{xy} c_2' \end{bmatrix}$$

This gives the vector,

$$\begin{bmatrix} 2h_{xy}c_3' - h_{xxy}c_3' - 2\lambda h_{xy}^2 c_2' \\ \lambda h_{xxx} c_3' \\ \lambda^2 h_{xxx} h_{xy} \end{bmatrix} \tag{3.3}$$

in (x, y, t) space. Projected into the parameter space of M gives the vector $(2h_{xy}c_3' - h_{xxy}c_3' - 2\lambda h_{xy}^2 c_2', \lambda h_{xxx} c_3')$. Then $\widetilde{L}$ is tangent to the x-axis iff $c_3' h_{xxx} = 0$. Note the similarity with Lemma 3.12. □

3.2.3 The Image Sphere

We now wish to map the locus of cusps on the spatio-temporal surface to the image sphere, and we shall call this curve C. There are some subtleties to be observed, in particular a point on the locus of cusps at time t is mapped to an image sphere at a position varying with time t. So essentially it is a one parameter family of maps from the surface to the sphere. Then we identify the spheres to create a curve on the so called, standard image sphere.

The map chosen is,

$$G : \widetilde{M} \to S^2$$
$$G(x, y, t) = \frac{(x, y, h(x,y)) - (c_1(t), c_2(t), c_3(t))}{\|(x, y, h) - (c_1(t), c_2(t), c_3(t))\|}$$

We recall (Subsection 2.2.3) the original formula for the visual mapping of the surface onto the sphere positioned at $\mathbf{c}(t)$; $\mathbf{r} = \mathbf{c} + \lambda \mathbf{p}$. Here $\mathbf{r}$ is a point on the surface and $\mathbf{p}$ is a unit vector that indicates a point on the sphere. Thus we see that the map G simply maps points on the t^{th} critical set to the vector $\mathbf{p}$, on the standard image sphere located at the origin.

For the purposes of calculation we take local coordinates on the standard image sphere located at the origin by projecting points out from the centre onto the $x = -1$ plane, Figure 3.6. We choose the $x = -1$ plane since we are interested in the local picture around the origin, and this will appear at the point $(0, 0, -1)$ on the image sphere at time 0. Thus a point (u, v, w) on the

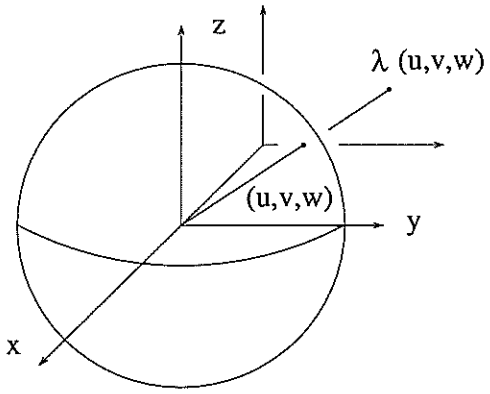

Figure 3.6: Local coordinates on the standard image sphere.

sphere goes to $(\frac{-v}{u}, \frac{-w}{u})$ on the plane. We now observe that given a curve on the standard image sphere we can examine the derivatives of this curve simply by taking measurements in the local coordinates.

If $(p_1(t), p_2(t), p_3(t))$ is a curve on the image sphere with $(p_1(0), p_2(0), p_3(0)) = (-1, 0, 0)$ then the curve in local coordinates, which we denote by $a(t)$ is,

$$a(t) = \left(-\frac{p_2(t)}{p_1(t)}, -\frac{p_3(t)}{p_1(t)} \right).$$

We can take the derivative of $a(t)$ and evaluate at zero to get,

$$\begin{aligned} a'(0) &= \left(\frac{-p_1 p_2' + p_2 p_1'}{p_1^2}, \frac{-p_1 p_3' + p_3 p_1'}{p_1^2} \right)_{t=0} \\ &= (p_2'(0), p_3'(0)) \end{aligned}$$

Also observe that since $p_1^2 + p_2^2 + p_3^2 = 1$ then $p_1'(0) = 0$. Calculation reveals that the second derivative of $a(t)$ is given by,

$$a''(0) = (p_2''(0), p_3''(0)). \tag{3.4}$$

Thus our local coordinate map is a 'good' one, in the sense that we can deduce the acceleration and velocity of the original curve from measurements in the local approximation.

The map G in local coordinates is therefore,

$$G(x, y, t) = \left(\frac{c_2(t) - y}{x - c_1(t)}, \frac{c_3(t) - h}{x - c_1(t)} \right) \tag{3.5}$$

3.9 Proposition: *The locus of cusps on the image sphere, $G(\widetilde{L})$ is singular iff either of the following conditions hold.*

- *The point is not on a frontier and on a swallowtail point. ($c_3' \neq 0$ and $h_{xxx} = 0$).*
- *The point is on the frontier, and either the point is a swallowtail or parabolic or a collision point. i.e. one of h_{xxx}, h_{xy}, c_2' is equal to zero.*

Proof: We calculate the Jacobian matrix of the map G, evaluated at the origin.

$$\begin{bmatrix} 0 & \frac{1}{\lambda} & \frac{-c_2'}{\lambda} \\ 0 & 0 & \frac{-c_3'}{\lambda} \end{bmatrix}$$

The locus of cusps will be singular on the image sphere if the tangent to the curve is in the kernel of $DG(0)$. This is the situation when a vector is both in the kernel of $DF(0)$ (see Definition 3.2) and $DG(0)$. We can determine the conditions for this by examining the 4×3 matrix below and we will have the above situation if the rank drops below three.

$$\begin{bmatrix} 0 & \lambda h_{xy} & -c_3' \\ \lambda^2 h_{xxx} & \lambda^2 h_{xxy} - 2\lambda h_{xy} & 2h_{xy}\lambda c_2' \\ 0 & 1 & -c_2' \\ 0 & 0 & -c_3' \end{bmatrix}$$

Thus the rank drops below three precisely when the stated conditions hold. □

We now turn our attention to when the local coordinates in each of the image-spheres is rotated with respect to some fixed coordinate system with the surface. All the previous work has assumed no rotation and this has enabled us to identify image-spheres at different times. Recall Section 2.3 for an explanation of $\mathbf{p}$ and $\mathbf{q}$ coordinates and $\mathbf{p} = \mathbf{R}(t)\mathbf{q}$.

We take a very similar map as before, except we now map $\widetilde{L}$ to the $\mathbf{q}$ coordinates.

$$Q : \widetilde{M} \to S^2$$
$$Q(x, y, t) = \mathbf{R}^{-1} \left(\frac{(x,y,h(x,y)) - (c_1,c_2,c_3)}{\|(x,y,h) - (c_1,c_2,c_3)\|} \right)$$

where $\mathbf{R}^{-1}(t)$ is the inverse rotation for $\mathbf{p} = \mathbf{R}\mathbf{q}$. We wish to map $\widetilde{L}$ and examine the singular occurrences of the image under Q.

We represent our surface in Monge form as before with the view direction along the x-axis and asymptotic. The camera trajectory is given by, $\mathbf{c}(t) = (\lambda + c_{11}t + \cdots, c_{21}t + \cdots, c_{31}t + \cdots)$ The instantaneous rotation vector $\boldsymbol{\Omega}$, is written in coordinates as $(\Omega_1, \Omega_2, \Omega_3)$.

3.10 Proposition: *If $\widetilde{L}$ is smooth then $Q(\widetilde{L})$ is singular if and only if either of the following conditions hold.*

- *The locus of camera centres intersects with the flecnodal scroll.*
- $\lambda = \frac{-c_{31}}{\Omega_2}$ *and* $c_{31} + \frac{c_{21}c_{31}}{\Omega_2}h_{xy} + \frac{c_{31}^2}{\Omega_2^2}\Omega_3 h_{xy} = 0$

Proof: Calculation reveals the Jacobian matrix of this mapping to be the 3×3 matrix,

$$\frac{1}{\lambda}\left[\mathbf{R}^{-1}\pi_p(\mathbf{r}_x),\ \mathbf{R}^{-1}\pi_p(\mathbf{r}_y),\ \lambda\mathbf{R}_t^{-1}\mathbf{p} + \mathbf{R}^{-1}\pi_p(\mathbf{c}_t)\right]$$

where the elements are column vectors and π_p is the projection mapping onto the plane perpendicular to the $\mathbf{p}$ vector. If we have our surface in Monge form with the standard camera motion then $\mathbf{p}$ is $(-1, 0, 0)$ and at $t = 0$ we have,

$$\begin{aligned}\pi_p(\mathbf{r}_x) &= (0, 0, h_x)\\ \pi_p(\mathbf{r}_y) &= (0, 1, h_y)\\ \pi_p(\mathbf{c}_t) &= (0, -c_{21}, -c_{31}).\end{aligned}$$

If we then evaluate the matrix at the origin we get,

$$\frac{1}{\lambda}\begin{bmatrix} 0 & 0 & 0 \\ 0 & 1 & \lambda\Omega_3 - c_{21} \\ 0 & 0 & \lambda\Omega_2 - c_{31} \end{bmatrix}.$$

We can now operate on the tangent to $\widetilde{L}$ (equation 3.3) to get the vector,

$$\begin{bmatrix} 0 \\ h_{xxx}c_{31} - c_{21}\lambda h_{xxx}h_{xy} + \lambda^2\Omega_3 h_{xxx}h_{xy} \\ -c_{31}\lambda h_{xxx}h_{xy} - \lambda^2\Omega_2 h_{xxx}h_{xy} \end{bmatrix} \text{ i.e. } \begin{bmatrix} 0 \\ h_{xxx}(c_{31} - c_{21}\lambda h_{xy} + \lambda^2\Omega_3 h_{xy}) \\ h_{xxx}h_{xy}\lambda(-c_{31} - \lambda\Omega_2) \end{bmatrix}$$

This gives us the tangent to the locus of cusps in the standard image sphere (in q coordinates). Clearly the locus of cusps will be singular iff the above vector is identically zero. Hence result. □

3.2.4 Conclusion

Items to note are,

- Swallowtail points always give a singular locus of cusps irrespective of the frontier and camera rotation.
- Parabolic points are innocuous unless on the frontier (at which point even the spatio-temporal surface itself is singular !).
- Collision points give a singular locus of cusps, but just frontier points do not. This condition is replaced in the $\mathbf{q}$ coordinate situation with a much stranger condition linking the surface geometry with the camera motion and rotation.
- The conditions for $\tilde{L}$ to be singular ($\mathbf{c}(t)$ tangent to either cylinder-axis developable or flecnodal scroll) are non-generic. We mean non-generic in the context of a generic surface and a single camera trajectory. Thus we may eliminate a singularity on $\tilde{L}$ by an arbitrarily small change in the camera trajectory.

The results are summarised in the table below (Figure 3.7), and the reader should recall that the x-axis is taken to be the view direction in the standard setup.

3.3 Versal Unfoldings.

3.3.1 Basic Definitions

The previous section gave results for determining when the locus of cusps is singular. This section will build on the results already obtained and give results that use some singularity theory, which can be found for example in [M]. For the following we now assume that $\tilde{L}$ is non-singular (which is generic for a generic surface and a single camera trajectory) and the points are not collision points. We also assume in this section that we are away from the frontier.

Name	Parametrised by x on $\widetilde{M}$?	by y on $\widetilde{M}$?	by t on $\widetilde{M}$?	Singular on $\widetilde{M}$?	on M?	on S^2?
$\mathbf{c}$(t) tangent to C.A.Developable	×	×	×	√	√	√
$\mathbf{c}$(t) transverse to C.A Developable and Flec. Scroll	√	×	×	×	×	√
$\mathbf{c}$(t) transverse to C.A. Developable and $h_{xxy} = 0$	×	√	×	×	×	×
$\mathbf{c}$(t) transverse to C.A Developable	√	√	×	×	×	×
$\mathbf{c}$(t) tangent to Flec. Scroll.	×	×	×	√	√	√
$\mathbf{c}$(t) transverse to Flec. Scroll	√	×	×	×	×	√
Collision pt.	×	×	√	×	√	√
Frontier pt.	√	√	√	×	×	×

Figure 3.7: Table showing cases for locus of cusps to be singular.

3.11 Definition: *(i) Let $f \in \mathcal{M}(n)$ be a germ of a function of n variables $x_1, \ldots, x_n$. A p-parameter* **unfolding** *of f is, by definition, a germ*

$$F : \mathbf{R}^n \times \mathbf{R}^p, 0 \to \mathbf{R}, 0$$

with $F(x, 0) = f(x)$.

(ii) Two p-parameter unfoldings F and G, of the same germ f are **isomorphic** *if there exists a local diffeomorphism $\phi : \mathbf{R}^n \times \mathbf{R}^p, 0 \to \mathbf{R}^n \times \mathbf{R}^p, 0$ such that*

1. *$\phi(x, u) = (\psi(x, u), u), \psi(x, 0) = x$,*
2. *$G = F \circ \phi$ that is $G(x, u) = F(\psi(x, u), u)$.*

(iii) An unfolding will be called **trivial** *if it is isomorphic to the constant unfolding $F(x, u) = f(x)$ (so $G(x, u) = (f(\psi(x, u))$ for some ψ).*

(iv) If F is a p -parameter unfolding of f let $h : \mathbf{R}^q \to \mathbf{R}^p$ be a smooth map with $h(0) = 0$. One can define a q-parameter unfolding of f by $(h^*F)(x, v) = F(x, h(v))$. The unfolding h^*F is said to be the **pull back** *of F by h.*

(v) Two p-parameter unfoldings F, G of f are called **equivalent** *if there exists a local diffeomorphism $h : \mathbf{R}^p, 0 \to \mathbf{R}^p, 0$ such that G is isomorphic to h^*F.*

(vi) A deformation F of f is said to be **versal** *if any other deformation G of f is isomorphic to the pull back of F by some suitable map h.*

Parts (v) and (vi) have the following interpretations: if F and G are equivalent there are smooth maps $\phi : \mathbf{R}^n \times \mathbf{R}^p, 0 \to \mathbf{R}^n \times \mathbf{R}^p, 0$, $h = \mathbf{R}^p, 0 \to \mathbf{R}^p, 0$ satisfying $\phi(x, u) = (\psi(x, u), u), \psi(x, 0) = x$, dh_0 invertible and $G(x, u) = F(\psi(x, u), h(u))$. If F is versal then for any G we can find ψ, h satisfying this equation but h now is simply a smooth map $h : \mathbf{R}^q, 0 \to \mathbf{R}^p, 0$ where F (resp. G) is a p (resp. q) parameter family.

3.3.2 Application of Versal Unfoldings

We provide some more results concerning the situation when the camera pierces the flecnodal scroll and cylinder axis developable.

The main result uses techniques from singularity theory that tells us that our family of visual maps versally unfolds the swallowtail and the lips/beaks.

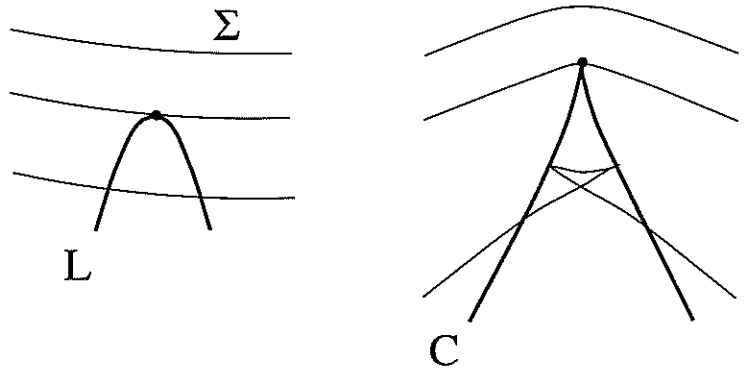

Figure 3.8: Schematic drawings of the case when the camera centre **c** passes through the flecnodal scroll: (left) Critical sets Σ and cusp generator curve L on M. Note that these curves are tangent at the swallowtail point and that two cusps on the profile come into coincidence here; (right) profiles and cusp locus C in the image sphere.

Figure 3.8(right) shows a typical view of the profiles on the image sphere that occur when the camera pierces the flecnodal scroll. It is the purpose of this sub-section to explain this picture.

The following Lemma gives us some information as to how two cusps come together in the profile and form a swallowtail transition.

3.12 Lemma: *Provided $\widetilde{L}$ is smooth (see Proposition 3.5) at a point $p \in M$ and the critical set is smooth at p, then $\widetilde{L}$ is tangent to the lifted critical set if and only if p is a swallowtail point (i.e. p is a flecnodal point and the flecnodal direction is the view direction).*

Proof: We find the tangent to $\widetilde{L}$ by examining the kernel of dF (3.1), the matrix,

$$\begin{bmatrix} 0 & \lambda h_{xy} & -c_3' \\ \lambda^2 h_{xxx} & \lambda^2 h_{xxy} - 2\lambda h_{xy} & 2\lambda h_{xy} c_2' \end{bmatrix}$$

This gives the vector,

$$\begin{bmatrix} 2h_{xy}c_3' - h_{xxy}c_3' - 2\lambda h_{xy}^2 c_2' \\ \lambda h_{xxx} c_3' \\ \lambda^2 h_{xxx} h_{xy} \end{bmatrix}$$

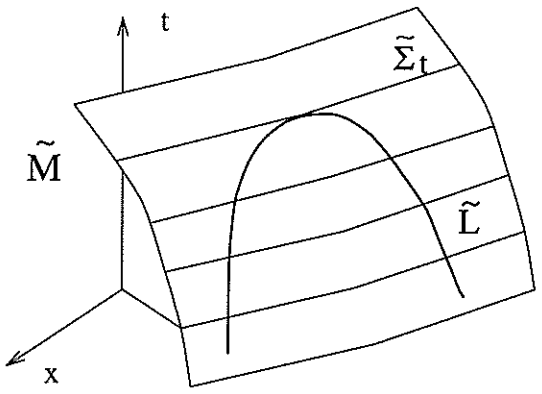

Figure 3.9: Lifted cusp generator curve (bold) through a swallowtail point with the lifted critical sets shown.

which is not the zero vector by our assumption that $\widetilde{L}$ is smooth. A vector is tangent to the critical set provided the component in the t direction (t is the last variable) is zero, since the lifted critical sets are horizontal (with respect to the t-direction) cross-sections of $\widetilde{M}$ i.e. provided $h_{xxx}h_{xy} = 0$. Along an asymptotic direction at a parabolic point the critical set is singular, so $h_{xy} \neq 0$, and $h_{xxx} = 0$ is the swallowtail condition. □

Thus at a swallowtail point the lifted cusp generator curve is tangent to the lifted critical set. See Figure 3.9. Note that critical sets near to the tangency point intersect $\widetilde{L}$ either in two places or not at all. This corresponds to the two cusps coming together on a profile and disappearing. The locus of cusps on the image sphere can be seen to cusp in this case (see Figure 3.8). Compare with Proposition 3.9.

At a parabolic point the critical set itself is not smooth so clearly there is no analogous lemma for this case. In fact Σ_t is a point or a crossing and L passes straight through it. The critical sets are shown in Figure 3.10(left) and the cusp generator curve is bold. This is smooth since $\widetilde{L}$ is and there are no collision points (Lemma 3.7). Again we see that $\widetilde{L}$ intersects nearby critical sets twice, and in the case of a crossing it may not intersect some critical sets at all. Thus we have a similar situation to a swallowtail with two cusps coming together in a lips/beaks transition and disappearing. The projection on the image sphere is shown in Figure 3.11 for the beaks transition. Note the non-singular cusp locus.

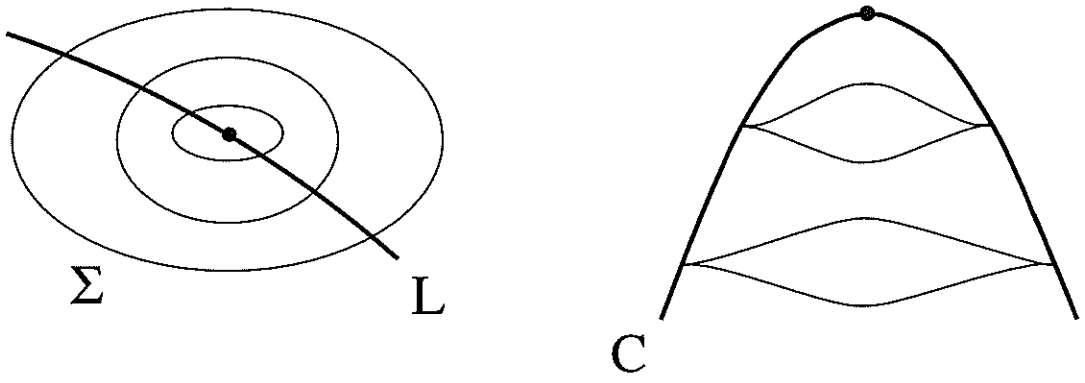

Figure 3.10: Schematic drawings of the case when the camera centre $\mathbf{c}$ passes through the CAD: (left) critical sets Σ and cusp generator curve L on M; (right) profiles and cusp locus C in the image sphere.

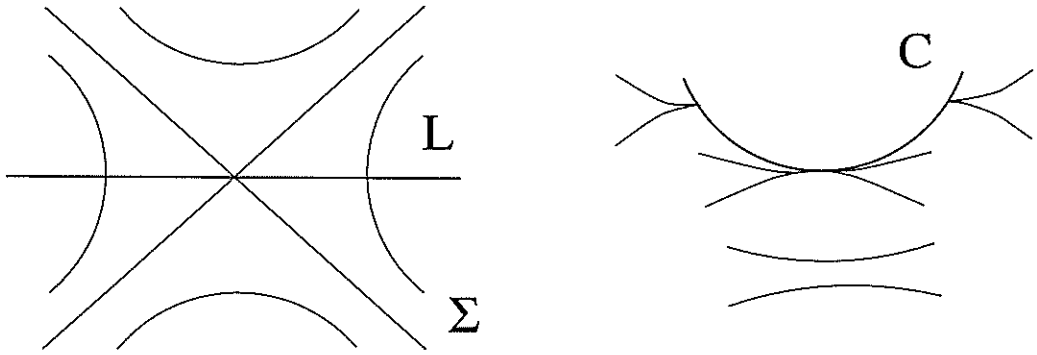

Figure 3.11: Left: cusp generator curve L passing through the critical sets Σ for a beaks transition. Right: locus of cusps C through a parabolic point (beaks transition) with the profiles at different times shown.

Now consider our surface M in Monge form and the unfolding map,

$$\begin{array}{ccc} & F & \\ M \times I & \rightarrow & S^2 \times I \\ x, y, t & \rightarrow & \mathbf{p}(x, y, t), t \end{array}$$

We consider the local picture and take local coordinates of the image sphere, as detailed in Subsection 3.2.3.

3.13 Definition: *The set $\Sigma^1 F$ of the map F consists of those points in $M \times I$ where the rank of the differential map dF is 2.*

Since $\widetilde{M}$ consists precisely of the critical sets we expect the following result to hold.

3.14 Lemma: $\Sigma^1 F = \widetilde{M}$

Proof: With M in Monge form and $\mathbf{c}(0) = (\lambda, 0, 0)$, and taking the image sphere in local coordinates (see Subsection 3.2.3 and equation 3.5) the map F is,

$$F(x, y, t) = \left(\frac{c_2(t) - y}{x - c_1(t)}, \frac{c_3(t) - h(x, y)}{x - c_1(t)}, t \right)$$

The derivative of this map is,

$$\begin{bmatrix} \frac{y - c_2}{(x - c_1)^2} & \frac{-1}{x - c_1} & \frac{c_2'(x - c_1) + c_1'(c_2 - y)}{(x - c_1)^2} \\ \frac{-h_x(x - c_1) - (c_3 - h)}{(x - c_1)^2} & \frac{-h_y}{x - c_1} & \frac{c_3'(x - c_1) + c_1'(c_3 - h)}{(x - c_1)^2} \\ 0 & 0 & 1 \end{bmatrix}$$

with c_i and its derivatives functions of time. This drops in rank iff,

$$\frac{1}{(x - c_1)^3} \Big(h_y(c_2 - y) + h_x(c_1 - x) - c_3 + h \Big) = 0$$

and has rank at least one. The above equation in the brackets defines $\widetilde{M}$ (i.e. $(\mathbf{r} - \mathbf{c}).\mathbf{n} = 0$). Therefore the result holds. □

3.15 Definition: *The set of points on $\widetilde{M}$ where the rank of the restriction of the unfolding map F to $\widetilde{M}$ is equal to one is called $\Sigma^{1,1}$. In other words $F|\widetilde{M} : \widetilde{M} \rightarrow S^2 \times I$ has rank equal to one.*

The following lemma describes the lifted cusp generator curve as the $\Sigma^{1,1}$ set of F.

3.16 Lemma: $\Sigma^{1,1}F = \widetilde{L}$

Proof: The equation defining $\widetilde{M}$ is,

$$h_x(c_1(t) - x) + h_y(c_2(t) - y) + h - c_3(t) = 0$$

The differential of this function is,

$$\Big[h_{xx}(c_1 - x) + h_{xy}(c_2 - y),\ h_{xy}(c_1 - x) + h_{yy}(c_2 - y),\ c_1'h_x + c_2'h_y - c_3'\Big]$$

A vector lies in the $\Sigma^{1,1}$ set of F if it lies in the kernel of the above matrix for $\widetilde{M}$ and the kernel of dF. This is equivalent to saying that the matrix,

$$\begin{bmatrix} h_{xx}(c_1 - x) + h_{xy}(c_2 - y) & h_{xy}(c_1 - x) + h_{yy}(c_2 - y) & c_1'h_x + c_2'h_y - c_3' \\ \frac{y - c_2}{(x - c_1)^2} & \frac{-1}{x - c_1} & \frac{c_2'(t)(x - c_1) + c_1'(t)(c_2 - y)}{(x - c_1)^2} \\ \frac{-h_x(x - c_1) - (c_3 - h)}{(x - c_1)^2} & \frac{-h_y}{x - c_1} & \frac{c_3'(x - c_1) + c_1'(c_3 - h)}{(x - c_1)^2} \\ 0 & 0 & 1 \end{bmatrix}$$

drops in rank from three to two. Note that it cannot drop in rank to one since that would require the first two columns to be identically zero. This can not be the case, since we have a $\frac{-1}{x - c_1(t)}$ term. We now examine 2×2 minors of the upper left 3×2 sub-matrix. These are,

$$\begin{aligned} \frac{1}{(x - c_1)^2} \quad & [h_{xx}(c_1 - x)^2 + 2h_{xy}(c_1 - x)(c_2 - y) + h_{yy}(c_2 - y)^2] \\ \frac{1}{(x - c_1)^3} \quad & [(c_1 - x)h_x + (c_2 - y)h_y + h - c_3] \\ \frac{1}{(x - c_1)^2(c_2 - y)} \quad & [((c_1 - x)h_x - c_3 + h)\,(h_{xy}(c_1 - x)(c_2 - y) + h_{yy}(c_2 - y)^2) \\ & -h_y(c_2 - y)\,(h_{xx}(c_1 - x)^2 + h_{xy}(c_2 - y)(c_1 - x))] \end{aligned}$$

From the definition of $\widetilde{L}$ (3.2) we see that the first two minors equal to zero is equivalent to being on the cusp locus. By observation, the third minor is zero if the first two are, hence result. □

3.17 Corollary: *The set $\Sigma^{1,1}F$ is smooth provided the camera trajectory is not tangent to either the the cylinder axis developable or the flecnodal scroll.*

Proof: This is simply a restatement of Proposition 3.5. □

Using the previous corollary, and the following criterion due to J.W.Bruce and F.Tari we can deduce that our map F is a versal unfolding of the swallowtail singularity.

3.18 Proposition: *Let $F(x,y,t)$ be an unfolding of a swallowtail map. Then F is a versal unfolding if and only if $\Sigma^{1,1}$ is a smooth curve.*

Proof: [RY, p.117] □

We have a versal unfolding of minimum dimension i.e. 1. This is isomorphic to the standard versal unfolding of the standard swallowtail since that has dimension 1 as well. This will ensure that there is a family of local diffeomorphisms of the plane (parametrised by t) taking the profiles (see Figure 3.8(right)) to profiles in the standard picture.

We also have a similar result for showing if our map is a versal unfolding of a lips/beaks map. The following criterion is due to J.W.Bruce and the proof due to F.Tari.

3.19 Proposition: *Let F be an unfolding of a lips/beaks map at the point (x_0,y_0) and the critical set of F be given by the equation,*

$$\Sigma F = \{(x,y,t) : \sigma(x,y,t) = 0\}$$

where 0 is a regular value of σ. The map $F(x,y,t)$ is a versal unfolding of $F(x,y,0)$ if and only if $\frac{\partial \sigma}{\partial t}(x_0,y_0,0) \neq 0$.

Proof: [RY, pp.108] □

For our map F, the critical set is simply $\widetilde{M}$ which is given by the equation $(\mathbf{r}(x,y) - \mathbf{c}(t)).\mathbf{n}(x,y) = 0$ where M is parametrised be x and y. We can thus apply the above condition in the following corollary.

3.20 Corollary: *If the map $F(x,y,0) = (\mathbf{p}(x,y,0),0)$ is a lips/beaks map at the point (x_0,y_0) then F is a versal unfolding if and only if the point (x_0,y_0) is not a frontier point.*

Proof: The critical set of F is given by the equation,

$$(\mathbf{r} - \mathbf{c}).\mathbf{n} = 0.$$

The condition $\frac{\partial \sigma}{\partial t}(x_0,y_0,0) \neq 0$, which is thus equivalent to $\mathbf{c}_t(0).\mathbf{n}(x_0,y_0) \neq 0$. Which is the condition for a non frontier point. □

Chapter 4

Tracking Cusps: Computer Vision Aspects.

> But having found by Experience, the great Difficulty of describing these round things, I have long since made use of another method.
> *Sixty-Fourth Figure* [Poz]

4.1 Introduction

This chapter will consider aspects of tracking cusps that are of relevance to the area of computer vision.

In the second section we prove that by tracking cusps the depth, Gauss and Mean curvatures can be recovered thus enabling the recovery of the cusp generator curve L and the second fundamental form along L. Indeed the formula for the Gauss curvature is considerably simpler than that of [CB]. It involves only first order temporal derivatives whereas [CB] uses up to second order spatio-temporal derivatives. Another simplification is that the formulae for the Gauss and Mean curvatures are independent of the spatio-temporal parametrisation. Recall that the parametrisation is fundamentally arbitrary but the formulae in [CB] are valid only for the epipolar parametrisation, see Subsection 2.2.4.

The third section considers the natural question, 'Does tracking cusps place a restriction on the camera motion?'. The answer is 'No', but this perhaps disappointing result is used to great advantage later in the chapter to generate many examples to perform an error analysis.

The fourth section gives some numerical examples that illustrate some of the techniques and difficulties that would be experienced in a practical demonstration of tracking cusps. This then motivates a more systematic analysis of the errors that one would need to quantify and control in a practical situation. We find that the depth and Gauss curvature formula seem to be stable even under relatively large errors.

Some of these results have appeared in [CFG] and [CFG2].

4.2 Surface Curvature from L

We now show that intrinsic information about the surface, namely the Gauss and Mean curvature, can be obtained by tracking singular profiles. We consider a surface marking (i.e. a smooth curve C) passing through a point on a critical set that generates a cusp. We then measure the instantaneous velocity of C with respect to the cusp in the image sphere. The calculation is initially done in unrotated $(\mathbf{p})$ coordinates.

If C is parametrised by time then let $\mathbf{p}(t)$ be the image of C in the standard image sphere, $\mathbf{n}$ the unit surface normal and define $\mathbf{t}$, the tangent (or limiting tangent) to the profile, as $\mathbf{t} = \mathbf{n} \wedge \mathbf{p}$.

4.1 Lemma: *Let C be a smooth curve on the surface, parametrised by t (hence locally intersecting each critical set in one point). Let the image of C in the standard image sphere be $\mathbf{p}(t)$ and the point $\mathbf{p}(t_0)$ be a singular point of the profile. Then,*

$$\begin{aligned} \mathbf{p}_t.\mathbf{t} &= \frac{\mathbf{c}_t.\mathbf{n}}{\lambda^2\sqrt{-K}} - \frac{\mathbf{c}_t.\mathbf{t}}{\lambda} \\ \mathbf{p}_t.\mathbf{n} &= -\frac{\mathbf{c}_t.\mathbf{n}}{\lambda} \end{aligned}$$

where everything is evaluated at t_0 and K is the Gaussian curvature.

Proof: We take our surface in Monge form with a rotation so that the x-axis is coincident with an asymptotic direction. Take the lifted curve $\tilde{C}$ on the spatio-temporal surface, parametrised by time and passing through the origin. Let $\tilde{C}$ be given by,

$$(\alpha t + \cdots, \beta t + \cdots, t)$$

The surface and its derivatives are written,

$$\begin{aligned} z &= \frac{1}{2}(2b_1xy + b_2y^2) + \frac{1}{6}(d_1x^3 + 3d_2x^2y + 3d_3xy^2 + d_4y^3) + \cdots \\ z_x &= b_1y + \frac{1}{2}(d_1x^2 + \cdots) + \cdots \\ z_y &= b_1x + b_2y + \frac{1}{2}(d_2x^2 + \cdots) + \cdots \end{aligned}$$

We write the camera motion as the vector,

$$\mathbf{c}(t) = (c_1(t), c_2(t), c_3(t)) = (\lambda + c_{11}t + \cdots, c_{21}t + \cdots, c_{31}t + \cdots)$$

The lifted curve $\widetilde{C}$ lies on $\widetilde{M}$ and thus points must satisfy the equation,

$$h_x(\lambda + c_{11}t + \cdots - x) + h_y(c_{21}t + \cdots - y) + h - c_{31}t + \cdots = 0$$

We substitute the curve into this equation and compare coefficients of t, to get $\beta = \frac{c_{31}}{\lambda b_1}$. Now we map from $\widetilde{M}$ to S^2 by the map G (see Subsection 3.2.3). We consider local coordinates of the image-sphere and so the image of the curve C under this map is,

$$G(\alpha t + \cdots, \beta t + \cdots, t) = \left(\frac{(c_{21} - \beta)t + O(t^2)}{-\lambda(\alpha - c_{11})t + O(t^2)}, \frac{c_{31}t + O(t^2)}{-\lambda + (\alpha - c_{11})t + O(t^2)} \right)$$

This is the observed path of the curve C parametrised by time, in local coordinates of the image sphere. We wish to find the instantaneous velocity at the origin, and thus calculate the derivative and evaluate at $t = 0$. This is,

$$\left(\frac{(c_{21} - \beta)\lambda}{\lambda^2}, \frac{-c_{31}\lambda}{\lambda^2} \right) = \left(\frac{c_{31}}{\lambda^2 b_1} - \frac{c_{21}}{\lambda}, \frac{-c_{31}}{\lambda} \right)$$

in the yz plane. We now wish to give this a coordinate-free description. Remember that $\mathbf{n}$ is the vector $(1, 0, 0)$, the view direction is $(-1, 0, 0)$, $\mathbf{t}$ is $(0, 1, 0)$ and $b_1 = \sqrt{-K}$.

Hence result. □

We also have an equivalent result for the rotating $\mathbf{q}$ coordinates (Section 2.3).

4.2 Corollary: *With the hypotheses of the previous lemma we have,*

$$\begin{aligned} \mathbf{q}_t.\mathbf{t} &= \frac{\mathbf{c}_t.\mathbf{n}}{\lambda^2\sqrt{-K}} - \frac{\mathbf{c}_t.\mathbf{t}}{\lambda} + \boldsymbol{\Omega}.\mathbf{n} \\ \mathbf{q}_t.\mathbf{n} &= -\frac{\mathbf{c}_t.\mathbf{n}}{\lambda} - \boldsymbol{\Omega}.\mathbf{t} \end{aligned}$$

Proof: We follow closely the method used in the proof of the previous lemma. The tangent vector to the curve $\widetilde{C}$ on $\widetilde{M}$ is $(\alpha, \beta, 1)$. We can map this by means of the derivative of the projection map in $\mathbf{q}$ coordinates, see Subsection 3.2.3

$$\frac{1}{\lambda}\begin{bmatrix} 0 & 0 & 0 \\ 0 & 1 & \lambda\Omega_3 - c_{21} \\ 0 & 0 & -\lambda\Omega_2 - c_{31} \end{bmatrix}\begin{bmatrix} \alpha \\ \beta \\ 1 \end{bmatrix} = \frac{1}{\lambda}\begin{bmatrix} 0 \\ \beta + \lambda\Omega_3 - c_{21} \\ -\lambda\Omega_2 - c_{31} \end{bmatrix}$$

We also have $\beta = \frac{c_{31}}{\lambda b_1}$. In local $\mathbf{q}$ coordinates of the image sphere we have the tangent to the image curve as,

$$\frac{1}{\lambda}\left(\frac{c_{31}}{\lambda b_1} + \lambda\Omega_3 - c_{21}, -\lambda\Omega_2 - c_{31}\right)$$

We interpret this in coordinate-free language to obtain the result. □

Comments:

- The critical set Σ_0 at $t = 0$ is tangent to the view direction.
- The variable β measures the speed at which critical sets depart from Σ_0.
- This surface marking is *any* curve parametrised by time. It could equally well be L which is parametrised by time. The hypotheses required are detailed in the following corollary. The important fact is that we examine the speed at the cusp point.

It may be useful to take the cusp generator curve as our curve, and track that through a cusp point. The following corollary details when this is possible.

4.3 Corollary: *If the camera centre does not intersect the cylinder-axis developable or the flecnodal scroll and we now take* $\mathbf{p}(t)$ *to be the locus of cusps in the image-sphere then,*

$$\begin{aligned} \mathbf{p}_t.\mathbf{t} &= \frac{\mathbf{c}_t.\mathbf{n}}{\lambda^2\sqrt{-K}} - \frac{\mathbf{c}_t.\mathbf{t}}{\lambda} \\ \mathbf{p}_t.\mathbf{n} &= -\frac{\mathbf{c}_t.\mathbf{n}}{\lambda} \end{aligned}$$

Proof: We can parametrise $\widetilde{L}$ by time provided the camera does not coincide with the cylinder axis developable or the flecnodal scroll. See table 3.7 for a summary of these cases. □

With the following proposition we can calculate the Gauss curvature of a point on the locus of cusps by tracking *any* smooth curve (providing we can parametrise it by time on $\widetilde{M}$) passing through the cusp without knowing any details about the curve itself.

4.4 Proposition: *In the situation of Lemma 4.1 we have the formula for the depth λ, Gauss curvature and Mean curvature at a singular point of the profile,*

$$\begin{aligned}
\lambda &= -\frac{\mathbf{c}_t.\mathbf{n}}{\mathbf{p}_t.\mathbf{n}} \\
K &= -\frac{(\mathbf{p}_t.\mathbf{n})^4}{[\mathbf{p},\mathbf{c}_t,\mathbf{p}_t]^2} \\
H &= \frac{\mathbf{p}_t.\mathbf{n}}{2[\mathbf{p},\mathbf{c}_t,\mathbf{p}_t]^2}\left(\mathbf{c}_{tt}.\mathbf{n}\ \mathbf{p}_t.\mathbf{n} - \mathbf{c}_t.\mathbf{n}\ \mathbf{p}_{tt}.\mathbf{n} - 2\mathbf{p}.\mathbf{c}_t\ (\mathbf{p}_t.\mathbf{n})^2\right).
\end{aligned}$$

Proof: The depth formula is identical to that of [CB].

For the Gauss and mean curvature we set the surface in Monge form. Evaluated at the origin we have

$$\begin{aligned}
\mathbf{p} &= (-1,0,0) \\
\mathbf{c}_t &= (c_{11},c_{21},c_{31}) \\
\mathbf{p}_t &= \left(0,\frac{c_{31}}{\lambda^2\sqrt{-K}} - \frac{c_{21}}{\lambda},\frac{-c_{31}}{\lambda}\right)
\end{aligned}$$

We can evaluate the triple scalar product $[\mathbf{p},\mathbf{c}_t,\mathbf{p}_t]$, in terms of these coordinates to get,

$$[\mathbf{p},\mathbf{c}_t,\mathbf{p}_t] = \frac{c_{31}^2}{\lambda^2\sqrt{-K}}$$

The standard formula for the distance λ allows us to write,

$$(\mathbf{p}_t.\mathbf{n})^2 = \frac{(\mathbf{c}_t.\mathbf{n})^2}{\lambda^2} = \frac{c_{31}^2}{\lambda^2}$$

We can eliminate c_{31} to get the Gauss curvature.

For the mean curvature consider the surface again in Monge form with the x-axis as an asymptotic direction and the view direction at $t=0$.

Therefore,

$$\begin{aligned}
h &= \frac{1}{2}(2b_1xy + b_2y^2) + \frac{1}{6}(d_0x^3 + 3d_1x^2y + 3d_2xy^2 + d_4y^3) + \cdots \\
h_x &= b_1y + \cdots \\
h_y &= b_1x + b_2y + \cdots
\end{aligned}$$

The camera motion $\mathbf{c}(t) = (c_1, c_2, c_3)$ is,

$$\begin{aligned} c_1 &= \lambda + c_{11}t + c_{12}t^2 + \cdots \\ c_2 &= c_{21}t + c_{22}t^2 + \cdots \\ c_3 &= c_{31}t + c_{32}t^2 + \cdots \end{aligned}$$

Our curve C is parametrised by time so for some real numbers α_i and β_i then,

$$\begin{aligned} x &= \alpha_1 t + \alpha_2 t^2 + \cdots \\ y &= \beta_1 t + \beta_2 t^2 + \cdots. \end{aligned}$$

The equation for the spatio-temporal surface is,

$$h_x(x - c_1(t)) + h_y(y - c_2(t)) = h(x, y) - c_3(t).$$

We now insist that our curve $\widetilde{C}$ lies on $\widetilde{M}$ and so must satisfy the above equation. We substitute in the relevant values and equate the coefficients of t to get an expression for β_1,

$$\beta_1 = \frac{c_{31}}{b_1 \lambda}.$$

Our map is,

$$a(t) = \left(\frac{y - c_2(t)}{c_1(t) - x}, \frac{z - c_3(t)}{c_1(t) - x} \right).$$

If we examine the image of our curve then the second component is,

$$\frac{-c_{31}t + (b_1\alpha_1\beta_1 + \frac{1}{2}b_2\beta_1^2 - c_{32})t^2 + \cdots}{\lambda(1 + \frac{c_{11} - \alpha_1}{\lambda}t + \frac{c_{12} - \alpha_2}{\lambda}t^2 + \cdots)}$$

and by the binomial theorem this is equal to,

$$\frac{1}{\lambda}\left(-c_{31}t + \left(b_1\alpha_1\beta_1 + \frac{1}{2}b_2\beta_1^2 - c_{32} + c_{31}\left(\frac{c_{11} - \alpha_1}{\lambda}\right)\right)t^2 + \cdots\right).$$

Observe that the terms containing α_1 vanish since $\beta_1 = \frac{c_{31}}{b_1\lambda}$ and the coefficient of α_1 is $b_1\beta_1 - \frac{c_{31}}{\lambda}$. Thus the second derivative of the second component of $a(t)$ evaluated at $t = 0$ is,

$$a_2''(0) = \frac{2}{\lambda}\left(\frac{1}{2}b_2\beta_1^2 - c_{32} + \frac{c_{31}c_{11}}{\lambda}\right).$$

Since in this case it is true that $b_2 = 2H$, then we can rearrange the above to get,

$$\frac{c_{31}^2}{b_1^2\lambda^2}H = \frac{1}{2}\left(\lambda a_2''(t) + 2c_{32} - 2\frac{c_{31}c_{11}}{\lambda}\right). \tag{4.1}$$

We now wish to interpret this in a coordinate free manner. Thus,

$$\begin{aligned} a_2''(0) &= \mathbf{p}_{tt}.\mathbf{n} \ (see(3.4)) \\ 2c_{32} &= \mathbf{c}_{tt}.\mathbf{n} \\ \lambda &= -\frac{\mathbf{c}_t.\mathbf{n}}{\mathbf{p}_t.\mathbf{n}} \\ -c_{11} &= \mathbf{p}.\mathbf{c}_t \\ b_1 &= \sqrt{-K}. \end{aligned}$$

From the result about K we have,

$$\sqrt{-K} = \frac{(\mathbf{p}_t.\mathbf{n})^2}{[\mathbf{p}, \mathbf{c}_t, \mathbf{p}_t]}.$$

Therefore we can interpret and rearrange equation 4.1 to get the result. □

4.3 General Motion Constraint

Here, we show that in a certain precise sense there is no general constraint on the motion obtainable from following cusps (that is, not making use of parallax). In fact we show that, using the locus of cusps as a parametrised curve $\mathbf{q}(t)$ (using rotated coordinates) in the sphere, and using also the normal lines to the cusps, there cannot be any constraint on the motion. Explicitly, we claim the following, where t is a real number lying in some (small) open interval $t_1 < t < t_2$.

4.5 Proposition: *Suppose that* $\mathbf{q}(t), \mathbf{n}(t)$ *are given smooth families of orthogonal unit vectors, that* $\mathbf{R}(t)$ *is a smooth family of 3-dimensional rotations, and that* $\mathbf{c}(t)$ *is a smooth space curve with* $\mathbf{c}_t.\mathbf{Rn} \neq 0$ *and* $(\mathbf{Rq})_t.\mathbf{Rn} \neq 0$. *Then we can find a smooth surface* M *in 3-space for which* $\mathbf{q}(t)$ *is the locus of cusps of profiles arising from camera centres* $\mathbf{c}(t)$, *with rotated* $\mathbf{q}$ *coordinates (*$\mathbf{p} = \mathbf{Rq}$ *in the usual notation) and* $\mathbf{n}(t)$ *is the normal to the profile at the cusp point.*

Proof Let $\mathbf{p}(t) = \mathbf{R}(t)\mathbf{q}(t)$ and replace also $\mathbf{n}$ by its rotated form $\mathbf{R}(t)\mathbf{n}(t)$ (we shall continue to use $\mathbf{n}$). We then seek a surface M with the following properties:

- for each t, there is a point $\mathbf{r}(t) = \mathbf{c}(t) + \lambda(t)\mathbf{p}(t)$ on M for some $\lambda(t)$,
- the normal to M at $\mathbf{r}(t)$ is $\mathbf{n}(t)$,

- for each t, the vector $\mathbf{p}(t)$ is in an asymptotic direction at $\mathbf{r}(t)$ (this ensures that the profile at 'time' t has a cusp at the profile point $\mathbf{c}(t) + \mathbf{p}(t)$).

There is no choice for the function λ, since we require (using subscripts to denote differentiation as usual) $\mathbf{r}_t = \mathbf{c}_t + \lambda \mathbf{p}_t + \lambda_t \mathbf{p}$, and since $\mathbf{n}(t)$ is required to be normal to the surface so that $\mathbf{r}_t.\mathbf{n} = 0$, we deduce the usual formula $\lambda(t) = -\mathbf{c}_t.\mathbf{n}/\mathbf{p}_t.\mathbf{n}$, noting here that $\mathbf{p}$ is a function of *one* variable t, since it gives the position of the cusp (in unrotated $\mathbf{p}$ coordinates). Note that $\mathbf{q}$ and $\mathbf{n}$ were chosen so that $\mathbf{p}_t.\mathbf{n} \neq 0$ and $\mathbf{c}_t.\mathbf{n} \neq 0$.

We now have a space curve $\mathbf{r}(t)$, and, along that curve, we shall require our surface M to have normal $\mathbf{n}(t)$ (for this is parallel to the profile normal in the unrotated coordinates). This gives us a 'surface strip' in the language of Koenderink [K, p.195].

The final requirement on M is that, at each point $\mathbf{r}(t)$, an asymptotic direction is in the specified direction $\mathbf{p}(t)$. This amounts to saying that, in the direction $\mathbf{p}(t)$, the sectional curvature of M is zero, that is the section of M by the plane through $\mathbf{r}(t)$ containing $\mathbf{p}(t)$ and $\mathbf{n}(t)$ has an (ordinary) inflection at $\mathbf{r}(t)$. There is no difficulty in constructing an M with this property, so long as the asymptotic direction does not actually coincide with the tangent to the curve $\mathbf{r}(t)$. But in that case it is easy to check that the locus of cusps $\mathbf{p}(t)$ in the image sphere would be singular or the surface point is on the frontier.

We can provide an explicit construction of a surface that satisfies the given data. If we let $\mathbf{r}(s,t)$ be a parametrisation of M where

$$\mathbf{r}(s,t) = \mathbf{c}(t) + \lambda(t)\mathbf{p}(t) + s\mathbf{p}(t) + s^3\mathbf{n}(t)$$

then $\mathbf{r}(0,t)$ is still the locus of cusps (see Figure 4.1 for an illustration of this construction). By taking a normal section containing $\mathbf{p}$ through M we have an inflectional curve making $\mathbf{p}$ an asymptotic direction as required. The normal to M along the locus of cusps is,

$$\mathbf{r}_s(0,t) \wedge \mathbf{r}_t(0,t) = \mathbf{p} \wedge (\mathbf{c}_t + \lambda \mathbf{p}_t).$$

Since $\mathbf{r} = \mathbf{c} + \lambda \mathbf{p}$ then $\mathbf{r}_t = \mathbf{c}_t + \lambda_t \mathbf{p} + \lambda \mathbf{p}_t$ and $\mathbf{p} \wedge \mathbf{r}_t = \mathbf{p} \wedge (\mathbf{c}_t + \lambda \mathbf{p}_t)$, resulting in a non singular surface since $\mathbf{r}_t$ is not parallel to $\mathbf{p}$ for the reason given at the end of the last paragraph.

(Another way of thinking of this reconstruction is to say that we are specifying the second fundamental form of M at each point of a curve on M, for specifying

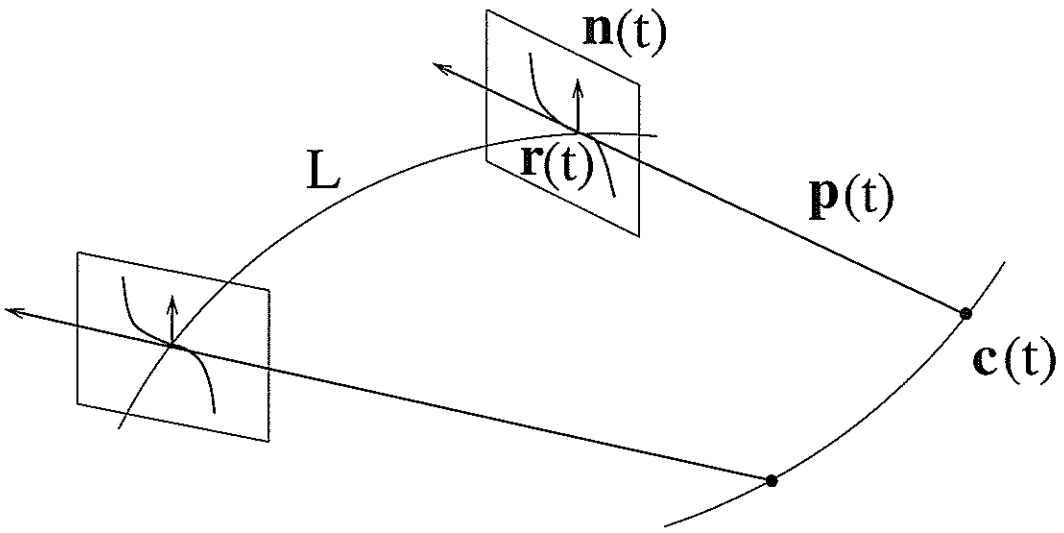

Figure 4.1: Illustration of the explicit surface construction used in proof of theorem.

one asymptotic direction and the derivative of the normal in a *different* direction (along the curve) is precisely enough to fix the second fundamental form. Of course there is no claim here that the surface constructed is unique, away from the curve $\mathbf{r}(t)$.)

4.4 Examples

We now present some examples of tracking cusps.

4.4.1 Example 1

We start with a general calculation and then consider a specific example. When the surface M is given by an equation $z = h(x, y)$, and the camera motion is given by a vector-valued function $\mathbf{c}(t) = (c_1(t), c_2(t), c_3(t))$, then it is straightforward to write down the conditions which must be satisfied by the cusp generator curve $\mathbf{r}(t) = (x(t), y(t), h(x(t), y(t)))$ on M. There are two conditions, both of which are obtained in the same way, as follows. Consider, for a fixed t, the line joining

$\mathbf{r}(t)$ to $\mathbf{c}(t)$. This line consists of points (omitting the variable t)

$$\mathbf{r} + \mu(\mathbf{r} - \mathbf{c}) = (x + \mu(x - c_1), y + \mu(y - c_2), z + \mu(z - c_3)),$$

where μ is an arbitrary real number, taking the value 0 at $\mathbf{r}(t)$. This line meets the surface where

$$z + \mu(z - c_3) = h(x + \mu(x - c_1), y + \mu(y - c_2)). \tag{4.2}$$

This equation for μ naturally has $\mu = 0$ as a solution; we want to impose the condition that $\mu = 0$ is a *triple* solution, since this means that the line has 3 points of contact with the surface, that is in an asymptotic direction. Thus we want the equations obtained by differentiating 4.2 once and twice with respect to μ to hold. With a little manipulation these come to

$$(x - c_1, y - c_2, h(x, y) - c_3)(-h_x, -h_y, 1) = 0, \tag{4.3}$$

$$h_{xx}(x - c_1)^2 + 2h_{xy}(x - c_1)(y - c_2) + h_{yy}(y - c_2)^2 = 0. \tag{4.4}$$

Here, h and its derivatives are evaluated at $(x(t), y(t))$. Of course, (4.3) says merely that $\mathbf{r} - \mathbf{c}$ is perpendicular to the normal to M, which is the critical set condition.

We now apply the above to the surface M with equation

$$z = h(x, y) = -xy + \frac{1}{3}(x^3 + y^3).$$

Let us further consider the straight line motion $\mathbf{c}(t) = (c_1(t), c_2(t), c_3(t)) = (1 + t, 2t, 3t)$. See Figure 4.2. We show how to obtain the Gauss curvature of M at the origin, by using the formula for tracking cusps. Note that the curvature is actually -1 from the equation h of the surface.

First we use (4.3), (4.4) to find out about the cusp generator curve on M close to the origin. Consider a curve in the x, y parameter plane, passing through the origin:

$$x = x_1 t + x_2 t^2 + \ldots, \quad y = y_1 t + y_2 t^2 + \ldots$$

We substitute these into (4.3). Comparing coefficients of t gives $y_1 = -3$ and comparing coefficients of t^2 gives $y_2 = x_1^2 - 8x_1 + 3$. That is, y_1 is fixed but we can choose x_1 and then deduce y_2. If we use (4.4) as well, than the curve on M is determined uniquely; the expansion of (x, y) starts off

$$(5t + 32t^2 + \ldots, -3t - 12t^2 + \ldots).$$

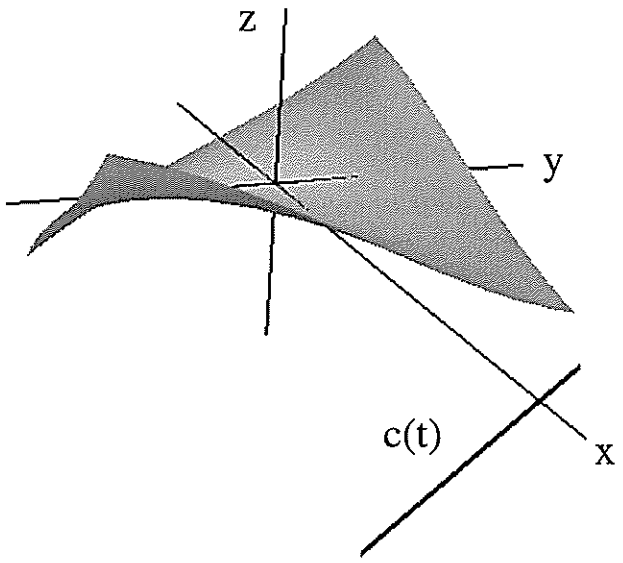

Figure 4.2: Graph of $h(x,y) = -xy + (1/3)(x^3 + y^3)$ and $\mathbf{c}(t) = (1+t, 2t, 3t)$

But to use the formula for K (and the corresponding formula for the mean curvature) *we do not need to know any more than* y_1, *which comes from the condition that* $\mathbf{r}(t)$ *lies on the critical set* $\Sigma(t)$.

In fact, the image $\mathbf{p}(t)$ of the curve $\mathbf{r}(t)$ comes to

$$(-1 + \ldots, -5t + \ldots, 3t + \ldots),$$

where in each case ... stands for terms of degree 2 or higher. This uses only $y_1 = -3$, *not* the extra conditions obtained from (4.3). Therefore, at $t = 0$, where we have the surface normal $\mathbf{n}$ equal to $(0,0,1)$, we have $\mathbf{p}_t.\mathbf{n} = -3$. Also $\mathbf{c}_t = (1,2,3)$ (for any t in our example), and $\mathbf{p}(0) = (-1,0,0)$, so $[\mathbf{p}, \mathbf{c}_t, \mathbf{p}_t] = -9$ and we then obtain $K = -(-3)^4/(-9)^2 = -1$ from Proposition 4.4.

4.4.2 Example 2

This example is in the form of a simulated experiment. We consider a camera flying past a surface taking 'snapshots' at set time intervals. We observe a cusp on the profile and track it. By estimating the velocity of the cusp and using

known 'observables' (time, camera velocity, cusp view direction, surface normal) we can estimate the Gauss curvature at the cusp point.

Recall the formula for K,

$$K = -\frac{\mathbf{p_t}.\mathbf{n}}{[\mathbf{c_t}, \mathbf{p_t}, \mathbf{p}]}$$

We have all the information apart from the derivative of $\mathbf{p}$ with respect to time. In the following we use a simple difference algorithm to estimate the derivative. If we wish to find $\mathbf{p_t}(t_0)$ then we estimate it by evaluating the difference,

$$\mathbf{p_t}(t_0) = \frac{\mathbf{p}(t_0 - 2h) - 8\mathbf{p}(t_0 - h) + 8\mathbf{p}(t_0 + h) - \mathbf{p}(t_0 + 2h)}{12h}$$

where h is the time difference between observed cusp points [PTVF].

The example surface is the graph of the function $f(x, y) = -xy + (1/3)(x^3 + y^3)$ and the camera motion we take is the trajectory, $\mathbf{c}(t) = (1+t, 2t, 3t)$ (Figure 4.2). Thus $\mathbf{c}_t$ is the constant vector (1,2,3). The table of observable data is contained in Figure 4.3. In general the camera path will be a space curve but in tracking cusps we only need knowledge of the camera velocity. We simplify the following calculations by taking the velocity to be constant. The directions $\mathbf{p}(t)$ for each t were found by solving (4.3) and (4.4) for x and y to get the cusp generator $\mathbf{r}(x(t), y(t))$ and then $\mathbf{p} = \frac{\mathbf{r}-\mathbf{c}}{\|\mathbf{r}-\mathbf{c}\|}$. The normals could then be calculated at $\mathbf{r}(x, y)$.

If we examine the cusp point at $t = 0$, then taking $h = 0.02$ and using the data in Figure 4.3 we get,

$$\begin{aligned} \mathbf{p}_t(0) &= \frac{(-.97, -.23, -.11) - 8(-.99, -.11, -.06)}{12 \times .02} \\ &\quad + \frac{8(-.99, .09, .06) - (-.98, .17, .12)}{12 \times .02} \\ &= (.042, 5.000, 3.042) \end{aligned}$$

Thus $\mathbf{p_t}.\mathbf{n} = 3.042$ and $[\mathbf{c_t}, \mathbf{p_t}, \mathbf{p}] = 8.917$. So our estimate for the Gauss curvature is -1.08. We can now take any time as our starting point and calculate the Gauss curvature at that time by taking the appropriate differences at that cusp point. Figure 4.4 shows the results of our calculation for some different times, and gives the exact analytically calculated values using the formula for the Gauss curvature of a parametrised surface in [ON, p.212].

Comment: This example used a known surface and a known camera locus. The cusp generator points were calculated with MAPLE and then the view

Time, t	View direction of cusp, $\mathbf{p} = \frac{\mathbf{r}-\mathbf{c}}{\|\mathbf{r}-\mathbf{c}\|}$	Surface normal at cusp generator, $\mathbf{n}$
-0.10	-.90, .34, .28	.11, -.45, .89
-0.08	-.93, .29, .23	.11, -.37, .92
-0.06	-.95, .24, .18	.11, -.28, .95
-0.04	-.98, .17, .12	.09, -.19, .98
-0.02	-.99, .09, .06	.05, -.10, .99
0.00	-1.00, 0.00, 0.00	0.00, 0.00, 1.00
0.02	-.99, -.11, -.06	-.07, .10, .99
0.04	-.97, -.23, -.11	-.16, .22, .96
0.06	-.92, -.37, -.14	-.26, .36, .89
0.08	-.78, -.62, -05	-.49, -.55, .67

Figure 4.3: Table showing observable data.

Time, t	Measured value of K.	Actual value of K.	Measured value of λ	Actual value of λ
0.00	-1.08	-1.00	0.99	1.00
-.02	-1.00	-1.00	1.10	1.08
-.04	-1.03	-0.99	1.14	1.16
-0.06	-1.09	-0.98	1.25	1.25

Figure 4.4: Table showing results (2 d.p's).

direction $\mathbf{p}$ could be calculated precisely. The only errors are those got from calculating the derivative of $\mathbf{p}$ from a difference formula. No error was added to $\mathbf{p}$.

4.4.3 Example 3

Comment: In constructing a numerical example we take a known surface and known camera motion and then calculate data concerning the motion of the observed cusp points. This is then taken to be *experimental* data and derivatives can be calculated via a difference method and we may wish to introduce noise to test the formulas. The following examples feature a ruled surface and a surface of revolution. The advantage in choosing a surface from a special class is that the calculations often simplify. We construct the examples in a different way to Example 1, by first taking a (relatively simple) curve on the surface and fixing that as the cusp generator curve L. We then calculate the direction of one flavour of asymptotic direction along L. Extending this vector in space gives a ruled surface. A camera motion on this surface (transverse to all rulings) will produce this L. This method is shown schematically in the illustrations below. Note that we can use this argument to argue that the curve L has no inherent geometrical restriction since we may take *any* curve on the hyperbolic region of M, and there are an infinite number of camera motions that produce this curve as a cusp generator curve.

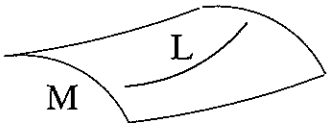

Create cusp generator.

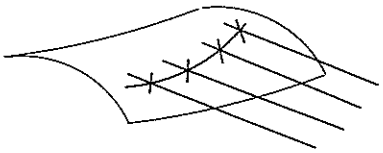
Extend asymptotic direction.

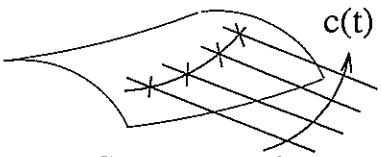

Create camera locus.

We take the ruled surface $\mathbf{r}(x,u) = (x, 0, x^2) + u(0, \cos x, \sin x)$ with Gauss curvature

$$K = \frac{-1}{(1+(u+2x\cos x)^2)^2},$$

Mean curvature

$$H = \frac{\cos x - 2x\sin x}{(1+(u+2x\cos x)^{3/2}},$$

and surface normal,

$$\mathbf{n} = \frac{(-u-2x\cos x, -\sin x, \cos x)}{\sqrt{1+(u+2x\cos x)^2}}.$$

Note that there are no parabolic rulings on the surface.

From [ON, p.230] we note that $a_1\mathbf{r}_x + a_2\mathbf{r}_u$ is an asymptotic direction iff $l(a_1)^2 + 2ma_1a_2 + n(a_2)^2 = 0$, where l, m, n are the usual coefficients of the shape operator. In our case this is made simpler because $n = 0$ for ruled surfaces.

This asymptotic direction will be our view direction $\mathbf{p}(t)$ in these examples. We take L parametrised by time so that $x = x(t)$ and $u = u(t)$. Recall that our surface is parametrised $\mathbf{r}(x, u) = (x, 0, x^2) + u(0, \cos x, \sin x)$ so we can calculate the first and second partial derivatives. We calculate the coefficients of the shape operator l, m and n and omitting a denominator that is common to all the terms we find,

$$\begin{aligned} l &= 2\cos x \\ m &= 1 \\ n &= 0. \end{aligned}$$

We find the asymptotic directions $a_1\mathbf{r}_x + a_2\mathbf{r}_u$ by solving $la_1^2 + 2ma_1a_2 = 0$ giving $a_1 = 0$ as a solution corresponding to the ruling, and $a_1 = -2m$ and $a_2 = l$ as the other direction. So the view direction $\mathbf{p}(t)$ is taken to be this direction.

$$\begin{aligned} \mathbf{p}(t) &= -2m\mathbf{r}_x + l\mathbf{r}_u \\ &= -2\mathbf{r}_x + 2\cos x\mathbf{r}_u \\ &= -2(1, -u\sin x, 2x + u\cos x) + 2\cos x(0, \cos x, \sin x). \end{aligned}$$

Normalising this vector to make it unit, gives

$$\mathbf{p}(t) = \frac{(1, -u\sin x - \cos^2 x, 2x + u\cos x - \cos x\sin x)}{\sqrt{(1 + 4x^2 + u^2 + \cos^2 x + 4ux\cos x - 4x\cos x\sin x)}}.$$

The camera path is given by $\mathbf{c} = \mathbf{r} - \lambda\mathbf{p}$ and we can take λ to be the denominator in $\mathbf{p}$ to ease the calculation. This gives,

$$\mathbf{c}(t) = (x - 1, u(\cos x + \sin x) + \cos^2 x, x^2 + u(\sin x - \cos x) + \cos x\sin x - 2x)$$

where $x = x(t)$ and $u = u(t)$. In this example we set $x = t$ and $u = t + t^2$. All the ingredients are now present for calculating data. We take a suitable discrete time step and calculate the position $\mathbf{p}(t)$ of the cusp, the normal and the camera velocity. We then use the same difference method described before for calculating the derivative $\mathbf{p}_t(t)$. This allows us to reconstruct depth, Gauss and

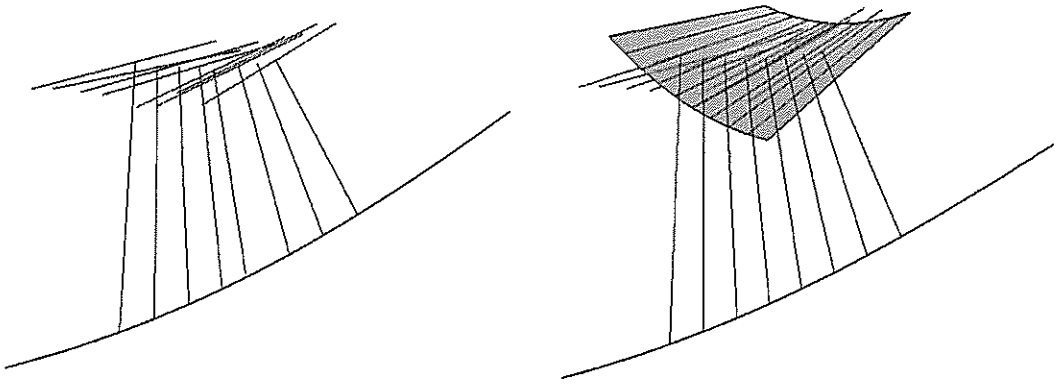

Figure 4.5: Left figure shows reconstructed rulings along the reconstructed cusp generator curve. Right figure superimposes model for comparison.

Mean curvature, and compare it with the actual values given above. Note that in this example the position of the cusp and surface normal are given exactly. In practice these (especially $\mathbf{p}(t)$) would be subject to noise.

The following table shows some results.

Time t	K (actual)	K (approx)	λ (actual)	λ (approx)	H (approx)
$-.075$	$-.91$	$-.92$	1.423	1.419	.92
$-.050$	$-.96$	$-.96$	1.415	1.418	1.04
$-.025$	$-.99$	$-.99$	1.415	1.415	1.03
.000	-1.00	-1.00	1.414	1.412	1.03
.025	$-.99$	$-.98$	1.416	1.422	.72
.050	$-.96$	$-.93$	1.418	1.429	1.22

If ϕ is the angle between asymptotic directions then it is well known [K, p.361] that $\tan\phi = \frac{\sqrt{-K}}{H}$. The view direction is asymptotic and we have calculated K and H, so with the surface normal we can reconstruct the direction of the ruling along the cusp generator. See Figure 4.5. This method of construction for ruled surfaces is expanded on in Chapter 5.

4.4.4 Example 4

In this example we take a surface of revolution and add noise to the position of the cusp points in the image. The normal is taken to be exact, as is the camera position. We use the same technique as in the last example where we fix an arbitrary cusp locus on the surface and then create a camera motion from that.

The surface is

$$\mathbf{r}(s,\theta) = ((s^2+1)\cos\theta, (s^2+1)\sin\theta, s),$$

with normal

$$\mathbf{n} = \frac{(-\cos\theta, -\sin\theta, 2s)}{\sqrt{1+4s^2}},$$

and Gauss curvature,

$$K = \frac{-2}{(1+4s^2)^2(1+s^2)}.$$

Our cusp generator is taken as the curve $x = t$ and $\theta = t + t^2$. Calculating the asymptotic direction as before gives the view directions of the cusps $\mathbf{p}(t)$. We extend and take the essentially arbitrary camera path,

$$\begin{aligned}\mathbf{c}(t) \;=\; & ((t^2+1)(\cos\theta - \sqrt{2}\sin\theta) + 2t\sqrt{t^2+1}\cos\theta, \\ & (t^2+1)(\sin\theta + \sqrt{2}\cos\theta) + 2t\sqrt{t^2+1}\sin\theta, \\ & \sqrt{t^2+1} + t)\end{aligned}$$

illustrated in Figure 4.6. Taking discrete time steps we calculate the position of the cusp point on the image sphere $\mathbf{p}(t)$. In this example we introduce some random noise. The noise is introduced artificially and the predominant component is along the limiting tangent to the cusp. For an opaque surface the cusp has only one visible branch and is often referred to as a *contour ending*. The principal error is in determining where the profile actually terminates. We can argue that the uncertainty is therefore in the direction of the limiting tangent.

The noisy points are then projected on to a plane, thus describing the cusp locus in local coordinates. We wish to fit a curve through these and in the following work a cubic curve was fitted with least squares estimation see Subsection 4.5.1. The best-fit curve is a parametrised curve and we are free to analytically calculate derivatives and do not have to use the difference formula.

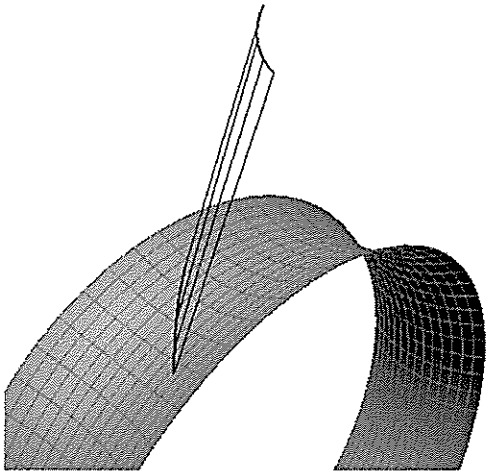

Figure 4.6: Camera motion, view directions and L shown for the surface of revolution example.

The results are tabulated below.

Time t	Depth (actual	Depth (noisy)	K (actual)	K (noisy)
$-.150$	1.79	1.80	-1.64	-1.79
$-.125$	1.77	1.77	-1.74	-1.79
$-.100$	1.76	1.76	-1.83	-1.79
$-.075$	1.75	1.74	-1.90	-1.80
$-.050$	1.74	1.73	-1.96	-1.82
$-.025$	1.73	1.73	-1.99	-1.82
.000	1.73	1.73	-2.00	-1.80
.025	1.73	1.74	-1.99	-1.76
.050	1.74	1.76	-1.96	-1.64
.075	1.75	1.80	-1.90	-1.40

4.5 Multiple Simulations.

We recall Proposition 4.5,

4.6 Proposition: *Suppose that* $\mathbf{q}(t), \mathbf{n}(t)$ *are given smooth families of orthogonal unit vectors, that* $\mathbf{R}(t)$ *is a smooth family of 3-dimensional rotations, and that* $\mathbf{c}(t)$ *is a smooth space curve with* $\mathbf{c}_t.\mathbf{Rn} \neq 0$ *and* $(\mathbf{Rq})_t.\mathbf{Rn} \neq 0$. *Then we*

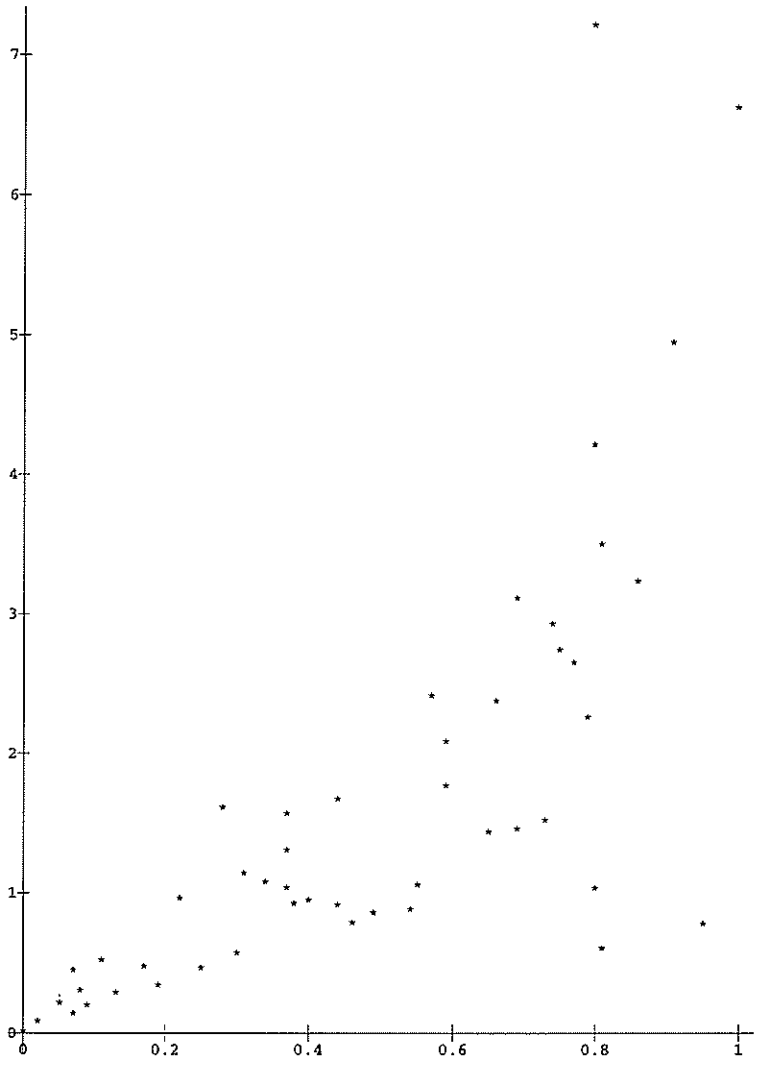

Figure 4.7: The result of many simulations, each with increasing amounts of noise (horizontal axis, noise in degrees), showing the resulting relative percentage error in Gauss curvature (vertical axis).

can find a smooth surface M in 3-space for which $\mathbf{q}(t)$ is the locus of cusps of profiles arising from camera centres $\mathbf{c}(t)$, with rotated $\mathbf{q}$ coordinates ($\mathbf{p} = \mathbf{Rq}$ in the usual notation) and $\mathbf{n}(t)$ is the normal to the profile at the cusp point.

For this set of examples we essentially create data given by unit (perpendicular) vectors $\mathbf{p}$ and $\mathbf{n}$ and a space-curve $\mathbf{c}(t)$. The previous theorem then tells us that there exists a surface whose cusp locus under this motion $\mathbf{c}$ is $\mathbf{p}$. This allows us to free ourselves of the constraint of calculating cusp loci for a specific surface and make examples easy to generate. We can readily investigate the addition of noise to this data.

In practice we take $\mathbf{p}$ as,

$$\mathbf{p}(t) = (\cos\theta\cos\phi, \cos\theta\sin\phi, \sin\theta)$$

with θ and ϕ as simple polynomials of t. The family of normal vectors are taken to be unit and perpendicular to $\mathbf{p}$. Observe that under this setup we can easily obtain a closed form for the derivative $\mathbf{p}_t$ and have no need to use the difference formula previously described.

We add noise to the functions $\theta(t)$ and $\phi(t)$ and to the normals by taking time increments $\{t_{-i}, \ldots t_0, \ldots t_i\}$ and adding a random amount to $\theta(t_k)$ and $\phi(t_k)$ $k = -i \ldots i$, upto a fixed threshold. So adding noise of 0.5° would add a random value to the angle up to 0.5 degrees to θ and ϕ. We then estimate the noisy cusp locus using the procedure that fitted a third degree polynomial to the noisy data via a least squares method described in Subsection 4.5.1. This gave us an equation for the noisy cusp locus that we could differentiate. We note that the formulae for depth and Gauss curvature rely on only the first order derivatives.

An error of x degrees means that up to x degrees of noise was added to the cusp locus on the image sphere as just described. For a camera with a focal length of 20mm and pixel density of 500 pixels per 5mm, we find that an angular separation of 0.03 degrees is about 1 pixel. So 0.3 degrees of error is equivalent to 10 pixels, generally seen as a 'large' error.

Figure 4.7 shows the result of fifty simulated experiments with varying cusp loci, and camera trajectories. The increase in error of the Gauss curvature with angular uncertainty of the cusp point on the image sphere can be seen to be roughly linear and stable for reasonable noise.

4.5.1 A Note On Curve Fitting.

As described above we add noise to the cusp locus on the image sphere and fit a 'best-fit' curve to this. The method used was the following.

Let n discrete (noisy) cusp points be given by (X_i, Y_i, Z_i). We wish to fit a curve $\gamma(t) = (x(t), y(t), z(t))$ to this data, parametrised such that $\gamma(t_i) = (X_i, Y_i, Z_i)$. It is common practice to take the functions $x(t), y(t)$ and $z(t)$ as cubic (sometimes quadratic) polynomials in t. There is no advantage to be gained in taking a higher degree polynomial since the fitted curve can be too 'wiggly'. Cubic curves can be fitted over intervals if necessary, and for greater sophistication one would fit a spline.

We let the curve be given,

$$\begin{aligned} x(t) &= a_0 + a_1 t + a_2 t^2 + a_3 t^3 \\ y(t) &= b_0 + b_1 t + b_2 t^2 + b_3 t^3 \\ z(t) &= c_0 + c_1 t + c_2 t^2 + c_3 t^3 \end{aligned}$$

where the a_i, b_i, c_i are to be calculated for each set of noisy data. The following set of linear equations can then be solved with MAPLE in a least-squares fashion to give the coefficients.

$$\begin{pmatrix} 1 & t_1 & t_1^2 & t_1^3 & 0 & 0 & 0 & 0 & 0 & 0 & 0 & 0 \\ \cdot & & & & & & & & & & & \cdot \\ \cdot & & & & & & & & & & & \cdot \\ \cdot & & & & & & & & & & & \cdot \\ 1 & t_n & t_n^2 & t_n^3 & 0 & 0 & 0 & 0 & 0 & 0 & 0 & 0 \\ 0 & 0 & 0 & 0 & 1 & t_1 & t_1^2 & t_1^3 & 0 & 0 & 0 & 0 \\ \cdot & & & & & & & & & & & \cdot \\ \cdot & & & & & & & & & & & \cdot \\ \cdot & & & & & & & & & & & \cdot \\ 0 & 0 & 0 & 0 & 1 & t_n & t_n^2 & t_n^3 & 0 & 0 & 0 & 0 \\ \cdot & & & & & & & & & & & \cdot \\ \cdot & & & & & & & & & & & \cdot \\ \cdot & & & & & & & & & & & \cdot \\ 0 & 0 & 0 & 0 & 0 & 0 & 0 & 0 & 1 & t_1 & t_1^2 & t_1^3 \\ \cdot & & & & & & & & & & & \cdot \\ \cdot & & & & & & & & & & & \cdot \\ \cdot & & & & & & & & & & & \cdot \\ 0 & 0 & 0 & 0 & 0 & 0 & 0 & 0 & 1 & t_n & t_n^2 & t_n^3 \end{pmatrix} \begin{pmatrix} a_0 \\ a_1 \\ a_2 \\ a_3 \\ b_0 \\ b_1 \\ b_2 \\ b_3 \\ c_0 \\ c_1 \\ c_2 \\ c_3 \end{pmatrix} = \begin{pmatrix} X_1 \\ \cdot \\ \cdot \\ \cdot \\ X_n \\ Y_1 \\ \cdot \\ \cdot \\ \cdot \\ Y_n \\ Z_1 \\ \cdot \\ \cdot \\ \cdot \\ Z_n \end{pmatrix}$$

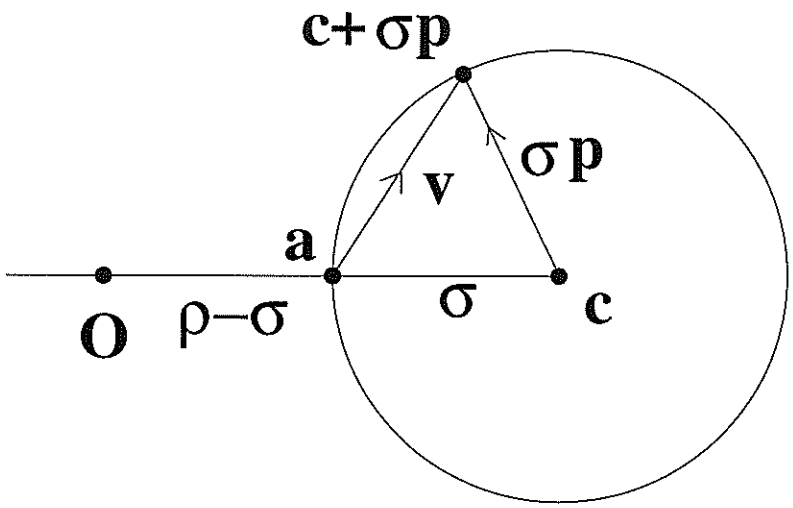

Figure 4.8: Passing from general motion to circular motion (see text).

If A is the large matrix, b the solution vector to the linear equation and x the vector of coefficients then the following MAPLE commands

```
with(linalg);
leastsqrs(A,b);
```

returns the vector x where x best satisfies $Ax = b$ for least squares. i.e. x minimises $\|Ax - b\|$.

4.6 Tracking Cusps with Parallel Projection and Circular Motion.

In this section we show how the formulae of Proposition 4.4 can be used to reprove those of [GS], which were for the special case of parallel projection. The reduction is instructive in that it brings out some of the differences between perspective projection and parallel projection. We also give the formulae for the case of 'circular motion', which is in effect motion of the view direction along a parallel of latitude on the view sphere.

We recap certain results from Section 2.5; when we use parallel projection to an image plane, with view direction $\mathbf{w}$, say, there is no longer any canonical way of using 'the same' coordinates in all the images, as there was using the '$\mathbf{p}$' coordinates for perspective projection. Indeed, in the limit as we pass from

perspective to parallel projection, the directions $\mathbf{p}$, for a fixed camera position, all tend to the *same* limit, which is the view direction $\mathbf{w}$. To effect this transition we altered the image sphere to have a radius σ rather than 1. The centre $\mathbf{c}$ of the sphere recedes to infinity at the same time as the radius σ tends to infinity, in such a way that the spherical surface has limit which is our image plane.

Consider the special motion (as in the situation of [GS]), that is, consider the centre $\mathbf{c}(t)$ to be moving on a circle, centred at the origin O, and of radius ρ, while the image sphere is, as above, centred at $\mathbf{c}(t)$ and of radius σ. Note that ρ here is not to be confused with the ρ used in Section 2.5. Then the ray from the origin to $\mathbf{c}(t)$ meets the sphere in $\mathbf{a}(t) = (1 - \sigma/\rho)\mathbf{c}(t)$. See Figure 4.8. This point will form the origin in our image plane, which is the limit of the sphere as ρ and σ tend to infinity in such a way that σ/ρ tends to a finite limit. (If the limit is 1 then all the image planes will pass through O.) In the limit, the image plane is therefore perpendicular to the vector $\mathbf{c}(t)$.

If $\mathbf{r}$ is a point on the surface then we still regard $\mathbf{p}$ as the *unit* vector in the direction from $\mathbf{c}$ to $\mathbf{r}$. However, the image vector we are actually interested in is say $\mathbf{v}$, where

$$\mathbf{c} + \sigma\mathbf{p} = (1 - \sigma/\rho)\mathbf{c} + \mathbf{v}.$$

Thus $\mathbf{v}$ is the vector from the point $\mathbf{a}$ to the point where the visual ray (from $\mathbf{c}$ in direction $\mathbf{p}$) meets the image sphere. Hence

$$\mathbf{c} = (\rho/\sigma)\mathbf{v} - \rho\mathbf{p},$$

and the following expression holds,

$$[\mathbf{p}, \mathbf{c}_t, \mathbf{p}_t] = [\mathbf{p}, (\rho/\sigma)\mathbf{v}_t - \rho\mathbf{p}_t, \mathbf{p}_t] = [\mathbf{p}, (\rho/\sigma)\mathbf{v}_t, \mathbf{p}_t].$$

Now we let ρ, σ tend to infinity, with $\rho/\sigma \to 1$. For a fixed t, the vectors $\mathbf{p}$ along the visual ray through $\mathbf{c}$ all become parallel, and their limit is the *view direction* $\mathbf{w}$ for that value of t. Likewise $\mathbf{p}_t$ becomes $\mathbf{w}_t$ (and this is a function of t only, not dependent on the particular profile point anymore). Thus the formula for K in Corollary 4.4 becomes:

4.7 Proposition *For parallel projection and circular motion,*

$$K = -\frac{(\mathbf{w}_t.\mathbf{n})^4}{[\mathbf{w}, \mathbf{v}_t, \mathbf{w}_t]^2}.$$

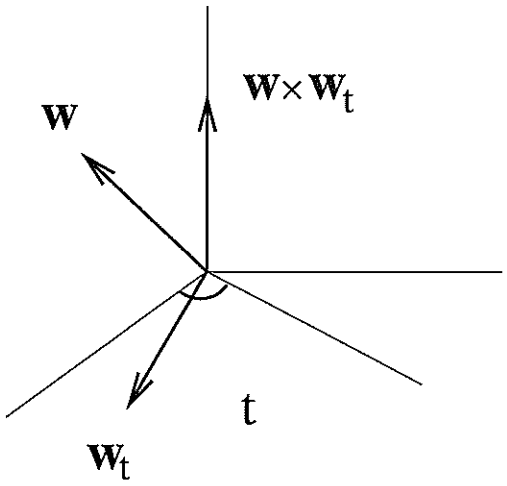

Figure 4.9: The coordinate frame used for circular motion.

To square this with the formula given in [GS] we take coordinates (Figure 4.9):

$$\mathbf{w}(t) = (-\cos t, -\sin t, 0), \mathbf{w}_t = (\sin t, -\cos t, 0), \mathbf{w} \wedge \mathbf{w}_t = (0, 0, 1).$$

Let us write $\boldsymbol{\Omega} = (0, 0, 1)$ (the axis direction) and use coordinate directions $\mathbf{w}_t$, $\boldsymbol{\Omega}$ in the image plane, that is write

$$\mathbf{v} = A\mathbf{w}_t + B\boldsymbol{\Omega},$$

so that (A, B) are the measured coordinates of the cusp in the image plane. Then $\mathbf{v}_t.\boldsymbol{\Omega} = B_t$, is the speed of the cusp in the direction of the axis (this appears as X' in [GS]). Writing θ for the angle between the $\mathbf{w}_t$-direction and the normal $\mathbf{n}$ to the cusp ($\tan\theta$ appears as m in [GS]), we have $\mathbf{w}_t.\mathbf{n} = \cos\theta$ (note that $\mathbf{w}_t$ is a unit vector) and the expression for K above becomes $K = -\cos^4\theta/(B_t)^2$, which is the same as the expression in [GS].

We can rederive the expression for H given in [GS]. The limiting version is,

$$H = \frac{\mathbf{w}_t.\mathbf{n}(\mathbf{v}_{tt}.\mathbf{n}\ \mathbf{w}_t.\mathbf{n} - \mathbf{v}_t.\mathbf{n}\ \mathbf{w}_{tt}.\mathbf{n} - 2\mathbf{w}.\mathbf{v}_t(\mathbf{w}_t.\mathbf{n})^2)}{2[\mathbf{w}_t, \mathbf{w}, \mathbf{v}_t]^2}.$$

The only extra complication is that here we have, using the same A, B notation as above,

$$\mathbf{v}_{tt}.\mathbf{n} = (A_{tt} - A)\mathbf{w}_t.\mathbf{n} + B_{tt}\Omega.\mathbf{n}.$$

Note that in this special case, $\mathbf{w}_{tt} = -\mathbf{w}$ and so $\mathbf{w}_{tt}.\mathbf{n} = 0$. We also have $\mathbf{v}_t = A_t\mathbf{w}_t + A\mathbf{w}_{tt} + B_t\Omega$, giving $\mathbf{v}_t.\mathbf{w} = -A$ and $\mathbf{v}_t.\mathbf{n} = A_t\cos\theta + B_t\sin\theta$.

Substituting in the limiting version for H above we obtain

$$H = \frac{\cos^2\theta(-(A_{tt}+A)\cos\theta + B_{tt}\sin\theta)}{2B_t^2}.$$

In [GS] we find that $W = A$ and we rederive the formula

$$H = \frac{-(W''+W)+mX''}{2X'^2(1+m^2)^{3/2}}.$$

It is not hard to generalise the above to the case of **circular motion**, which we take to mean $\mathbf{c}(t)$ moves on a 'circle of latitude' at latitude β on a sphere, centre O, of radius ρ. See Figure 4.10. We take an image sphere centred at $\mathbf{c}(t)$, radius σ, and the origin of coordinates on this sphere (and so, as $\rho \to \infty$, on the image plane) at the point of intersection $\mathbf{a}(t)$ of the line from O to $\mathbf{c}(t)$ with the image sphere. This point is $\mathbf{a}(t) = (1-\sigma/\rho)\mathbf{c}(t)$, as before. However we have

$$\mathbf{w}(t) = (-\cos\beta\cos t, -\cos\beta\sin t, -\sin\beta)\mathbf{c}(t) = -\rho\mathbf{c}(t).$$

The natural choice of axes in the image plane will be along the horizontal vector $\mathbf{e}_1 = (-\sin t, \cos t, 0)$ and along $\mathbf{e}_2 = (\sin\beta\cos t, \sin\beta\sin t, -\cos\beta)$, so that $\mathbf{e}_1.\mathbf{e}_2$, $\mathbf{w}$ is a right-handed orthonormal triad of vectors. Writing $\mathbf{v}$, as before, for the vector from $\mathbf{a}$ to the image point, so that $(1-\sigma/\rho)\mathbf{c} + \mathbf{v} = \mathbf{c} + \sigma\mathbf{p}$, and writing $\mathbf{v} = A\mathbf{e}_1 + B\mathbf{e}_2$ we find the following formula for K by following cusps under circular motion.

4.8 Proposition: *For parallel projection and circular motion at latitude β, taking the axes as above,*

$$K = -\frac{\cos^2\beta\cos^4\theta}{(A\sin\beta - B_t)^2},$$

where, as before, θ is the angle between the cusp normal and the $\mathbf{e}_1$-direction.

In a similar way one can generalise the formula for H in [GS] to the case of parallel projection and circular motion.

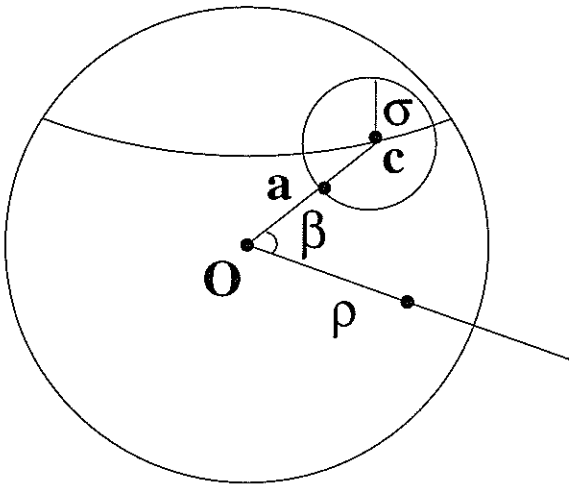

Figure 4.10: Illustration of circular motion, with the camera moving along the β circle of latitude.

Chapter 5

Tracking Cusps on Special Surfaces.

We thought it not improper, to describe
something more particularly. *Preface* [Poz]

5.1 Introduction.

We present methods for the *global* reconstruction of some classes of special surfaces by tracking cusps (contour endings) [1] of the profile (also known as the apparent contour and the occluding contour) under a known dynamic monocular perspective observer.

There has been considerable interest in the computer vision community concerning special families of surfaces ([BGT2], [FMZR], [GDL], [P], [ZM], [ZN] for instance). Much of the literature exploits *rich image features*, such as inflections, bitangents, the symmetry set, to aid reconstruction and viewpoint-invariant representation. While there have been some theoretical results concerning the cusps of profiles on special surfaces [PC],[R92], there has been little exploitation of the geometry with regard to reconstruction. Working within a particular family can present certain challenges, since often certain phenomena can be more degenerate than in the generic case, but also the sharply constrained structure can be exploited to provide powerful results.

[1] We use the terms 'contour ending' and 'cusp' synonymously. A cusp is observed in the image for a transparent surface and for brevity we often refer to 'cusps'.

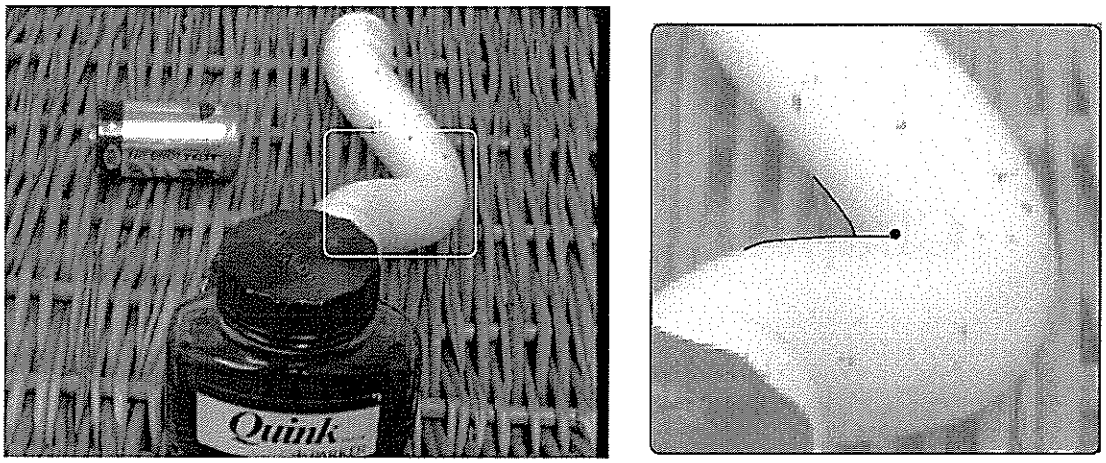

Figure 5.1: Canal surface with a T-junction and a contour ending magnified on the right. Thanks to Dr.A. Zisserman and his student for this picture.

We examine surfaces of revolution (SOR), canal surfaces (piped) and ruled surfaces. Each of these special types of surface is generated in a special way by a moving curve. For example the ruled surface is generated by a sweeping line, the SOR generated by a varying radius circle centred on a straight line and the canal surface is described by sweeping a circle along a space curve, keeping it in the normal plane. (The canal surface can also be considered as an envelope of spheres of constant radius centred along a space curve.) If we can recover the generator curve then we recover part of the original surface, even resulting in areas that are unseen and beyond the *frontier* (Section 2.7). O'Neill [ON] provides a good introduction to the differential geometry of the above classes of surfaces.

For each class of surface we provide simulated experiments that illustrate the technique and demonstrate the stability of the reconstruction under extremely noisy data. This simulates the uncertainty in the detection of the contour ending that is present in any practical situation. A contour ending can be seen in Figure 5.1 where it appears as a dark blob, but the observed location is subject to error.

Some of the material in this chapter has appeared in [FG].

5.2 Experimental Technique.

In the sequel we present synthetic examples that were calculated to demonstrate the stability and accuracy of the reconstruction techniques employed. Chapter 4 gives many examples of tracking cusps and the methods that were used in this chapter are described in Subsection 4.4.3. All calculations and diagrams were performed on MAPLE V.3 the computer algebra package.

The general technique is to draw any curve on the hyperbolic part of a surface M and extend one flavour of asymptotic direction. This forms a ruled surface, and taking our camera motion $\mathbf{c}$ on this surface transverse to the rulings will make our original curve the cusp generator curve with respect to $\mathbf{c}$ and M. We now present a specific calculation that demonstrates this for a canal surface. The calculation is similar for the ruled surface and surface of revolution.

We parametrise our canal surface by t and θ and the usual parametrisation is

$$\sigma(t,\theta) = \gamma(t) + r(N(t)\cos\theta + B(t)\sin\theta),$$

where r is a constant radius, $\gamma(t)$ is a smooth space curve (the 'core curve'), with non-vanishing curvature, and N and B are from the Serret Frenet frame of γ. It is then possible (e.g. [ON, p.69]) to show the following where κ and τ is the curvature and torsion of γ respectively,

$$T = \frac{\gamma'}{\|\gamma'\|}, \qquad B = \frac{\gamma' \wedge \gamma''}{\|\gamma' \wedge \gamma''\|}, \qquad N = B \wedge T,$$

$$\kappa = \frac{\|\gamma' \wedge \gamma''\|}{\|\gamma'\|^3}, \quad \tau = \frac{(\gamma' \wedge \gamma'') \cdot \gamma'''}{\|\gamma' \wedge \gamma''\|^2}.$$

From [ON, p.230] we have the result that says the direction $a_1\sigma_t + a_2\sigma_\theta$ is asymptotic if and only if, $l(a_1)^2 + 2ma_1a_2 + n(a_2)^2 = 0$ where l, m, n are the usual coefficients of the shape operator. We can calculate l, m, n and up to some uniform multiple they are,

$$\begin{aligned} l &= r\tau^2 - (1 - r\kappa\cos\theta)\kappa\cos\theta \\ m &= r\tau \\ n &= r. \end{aligned}$$

This enables us to calculate a_1 and a_2 giving,

$$\begin{aligned} a_1 &= r\tau \pm \sqrt{(1 - r\kappa\cos\theta)r\kappa\cos\theta} \\ a_2 &= r\tau^2 - (1 - r\kappa\cos\theta)\kappa\cos\theta \end{aligned}$$

and we know σ_t and σ_θ, so we have calculated the asymptotic directions. By taking a cusp generator curve $(t, \theta(t)) = (t, \theta_0 + \theta_1 t + \theta_2 t^2 + \cdots)$ for example, we can take all the asymptotic directions along this curve.

We then form the camera motion $\mathbf{c}(t)$ in the following way,

$$\mathbf{c}(t) = \sigma(t, \theta(t)) + \mu(t)[a_1(t, \theta(t))\sigma_t + a_2(t, \theta(t))\sigma_\theta] \cdot$$

where $\mu(t)$ is some non zero function of t that gives the depth from the camera to the cusp generator curve on the surface.

So starting from a core curve $\gamma(t)$, a fixed radius r and a cusp generator curve we can create a camera motion consistent with this. We know the true depth (μ above) and can calculate the true Gauss and Mean curvature on the surface from the formulae in [ON, p.212]. The method is to add noise to the view directions up to a fixed angular threshold on the image sphere and note the effect on the errors in the formulae and subsequent reconstruction. This is done in MAPLE where random noise can be added to the data and the least squares facility can be used to calculate cubic curve approximations to the cusp loci (see Subsection 4.5.1).

5.3 Surfaces of Revolution.

5.3.1 Theory.

We now show that by tracking a cusp pair on a surface of revolution (SOR) global information about the surface can be found. More specifically, we assert that by tracking the cusp pair over parallels of our SOR we can reconstruct those parallels. A parallel (section) of a SOR is a plane section of a SOR perpendicular to the axis of rotation. It is a plane circle.

We shall need the following lemmas.

5.1 Lemma: *If the point* $\mathbf{r}$ *generates an ordinary cusp for a certain camera position then there exists another point* $\mathbf{r}'$ *on the same parallel that also generates a cusp. The surface at* $\mathbf{r}$ *is congruent to that at* $\mathbf{r}'$*, in particular the Gauss curvatures are equal. See Figure 5.2.*

Proof: We can parametrise our SOR by making the axis of revolution the

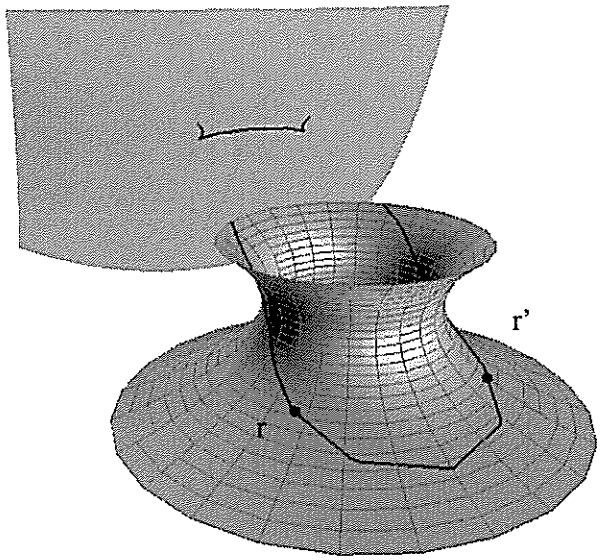

Figure 5.2: Profile (projected on to image sphere) and critical set (on surface) shown for some time. Observe the cusp generator pair $\mathbf{r}$ and $\mathbf{r}'$ on the same parallel.

z-axis (without significant loss in generality) in the following way,

$$(x, y, z) = (r(t)\cos\theta, r(t)\sin\theta, t),$$

with $r(t) > 0$ for all t. Alternatively we can describe the surface by an equation $x^2 + y^2 = (r(z))^2$. Now a view line joining a centre of projection (u, v, w) and a general point on the surface is,

$$(1-\lambda)(r\cos\theta, r\sin\theta, t) + \lambda(u, v, w).$$

We compose this with the equation of the surface to get,

$$((1-\lambda)r\cos\theta + \lambda u)^2 + ((1-\lambda)r\sin\theta + \lambda v)^2 = (r(1-\lambda)t + \lambda w)^2 \qquad (5.1)$$

We are interested in the number of derivatives with respect to λ that vanish at $\lambda = 0$. This tells us the *order of contact* of the line with the surface [BG, p.19]. A direction is asymptotic at a point p if and only if the line in that direction has three points of contact at p, i.e. the first two derivatives of equation 5.1 vanish at $\lambda = 0$. First and second derivatives of equation 5.1 at $\lambda = 0$ give,

$$\begin{aligned} -r + u\cos\theta + v\sin\theta &= r'(w-t) \\ -r^2 - 2rr'(w-t) + u^2 + v^2 &= (r'^2 + rr'')(w-t)^2 \end{aligned}$$

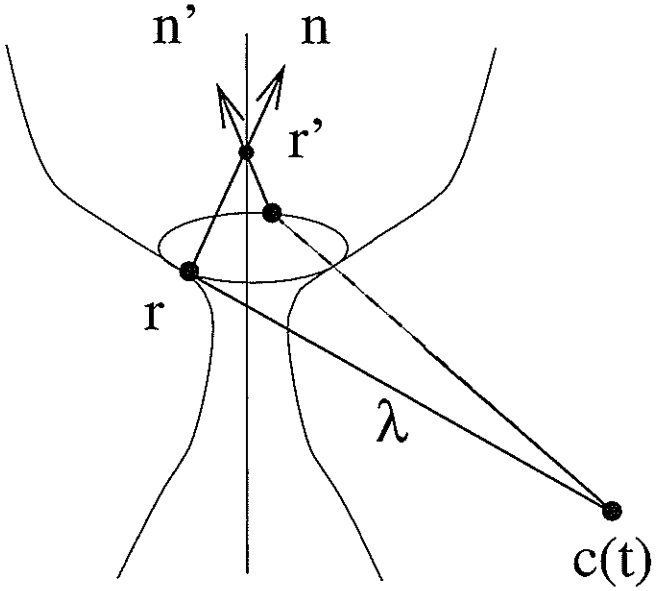

Figure 5.3: Cusp generator pair $\mathbf{r}$ and $\mathbf{r}'$ on a surface of revolution with surface normals $\mathbf{n}$ and $\mathbf{n}'$ intersecting on the axis.

where a prime indicates d/dt, and r, r', r'' are evaluated at t. The last equation is for t alone. Given a solution for t the first equation is then in the form,

$$u\cos\theta + v\sin\theta = k.$$

If $k^2 < u^2 + v^2$ then this has two solutions

$$\theta = \cos^{-1}\left(\frac{u}{\sqrt{u^2+v^2}}\right) \pm \cos^{-1}\left(\frac{k}{\sqrt{u^2+v^2}}\right)$$

corresponding to two points on the same parallel. These solutions coalesce into a single solution, giving a higher codimension singularity on the profile, in the non-generic situation where $k^2 = u^2 + v^2$. If $k^2 > u^2 + v^2$ there are no cusps. □

This lemma tells us that cusps always appear in the image in pairs, and resulting from the same parallel. The following lemma will be used in the reconstruction process.

5.2 Lemma: *The normals to a SOR along a parallel all intersect at a point on the axis, see Figure 5.3.*

□

The basic reconstruction technique is as follows.

1. We observe a cusp pair in the image. Note that cusp pairs from the same parallel on the SOR have equal Gauss curvatures by Lemma 5.1, so we can easily verify from the image which of the cusps we observe do in fact arise from the same parallel by calculating the Gauss curvature for each cusp. Clearly if the Gauss curvatures are unequal then they can not be cusps arising from the same parallel.

2. We reconstruct the depth using Proposition 4.4 to get two points $\mathbf{r}, \mathbf{r}'$ (These are the so-called cusp-generator points).

3. The surface normals are preserved under perspective projection since the normal to the profile is parallel to the normal to the surface, and so extending the normals at $\mathbf{r}$ and $\mathbf{r}'$ points must give us an intersection on the axis by Lemma 5.2.

4. Tracking the cusps over time gives us the reconstructed axis.

5. The parallel through $\mathbf{r}$ is then the circle perpendicular to the axis with centre on the axis and passing through $\mathbf{r}$.

As our camera moves the cusp pair sweeps along the parallels and we are able to reconstruct them.

5.3.2 Experiment.

It is clear that in practice this technique will be susceptible to errors. The image may contain several cusps but it is straightforward to select the correct pair since these cusps arise from points on the surface having the same Gauss curvature (see Proposition 4.4). This provides a consistency check as described in part 1. above.

In practice when we reconstruct the cusp generator points and extend the normals we find they do not quite intersect. We take the nearest point in this instance and fit an axis to the noisy points. The method of curve fitting is described in 4.5.1.

The reconstruction technique was tested for different amounts of error in the observation of the cusp images. An error of x degrees means that up to x degrees

of noise was added to the cusp locus on the image sphere to give a noisy locus. For a camera with a focal length of 20mm and pixel density of 500pixels per 5mm, we find that an angular separation of 0.03 degrees is about 1 pixel. For the following SOR experiments errors of 0.3 degrees (10 pixels) and 0.6 degrees (20 pixels) were used.

We now produce some simulated examples which demonstrate the reconstruction technique. The surface used was the following,

$$\mathbf{r}(s,\theta) = ((1+s^2)\cos\theta, (1+s^2)\sin\theta, s)$$

and the camera motion,

$$\mathbf{c}(t) = (10+2t, 0.3t+0.1t^2, -5+4t).$$

Note that the axis of the SOR is the z-axis (0,0,1). We observed a cusp pair at discrete times and added some noise of various amounts. This was then smoothed with a cubic curve via a least-squares method to give the observed cusp loci. Figure 5.4 and 5.6 shows the noisy cusp loci sampled over time with a cubic curve fitted in local coordinates on the image sphere. (Recall that we track a cusp pair and there is one locus per cusp.) The depth was calculated and then the nearest intersection point to the normals was calculated. This gave points on the SOR axis, and a straight axis was fitted. The parallels could then be generated resulting in a radius function that could be smoothed giving a complete SOR.

We now illustrate some of the results for an error of 0.3 degrees and 0.6 degrees. The reconstructed axis for an error of 0.3 degrees was calculated as

$$[.051 - .001u, -.013 + .003u, -1.198 + .999u],$$

recall that the actual axis is $[0,0,u]$. The axis for 0.6 degrees is

$$[.158 - .012u, -.074 + .013u, -1.142 + .999u].$$

See Figures 5.5 and 5.7.

5.4 Canal Surfaces.

5.4.1 Theory

Let $\gamma(t)$ be a space curve with nowhere vanishing curvature and $N(t)$ be its principal normal and $B(t)$ be the binormal then the standard parametrisation

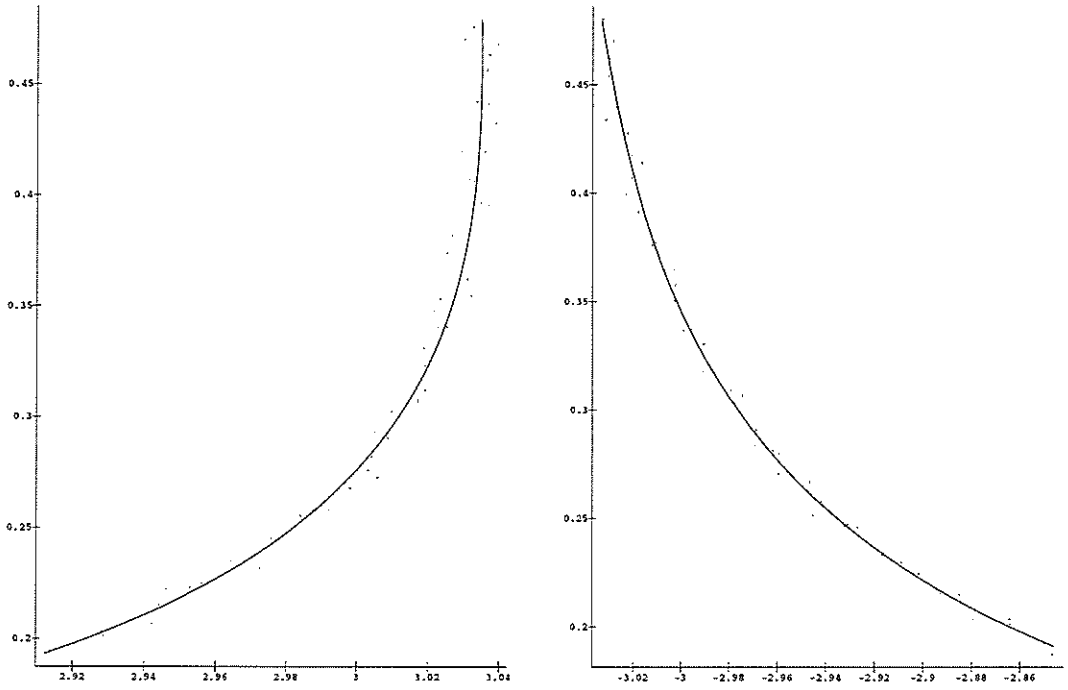

Figure 5.4: Cusp locus 1 and 2 showing the noisy data points of 0.3 degrees, with the axes giving local θ ϕ coordinates on the image sphere.

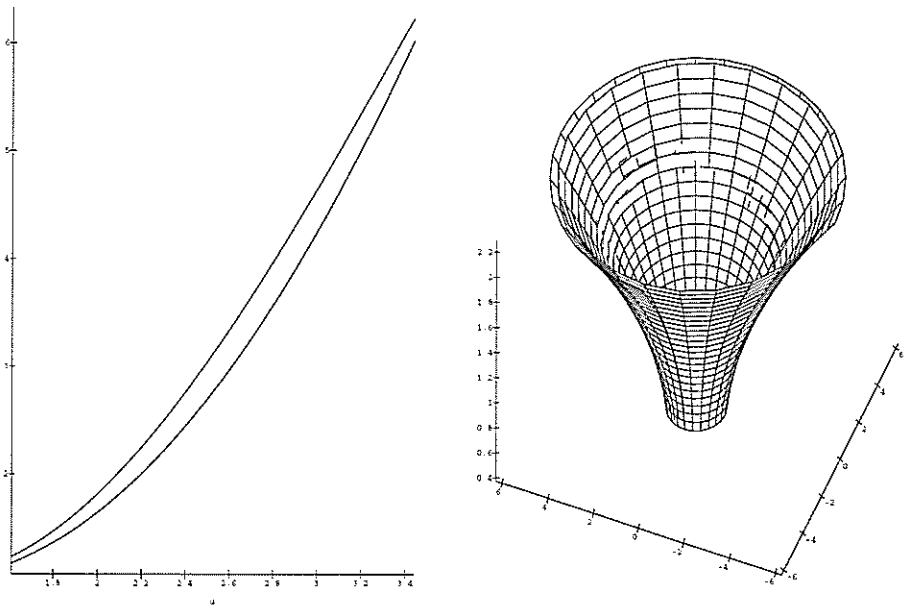

Figure 5.5: Actual SOR generating curve compared with reconstructed curve (left) shown in the yz plane. Actual surface (cut away) compared with reconstructed surface (0.3 degs).

for a canal surface is the following,

$$\mathbf{r}(t,\theta) = \gamma(t) + r(\cos\theta N(t) + \sin\theta B(t)). \tag{5.2}$$

We can also think of the canal surface as an envelope of a family of spheres of constant radius r centred on $\gamma(t)$.

5.3 Definitions. *The space-curve γ is the* **core curve**, *the factor r is the (constant)* **radius** *of the canal surface. The circle $\gamma(t_0) + r(\cos\theta N(t_0) + \sin\theta B(t_0))$ is the* **characteristic circle** *for $t = t_0$.*

We assert that by tracking a single cusp along the canal surface we can reconstruct the characteristic circles (and hence the complete surface) as the cusp sweeps along the surface. We note that this reconstruction technique works with incomplete viewer information, such as when only one 'side' of the canal surface is visible.

We shall need the following lemma.

5.4 Lemma:

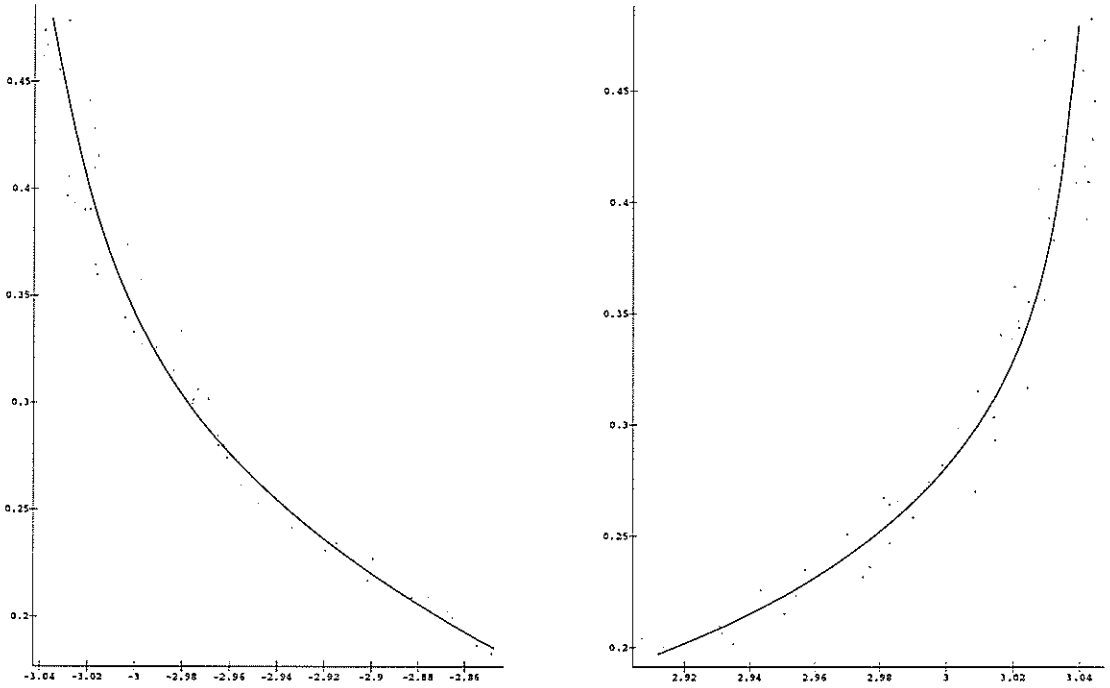

Figure 5.6: Cusp locus 1 and 2 showing the noisy data points of 0.6 degrees, with the axes giving local θ ϕ coordinates on the image sphere.

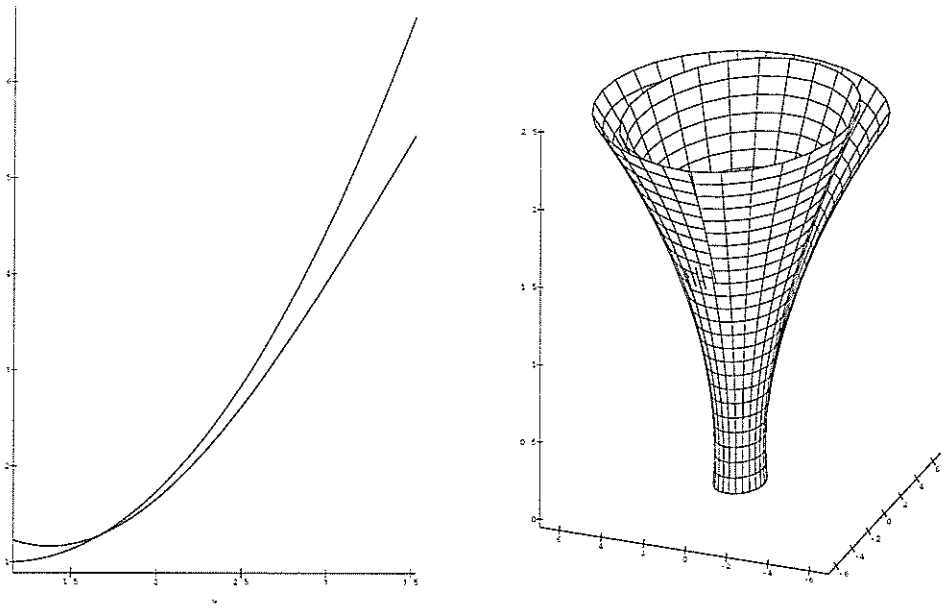

Figure 5.7: Actual SOR generating curve compared with reconstructed curve (left) shown in the yz plane. Actual surface (cut away) compared with reconstructed surface (0.6 degs).

1. *The radius of a canal surface can be expressed in terms of the Gauss curvature K, and the Mean curvature H,*

$$r = \frac{H - \sqrt{H^2 - K}}{K}.$$

2. *The normal to a canal surface at a point p passes through the centre of the characteristic circle of p.*

Proof:

We use the parametrisation given in the main text (equation 5.2). It is straightforward to show that the normal to the canal surface is along the radius, i.e. $\cos\theta N + \sin\theta B$. We use the formulae for the Gauss and Mean curvature from [ON, p.212],

$$K = -\frac{\kappa\cos\theta}{r(1 - r\kappa\cos\theta)}$$

and

$$H = \frac{1 - 2r\kappa\cos\theta}{2r(1 - r\kappa\cos\theta)}$$

where κ is the curvature of the space curve $\gamma(t)$. These two equations allow us to eliminate $\kappa \cos\theta$ and we find that $Kr^2 - 2Hr + 1 = 0$. Since $K < 0$ at the points we are interested in, the positive root for r is taken as stated in Lemma 5.4. □

Recall that we can calculate K and H from tracking cusps using Proposition 4.4 and so can recover the radius. The reconstruction technique is as follows,

1. Track cusp to recover depth, Gauss and Mean curvature.
2. Calculate the radius r via Lemma 5.4.
3. Using the recovered depth we can recover the cusp generator point and then move along the normal a distance r to recover the core curve by 5.4.
4. The core curve and radius completely determine the canal surface.

5.4.2 Experiment.

We simulate the reconstruction process with a simple example. Again noise was added to the image of the cusp points to simulate the uncertainty in detecting the cusp points. Figure 5.8 shows the cusp points on the image sphere in theta/phi coordinates. The core-curve used was, $\gamma(t) = (2t, 0.6t^2, 0)$ and the radius 1. Note that the core curve of this canal surface is planar; this is just to simplify the calculations and does not imply a restriction inherent in the technique used. An error of 0.5 degrees was added in this example and the recovered radius was 0.973. It is difficult to quantify the error in the core curve, but Figure 5.9 shows the actual and recovered core curves. The recovered and actual surfaces are shown in Figure 5.9.

It is unclear how best to empirically measure the 'success' of the reconstruction, other than simply a visual inspection. Figure 5.10 shows a series of experiments performed on different canal surfaces all with radius one, and varying camera motions. The horizontal axis indicates increasing noise added, and the vertical axis shows the recovered radius. A deviation from a radius equal to one, shows the effect of the noise. We don't expect this relationship to be simple since the radius depends on second derivatives of the cusp locus (Lemma 5.4). We merely wish to assess the stability under large noise.

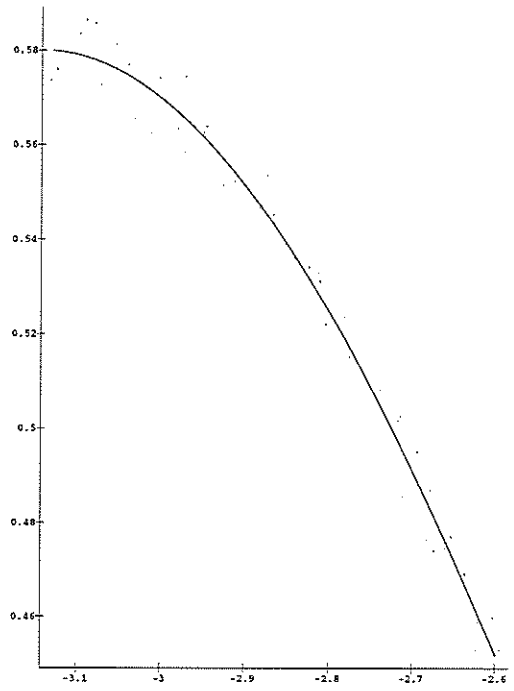

Figure 5.8: Image of noisy cusp points with a cubic curve fitted.

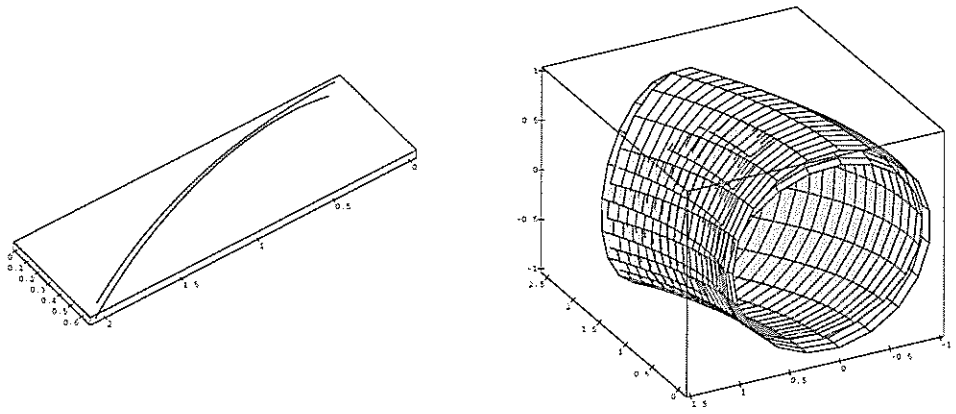

Figure 5.9: Actual and recovered core curves (left), and actual and recovered surfaces (right). Note that the scale and orientation are different in each picture.

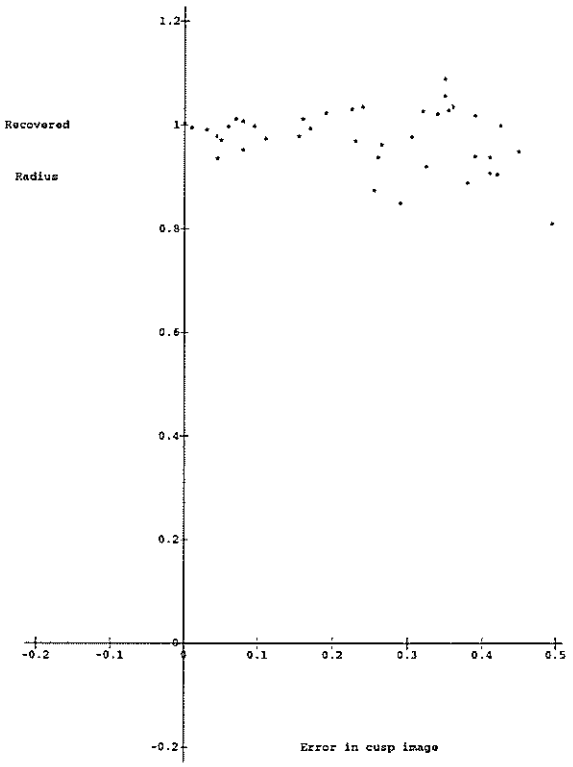

Figure 5.10: Increase in maximum angular error of cusp points (horizontal) with recovered radius of canal surface (vertical).

5.5 Ruled surfaces.

5.5.1 Theory.

We now consider tracking a cusp on a ruled surface. As the cusp sweeps across the rulings we find that we are able to reconstruct the rulings and hence the whole surface. The crucial observation is contained in the following lemma from [K, p.361].

5.5 Lemma: *If the angle between asymptotic directions at a hyperbolic point of a surface is ϕ, then*

$$\tan\phi = \frac{\sqrt{-K}}{H}.$$

Proof: We work with the surface in Monge form, rotated so that one asymptotic direction is along $(1,0,0)$. Let the surface be parametrised $(x, y, h(x,y))$ with

$$h(x,y) = \frac{1}{2}(2a_1xy + a_2y^2) + \cdots.$$

Take the line parametrised by u, $(x,y,z) = u(1,p,0)$. We substitute this in the equation $z - h(z,y) = 0$ of the surface and find the condition for there to be a triple root at $u = 0$. This gives $2a_1u^2p + a_2u^2p^2 + \cdots$ where $\cdots$ denotes terms of u^3 and higher. The first derivative evaluated at $u = 0$ is zero but the second derivative gives the equation,

$$2a_1 + a_2p = 0.$$

If ϕ is the angle between $(1,0,0)$ and $(1,p,0)$ then $\tan\phi = -\frac{2a_1}{a_2}$ and calculating K and H at the origin gives the result. □

By tracking cusps we can recover K, H, the depth, the surface normal and one asymptotic direction (namely the view direction). Recall that for a ruled surface one asymptotic direction is always along the ruling. The ingredients are now all present along with Lemma 5.5, and the recipe is now given.

1. Track cusp and recover the depth, K and H.
2. The view direction is one asymptotic direction and the other is the ruling. Calculate the angle between them by Lemma 5.5 and since we know that the ruling lies in the tangent plane this constrains it.

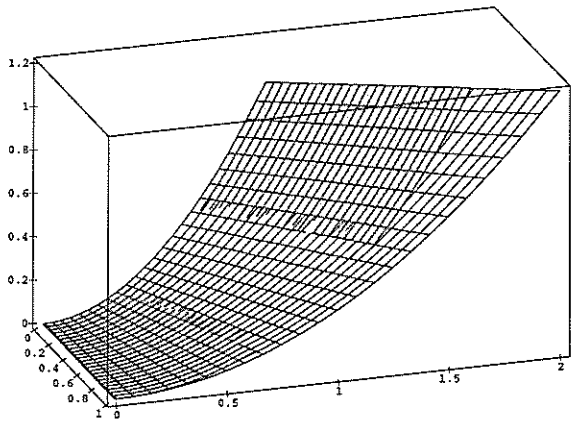

Figure 5.11: Actual and reconstructed ruled surface with an error of 0.3 degrees.

3. This gives the direction of the ruling, and it passes through the cusp generator point which can be recovered with knowledge of the depth.

Figure 5.11 shows the result of a reconstruction experiment on a ruled surface where the maximum error in observed cusp points was 0.3 degrees.

5.6 Conclusion

We have shown that the cusps on the profiles of certain classes of smooth surfaces give enough information to enable the *complete* reconstruction of the surface by tracking cusps alone. This work has built on the theory developed in Chapter 4 and [CFG2], and has added to the accumulating body of work concerning differential geometric aspects of special surface classes.

Recognising that cusps are hard to detect in real images we have given an

analysis with errors that demonstrates the stability and accuracy of the reconstruction even under large image perturbation.

Future work will include extending the methods to other classes of special surfaces, and the analysis of real image data.

Chapter 6

Construction of Surfaces from Profiles.

> Fix one end of a thread in the point O; and extending the other to the vault, make use of it as a ray from the lamp or candle, for describing the place of shadows.
> *The method of drawing the Net or Lattice-Work on vaults* [Poz]

6.1 Construction vs Reconstruction.

This chapter considers the *frontier* of the surface. This curve separates the visible from the invisible or 'the place of shadows'.

Computer Vision has seen a great deal of research into the area of reconstruction of surfaces from profiles, see Chapter 1 for a discussion. Consider a smooth surface 'out there'; by taking different projection centres, with the resulting profiles, well known methods exist for the *reconstruction* of the visible portion of the surface. Figure 6.1 shows a schematic for this situation. The underlying smooth surface is shown dotted and the critical sets are reconstructed and lie on this surface. At the boundary between the visible and invisible region we can see that they form an envelope called the frontier curve (Section 2.7). We have effectively reconstructed a smooth surface with boundary. It is folded (close to the frontier) since two critical sets pass through each point. Also note that the reconstructed surface, as a surface parametrised by the critical sets, *not* the underlying surface, is singular and the singular curve is the frontier.

We can abstract this concept of reconstruction and we will call this *con-*

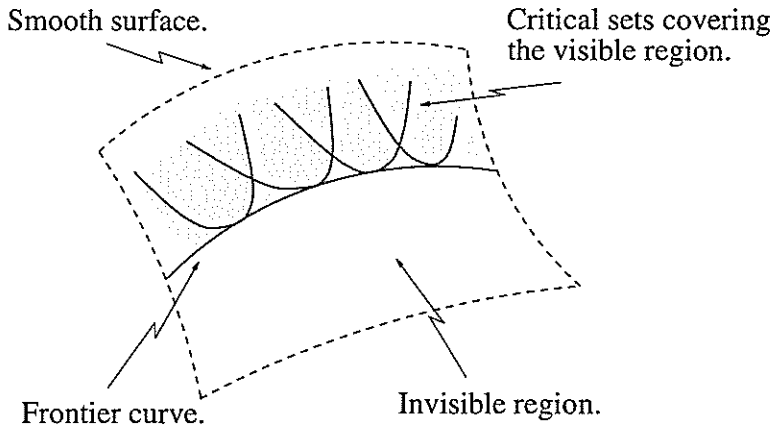

Figure 6.1: Surface reconstruction.

struction. We take the principal ingredients for constructing a surface, namely a camera motion $\mathbf{c}(t)$, which is just a space curve, a set of profiles $\mathbf{p}(s,t)$, though these are not now profiles of a surface but some arbitrary family of smooth curves in the unit sphere, and apply the well known reconstruction technique in order to construct a surface that previously was not available. In short: given a smooth set of curves in the sphere $\mathbf{p}$ (subject to some minor conditions) and a space curve $\mathbf{c}$ what sort of surfaces can we construct? To draw the reader into the mystery an example of such a constructed surface is shown in Figure 6.2. The bold curve on the surface is the frontier (in the sense of $\mathbf{c}_t.\mathbf{n} = 0$, Definition 2.15), and is certainly not the boundary of the visible region in this case! Perhaps the reader can also believe that at the left of the figure the surface has a cusp edge. The surface is singular but not along the frontier.

The construction of surfaces is more than an interesting exercise in differential topology and geometry, what we seek is the exact conditions on $\mathbf{p}$ and $\mathbf{c}$ for us to construct a surface that looks like Figure 6.1. If we can find these conditions, then it is possible that we can exploit them in surface reconstruction to get constraints on the viewer motion.

Some early results appear in [FG2].

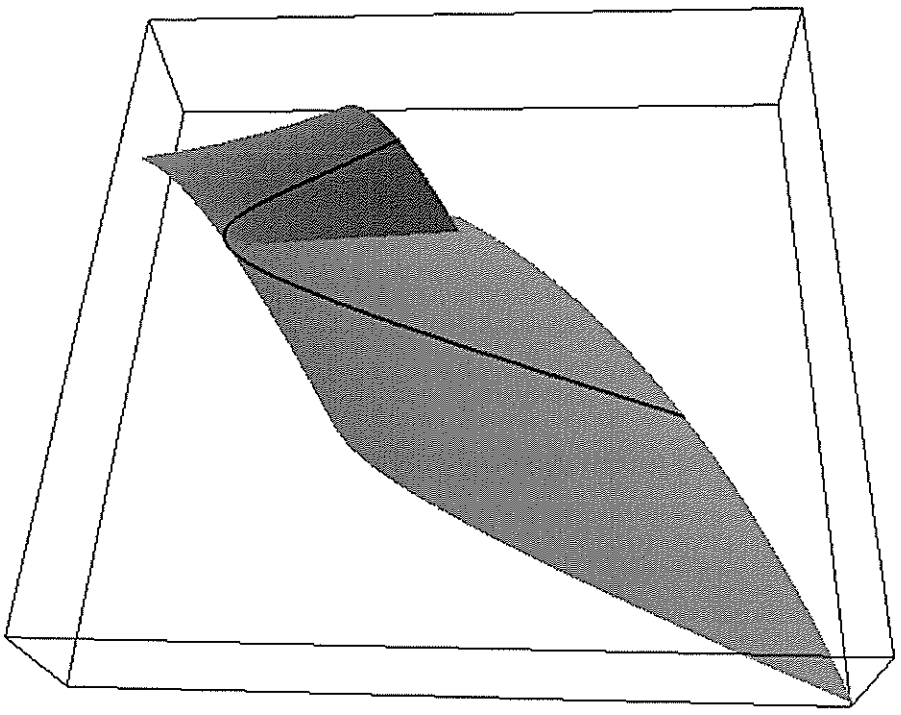

Figure 6.2: Surface construction.

6.2 Construction

Recall the following notation from Subsection 2.2.3. The family of profiles on the sphere is $\mathbf{p}(s,t)$ and the camera motion is $\mathbf{c}(t)$. If $\mathbf{r}(s,t)$ is a point on the surface then the vector $\mathbf{n}(s,t)$ is defined as $\mathbf{p}\wedge\mathbf{p}_s$. This is the normal to the reconstructed surface and so $\mathbf{r}_s.\mathbf{n}=0$ and $\mathbf{r}_t.\mathbf{n}=0$. Using the usual reconstruction formula

$$\mathbf{r}=\mathbf{c}+\lambda\mathbf{p},$$

we obtain the depth, $\lambda=\frac{-\mathbf{c}_t.\mathbf{n}}{\mathbf{p}_t.\mathbf{n}}$.

In the case of surface construction we choose a $\mathbf{c}(t)$ and $\mathbf{p}(s,t)$. If $\mathbf{c}_t.\mathbf{n}\neq 0$ and $\mathbf{p}_t.\mathbf{n}\neq 0$ then λ is well defined and non-zero. If the denominator is zero, we must also have the numerator zero and then define the value of lambda via L'Hopital's rule. Quite simply we can not take for granted the existence of a function λ satisfying $\lambda\mathbf{p}_t.\mathbf{n}+\mathbf{c}_t.\mathbf{n}=0$ for arbitrary $\mathbf{p}$ and $\mathbf{c}$.

> This immediately puts constraints on $\mathbf{p}(s,t)$ and $\mathbf{c}(t)$, and we insist in the remaining work that we choose $\mathbf{p}$ and $\mathbf{c}$ so that there exists a smooth function $\lambda(s,t)$ with $\mathbf{c}_t.\mathbf{n}+\lambda\mathbf{p}_t.\mathbf{n}=0$ holding identically.

We still refer to the 'frontier' in the case of construction, and this is the curve $\mathbf{c}_t.\mathbf{n}=0$.

One can view the construction process as being equivalent to forming the cones with vertex $\mathbf{c}(t)$ through $\mathbf{p}(s,t)$, and then the surface $\mathbf{r}(s,t)$ is the envelope of these cones (indexed by t). Let Δ be a one parameter family of cones parametrised by u and s, and indexed by t. Then

$$\Delta(u,s,t)=\mathbf{c}(t)+u\mathbf{p}(s,t)$$

and the envelope of cones is got by projecting (Δ,t) onto the first three components. The tangent space in $\mathbf{R}^4$ is spanned by the vectors $(\Delta_u,0)$, $(\Delta_s,0)$ and $(\Delta_t,1)$. This contains the kernel direction of the projection provided there exists α and β such that

$$\begin{array}{lrcl} & \alpha\Delta_u+\beta\Delta_s & = & -\Delta_t \\ \text{i.e.} & [\Delta_u,\Delta_s,\Delta_t] & = & 0 \\ \text{i.e.} & [\mathbf{p},u\mathbf{p}_s,\mathbf{c}_t+u\mathbf{p}_t] & = & 0 \\ \text{i.e.} & (\mathbf{c}_t+u\mathbf{p}_t).u\mathbf{n} & = & 0 \\ \text{i.e.} & \text{either } u=0 \text{ or } u & = & -\frac{\mathbf{c}_t.\mathbf{n}}{\mathbf{p}_t.\mathbf{n}}. \end{array}$$

The depth formula u is identical to that for surface reconstruction. If $u = 0$ then the curve $\mathbf{c}(t)$ appears as part of the envelope, and u is arbitrary if $\mathbf{c}_t.\mathbf{n} = \mathbf{p}_t.\mathbf{n} = 0$.

In the case of surface construction we will continue to call the $\mathbf{p}$ curves the 'profiles', even though they are arbitrary curves and one has to prove that they are in fact the profiles to the constructed surface. We will also refer to a 'normal' $\mathbf{n}(s,t)$. This is in fact defined as

$$\mathbf{n} = \mathbf{p} \wedge \mathbf{p}_s.$$

Recall that for reconstruction the surface normal is parallel to the profile normal. We can still talk about 'the normal $\mathbf{n}$', but it is understood to be defined in terms of the $\mathbf{p}$ curves in the manner just described.

6.3 A Specific Example.

In the example we will create a family of profiles on the image sphere starting from a given surface M and camera motion, and then for a variety of other camera motions examine the resulting constructed surface. Here we concern ourselves with the situation when the profiles form an *envelope.*

We now introduce the setup for this specific example. Suppose that the camera centre $\mathbf{c}(t)$ is moving in a circle centred at a point on the z-axis, and the surface M is a sphere centred at the origin, with the whole path $\mathbf{c}(t)$ outside M. See Figure 6.3. Then it is clear that the critical sets are all circles, forming an envelope along two latitude circles on M. The profiles are circles too, which in the unrotated coordinates will form an envelope on the unit sphere. *Given* these profile curves and using other camera motions we will construct different surfaces M'. We ask the question: will the critical sets necessarily form a frontier, that is an envelope on M'?

6.3.1 The Profiles.

Our family of profiles consists of circles lying between the parallels of latitude at say the angles α and β on the image sphere (see Figure 6.3). The envelope is along the two parallels of latitude. We now calculate the parametrisation of

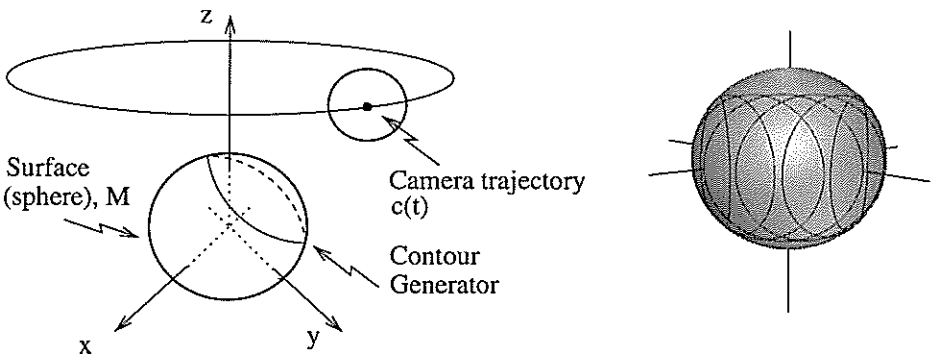

Figure 6.3: Left: Circular motion in the case when M is a sphere. Right: profiles in the image sphere, arising from the case where the centre of the $\mathbf{c}(t)$ circle is at the origin.

$\mathbf{p}(s,t)$. We have two parallels at angle α and β parametrised by ϕ given by the equations,

$$(\cos\alpha\cos\phi, \cos\alpha\sin\phi, \sin\alpha)$$
$$(\cos\beta\cos\phi, \cos\beta\sin\phi, \sin\beta).$$

The centre of the profile (which is a circle) at some time is then,

$$\left(\frac{1}{2}(\cos\alpha+\cos\beta)\cos\phi, \frac{1}{2}(\cos\alpha+\cos\beta)\sin\phi, \frac{1}{2}(\sin\alpha+\sin\beta)\right).$$

We write $a = \frac{1}{2}(\cos\alpha+\cos\beta)$ and $b = \frac{1}{2}(\sin\alpha+\sin\beta)$ for brevity. The radius of the circle is the magnitude of the following vector,

$$\frac{1}{2}((\cos\beta-\cos\alpha)\cos\phi, (\cos\beta-\cos\alpha)\sin\phi, \sin\beta-\sin\alpha),$$

which is $\frac{1}{\sqrt{2}}\sqrt{1-\cos(\beta-\alpha)}$. We denote this length as ρ. A horizontal vector in the plane of the circle is $(-\sin\phi, \cos\phi, 0)$, and the vertical vector is the position vector of the centre $(a\cos\phi, a\sin\phi, b)$, cross the horizontal vector, giving $(1/\sqrt{a^2+b^2})(-b\cos\phi, -b\sin\phi, a)$.

The parametrisation of $\mathbf{p}$ is then,

$$\begin{aligned}\mathbf{p}(s,t) &= (a\cos t, a\sin t, b)\\ &+ \frac{\rho}{\sqrt{1-\rho^2}}(-b\cos t, -b\sin t, a)\cos s\\ &+ \rho(-\sin t, \cos t, 0)\sin s\end{aligned} \tag{6.1}$$

where for convenience we have defined,

$$\begin{aligned}\rho &= (1/\sqrt{2})\sqrt{1-\cos(\beta-\alpha)} \\ a &= (1/2)(\cos\alpha+\cos\beta) \\ b &= (1/2)(\sin\alpha+\sin\beta)\end{aligned}$$

and note the equation, $\sqrt{a^2+b^2} = \sqrt{1-\rho^2}$.

6.3.2 The Construction Process.

We use the following family of camera motions, where the velocity is given as,

$$\mathbf{c}_t(t) = (-B(t)\sin t, B(t)\cos t, 0)$$

and $B(t)$ is some non–zero function of t. Therefore we can now choose different functions B and using the reconstruction formula create some surfaces. If B is constant this corresponds to our reconstructed surface being a sphere with the camera following our original circular path.

Recalling the discussion concerning the normal $\mathbf{n}$ at the end of the introductory section we have $\mathbf{n} = \mathbf{p} \wedge \mathbf{p}_s$ where $\|\mathbf{n}\| = \rho$ and

$$\begin{aligned}\mathbf{n} = \Bigg(&-\sqrt{1-\rho^2}\sin t\sin s - b\cos t\cos s - \frac{\rho}{\sqrt{1-\rho^2}}a\cos t\ , \\ &+\sqrt{1-\rho^2}\cos t\sin s - b\sin t\cos s - \frac{\rho}{\sqrt{1-\rho^2}}a\sin t, \\ &a\cos s - \frac{\rho}{\sqrt{1-\rho^2}}b\Bigg).\end{aligned}$$

It then follows that,

$$\mathbf{c}_t.\mathbf{n} = B\sqrt{1-\rho^2}\sin s$$

and

$$\mathbf{p}_t.\mathbf{n} = \frac{a\sin s}{\sqrt{1-\rho^2}},$$

giving the distance as

$$\lambda = -\frac{B(1-\rho^2)}{a}. \tag{6.2}$$

The cancellation of $\sin s$ is critical since now the depth formula is valid for all s and t and in fact independent of s. This is why we chose $\mathbf{c}_t$ in the form described

above. Note that the sets $\{(s,t) : \mathbf{p}_t.\mathbf{n} = 0\}$ and $\{(s,t) : \mathbf{c}_t.\mathbf{n} = 0\}$ are equal and given by the points $\sin s = 0$. In the image these points form the envelope of profiles. We interest ourselves in the pattern of critical sets and the form of the reconstructed surface.

Given the profiles and camera motion as detailed above we can form the surface $\mathbf{r} = \mathbf{c} + \lambda\mathbf{p}$ and calculate the coefficients of the second fundamental form. We can use equation 6.2 to eliminate B and then along the envelope of profiles (at $s = 0$) the coefficients are,

$$\begin{aligned}
l &= -\lambda\rho\sqrt{1-\rho^2} \\
m &= \lambda\rho\left(b + \frac{a\rho}{\sqrt{1-\rho^2}}\right) \\
n &= \frac{-\rho\lambda}{\sqrt{1-\rho^2}}\left(b + \frac{a\rho}{\sqrt{1-\rho^2}}\right)^2 \\
E &= \lambda^2\rho^2 \\
F &= -\lambda\rho\left(\frac{\lambda\rho b}{\sqrt{1-\rho^2}} - \lambda a - B\right) \\
G &= \left(\frac{\lambda\rho b}{\sqrt{1-\rho^2}} - \lambda a - B\right) + \frac{B'^2(1-\rho^2)^2}{a^4}
\end{aligned}$$

We observe that $ln - m^2 = 0$. We can not conclude however that the corresponding points on the surface are parabolic, since at a genuine frontier point we have $\mathbf{r}_s$ parallel to $\mathbf{r}_t$ which is equivalent to the condition $EG - F^2 = 0$ on the metric coefficients E, F and G. Thus the formula for the Gauss curvature,

$$K = \frac{ln - m^2}{EG - F^2}$$

is undefined since the numerator and denominator are both zero. Since $\lambda_s = 0$ then $\mathbf{r}_s = \lambda\mathbf{p}_s$ and $\mathbf{r}_t = \mathbf{c}_t + \lambda_t\mathbf{p} + \lambda\mathbf{p}_t$, and the condition for $\mathbf{r}_s$ and $\mathbf{r}_t$ to be parallel is then $\lambda_t = -\mathbf{c}_t.\mathbf{p}$. Now $\mathbf{c}_t.\mathbf{p} = B\rho\sin(t)$ and if we impose the condition $\lambda_t = -\mathbf{c}_t.\mathbf{p}$ at points where $\mathbf{c}_t.\mathbf{n} = 0$ (i.e. $\sin(s) = 0$) then we require $\lambda_t = 0$. In other words the condition for the critical sets to form an envelope for this example is $B'(t) = 0$ i.e. B =constant as in our original circular trajectory.

6.3.3 The Resulting Surfaces.

We now consider two different camera motions, when B is constant and $B = 2 + \sin t$. For the case when B is constant recall that the reconstructed surface is

a portion of a sphere between two parallels (which form the envelope of critical sets). For $B = 2 + \sin t$ the constructed surface is smooth and $\mathbf{r}_s$ is not parallel to $\mathbf{r}_t$ along $s = 0$, see Figure 6.4. We have a curve ($s = 0$) where $\mathbf{c}_t.\mathbf{n} = 0$ and another curve where $\mathbf{r}_s \| \mathbf{r}_t$, and these are not the same curve in the case of surface construction. This is a general phenomenon in surface construction that will be investigated further in later sections.

Further inspection of the case $B = 2 + \sin t$ reveals that in fact the view directions $\mathbf{p}(0,t)$ are asymptotic, and since the points $\mathbf{r}(0,t)$ are parabolic (since $ln - m^2 = 0$ and $EG - F^2 \neq 0$) the camera motion is in fact travelling along the Cylinder Axis Developable. Clearly an extremely non–generic situation.

From [ON, p.230] the direction $a_1\mathbf{r}_s + a_2\mathbf{r}_t$ is asymptotic iff $la_1^2 + 2ma_1a_2 + na_2^2 = 0$. Therefore at a parabolic point the unique asymptotic direction is $-m\mathbf{r}_s + l\mathbf{r}_t$. For our example this is the direction,

$$\left(\frac{a\rho}{\sqrt{1-\rho^2}} + b\right)\mathbf{r}_s(0,t) + \sqrt{1-\rho^2}\mathbf{r}_t(0,t).$$

Calculation reveals this to be equal to the direction,

$$\frac{-B'(1-\rho^2)^{3/2}}{a^2}\left(\left(a - \frac{\rho b}{\sqrt{1-\rho^2}}\right)\cos t, \left(a - \frac{\rho b}{\sqrt{1-\rho^2}}\right)\sin t, b + \frac{\rho a}{\sqrt{1-\rho^2}}\right),$$

and parallel to the direction of $\mathbf{p}(0,t)$ (equation 6.1).

6.3.4 Summary.

What we have shown in this example is that reconstruction and construction are fundamentally different. We started with a sphere M, and by taking a circular camera motion were able to generate a set of profiles of the sphere. These profiles were circles on the image sphere that had an envelope. Using the same camera motion we could reconstruct M, or at least the visible part of it. The critical sets formed an envelope at the boundary of the visible part.

We then used the same set of profiles but changed the camera motion. The camera motion was essentially arbitrary subject to the provision that $\mathbf{p}_t.\mathbf{n}$ and $\mathbf{c}_t.\mathbf{n}$ had the same zero sets so that the depth was finite and non zero. Then a new surface M' was constructed from this data. The surface M' was smooth at the 'frontier' (taken as the image of the envelope of profiles) and had cusp edges separate to this. Moreover the frontier was a parabolic curve and all the view

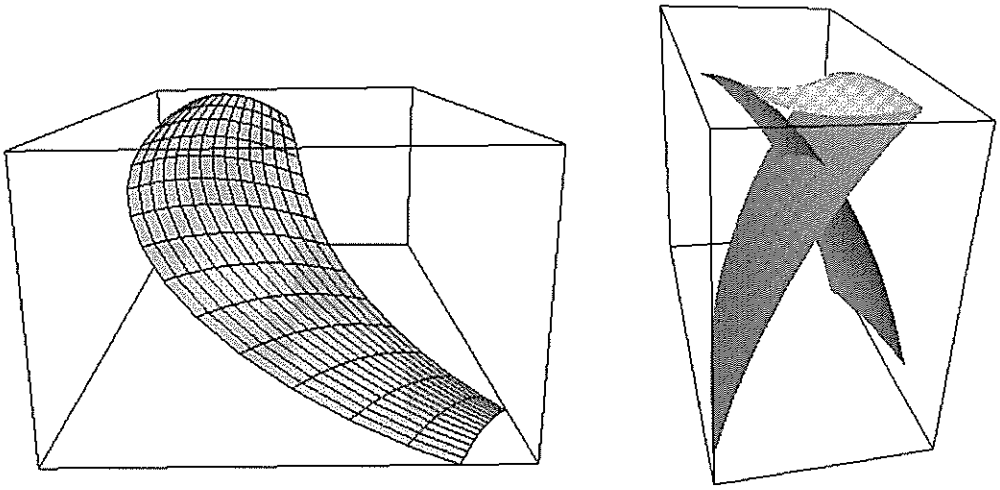

Figure 6.4: Left: The part of M' constructed from a neighbourhood of the envelope of profiles—note that there is no frontier. Right: the part of M' in a neighbourhood of the $\mathbf{r}_s||\mathbf{r}_t$ curve—note that M', has two cusp edges.

directions at these points were asymptotic. This would make the true critical sets of M' with the same camera motion all singular. Recall that the critical set is singular iff the point is parabolic and the view direction asymptotic. We must conclude that the $\mathbf{p}$ curves are not the true profiles since the true profiles must also be singular.

6.4 General Theory.

In this section we examine the constructed surface $\mathbf{r}(s,t)$. We will be primarily interested in the behaviour of $\mathbf{r}$ around two curves on the surface, the frontier and the singular curve. When constructing a surface from $\mathbf{p}(s,t)$ and $\mathbf{c}(t)$ we expect a curve of solutions for $[\mathbf{c}_t, \mathbf{p}, \mathbf{p}_s] = \mathbf{c}_t.\mathbf{n} = 0$. In the case of projections of a genuine surface where we reconstruct, this curve is the frontier or envelope of critical sets, i.e. the curve that forms the boundary of the visible region of the reconstructed surface with the invisible region. We show that this is not necessarily the case when starting from general $\mathbf{p}$ and $\mathbf{c}$. We find that the curve $\mathbf{c}_t.\mathbf{n} = 0$ does *not* form the boundary to a surface and is not the envelope of

critical sets. We prove the surprising result that the surface is in fact smooth at a general point of this curve and in fact the curve is parabolic and the view directions asymptotic.

For a general $\mathbf{p}$ and $\mathbf{c}$ we find that the surfaces we construct are singular. Moreover these singularities occur along a curve, for the following reason. The construction method we use gives $\mathbf{r}_s.\mathbf{n} = 0$ and $\mathbf{r}_t.\mathbf{n} = 0$ holding identically, thus the condition that $\mathbf{r}_s$ and $\mathbf{r}_t$ are parallel is only one condition which we therefore expect to hold along a curve in (s,t) space. The points $\mathbf{r}(s,t)$ where $\mathbf{r}_s$ is parallel to $\mathbf{r}_t$ is the 'singular curve' on $\mathbf{r}$. We prove that the dual is smooth at general points of this curve leading us to suspect that $\mathbf{r}$ has a cuspidal edge.

At points where the singular curve and the $\mathbf{c}_t.\mathbf{n} = 0$ curve cross, the behaviour of $\mathbf{r}$ is surprisingly complicated. In a later section we devise a general example to examine this situation and come to the compelling conclusion that $\mathbf{r}$ is a cuspidal cross cap.

The following result describes the case where $\mathbf{c}_t.\mathbf{n} = 0$ and $\mathbf{r}_s$ and $\mathbf{r}_t$ are independent.

6.1 Proposition: *Given nonsingular* $\mathbf{p}(s,t)$ *with* $\|\mathbf{p}\| = 1$ *where* $\mathbf{p}(s,t_0)$ *has no geodesic inflections for any fixed* t_0 *and* $\mathbf{c}(t)$ *a space curve with* $\mathbf{c}_t$ *not parallel to* $\mathbf{p}$ *we construct a surface* $\mathbf{r}$ *in the usual fashion (Section 6.2). At points on* $\mathbf{r}$ *where* $\mathbf{c}_t.\mathbf{n} = 0$ *(with* $\mathbf{n} = \mathbf{p} \wedge \mathbf{p}_s$*), and* $\mathbf{r}$ *is nonsingular then the surface* $\mathbf{r}$ *has a parabolic point and* $\mathbf{p}$ *is an asymptotic direction. Also the profile of* $\mathbf{r}$ *consists of* $\mathbf{p}(s,t_0)$ *and another branch.*

Proof: We first prove that at nonsingular points where $\mathbf{c}_t.\mathbf{n} = 0$ the surface is parabolic and the view direction is asymptotic.

When we construct a surface from profiles it is constructed so that the following identity holds in s and t,

$$(\mathbf{r}(s,t) - \mathbf{c}(t)).\mathbf{n}(s,t) = 0, \tag{6.3}$$

where $\mathbf{n}(s,t)$ is parallel to $\mathbf{p} \wedge \mathbf{p}_s$ and $\mathbf{r}_s.\mathbf{n} = 0$ and $\mathbf{r}_t.\mathbf{n} = 0$ identically. Differentiating (6.3) by s gives, $(\mathbf{r} - \mathbf{c}).\mathbf{n}_s = 0$. Note that $\mathbf{n}_s$ means differentiating the unit normal in the direction $\mathbf{r}_s$ and since we have assumed that the surface is non-singular we are free to use the shape operator, and this means that $S(\mathbf{r}_s) = -\mathbf{n}_s$ and hence we can interpret this as $II(\mathbf{r} - \mathbf{c}, \mathbf{r}_s) = 0$ which is the

standard result about the view direction being conjugate to the tangent to the critical set.

Differentiating (6.3) with respect to t gives, $-\mathbf{c}_t.\mathbf{n} + (\mathbf{r} - \mathbf{c}).\mathbf{n}_t = 0$ and since we are considering points where $\mathbf{c}_t.\mathbf{n} = 0$ we have $II(\mathbf{r} - \mathbf{c}, \mathbf{r}_t) = 0$. Because $\mathbf{r}_s$ is not parallel to $\mathbf{r}_t$ we must conclude that the point is parabolic and the view direction is asymptotic.

We now prove that the profile of the constructed surface from $\mathbf{c}(t_0)$ consists of $\mathbf{p}(s, t_0)$ and another branch. We wish to find the critical set on the constructed surface from the projection centre $\mathbf{c}_0 = \mathbf{c}(t_0)$. Using the formula $\mathbf{r} = \mathbf{c}_0 + \lambda\mathbf{p}$ this is precisely given by the points (s, t) where

$$(\mathbf{r}(s,t) - \mathbf{c}_0).\mathbf{n}(s,t) = 0, \tag{6.4}$$

recalling that $\mathbf{n} = \mathbf{p} \wedge \mathbf{p}_s$. Clearly $t = t_0$ is a solution for arbitrary s but is this the only solution?

In fact (6.4) will be a smooth curve in the (s, t) plane and hence on $\mathbf{r}$ unless the following hold,

$$\begin{aligned} (\mathbf{r} - \mathbf{c}_0).\mathbf{n}_s &= 0 \\ (\mathbf{r} - \mathbf{c}_0).\mathbf{n}_t + \mathbf{c}_t.\mathbf{n} &= 0. \end{aligned}$$

At the point $\mathbf{r}(s_0, t_0)$ where $\mathbf{c}_t.\mathbf{n} = 0$ we see that the curve is not smooth. We prove below that it is a crossing in the s, t plane. Since we assume that $\mathbf{r}$ is a local diffeomorphism then we will obtain a crossing on the surface. In the case of reconstruction $\mathbf{r}$ is *not* a local diffeomorphism at frontier points. We now wish to find out if it is a point or a crossing, and so examine the quadratic part of (6.4). Setting $f(s, t)$ =l.h.s. of (6.4), at $t = t_0$ we find $f_{ss} = 0$ and so $f_{ss}f_{tt} - f_{st}^2 = [\mathbf{c}_t, \mathbf{p}, \mathbf{p}_{ss}]$ is always negative and the curve is always a crossing. It is more degenerate than Morse iff $[\mathbf{c}_t, \mathbf{p}, \mathbf{p}_{ss}] = 0$. Since we are at a point where $\mathbf{c}_t.\mathbf{n} = 0$ then $\mathbf{c}_t$ is perpendicular to $\mathbf{n}$, and $\mathbf{p}$ is perpendicular to $\mathbf{n}$ by the construction $\mathbf{n} = \mathbf{p} \wedge \mathbf{p}_s$ and so this condition is equivalent to $\mathbf{p}_{ss}.\mathbf{n} = 0$ since $\mathbf{c}_t$ is not parallel to $\mathbf{p}$. We can make $\|\mathbf{p}_s\|$ identically one then $\mathbf{p}_{ss}.\mathbf{p}_s = 0$ and so $\mathbf{p} \wedge \mathbf{p}_{ss} = 0$, i.e. $\mathbf{p}$ has a geodesic inflection. □

Notes on the Proposition.

1. We have found that nonsingular points where $\mathbf{c}_t.\mathbf{n} = 0$ are parabolic points on the constructed surface. Moreover the view directions at these parabolic

points are asymptotic. Recalling Definition 1.16 we see that the camera is travelling along the Cylinder Axis Developable. For the case when we are observing an external surface this would be extremely non generic, and results in all the critical sets being singular along this curve.

2. Since the critical sets are singular the profiles are singular. Recall that the curves $\mathbf{p}(s,t)$ were designed to be the profiles and so we must conclude that there is an extra branch to $\mathbf{p}$ in order to make the actual profile to the constructed surface complete. Starting with some 'profile' curves $\mathbf{p}(s,t)$ and constructing a surface in the usual way we find that $\mathbf{p}$ is not the complete profile.

3. The condition that the curves $\mathbf{p}$ do not have geodesic inflections is to eliminate the complication of expected 'parabolic' points. We expect a parabolic point on the constructed surface if the profile inflects, since this is the well known result of Koenderink, Section 2.5. We have found that the $\mathbf{c}_t.\mathbf{n} = 0$ curve is parabolic which is entirely unexpected. In fact when the 'real' parabolic curve (i.e. locus of geodesic inflections on $\mathbf{p}$) hits the $\mathbf{c}_t.\mathbf{n} = 0$ curve we find that this is precisely the point where $\mathbf{c}_t.\mathbf{n} = 0$ can not be parametrised by t. Observe that $\mathbf{c}_t.\mathbf{n} = 0$ can not be parametrised by t iff $\frac{\partial}{\partial s}\mathbf{c}_t.\mathbf{n} = 0$ which is the condition found in the above proof, $[\mathbf{c}_t, \mathbf{p}, \mathbf{p}_{ss}] = 0$. For our case the profiles do not form an envelope along the $\mathbf{c}_t.\mathbf{n} = 0$ curve, they are singular as we have shown above.

6.4.1 The Dual.

We now turn our attention to points on the constructed surface where the surface is singular ($\mathbf{r}_s$ parallel to $\mathbf{r}_t$) and $\mathbf{c}_t.\mathbf{n}$ is not equal to zero. We call the dual of the constructed surface R.

It is possible to view the profiles $\mathbf{p}(s,t)$ and the camera motion $\mathbf{c}(t)$ as providing enough information to construct all the tangent planes. If $\mathbf{n} = \mathbf{p} \wedge \mathbf{p}_s$ then the equation of the tangent planes is

$$(\mathbf{x} - \mathbf{c}).\mathbf{n} = 0.$$

These are planes passing through $\mathbf{c}$ and spanned by the view direction $\mathbf{p}$ and the

tangent to the profile $\mathbf{p}_s$. We can parametrise these planes in the following way,

$$\begin{aligned} \mathbf{R}^2 &\rightarrow \mathbf{R} \times \mathbf{S}^2 \\ s,t &\mapsto \mathbf{c}.\mathbf{n}, \mathbf{n} \end{aligned}$$

and if we avoid points where $\mathbf{c}.\mathbf{n} = 0$ we can map to $\mathbf{R}^3$ via,

$$\begin{aligned} \mathbf{R} \times \mathbf{S}^2 &\rightarrow \mathbf{R}^3 \\ \mathbf{c}.\mathbf{n}, \mathbf{n} &\mapsto (\mathbf{c}.\mathbf{n})\mathbf{n}. \end{aligned}$$

Certainly one advantage in considering the dual is that it does not involve the depth function λ. In the following result we prove that the dual is singular at frontier points ($\mathbf{c}_t.\mathbf{n} = 0$). The dual is smooth at singular points of $\mathbf{r}$ suggesting that $\mathbf{r}$ is no worse than a cusp edge. The singularities of $\mathbf{r}$ are dealt with in more detail in a subsequent section. The following lemma gives the condition for the normal map to the surface to be singular.

6.2 Lemma: *Given smooth* $\mathbf{p}(s,t)$ *and* $\mathbf{c}(t)$ *let the normal (see end of Section 6.2) be* $\mathbf{n} = \mathbf{p} \wedge \mathbf{p}_s$. *Then* $\mathbf{n}_s$ *is parallel to* $\mathbf{n}_t$ *if and only if either* $\mathbf{p}$ *has a geodesic inflection or* $\mathbf{c}_t.\mathbf{n} = 0$.

Proof: From the definition we can differentiate and obtain,

$$\mathbf{n}_s \wedge \mathbf{n}_t = \mathbf{p}_t[\mathbf{p}, \mathbf{p}_{ss}, \mathbf{p}_s] - \mathbf{p}_s[\mathbf{p}, \mathbf{p}_{ss}, \mathbf{p}_t] + \mathbf{p}[\mathbf{p}, \mathbf{p}_{ss}, \mathbf{p}_{st}].$$

Thus $\mathbf{n}_s$ is parallel to $\mathbf{n}_t$ if and only if $\mathbf{p}$ is parallel to $\mathbf{p}_{ss}$, which is the condition for a geodesic inflection by Subsection 2.5.2, or $\mathbf{p}$, $\mathbf{p}_s$ and $\mathbf{p}_t$ lie in a plane. This is equivalent to $[\mathbf{p}_t, \mathbf{p}, \mathbf{p}_s] = 0$, and recalling that $\mathbf{n} = \mathbf{p} \wedge \mathbf{p}_s$ we have $\mathbf{p}_t.\mathbf{n} = 0$ which is equivalent to $\mathbf{c}_t.\mathbf{n} = 0$ by the global assumption of the existence of λ ($\mathbf{c}_t.\mathbf{n} + \lambda \mathbf{p}_t.\mathbf{n} = 0$). □

6.3 Proposition: *The dual surface* $R(s,t) = (\mathbf{c}.\mathbf{n})\mathbf{n}$ *is singular if and only if* $\mathbf{p}$ *has a geodesic inflection or* $\mathbf{c}_t.\mathbf{n} = 0$.

Proof: Calculation gives,

$$\begin{aligned} R_s &= (\mathbf{c}.\mathbf{n}_s)\mathbf{n} + (\mathbf{c}.\mathbf{n})\mathbf{n}_s \\ R_t &= (\mathbf{c}_t.\mathbf{n} + \mathbf{c}.\mathbf{n}_t)\mathbf{n} + (\mathbf{c}.\mathbf{n})\mathbf{n}_t \end{aligned}$$

and given $\mathbf{c}.\mathbf{n} \neq 0$, for R to be singular it is necessary to have $\mathbf{n}_s$ and $\mathbf{n}_t$ parallel since $\mathbf{n}_s$ and $\mathbf{n}_t$ are perpendicular to $\mathbf{n}$ and in addition,

$$(\mathbf{c}_t.\mathbf{n} + \mathbf{c}.\mathbf{n}_t)(\mathbf{c}.\mathbf{n})\|\mathbf{n}_s\| = (\mathbf{c}.\mathbf{n}_s)(\mathbf{c}.\mathbf{n})\|\mathbf{n}_t\|. \tag{6.5}$$

If $\mathbf{n}_s$ and $\mathbf{n}_t$ are parallel and non zero then (6.5) reduces to the condition $\mathbf{c}_t.\mathbf{n} = 0$. From the result of the previous lemma we can conclude that if $\mathbf{n}_s$ and $\mathbf{n}_t$ are non zero then R is singular if and only if $\mathbf{c}_t.\mathbf{n} = 0$, using $\mathbf{n} = \mathbf{p} \wedge \mathbf{p}_s$.

Observe that if $\mathbf{n}_s = 0$ then the dual is singular. The condition for this is $\mathbf{p} \wedge \mathbf{p}_{ss} = 0$ which is a geodesic inflection. Therefore the condition for the dual to be singular is that either the profiles have a geodesic inflection or that $\mathbf{c}_t.\mathbf{n} = 0$. □

6.5 General Example.

In this section we devise a general example for examining the construction of surfaces from profiles. It is far from obvious how to achieve this since we have the constraint that there must exist a $\lambda(s,t)$ such that $\mathbf{c}_t.\mathbf{n} + \lambda\mathbf{p}_t.\mathbf{n} = 0$ holds identically. In the following example we take $\mathbf{p}_t.\mathbf{n} = 0$ and $\mathbf{c}_t.\mathbf{n} = 0$ along the $s = 0$ curve and then using this fact we can perform some calculations detailed in the text for finding a well defined λ.

We consider perspective projection but for simplicity we show that we can work with a family of curves $\mathbf{P}(s,t)$ in the plane and not on the image sphere. These curves, which we call 'profile curves' though strictly they do not start life as the profiles of any surface and one should prove that they are in fact the profiles of the constructed surface, are given as power series expansions. We make some assumptions that restrict certain coefficients but these do not restrict the generality of the example. The camera motion is also given as a general power series.

Let $\mathbf{P}(s,t)$ be a family of curves in the $x = 1$ plane given as

$$\mathbf{P}(s,t) = (1, X(s,t), Y(s,t)),$$

then if $\mathbf{p}(s,t)$ is the family of profiles in the image sphere we have, $\mathbf{p} = \mathbf{P}/\|\mathbf{P}\|$, see Figure 6.5.

We are interested in $\mathbf{r}$ around the curve $\mathbf{c}_t.\mathbf{n} = 0$ and the singular curve where $\mathbf{r}_s$ is parallel to $\mathbf{r}_t$. We now prove some results concerning the plane profiles $\mathbf{P}$.

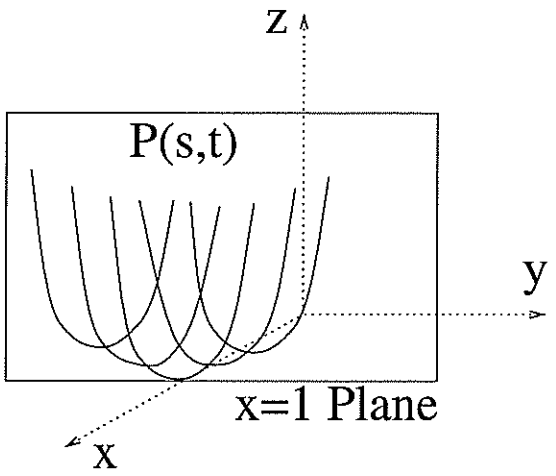

Figure 6.5: Schematic showing the curves $\mathbf{P(s,t)} = (1, X(s,t), Y(s,t))$.

6.4 Lemma: *In the situation above where* $\mathbf{P} = (1, X(s,t), Y(s,t))$, $\mathbf{p}(s,t) = \mathbf{P}/\|\mathbf{P}\|$ *and writing* $\mathbf{N} = \mathbf{P} \wedge \mathbf{P}_s$ *and,* $\mathbf{n} = \mathbf{p} \wedge \mathbf{p}_s$ *we have,*

1. $\mathbf{n} = \frac{\mathbf{N}}{\|\mathbf{P}\|^2}$,
2. $\mathbf{p}_t.\mathbf{n} = 0 \Leftrightarrow \mathbf{P}_t.\mathbf{N} = 0$,
3. $\mathbf{c}_t.\mathbf{n} = 0 \Leftrightarrow \mathbf{c}_t.\mathbf{N} = 0$.

Proof:

1. Firstly $\mathbf{p}\|\mathbf{P}\| = \mathbf{P}$, and differentiating both sides gives, $\mathbf{p}_s\|\mathbf{P}\| + \mathbf{p}\frac{\mathbf{P}.\mathbf{P}_s}{\|\mathbf{P}\|} = \mathbf{P}_s$. Then crossing with $\mathbf{p}$ gives, $\mathbf{p} \wedge \mathbf{p}_s = \frac{\mathbf{P} \wedge \mathbf{P}_s}{\|\mathbf{P}\|^2}$ and using the definitions of $\mathbf{n}$ and $\mathbf{N}$ given in the statement we obtain the result.
2. Since $\mathbf{p}\|\mathbf{P}\| = \mathbf{P}$ we differentiate to get, $\mathbf{p}_t\|\mathbf{P}\| + \mathbf{p}\frac{\mathbf{P}.\mathbf{P}_t}{\|\mathbf{P}\|} = \mathbf{P}_t$ and dotting with $\mathbf{n}$ and using the first result of this lemma gives $\mathbf{p}_t.\mathbf{n} = \frac{\mathbf{P}_t.\mathbf{N}}{\|\mathbf{P}\|^3}$.
3. From the first result of this lemma we see that $\mathbf{n}$ is parallel to $\mathbf{N}$, and the result is straightforward.

□

This lemma essentially tells us that we can work with the curves $\mathbf{P}$ and still easily interpret the conditions with respect to the $\mathbf{p}$ curves. In setting up this

general example we shall insist that $\mathbf{c}_t.\mathbf{n} = 0$ and $\mathbf{p}_t.\mathbf{n} = 0$ is the curve $s = 0$. Or to be more precise the curves $\mathbf{c}_t.\mathbf{n} = 0$ and $\mathbf{p}_t.\mathbf{n} = 0$ have a common non singular branch that is $s = 0$. This of course does not restrict the generality of the example. We thus want to find the conditions on $\mathbf{P}$ and $\mathbf{c}$ for $\mathbf{P}_t.\mathbf{N} = 0$ and $\mathbf{c}_t.\mathbf{N} = 0$ along $s = 0$.

Writing $\mathbf{P}$ as $(1, X, Y)$ we have $\mathbf{P}_s = (0, X_s, Y_s)$ and $\mathbf{P}_t = (0, X_t, Y_t)$, it is then straightforward to calculate the condition for $\mathbf{P}_t.\mathbf{N} = [\mathbf{P}_t, \mathbf{P}, \mathbf{P}_s] = 0$. This is $X_s Y_t - X_t Y_s = 0$. We require this quantity to be identically zero when $s = 0$. We can assume $\mathbf{P}_s(0,0) = (0,1,0)$ so that $X_s(0,0) = 1$ and $Y_s(0,0) = 0$ and then write

$$Y_t(0,t) = \frac{X_t(0,t)Y_s(0,t)}{X_s(0,t)},$$

where we have now made the denominator non zero at 0. We split Y into two parts $Y = sY_3(s,t) + Y_2(t)$ where the function Y_2 of t only, is given as the following integral,

$$Y_2(t) = \int_0^t \frac{X_t(0,t)Y_s(0,t)}{X_s(0,t)} dt.$$

This imposition on Y_2 will make the condition $\mathbf{P}_t.\mathbf{N}(0,t) = 0$ hold identically, even for arbitrary $Y_3(s,t)$. In fact in the MAPLE program we write,

$$Y_3(s,t) = z_{10}s + z_{01}t + z_{20}s^2 \cdots.$$

We now wish to impose a condition on the camera motion $\mathbf{c}(t)$ so that $\mathbf{c}_t.\mathbf{N}(0,t) = 0$ is an identity. Write $\mathbf{c}(t) = (c_1(t), c_2(t), c_3(t))$ and the condition $\mathbf{c}_t.\mathbf{N} = [\mathbf{c}_t, \mathbf{P}, \mathbf{P}_s] = 0$ becomes,

$$-c_{2t}Y_s + c_{3t}X_s + c_{1t}(XY_s - X_sY) = 0.$$

We choose c_{3t} to take the value that satisfies this at $s = 0$ and so c_3 is defined by the following integral,

$$c_3 = \int_0^t \frac{c_{2t}Y_s(0,t) - c_{1t}(X(0,t)Y_s(0,t) - X_s(0,t)Y(0,t))}{X_s(0,t)} dt.$$

Therefore the functions $\mathbf{c}_t.\mathbf{N}$ and $\mathbf{P}_t.\mathbf{N}$ are divisible by s and we define the functions $f(s,t)$ and $g(s,t)$ so that

$$\begin{aligned} \mathbf{c}_t.\mathbf{N} &= sf(s,t) \\ \mathbf{P}_t.\mathbf{N} &= sg(s,t). \end{aligned}$$

Recall that the depth λ is defined as $\frac{-\mathbf{c}_t.\mathbf{n}}{\mathbf{p}_t.\mathbf{n}}$ or equally well as the identity $\mathbf{c}_t.\mathbf{n}+\lambda\mathbf{p}_t.\mathbf{n}=0$. This is equivalent to $\frac{\mathbf{c}_t.\mathbf{N}}{\|\mathbf{P}\|^2}+\lambda\frac{\mathbf{P}_t.\mathbf{N}}{\|\mathbf{P}\|^3}=0$ and so defining $\Lambda=\frac{\lambda}{\|\mathbf{P}\|}$ we have,

$$\mathbf{r}=\mathbf{c}+\lambda\mathbf{p}=\mathbf{c}+\Lambda\|\mathbf{P}\|\frac{\mathbf{P}}{\|\mathbf{P}\|}=\mathbf{c}+\Lambda\mathbf{P}=\mathbf{c}-\frac{f}{g}\mathbf{P}.$$

The calculations described can be accomplished with MAPLE. We can specify $\mathbf{P}$ as a power series and c_1 and c_2 similarly. MAPLE can integrate to find $Y_2(t)$ and $c_3(t)$ described previously and then find f and g. This gives the ingredients necessary to construct the surfaces.

We now present a short digression on possible recognition criteria for cusp edges and cuspidal cross caps.

6.5.1 Cuspidal Cross Caps and Cusp Edges.

In [MO2] the class of maps from the plane to 3-space with cuspidal edges is studied. The following definition is from [MO2], and we note that the class of maps we are considering belongs to 'CE'. Recall that we observed in Section 6.4 that we expect $\mathbf{r}_s$ and $\mathbf{r}_t$ to be dependent along a curve in the s,t plane.

6.5 Definition: *A map-germ $f:(\mathbf{R}^2,0)\to(\mathbf{R}^3,0)$ has a cuspidal edge if there is a 1-manifold germ $(C,0)\subset(\mathbf{R}^2,0)$ such that for each $x\in C$, $rank\,df_x=1$. The class of all germs like this will be denoted CE.*

One method to distinguish corank one maps is to investigate the doublepoint space. Intuitively one expects the doublepoint space of the cuspidal cross cap to be more complicated than that of the cuspidal edge, see Figure 6.6. For a corank 1 map of the form $h(x,y)=(x,p(x,y),q(x,y))$ the doublepoint space $D^2(h)$ as a subset of $C^3=(x,y,y')$ space, is defined by the equations

$$\frac{p(x,y)-p(x,y')}{y-y'}=0$$
$$\frac{q(x,y)-q(x,y')}{y-y'}=0.$$

Example: For the cuspidal edge let $f(x,y)=(x,y^2,y^3)$ and for the cuspidal cross cap $g(x,y)=(x,y^2,xy^3)$ then one finds that $D^2(f)$ is defined by $y+y'$ and $y^2+yy'+y'^2$, resulting in a single line $y=y'=0$. For the cuspidal cross cap

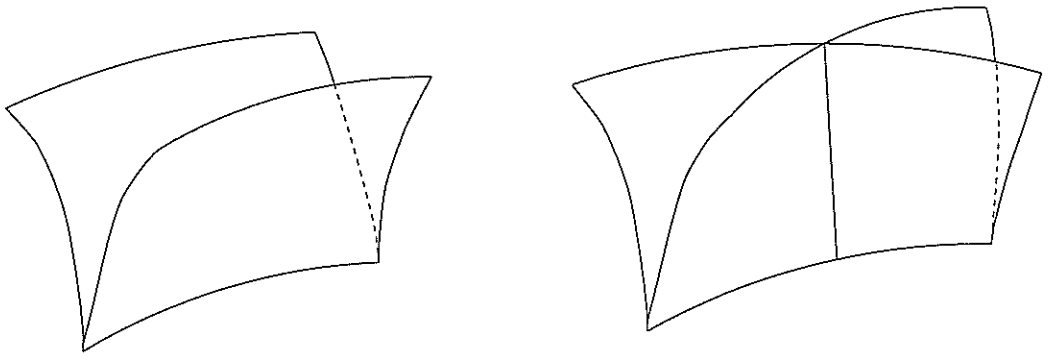

Figure 6.6: Cusp Edge and Cuspidal Cross Cap.

$D^2(g)$ is defined by $y+y'$ and $x(y^2+yy'+y'^2)$ and the double point space has two branches: the lines $y = y' = 0$ and the line $y = -y'$, $x = 0$, which is recognisably different to $D^2(f)$.

For our surface construction maps we do not expect them to come to this nice form but we can appeal to a method given in Section 3 of [MO1] which describes how to obtain $D^2(h)$ for a general corank 1 map. We consider pairs of points (x, y) and (x', y') and for each of the coordinate functions h_i $(i = 1, 2, 3)$ of h, we can find functions a_i, b_i of x, y, x', y' such that

$$h_i(x, y) - h_i(x', y') = (x - x')a_i + (y - y')b_i.$$

Then $D^2(h)$ is defined in x, y, x', y' space by the equations $h_i(x, y) - h_i(x', y') = 0$ $i = 1, 2, 3$ and by the vanishing of the 2×2 minors of the 3×2 matrix whose rows are the a_i and b_i. This gives six equations in four unknowns and we wish to find the solutions to all equations simultaneously. Due to the special nature of the equations we expect some considerable interdependnece and expect the solution to be a curve with possible singularities.

We can find the functions a and b in the following way. Let

$$\begin{aligned} a &= \frac{h(s, t') - h(s', t')}{s - s'}, \\ b &= \frac{h(s, t) - h(s, t')}{t - t'} \end{aligned}$$

and then a and b satisfy,

$$h(s, t) - h(s', t') = a(s - s') + b(t - t').$$

Observe that the numerator of a and b above is divisible by $s - s'$ and $t - t'$ respectively, and so for our method we take the Taylor expansion of these up to some sufficient jet level.

6.5.2 MAPLE Implementation.

We can use MAPLE to construct the jet of our map $\mathbf{r}$ from a given $\mathbf{P}$ and $\mathbf{c}$. Recall that $\mathbf{P} = (1, X(s,t), Y(s,t))$ and in Section 6.5 we described how Y was found from the function $Y_3(s,t)$. In the MAPLE implementation we write X, Y_3 and $\mathbf{c}(t) = (c_1, c_2, c_3)$ as power series in the following way,

$$\begin{aligned} X &= s + x_{01}t + x_{20}s^2 + x_{11}st + x_{02}t^2 + x_{30}s^3 + x_{21}s^2t + x_{12}st^2 + x_{03}t^3 \\ Y_3 &= z_{10}s + z_{01}t + z_{20}s^2 + z_{11}st + z_{02}t^2 \\ c_1 &= c_{10} + c_{11}t + c_{12}t^2 \\ c_2 &= c_{20} + c_{21}t + c_{22}t^2. \end{aligned}$$

Recall from Section 6.5 that c_3 is found from those variables given above.

To do this symbolically is extremely difficult due to the complexity of our maps and Figure 6.7 only shows the *two*–jet for *one* component of $\mathbf{r}$. Whilst the geometric construction and intuition behind $\mathbf{r}$ is straightforward the calculation in components rapidly becomes intractable even with powerful computer algebra packages.

We can however devise a suitably general example where numbers are substituted, and this is what is done in the following. We wish to examine the case when the singular curve and the frontier cross. We investigate the singularities of the image of $\mathbf{r}$ via the double–point space $D^2(\mathbf{r})$. Since initially we are in the frontier case the profiles form an envelope and we choose suitable values so as to make $\mathbf{P}$ a nice smooth family. Figure 6.8 shows the profiles $\mathbf{P}(s,t)$ that we will use plotted for a range of t and the example is set up so that they form an envelope along $s = 0$.

Appendix A shows the MAPLE code that was used to generate the example. We implement the method described above from [MO1] for finding the double-point curve. We find the functions a_i and b_i described in Subsection 6.5.1 and then form the six equations in four unknowns that define the double-point curve. We are able to solve for the variables s' and t' (called `s1` and `t1` in the MAPLE code) by substituting in two power series and iteratively solving to find the

$$
\begin{aligned}
&-\frac{1}{4}(32\,z10^4\,c21\,z01\,x01 - 8\,z10^3\,c21\,z01^2 + 8\,z10^5\,s^2\,c11\,x01 + 24\,z10^3\,s\,x01\,z20\,c21\,z01 - 32\,c21\,z10^5\,x01^2 \\
&\quad - 48\,c10\,z10^4\,x01^2\,z01 + 24\,c10\,z10^3\,x01\,z01^2 + 32\,c10\,z10^5\,x01^3 - 4\,c10\,z10^2\,z01^3 + 48\,t\,s\,z20\,c21\,z10^3\,z02\,x01 \\
&\quad - 64\,t\,s\,c21\,z10^5\,x11\,x02 - 16\,t\,s\,x20^2\,z01^3\,c21\,z10^2 - 16\,t\,s\,c21\,z10^5\,x11\,x01 - 16\,t\,s\,c21\,z10^4\,x11^2\,z01 \\
&\quad + 32\,t\,s\,c21\,z10^4\,x11\,z02 - 24\,t\,s\,z20\,c21\,z01^2\,z10^2\,x11 + 16\,t\,s\,z10^4\,c11\,x01\,z02 + 64\,t\,s\,c21\,z10^5\,x12\,x01 \\
&\quad - 32\,t\,s\,c21\,z10^3\,x20^2\,z01^2\,x01 - 16\,t\,s\,c21\,z10^4\,z02 - 32\,t\,s\,c21\,z10^4\,x12\,z01 - 30\,t\,s\,z20\,z01^2\,c11\,z10^2\,x01 \\
&\quad + 32\,t\,s\,z10^5\,c12\,x01^2 + 12\,t\,s\,z10^4\,c11\,z01\,x01 + 16\,t\,s\,z10^3\,c11\,x11\,z01^2 + 9\,t\,s\,z20\,z01^3\,c11\,z10 + 32\,t\,s\,c21\,z10^5\,x02 \\
&\quad - 4\,t\,s\,c21\,z01\,z10^4 - 24\,t\,s\,x30\,z01^2\,c21\,z10^3\,x01 + 48\,t\,s\,z10^5\,c11\,x11\,x01^2 - 48\,t\,s\,z20\,c21\,z01\,z10^3\,x01 \\
&\quad + 8\,t\,s\,c21\,z10^3\,x21\,z01^2 + 12\,t\,s\,x30\,z01^3\,c21\,z10^2 - 16\,t\,s\,z10^5\,c11\,x01^2 - 2\,t\,s\,z10^3\,c11\,z01^2 - 9\,t\,s\,z20^2\,c21\,z01^3 \\
&\quad - 48\,t\,s\,z20\,c21\,z10^3\,x02\,z01 + 8\,t\,s\,z10^3\,c12\,z01^2 + 24\,t\,s\,z20\,c21\,z01^2\,z10^2 - 56\,t\,s\,z10^4\,c11\,x11\,x01\,z01 \\
&\quad - 32\,t\,s\,z10^4\,c12\,z01\,x01 - 16\,t\,s\,z10^2\,c11\,x20\,z01^3 + 24\,t\,s\,z20\,z01\,x01^2\,z10^3\,c11 + 32\,t\,s\,c21\,z10^3\,x20\,z01^2\,x11 \\
&\quad + 16\,t\,s\,c21\,z10^5\,x01 - 16\,t\,s\,x20\,z01^2\,c21\,z10^3 - 32\,t\,s\,z10^5\,c11\,x01\,x02 + 12\,t\,s\,z10\,c21\,z01^3\,z20\,x20 \\
&\quad - 16\,t\,s\,c21\,z10^4\,x21\,z01\,x01 - 64\,t\,s\,c21\,z10^4\,x20\,z02\,x01 + 8\,t\,s\,c21\,z01\,z10^4\,x11 + 16\,t\,s\,z10^4\,c11\,z01\,x02 \\
&\quad + 48\,t\,s\,z10^3\,c11\,x20\,z01^2\,x01 + 32\,t\,s\,c21\,z10^4\,x20\,z01\,x11\,x01 + 48\,t\,s\,x20\,z01^2\,c21\,z10^2\,x01\,z20 \\
&\quad - 32\,t\,s\,z10^4\,c11\,x20\,z01\,x01^2 + 24\,z10^2\,s^2\,z20\,c21\,z01^2\,x20 - 36\,z10^2\,s^2\,z20^2\,c21\,z01\,x01 + 8\,z10^4\,s^2\,c11\,z20\,x01^2 \\
&\quad - 8\,t\,s\,z10^3\,c11\,z01\,z02 - 32\,z10^3\,s^2\,c21\,x20^2\,z01^2 + 48\,z10^3\,s^2\,c21\,x20\,z01\,x01\,z20 + 64\,z10^4\,s^2\,c21\,x20\,z01\,x11 \\
&\quad - 16\,z10^5\,s^2\,c11\,x01\,x11 - 20\,z10^3\,s^2\,c11\,z20\,x01\,z01 - 8\,z10^3\,s^2\,c11\,z01^2\,x20 + 8\,z10^4\,s^2\,c11\,z01\,x11 \\
&\quad + 16\,t\,s\,c21\,z10^4\,x20\,z01\,x01 + 64\,t\,s\,c21\,z10^4\,x20\,z01\,x02 - 48\,z10^4\,s^2\,c21\,x30\,z01\,x01 + 24\,z10^3\,s^2\,c21\,x30\,z01^2 \\
&\quad - 32\,z10^5\,s^2\,c21\,x11^2 - 48\,z10^3\,s^2\,c21\,x11\,z20\,z01 - 32\,z10^5\,s^2\,c21\,x20\,x01 + 32\,z10^5\,s^2\,c21\,x21\,x01 \\
&\quad - 16\,z10^4\,s^2\,c21\,x21\,z01 + 8\,z10^2\,s^2\,c11\,z20\,z01^2 + 16\,z10^4\,s^2\,c11\,x01\,x20\,z01 - 16\,z10^4\,s^2\,c21\,x20\,z01 \\
&\quad + 32\,z10^5\,s^2\,c21\,x11 + 24\,z10^4\,s^2\,z20\,c21\,x01 + 12\,z10^3\,s^2\,z20\,c21\,z01 - 8\,t^2\,z10^3\,c21\,z01^2\,x11 \\
&\quad - 24\,t^2\,c21\,z01^2\,z20\,x02\,z10^2 - 4\,t^2\,c12\,z10^2\,z01^3 + 8\,t^2\,x20\,z02\,c21\,z01^2\,z10^2 - 4\,z10^4\,s^2\,c11\,z01 \\
&\quad - 112\,t^2\,z10^4\,c12\,z01\,x01^2 - 48\,t^2\,c21\,z10^4\,x03\,z01 + 40\,t^2\,z10^3\,c12\,z01^2\,x01 - 8\,t^2\,x12\,z10^3\,c21\,z01^2 \\
&\quad + 96\,t^2\,z10^5\,c11\,x02\,x01^2 + 16\,t^2\,x12\,z10^4\,c21\,z01\,x01 + 32\,t^2\,z10^4\,c21\,z02\,x01 + 16\,t^2\,z10^4\,z01\,x01^2\,c11 \\
&\quad - 16\,t^2\,x21\,z01^2\,c21\,z10^3\,x01 - 16\,t^2\,x11\,z10^4\,c21\,z02\,x01 + 16\,t^2\,z10^4\,c21\,x02\,z01 - 6\,t^2\,x20\,z01^4\,c11\,z10 \\
&\quad - 24\,t^2\,z10^3\,c21\,z02\,z01 + 12\,t^2\,z10^3\,c21\,z01^2 + 96\,t^2\,c21\,z10^5\,x03\,x01 + 20\,t^2\,x20\,z01^3\,x01\,z10^2\,c11 \\
&\quad + 32\,t^2\,x20\,z01^2\,c21\,z10^3\,x02 - 16\,t^2\,x20\,z01^2\,x01^2\,z10^3\,c11 - 12\,t^2\,x20\,z01^3\,c21\,z10^2 + 96\,t^2\,z10^5\,c12\,x01^3 \\
&\quad + 8\,t^2\,x21\,z01^3\,c21\,z10^2 - 6\,t^2\,z10\,c21\,z01^3\,z20 + 6\,t^2\,x20\,z01^4\,c21\,z20 - 16\,t^2\,x20^2\,z01^3\,c21\,z10^2\,x01 \\
&\quad + 32\,t^2\,z10^3\,c11\,x02\,z01^2 + 16\,t^2\,x20\,z01^2\,c21\,z10^3\,x11\,x01 - 48\,t^2\,x20\,z02\,c21\,z10^3\,x01\,z01 \\
&\quad - 112\,t^2\,z10^4\,c11\,x02\,x01\,z01 + 32\,t^2\,x20\,z01^2\,c21\,z10^3\,x01 + 24\,t^2\,x11\,z10^3\,c21\,z02\,z01 - 32\,t^2\,x11\,z10^4\,c21\,x02\,z01 \\
&\quad - 20\,t^2\,z10^3\,z01^2\,c11\,x01 + 12\,t^2\,z10\,c21\,z01^2\,z20\,z02 - 32\,t^2\,z10^4\,c11\,x01^2\,z02 - 12\,t^2\,z01^2\,c11\,z10^2\,z02 \\
&\quad + 40\,t^2\,z01\,x01\,z10^3\,c11\,z02 + 6\,t^2\,z10^2\,z01^3\,c11 - 16\,t^2\,z10^4\,c21\,z01\,x01 - 16\,z10^3\,z01^2\,t\,x20\,c21\,x01 \\
&\quad + 8\,z10^2\,z01^3\,t\,x20\,c21 - 8\,z10^4\,z01\,t\,c21\,x01 + 4\,z10^3\,z01^2\,t\,c21 + 16\,z10^4\,z01\,t\,x11\,c21\,x01 - 8\,z10^3\,z01^2\,t\,c21\,x11 \\
&\quad - 8\,z10^5\,s^2\,c21 + 12\,z10^2\,z01^2\,t\,x01\,z20\,c21 - 6\,z10\,z01^3\,t\,c21\,z20 - 8\,z10^3\,z01^2\,t\,x01\,c11 + 2\,z10^2\,z01^3\,t\,c11 \\
&\quad + 8\,z10^4\,z01\,t\,c11\,x01^2 + 32\,z10^5\,s\,x11\,c21\,x01 - 16\,z10^4\,s\,c21\,z01\,x11 + 8\,z10^4\,s\,c21\,z01 - 16\,z10^4\,s\,z01\,x01\,c11 \\
&\quad + 4\,z10^3\,s\,z01^2\,c11 + 16\,z10^5\,s\,c11\,x01^2 - 32\,z10^4\,s\,x20\,z01\,c21\,x01 + 16\,z10^3\,s\,x20\,z01^2\,c21 - 16\,z10^5\,s\,c21\,x01 \\
&\quad - 12\,z10^2\,s\,c21\,z01^2\,z20)\Big/\left(z10^2\,(-2\,z10\,x01 + z01)^3\right)
\end{aligned}
$$

Figure 6.7: The two jet of one component of r (for illustrative purposes only!).

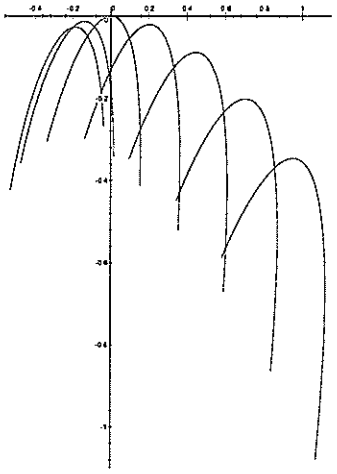

Figure 6.8:

coefficients, thus reducing the double–point space to two dimensions and then looking for the common solution in the remaining equations. On the penultimate page of the MAPLE listing we see the commands

```
s1_poly  =  u10*s+u01*t+u20*s^2+u11*s*t+u02*t^2+
            u30*s^3+u21*s^2*t+u12*s*t^2+u03*t^3
t1_poly  =  v10*s+v01*t+v20*s^2+v11*s*t+v02*t^2+
            v30*s^3+v21*s^2*t+v12*s*t^2+v03*t^3
```

These polynomial substitutions for s_1 and t_1 are substituted in one of the defining equations for the double point space, and then the coefficients `vij` and `uij` are solved iteratively. Once the jet of s_1 and t_1 is calculated it is substituted in the remaining equations of $D^2(\mathbf{r})$ to give the double point curve.

Working at the jet level we examine as far as the three jet of the double–point curve, this is sufficient for determining if the image is a cuspidal cross-cap [MO1].

When we run the MAPLE session MAPLE performs all the relevant integration described in Section 6.5 to obtain the camera motion. The depth formula for λ is calculated and along the frontier it is still defined. Figure 6.9 shows the depth $\lambda(s,t)$ plotted against s for three values of constant t. Note that λ is finite and non-zero.

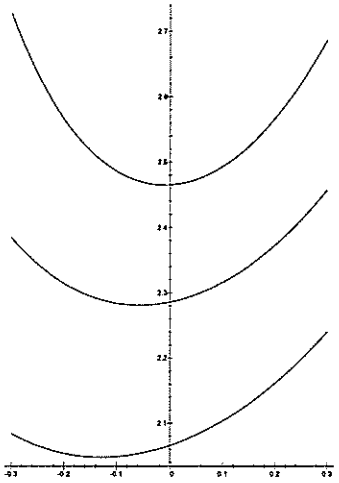

Figure 6.9: The calculated depth λ for three time periods.

At the termination of the MAPLE session in Appendix A MAPLE returns the three jet of the double–point curve. This is a function of just s and t. Recall that the the double–point space is four dimensional with coordinates s, t, s', t' but we have solved for s' and t' leaving an equation in two variables. The MAPLE session in Appendix A is for the case when the frontier curve crosses the singular curve, and we see that the double–point curve is

$$(t + 4s)(22937t + 160s)^2.$$

There are no terms of degree two or less and the double–point curve is branched with a multiple root. This is exactly what we expect for the cuspidal cross cap, where the double root indicates a cusp edge and the other branch is the double–point curve of the cross cap [MO3]. Moreover we can also conclude that it is no worse than a cuspidal cross cap. This is a significant result since this rather general example seems to indicate that when the singular curve and frontier cross a cuspidal cross cap is the result. It also seems that the only barrier to actually proving this is a computational one. MAPLE is extremely sophisticated in its algebraic manipulation but it seems that at present the size of the resulting expressions precludes a complete general proof. So we must satisfy ourselves with the overwhelming circumstantial evidence and conclude with the following hypothesis.

6.6 Conjecture: *In constructing a surface* $\mathbf{r}$ *in the usual way from* $\mathbf{p}(s,t)$ *and* $\mathbf{c}(t)$*, at points where the curves* $\mathbf{c}_t.\mathbf{n} = 0$ *and* $\mathbf{r}_s \| \mathbf{r}_t$ *cross transversely* $\mathbf{r}$ *is a cuspidal cross cap.*

We can of course adapt the MAPLE session from Appendix A to deal with other situations. At points where the frontier curve does not meet the singular curve we expect $\mathbf{r}$ to have a cusp edge. This is supported by previous work concerned with the dual of $\mathbf{r}$ where it was found that in this case the dual is smooth, Proposition 6.3.

Running the MAPLE session where we choose our profiles so that they do not form an envelope and thus $\mathbf{c}_t.\mathbf{n} \neq 0$ and $\mathbf{p}_t.\mathbf{n} \neq 0$, we find that the resulting double–point curve has quadratic terms with a double root. This is expected [MO3] and reflects the fact that in this formulation the cusp edge has multiplicity two in some sense. We conclude therefore that the surface $\mathbf{r}$ is a cusp edge away from the frontier.

We can do some calculations to investigate degeneracies of $\mathbf{r}$. Recall that in the actual case of reconstruction we have the infinite degeneracy where the two sheets are folded flat and doubly cover $\mathbf{r}$. What if the frontier curve is tangent to the singular curve, and so they now share two points in common? We can set up the MAPLE session to allow for this and we find that the double–point curve has no cubic terms indicating a worse singularity than the cuspidal cross cap.

As mentioned in Section 6.1, in the reconstruction case the frontier marks the boundary of $\mathbf{r}$, and the singular curve and frontier are identical. We may perhaps conclude that during reconstruction we are obtaining a cuspidal cross cap at *every* point along the frontier and the double–point curves sweep out a doubly covered surface.

We can also perform the same calculation by adapting the MAPLE code to calculate the double point space for the dual R of the constructed surface $\mathbf{r}$. We were able to do this for the general example and found that when the singular curve $(\mathbf{r}_s \| \mathbf{r}_t)$ and frontier curve $(\mathbf{c}_t.\mathbf{n} = 0)$ cross, the dual also has a cuspidal cross cap. Recall from Proposition 6.3 that the dual is singular along the frontier (we proved in Proposition 6.1 that the frontier for surface construction is a parabolic curve) and smooth along the singular curve of $\mathbf{r}$.

We therefore have a strange self duality. On $\mathbf{r}$ there are two curves of interest, the frontier (though of course in *construction* this is not the envelope of critical sets as normally happens) and the singular curve. The constructed surface has

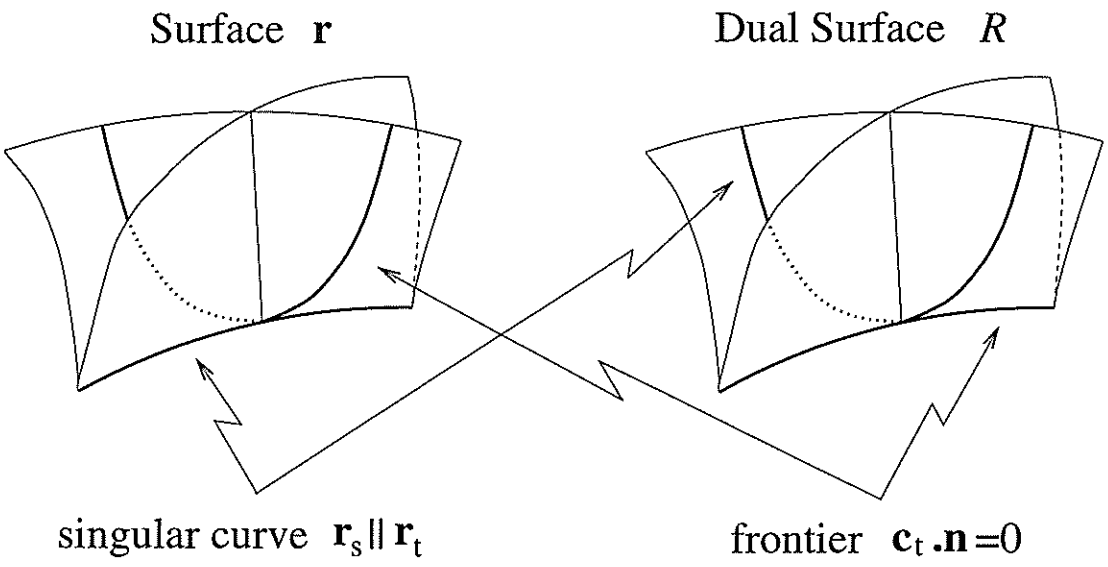

Figure 6.10: Schematic diagram showing the self-duality property described in the text.

a cusp edge along the singular curve and smooth parabolic points along the frontier. Where they cross we find a cuspidal cross cap. On the dual the frontier curve is a cusp edge and the singular curve is smooth on R. Where they cross we get a cuspidal cross cap, see Figure 6.10.

6.6 Conclusion

We set out to investigate what the precise conditions on the profiles $\mathbf{p}$ and camera motion $\mathbf{c}$ were in the case when the critical sets formed a frontier. We constructed an example based on circular camera motion around a sphere, and found that it is not simply sufficient to assume that the profiles formed an envelope. Indeed assuming the existence of a depth $\lambda(s,t)$ satisfying

$$\mathbf{c}_t.\mathbf{n} + \lambda \mathbf{p}_t.\mathbf{n} = 0$$

is not enough to ensure that the surface is a doubly covered surface with boundary.

We found that the singular curve and the frontier somehow became 'detached' in construction, whereas in reconstruction they are identically the same curve.

Some general results were formed for the cases of singular/non-frontier and non-singular/frontier cases. This was helped by an excursion into the dual. For the case of frontier/singular points more sophisticated techniques were used.

From the computer pictures it seemed that at points where the singular curve and frontier crossed the singularity was a cuspidal cross cap. We then implemented a method from D.Mond for finding the double point space. Performing everything at the jet level, as we were required, was a formidable task since our map rapidly increased in complexity. In fact MAPLE was unable to perform the calculations and we had to substitute values for the profiles. The proofs concerning the crossing of the singular curve and the frontier are thus for the 'general example'.

Our initial goal of finding constraints usable in a computer vision context was perhaps overshadowed by the fascinating differential topology and singularity theory that was uncovered. Recent results with K. Åström (not included in this thesis) show that it is possible to write down a complete necessary and sufficient condition for the constructed surface to be a doubly covered surface with boundary, by utilising *discrete* epipolar constraints. These are obtained by using tangent planes defined by camera positions at time instants separated by a finite, rather than infinitesimal, time.

Chapter 7

The Conjugate Curve Congruence.

> These ... are form'd without the Help of Occult Lines, by making use only of the heights and breadths of the Angles.
> *The Fifth Figure* [Poz]

7.1 Introduction.

A curve congruence is a family of curves on a surface, an example of which is the principal curve congruence. We introduce a one parameter family of curve congruences on an oriented surface. This family includes the principal curve congruence and the asymptotic curve congruence.

We consider all directions v in all tangent planes whose conjugate $\overline{v}$ makes a fixed angle angle α with v. The angle α is then the parameter of the family of congruences which we call $\mathcal{C}_\alpha$. Thus the $\alpha = 0$ conjugate curve congruence is simply the asymptotic directions, since it consists of all directions whose conjugate is equal (i.e. has zero angle) with itself. The $\alpha = \pi/2$ conjugate curve congruence is the principal curve congruence.

The second section describes the configuration of curves at a point of the surface for a general conjugate curve congruence. It is found that for a given α up to two conjugate pairs can be seen. For a general angle α we obtain up to two directions which we label light red and light blue. These directions have conjugates which we label dark red and dark blue respectively. Since our surfaces are oriented we can assign a 'sense' to the tangent planes, and so we say that the light directions make an angle α with the dark ones, and the dark ones make

an angle $-\alpha$ with the light ones.

The third section formulates the conjugate curve congruence in the more sophisticated setting of a family of Binary Differential Equations. We use results of Bruce and Tari to provide generic topological pictures. We can view this section as an investigation into how a fixed congruence varies over the surface. The previous section investigates how the congruence changes when we fix a point on the surface and vary α.

The fourth section introduces the spherical image of $\mathcal{C}_\alpha$ and the critical set of this is the fold curves. We have a one-parameter family of fold curves, one for each curve congruence. It is proved that the light red fold curves are the loci of geodesic inflections of the conjugate (dark red) integral curves.

The fifth section introduces the cubic form Γ which is a cubic form on the tangent spaces of our surface, that generalises the classifying cubic form at umbilics. Initially there seems no connection between this and the conjugate curve congruence, but later results concerning the projections of surfaces reveal a surprising relationship.

The sixth section characterises geodesic inflections of the critical set of a parallel projection by means of the singularites of the spherical image of $\mathcal{C}_\alpha$.

The seventh section characterises the geodesic inflections of the critical set of a parallel projection by means of the root directions of Γ. We provide a new characterisation of the subparabolic lines and flecnodal curves of a surface, and show that the envelope of fold curves is the discriminant of Γ.

The eighth and ninth section investigates the zeros of $\mathcal{C}_\alpha$, including the saddle node and Morse discriminant bifurcation, and introduces the umbilical cords of a surface.

7.1.1 Conjugacy

We now give a short review of conjugate directions in the context of surface shape.

Eisenhart defines conjugacy in terms of the Dupin Indicatrix. This is a conic defined at each point of the surface by taking the locus of points $\mathbf{t}$ on the tangent plane for which $\frac{1}{2}II(\mathbf{t},\mathbf{t})$ is equal to plus or minus one, where II is the

second fundamental form [K, p.229]. As observed in [E, p.125] one can think of Dupin's Indicatrix as the curve one obtains by slicing the surface very close to a point p with a plane perpendicular to the normal at p. Elliptic points give an elliptical indicatrix, hyperbolic points hyperbolas, and at a parabolic point the conic degenerates into two parallel straight lines. The umbilic has a circular indicatrix. Classically one would then consider conjugate directions in the sense of conjugate directions to the conic. Thus if $\mathbf{a}$ and $\mathbf{b}$ are directions in the tangent plane passing through the origin of the conic, then these are conjugate iff they are conjugate diameters of the indicatrix [K, p.230].

It is straightforward to see that for an elliptical point there is a direction $\mathbf{v}$ whose conjugate makes a minimal angle with $\mathbf{v}$ and for a hyperbolic point these are the asymptotes, and the angle is zero.

Another result concerning conjugacy is that the characteristic [BG, p.102] of a one parameter family of tangent planes along a curve σ through a point p is conjugate to the tangent to σ at p. One often sees this construction in the proofs in old geometry books.

In the following we say that $\mathbf{v}$ and $\mathbf{w}$ are conjugate iff $II(\mathbf{v},\mathbf{w}) = II(\mathbf{w},\mathbf{v}) = 0$ or in terms of the shape operator S, $S(\mathbf{v}).\mathbf{w} = \mathbf{v}.S(\mathbf{w}) = 0$.

7.2 Preliminary Results.

Since we only consider oriented surfaces, we can assign a sign to angles in the tangent space.

7.1 Definition.

1. *If $v \in T_pM$ then we write $\overline{v} \in T_pM$ for the conjugate vector to v with respect to the second fundamental form, i.e. a vector satisfying $II_p(v,\overline{v}) = 0$. Note that $\overline{v}$ is only well defined upto multiplication by a non zero factor, and that in the case when v is an asymptotic direction at a parabolic point any vector is conjugate to v.*

2. *Define the the real valued function Θ on the tangent bundle TM (strictly the projectivised bundle),*

$$\Theta$$

$$\begin{aligned} TM &\to [-1,1] \\ p, v &\mapsto \sin\alpha \end{aligned}$$

where α denotes the positive angle in $[0, \pi/2]$ between v and $\overline{v}$. Again we note that Θ is ill defined at points of the tangent bundle corresponding to asymptotic directions at parabolic points.

3. *The* **conjugate curve congruence** *for a fixed α is the set $\Theta^{-1}(\sin\alpha)$ which we denote $\mathcal{C}_\alpha$. The conjugate directions to $\mathcal{C}_\alpha$ are $\mathcal{C}_{-\alpha}$.*

Notes on the Definition. Observe that $\Theta^{-1}(1)$ gives all the principal directions and $\Theta^{-1}(0)$ gives all the asymptotic directions. For a general angle α, $\Theta^{-1}(\alpha)$ gives up to two directions at each point on the surface. Thus there are different 'flavours' or 'colours' of direction at a point for any α. This is analogous to there being two colours of principal direction at a point. Given a vector $v \in T_pM$ we can find the whole conjugate curve congruence that has v as a member by taking $\Theta^{-1}(\Theta(v))$. Also note that $\Theta^{-1}(\alpha)$ is defined for all α and contains the asymptotic directions at parabolic points for any α.

The following lemma gives a useful expression for the above map Θ.

7.2 Lemma: *For any $v \in T_pM$ of unit length (that is not asymptotic at a parabolic point) and its unique conjugate $\overline{v}$ let α be the positive angle between v and $\overline{v}$. We have*

$$\sin\alpha = \frac{S_p(v).v}{\|S_p(v)\|}$$

where S_p is the shape operator at the point p.

Proof: Let e_1 and e_2 be the two principal directions and let $v = \cos\theta e_1 + \sin\theta e_2$. Then it is easy to see that the conjugate is $\overline{v} = \kappa_2 \sin\theta e_1 + \kappa_1 \cos\theta e_2$ where κ_1 and κ_2 are principal curvatures. Now we have,

$$\begin{aligned} \|v \wedge \overline{v}\| &= \|\overline{v}\| \sin\alpha \\ &= \sin\alpha . \sqrt{\kappa_2^2 \sin^2\theta + \kappa_1^2 \cos^2\theta} \end{aligned}$$

Calculation also reveals that $v \wedge \overline{v} = (0, 0, \kappa_1 \cos^2\theta + \kappa_2 \sin^2\theta)$, and so,

$$\sin\alpha = \frac{\kappa_1 \cos^2\theta + \kappa_2 \sin^2\theta}{\sqrt{\kappa_2^2 \sin^2\theta + \kappa_1^2 \cos^2\theta}}. \tag{7.1}$$

A short calculation gives,

$$\frac{S_p(v).v}{\|S_p(v)\|} = \frac{\kappa_1 \cos^2\theta + \kappa_2 \sin^2\theta}{\sqrt{\kappa_2 \sin^2\theta + \kappa_1^2 \cos^2\theta}}$$

which is the same as (7.1). □

We now examine the fibres of the map Θ that give the individual conjugate curve congruences. We are interested in the local picture, namely the number and directions of curves in a tangent plane, and the local topological pictures of the curves in the vicinity of a point. We first examine the congruence in a tangent plane.

7.3 Lemma: *If the tangent directions v in T_pM are parametrised by the angle $\theta \in [-\pi, \pi]$ between v and a principal direction then the restriction of Θ to a point p of our surface can be written,*

$$\Theta(p, v(\theta)) = \frac{\kappa_1 + (\kappa_2 - \kappa_1)\sin^2\theta}{\sqrt{\kappa_1^2 + (\kappa_2^2 - \kappa_1^2)\sin^2\theta}}.$$

where κ_1 and κ_2 are principal curvatures in T_pM.

Proof: Construct local coordinates where the principal directions are $(1,0)$ and $(0,1)$, and $v = (\cos\theta, \sin\theta)$. Then using Lemma 7.2 it is easy to verify the result. □

Notes on the lemma.

- The level sets (where the target is in $[-1,1]$) of this function $\Theta(p,\cdot)$ give us the values of θ (i.e. tangent vectors) where the conjugate vector $\overline{v}$ makes a fixed angle with $v(\theta)$.
- Observe that at an umbilic the function Θ becomes ± 1 and every direction has the angle $\pi/2$ with its conjugate, i.e. every direction is principal.

We wish to examine the level sets of $\Theta(p,\cdot)$, and in order to sketch the function we note some elementary facts.

7.4 Lemma:

- $\Theta(p, v(\theta))$ *has period* π.

- *If p is not an umbilic then the only values of θ for which $\Theta(p, v(\theta)) = \pm 1$ are $\theta = 0, \pi/2, \pi \ mod\ \pi/2$.*
- *If p is not an umbilic then the only turning points of $\Theta(p, -)$ occur at $\theta = 0, \pi/2, \pi$ and when p is an elliptic point, $\sin^2\theta = \frac{\kappa_1}{\kappa_1+\kappa_2}$.*

Proof: Clearly Θ has period π since $\sin^2$ has.

The function is ± 1 when

$$(\kappa_1 + (\kappa_2 - \kappa_1)\sin^2\theta))^2 = \kappa_1^2 + (\kappa_2^2 - \kappa_1^2)\sin^2\theta,$$

i.e. when $\kappa_2 = \kappa_1$ or $\sin^2\theta = 1$ or $\sin\theta = 0$. This gives the required result.

To find the turning points we differentiate and obtain the result. For $\sin^2\theta = \frac{\kappa_1}{\kappa_1+\kappa_2}$ we have

$$0 \leq \frac{\kappa_1}{\kappa_1 + \kappa_2} \leq 1$$

and consider two cases.

(a) $\kappa_1 + \kappa_2 < 0$ so $0 \geq \kappa_1 \geq \kappa_1 + \kappa_2$ and $\kappa_2 \leq 0$ and p is elliptic.

(b) $\kappa_1 + \kappa_2 > 0$ so $0 \leq \kappa_1 \leq \kappa_1 + \kappa_2$ and $\kappa_2 \geq 0$ and p is elliptic. □

7.2.1 Hyperbolic Points.

The following diagram shows the function $\Theta(p, v(\theta))$ and $-\Theta(p, v(\theta))$ (left hand side) for a hyperbolic region of the surface with the accompanying sketches of the vectors in the tangent plane (right hand side). We see that for $\Theta = 1$ the resulting vectors are the principal directions e_1 and e_2. For $\Theta = 0$ we capture the asymptotic directions.

When Θ takes a value in $(0, 1)$ we obtain four directions, or two conjugate pairs. We can label these pairs, a blue pair and a red pair. (In the absence of colour diagrams they are represented by black lines for one pair, and grey lines for the other pair.) Within the pair we can have a light and a dark colour. Then light is conjugate to dark. Between the red pair there is an asymptotic direction (shown dotted) and the same between the blue pair.

For the asymptotic directions we see that the light and dark directions of the same colour have come together to make a self conjugate direction. In the

case of the principal directions the two light and two dark directions have come together.

Conclusion. For hyperbolic points we expect the conjugate curve congruence $\mathcal{C}_\alpha$ and $\mathcal{C}_{-\alpha}$ to have two directions for an angle 0 or $\pi/2$, and four directions otherwise.

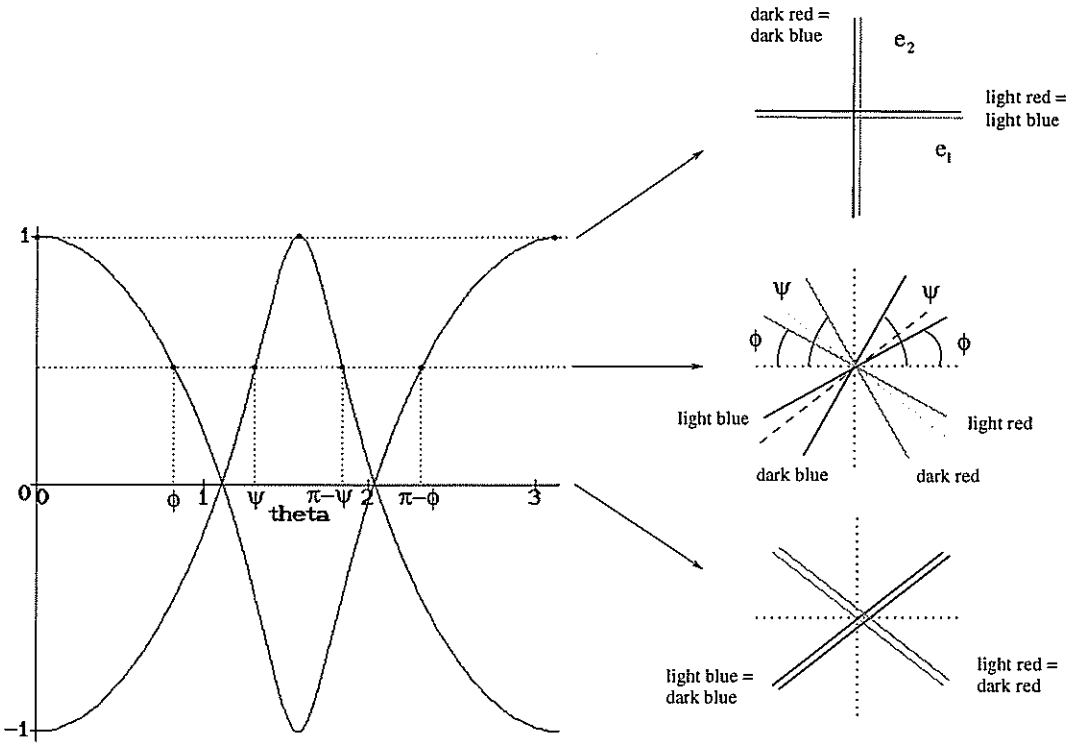

7.2.2 Elliptic Points.

The following diagram shows the function $\Theta(p, v(\theta))$ and $-\Theta(p, v(\theta))$(left hand side) for an elliptic region of the surface with the accompanying sketches of the vectors in the tangent plane (right hand side). We see that for $\Theta = 1$ the resulting vectors are the principal directions e_1 and e_2. For $\Theta = 0$ there are no solutions, indicating that there are no asymptotic directions on an elliptic patch.

When Θ takes a value in (0,1) we see that there are either no solutions, corresponding to no vectors v having the property that the angle they make with their conjugate $\overline{v}$ is the required angle, two solutions or four solutions.

It can be shown that the condition for Θ to have a repeated solution on an elliptic patch is that $\Theta(p, v(\theta)) = \frac{2\sqrt{\kappa_1\kappa_2}}{\kappa_1+\kappa_2}$ i.e. $\sin\alpha = \frac{\sqrt{K}}{H}$. So for some given fixed angle we expect a curve of solutions on the surface, since this is one condition. Thus the elliptic part is split into two regions of four solutions (two conjugate pairs) and zero solutions, for our curve congruence. We will see later that when we formulate $\mathcal{C}_\alpha$ as a binary differential equation this curve will be the discriminant (7.8).

For the four solutions, we have a blue and a red conjugate pair as before, and we can label the members of the pair light and dark. The dotted lines between the blue and red lines are the directions they converge to when the four directions become two, shown in the diagram below it. Unlike the hyperbolic case the coincident directions are not self conjugate, they are of different colours.

Conclusion. For elliptic points for we expect the surface to be divided into two regions separated by a discriminant curve (possibly singular), with each point contributing two directions to the curve congruence in one region, one direction on the discriminant and no directions in the other region.

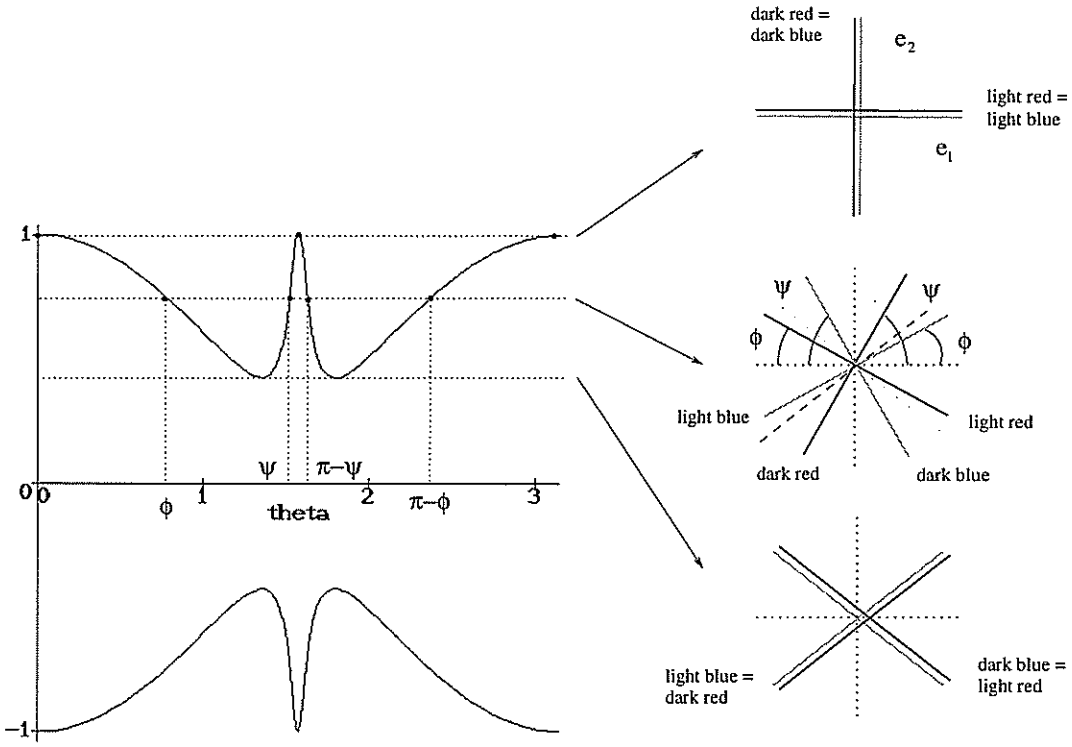

7.2.3 Parabolic Points.

At parabolic points for a generic surface there is one asymptotic direction and two principal directions. We discount flat umbilics as non generic in the surfaces we consider.

The following diagrams show the configurations of directions we expect at parabolic points in our family of conjugate curve congruences. The asymptotic direction has been taken as the x-axis, that is $\theta = 0$. For $\Theta = 1$ we have picked out the principal direction with non zero curvature. This is conjugate with the asymptotic direction. It is impossible to say what angle the asymptotic direction makes with its conjugate since it is conjugate to *every* direction.

For $\Theta = 0$ we find that the unique asymptotic direction is the only direction that is coincident with its conjugate, as expected.

We then get just one pair of conjugate directions for all other angles.

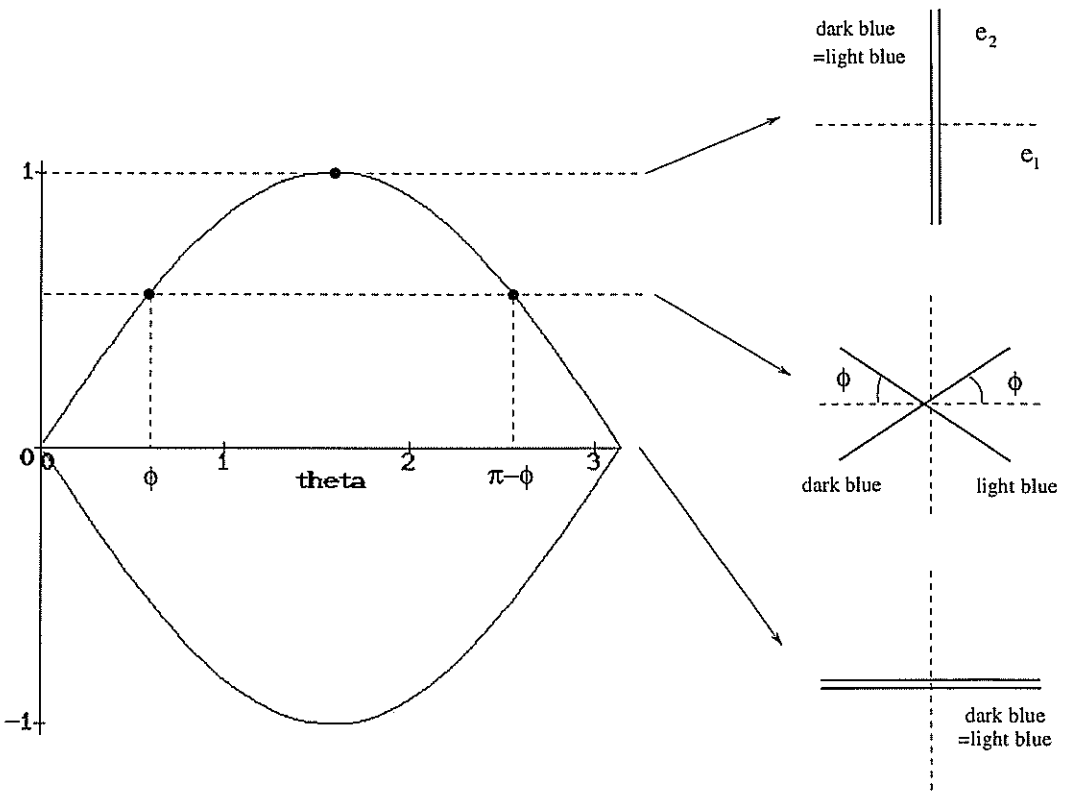

7.2.4 Umbilics.

For the umbilic we see that Θ is constant, and the conjugate curve congruence is empty for all angles except $\pi/2$, where all directions make an angle $\pi/2$ with their conjugate, as expected.

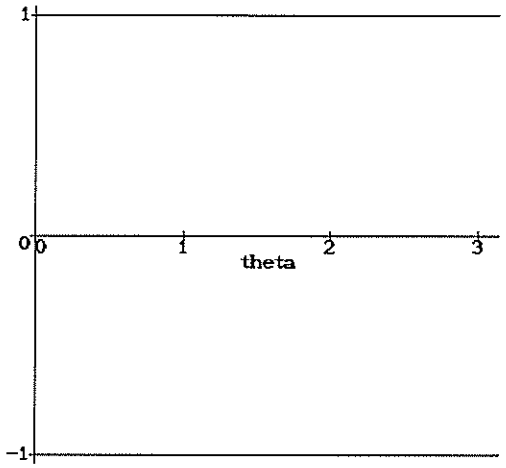

7.3 $\mathcal{C}_\alpha$ As A Binary Differential Equation.

In this section we consider our family of congruences $\mathcal{C}_\alpha$ as a family of binary differential equations (BDEs). Much work has been done on these objects [BF], [D], [BT1], [BT2] and we seek to apply some of the results to provide generic pictures of the family of integral curves and discriminants.

We consider BDEs of the form

$$a(x,y,\alpha)dy^2 + 2b(x,y,\alpha)dydx + c(x,y,\alpha)dx^2 = 0$$

where we think of α as the parameter of our family. The discriminant for some α is $b^2 - ac = 0$. Figure 7.1 shows the family $\mathcal{C}_\alpha$ for some example surface. In this section a, b and c always refer to the coefficients of the BDE.

We establish some notation.

7.5 Definition: *The* **discriminant** $b^2 - ac = 0$ *of the congruence* $\mathcal{C}_\alpha$ *is denoted* $\Delta(\mathcal{C}_\alpha)$.

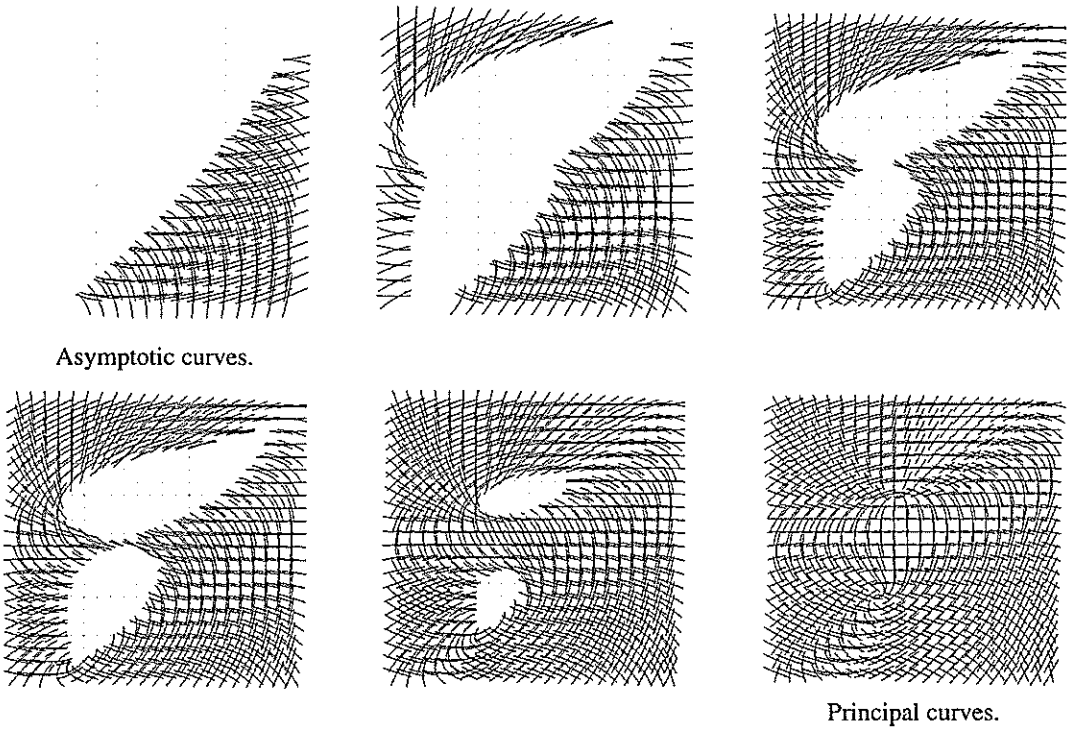

Figure 7.1: Integral curves of C_α with increasing α left to right. The figure includes many features that will be discussed later in the text.

We now establish the form of the BDE for a surface in Monge form.

7.6 Proposition:

For a surface in Monge form $(x, y, h(x, y))$ with E, F, G, l, m and n the usual coefficients of the first and second fundamental form we can write $\mathcal{C}_\alpha$ as,

$$\begin{aligned} dy^2(\sin\alpha(Gm - Fn) - n\sqrt{1 + h_x^2 + h_y^2}\cos\alpha) + \\ dydx(\sin\alpha(Gl - En) - 2m\sqrt{1 + h_x^2 + h_y^2}\cos\alpha) + \\ dx^2(\sin\alpha(Fl - Em) - l\sqrt{1 + h_x^2 + h_y^2}\cos\alpha) = 0. \end{aligned}$$

Proof: Let S be the shape operator, $\mathbf{r}(x, y) = (x, y, h(x, y))$ and,

$$\begin{aligned} l = S(\mathbf{r}_x).\mathbf{r}_x \quad E = \mathbf{r}_x.\mathbf{r}_x \\ m = S(\mathbf{r}_x).\mathbf{r}_y \quad F = \mathbf{r}_x.\mathbf{r}_y \\ n = S(\mathbf{r}_y).\mathbf{r}_y \quad G = \mathbf{r}_y.\mathbf{r}_y. \end{aligned}$$

Let v be a tangent vector. We let $v = (1, b)$ which means $v \equiv \mathbf{r}_x + b\mathbf{r}_y$. Since S is linear we have,

$$\begin{aligned} S(v).\mathbf{r}_x &= S(\mathbf{r}_x).\mathbf{r}_x + bS(\mathbf{r}_y).\mathbf{r}_x = l + bm \\ S(v).\mathbf{r}_y &= S(\mathbf{r}_x).\mathbf{r}_y + bS(\mathbf{r}_y).\mathbf{r}_y = m + bn. \end{aligned}$$

Define $A_1 = S(v).\mathbf{r}_x$ and $A_2 = S(v).\mathbf{r}_y$ and note well that we can not conclude that $S(v) = (A_1, A_1)$ since the Monge parametrisation is not orthonormal at every point on the surface.

Now for some s_1 and s_2 let $S(v) = (s_1, s_2)$ and perform the following,

$$\begin{aligned} S(v).\mathbf{r}_x &= s_1E + s_2F = A_1 \\ S(v).\mathbf{r}_y &= s_1F + s_2G = A_2. \end{aligned}$$

We can solve the above for s_1 and s_2 to get,

$$\begin{aligned} S(v) &= \frac{1}{EG - F^2}(A_1G - A_2F, A_2E - A_1F) \\ &= \frac{1}{EG - F^2}((l + bm)G - (m + bn)F, (m + bn)E - (l + bm)F). \end{aligned}$$

We will require $S(v).v$ which is,

$$\begin{aligned} S(v).v &= S(v).\mathbf{r}_x + bS(v).\mathbf{r}_y \\ &= A_1 + bA_2. \end{aligned}$$

Now if α is the (signed) angle between v and $\overline{v}$ then recall from (7.2) that,

$$\sin\alpha = \frac{S(v).v}{\|v\|\|S(v)\|}, \quad \cos\alpha = \frac{v.\overline{v}}{\|v\|\|\overline{v}\|}.$$

Since $S(v)$ and $\overline{v}$ are orthogonal then if u is normal to the surface we can write $\overline{v} = S(v) \times u$ and

$$\|\overline{v}\| = \|S(v)\|\|u\|. \tag{7.2}$$

So we have,

$$\cos\alpha = \frac{\overline{v}.v}{\|\overline{v}\|\|v\|} = \frac{S(v) \wedge u.v}{\|S(v)\|\|u\|\|v\|},$$

and

$$\sin\alpha = \frac{S(v).v}{\|S(v)\|\|v\|},$$

using (7.2) giving,

$$\tan\alpha = \frac{\|u\|S(v).v}{[S(v),u,v]}. \tag{7.3}$$

We can interpret our vectors in Monge form,

$$\begin{aligned} v &= (1,b) \equiv (1,b,h_x + bh_y) \\ u &= (h_x, h_y, -1) \\ S(v) &\equiv (s_1, s_2, s_1h_x + s_2h_y). \end{aligned}$$

Calculation reveals that $[v, S(v), u] = (bs_1 - s_2)(1 + h_x^2 + h_y^2)$. We can now expand (7.3) to get,

$$\begin{aligned} & [v,S(v),u]\sin\alpha = \|u\|S(v).v\cos\alpha \\ i.e. \quad & (bs_1 - s_2)(1 + h_x^2 + h_y^2)\sin\alpha = \\ & \sqrt{1 + h_x^2 + h_y^2}(A_1 + bA_2)\cos\alpha \\ i.e. \quad & (bA_1G - bA_2F - A_2E + A_1F)\sqrt{1 + h_x^2 + h_y^2}\sin\alpha = \\ & (A_1 + bA_2)(EG - F^2)\cos\alpha \\ i.e. \quad & (bG(l + bm) - bF(m + bn) - (m + bn)E + (l + bm)F)\sin\alpha = \\ & (l + 2bm + b^2n)\sqrt{1 + h_x^2 + h_y^2}\cos\alpha, \end{aligned}$$

where the last equivalence is got by noting that in Monge form $EG - F^2 = \|u\|^2$. We can now expand this to get a quadratic in b and $b = dy/dx$,

$$\begin{aligned} & b^2(\sin\alpha(Gm - Fn) - n\sqrt{1 + h_x^2 + h_y^2}\cos\alpha) + \\ & b(\sin\alpha(Gl - En) - 2m\sqrt{1 +_x^2 +h_y^2}\cos\alpha) + \\ & \sin\alpha(Fl - Em) - l\sqrt{1 + h_x^2 + h_y^2}\cos\alpha = 0. \end{aligned}$$

This completes the proof. □

Things are considerably simplified if we adopt a very special parametrisation of the surface; namely parametrising by the principal curves (away from umbilics).

7.7 Lemma: *If $\kappa_p(x,y)$ and $\kappa_q(x,y)$ are the principal curvatures at a non-umbilical point of the surface and we adopt a parametrisation away from umbilics where x-constant and y-constant curves are principal curves, then we can write the family $\mathcal{C}_\alpha$ as,*

$$\kappa_q \cos\alpha dy^2 + (\kappa_q - \kappa_p)\sin\alpha dy dx + \kappa_p \cos\alpha dx^2 = 0.$$

Proof: For this parametrisation we have the following identities,

$$\begin{aligned} l &= \kappa_p \quad E = 1 \\ m &= 0 \quad F = 0 \\ n &= \kappa_q \quad G = 1. \end{aligned}$$

If we write $v = (\gamma, \beta)$ then $S(v) = (\gamma l, \beta n)$, $\overline{v} = (-\beta n, \gamma l)$, so $\|S(v)\| = \|\overline{v}\|$. Calculation reveals that,

$$\begin{aligned} S(v).v &= \gamma^2 l + \beta^2 n \\ \overline{v}.v &= -\gamma\beta n + \gamma\beta l. \end{aligned}$$

If α is the angle between v and $\overline{v}$ then as usual we have ,

$$\sin\alpha = \frac{S(v).v}{\|S(v)\|\|v\|}, \quad \cos\alpha = \frac{v.\overline{v}}{\|\overline{v}\|\|v\|},$$

and since $\|S(v)\| = \|\overline{v}\|$ we have,

$$\sin\alpha(\gamma\beta(l-n)) = \cos\alpha(\gamma^2 l + \beta^2 n)$$

and making the substitutions for l, n we have the family of BDEs,

$$\kappa_q \cos\alpha dy^2 + (\kappa_q - \kappa_p)\sin\alpha dy dx + \kappa_p \cos\alpha dx^2 = 0.$$

□

A straightforward calculation gives the following corollary.

7.8 Corollary: *The discriminant of the family is given by*

$$H^2 \sin^2 \alpha - K = 0$$

where K is the Gauss curvature and H is the mean curvature.

Notes on Corollary:

- Thus we see that all the discriminant curves of our BDE family occur in the elliptic region of the surface.
- The mean curvature H is never zero on the discriminant curves by the previous note.
- When $\alpha = 0$, $\Delta(\mathcal{C}_\alpha)$ is the parabolic curve.
- When $\alpha = \pi/2$, $\Delta(\mathcal{C}_\alpha)$ consists of the umbilic points.

We wish to calculate the condition in Monge form for our discriminant to be singular. First we expand the coefficients a, b, c of the BDE in terms of the coefficients in the Monge expansion of the surface.

7.9 Lemma: *If our surface is given as the graph, $h = (1/2)(a_0x^2 + 2a_1xy + a_2y^2) + (1/6)(b_0x^3 + 3b_1x^2y + 3b_2xy^2 + b_3y^3) + \cdots$ then the linear and constant parts of the coefficients a, b, c of the BDE are,*

$$\begin{aligned}
a &= a_1 \sin\alpha - a_2 \cos\alpha + (b_1 \sin\alpha - b_2 \cos\alpha)x + (b_2 \sin\alpha - b_3 \cos\alpha)y \\
b &= (1/2)\sin\alpha(a_0 - a_2) - a_1 \cos\alpha + ((1/2)\sin\alpha(b_0 - b_2) - b_1 \cos\alpha)x + \\
&\quad ((1/2)\sin\alpha(b_1 - b_3) - b_2 \cos\alpha)y \\
c &= -a_1 \sin\alpha - a_0 \cos\alpha - (b_1 \sin\alpha + b_0 \cos\alpha)x - (b_2 \sin\alpha + b_1 \cos\alpha)y
\end{aligned}$$

Proof: With the Monge parametrisation we have,

$$\begin{aligned}
l &= a_0 + b_0x + b_1y + \cdots & E &= 1 + O(2) \\
m &= a_1 + b_1x + b_2y + \cdots & F &= O(2) \\
n &= a_2 + b_2x + b_3y + \cdots & G &= 1 + O(2).
\end{aligned}$$

We then just expand the coefficients from Proposition 7.6 to get the result. □

We use the previous lemma in the proof of the following lemma.

7.10 Lemma: *If our surface is given in the following Monge form with diagonalised quadratic part*

$$h = (1/2)(a_0x^2 + a_2y^2) + (1/6)(b_0x^3 + 3b_1x^2y + 3b_2xy^2 + b_3y^3) + \cdots,$$

then provided $a_0 \neq a_2$ *the direction of the normal to* $\Delta(\mathcal{C}_\alpha)$ *at the origin is*

$$(a_0b_2 - a_2b_0, a_0b_3 - a_2b_1),$$

and the condition for the origin to be a singular point of $\Delta(\mathcal{C}_\alpha)$ *is,*

$$\begin{aligned} \sin^2\alpha &= \tfrac{4a_0a_2}{(a_0+a_2)^2}, \\ a_0b_2 - a_2b_0 &= 0, \\ a_0b_3 - a_2b_1 &= 0. \end{aligned}$$

If the point is an umbilic and $\sin\alpha = \pm 1$ *then the discriminant is always singular at the origin.*

Proof: Calculate the linear and constant part of $b^2 - ac$ from the expansions in the previous lemma,

$$\begin{aligned} b^2 - ac \;=\; & \frac{\sin^2\alpha}{4}(a_0 + a_2)^2 - a_0a_2 + \\ & \left(\frac{\sin^2\alpha}{2}(a_0b_0 + a_0b_2 + a_2b_0 + a_2b_2) - a_0b_2 - a_2b_0\right)x + \\ & \left(\frac{\sin^2\alpha}{2}(a_2b_1 + a_2b_3 + a_0b_1 + a_0b_3) - a_0b_3 - a_2b_1\right)y + \cdots. \end{aligned}$$

Since the region is elliptic a_0 and a_2 are the same sign and never both zero so $a_0 + a_2 \neq 0$ and so substituting $\sin^2\alpha = \frac{4a_0a_2}{(a_0+a_2)^2}$ gives

$$b^2 - ac = \frac{(a_2 - a_0)}{a_0 + a_2}(a_0b_2 - a_2b_0)x + \frac{(a_2 - a_0)}{a_0 + a_2}(a_0b_3 - a_2b_1)y + \cdots,$$

hence result. □

Note on the Lemma: It is helpful to think of the discriminant $\sin^2\alpha = K/H^2$ as a surface in x, y, α space. Then the set of discriminant curves arise as level sets of this (generically) smooth surface. Figure 7.2 shows some discriminant curves for the family $\mathcal{C}_\alpha$ for an elliptic island in a hyperbolic sea, with one umbilic.

We have a one parameter family of BDEs and the previous lemma indicates that there are three conditions on the coefficients for a singular discriminant.

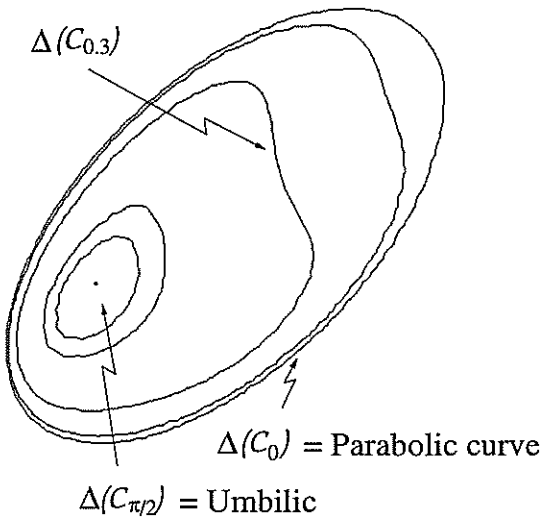

Figure 7.2: Some discriminant curves shown for an elliptic island with an umbilic in a hyperbolic sea.

For a generic surface we expect there to be isolated singularities in the family of discriminants. We also assume in the subsequent work that the singularites will be no worse than Morse. Since a non-Morse singularity would impose another condition we do not expect this to be satisfied in general. The condition for $\Delta(\mathcal{C}_\alpha)$ to be worse than Morse is extremely complicated.

7.3.1 One Parameter Families of BDEs

We have shown how the family $\mathcal{C}_\alpha$ can be considered as a one parameter family of binary differential equations. In this subsection we provide a short synopsis of the results in [BT2].

The paper [BT2] considers generic 1-parameter families of BDEs of the form

$$a(x,y,t)dy^2 + 2b(x,y,t)dydx + c(x,y,t)dx^2 = 0 \tag{7.4}$$

where the discriminant $b^2 - ac = 0$ has a Morse singularity at $t = 0$ and all the coefficients a, b and c vanish. The local topological classification of solution curves of BDEs of Morse type is given in [BT1]. This follows earlier work in [BF], and Davydov classified generic bivalued fields when the discriminant is smooth

[D].

For the family $\mathcal{C}_\alpha$ we observe that the discriminant undergoes Morse transitions where not all the coefficients of the BDE are zero. We expect this to happen for some α, with $0 < \alpha < \pi/2$. In this case it is not possible to apply the results of [BT1]. Consider the BDE

$$dy^2 + xydx^2 = 0,$$

the coefficients 1 and xy are not all zero but the discriminant $xy = 0$ is Morse. We can not use the results in [BT1] in this case.

We can however apply the results of [BT2] for when $\alpha = \pi/2$ and the discriminant is an umbilic. In this case we have some conditions to check and then we can use the pictures to give us the topological configuration of $\mathcal{C}_\alpha$ at an umbilic. The notion of fibre topological equivalence for families of bivalued vector fields is used in [BT2]. Two configurations are topologically equivalent if there is a homeomorphism of the plane taking one set of integral curves to the other. Two one parameter families of such configurations X_t and Y_s are called topologically equivalent if there exists a homeomorphism $s = \phi(t)$ between the parameter space and a family of homeomorphisms h_t of $\mathbf{R}^2$ depending on the parameter t such that for all t, h_t is a topological equivalence between X_t and $Y_{\phi(t)}$.

We now outline the conditions that are required. The results of [BT2] are only valid for families of BDEs that satisfy a so called 'versality condition'. We reproduce this here.

7.11 Proposition: *[BT2] We denote by $a_1x + a_2y + l_1t$, $b_1x + b_2y + l_2t$ and $c_1x + c_2y + l_3t$ the linear parts of a, b and c respectively. The 1-jet of equation (7.4) can be reduced to*

$$(y + t)dy^2 + 2(b_1x + b_2y)dydx \pm ydx^2$$

(with a new pair b_1, b_2) if the following 'versality condition' is satisfied

$$\begin{vmatrix} a_1 & a_2 & l_1 \\ b_1 & b_2 & l_2 \\ c_1 & c_2 & l_3 \end{vmatrix} \neq 0.$$

Our first job is therefore to verify this for $\mathcal{C}_\alpha$ at an umbilic, which is accomplished in the next subsection.

In [BT2] the BDE is lifted on to a doubly covered surface $F = 0$, where $F = ap^2 + 2bp + c$, and the lift ξ is

$$\xi = F_p \frac{\partial}{\partial x} + pF_p \frac{\partial}{\partial y} - (F_x + pF_y)\frac{\partial}{\partial p}.$$

It is then assumed that the cubic

$$\begin{aligned} \phi(p) &= (F_x + pF_y)(0,0,0,p) \\ &= a_2p^3 + (2b_2 + a_1)p^2 + (2b_1 + c_2)p + c_1 \end{aligned}$$

giving the zeros of the field $\xi_0 = \xi(x, y, 0, p)$ has no repeated roots and that the eigenvalues of these singularities are non-zero [BT2]. In the following subsection we calculate ϕ for $\mathcal{C}_\alpha$.

The theorem that we will require from [BT2] is the following

7.12 Theorem: *[BT2] Suppose that the family of BDEs is of Morse type at $t = 0$, the cubic ϕ has no repeated roots, the zeros of ξ_0 are normal and the family satisfies the versality condition above. Then the family is (fibre) topologically equivalent to one of the following normal forms.*

I. Δ_0 is an isolated point:

(a)	*Lemon (1 saddle)*	$(y+t)dy^2 + 2xdydx - ydx^2 = 0$
(b)	*Star (3 saddles)*	$(y+t)dy^2 - 2xdydx - ydx^2 = 0$
(c)	*Monstar (2 saddles +1 node)*	$(y+t)dy^2 + \frac{1}{2}xdydx - ydx^2 = 0.$

(Normality is a technical condition on eigenvalues of the zeros of a vector field that holds for "most" fields.) There are also results in [BT2] for when the discriminant is a crossing that we have not reproduced here.

In the next subsection we show that $\mathcal{C}_\alpha$ generically satisfies the hypotheses of the previous theorem at an umbilic.

7.3.2 $\mathcal{C}_\alpha$ At An Umbilic

Assuming then that $\Delta(\mathcal{C}_\alpha)$ is of Morse type we expect it either to be an isolated point or the transverse crossing of two curves. In the case of an umbilic we present a lemma that tells us that $\Delta(\mathcal{C}_{\pi/2})$ is (unsurprisingly) an isolated point. First we will need the conditions given in the following lemma for when an umbilic is degenerate. The umbilic can be degenerate in essentially two ways, either it is a non-versally unfolded D_4 of the distance squared function or is worse than a D_4.

7.13 Lemma: *Write our surface in Monge form at the origin with height function,*

$$h(x,y) = (\kappa/2)(x^2+y^2) + (1/6)(b_0x^3 + 3b_1x^2y + 3b_2xy^2 + b_3y^3) + \cdots$$

then the origin is a versally unfolded D_4 of the distance squared function iff the following hold

$$\text{The cubic } b_0x^3 + 3b_1x^2y + 3b_2xy^2 + b_3y^3 \text{ is non degenerate}$$
$$b_1b_3 - b_2^2 + b_0b_2 - b_1^2 \neq 0.$$

Proof:

The family of distance squared functions on our surface is

$$F(x,y,\mathbf{a}) = (x-a_1)^2 + (y-a_2)^2 + (h - a_3 - \frac{1}{2\kappa})^2 - \frac{1}{2\kappa}.$$

If we let $f = F(x,y,\mathbf{0})$ then

$$f = \frac{-1}{3\kappa}(b_0x^3 + 3b_1x^2y + 3b_2xy^2 + b_3y^3) + \cdots.$$

We see that f is at least a D_4, and worse if this cubic form degenerates.

We now wish to unfold the D_4 in our family F. Recall that in checking versal unfolding it is sufficient to work at the jet level and in the case of a D_4 we can work to the three level. It just becomes a matter of linear algebra. For functions we require $\frac{\partial F}{\partial a_i}(x,y,\mathbf{0})$ to span the real vector space,

$$\frac{\mathcal{E}(x,y)}{\mathcal{E}(x,y)\langle \partial f/\partial x, \partial f/\partial y\rangle}$$

equivalently,

$$\mathbf{R} + \mathcal{E}(x,y)\langle \partial f/\partial x, \partial f/\partial y\rangle + \mathbf{R}\langle \partial F/\partial a_i\rangle = \mathcal{E}(x,y).$$

We now perform some calculations to obtain the following,

$$\begin{aligned}
\frac{\partial F}{\partial a_1} &= -2x \\
\frac{\partial F}{\partial a_2} &= -2y \\
\frac{\partial F}{\partial a_3} &= \frac{2}{\kappa} - 2h \\
\frac{\partial f}{\partial x} &= \frac{-1}{\kappa}(b_0x^2 + 2b_1xy + b_2y^2) + \cdots \\
\frac{\partial f}{\partial y} &= \frac{-1}{\kappa}(b_1x^2 + 2b2xy + b_3y^2) + \cdots,
\end{aligned}$$

We can get four cubics (ignoring higher terms) by taking xf_x, yf_x, xf_y, yf_y, and then calculate the condition for us to obtain all cubic monomials. This is equivalent to the non-vanishing of the following jacobian,

$$\begin{vmatrix} b_0 & 2b_1 & b_2 & 0 \\ b_1 & 2b_2 & b_3 & 0 \\ 0 & b_0 & 2b_1 & b_2 \\ 0 & b_1 & 2b_2 & b_3 \end{vmatrix} = 6b_0b_1b_2b_3 - 4b_0b_2^3 - b_0^2b_3^2 - 4b_1^3b_3 + 3b_1^2b_2^2.$$

Observe that $\mathcal{E}J_f \supset \mathbb{I}_2^2$ so there is no need to consider the cubic parts. It remains to check the quadratic parts.

Ignoring the constant term of $\frac{\partial F}{\partial a_3}$, and using $\frac{\partial f}{\partial x}$ and $\frac{\partial f}{\partial y}$ we can obtain all quadratic monomials providing the following jacobian does not vanish

$$\begin{vmatrix} b_0 & 2b_1 & b_2 \\ b_1 & 2b_2 & b_3 \\ 1 & 0 & 1 \end{vmatrix} = b_1b_3 - b_2^2 + b_0b_2 - b_1^2.$$

Provided this is not zero we have satisfied the conditions for our family of distance squared functions to versally unfold the D_4. □

7.14 Lemma: *The discriminant $\Delta(C_{\pi/2})$ is an isolated point at an ordinary umbilic.*

Proof: Corollary 7.8 says that the discriminant is given by the equation $\sin^2\alpha = K/H^2$, i.e,

$$\sin^2\alpha(Gl + En - 2Fm)^2 = 4(ln - m^2)(EG - F^2).$$

Setting $\alpha = \pi/2$ we can expand the above equation in terms of x and y at an umbilic giving,

$$\begin{aligned} & (-2b_2b_0 + b_0^2 + b_2^2 + 4b_1^2)x^2 \\ + \; & (6b_1b_2 + 2b_2b_3 - 2b_0b_3 + 2b_1b_0)xy \\ + \; & (4b_2^2 - 2b_1b_3 + b_1^2 + b_3^2)y^2 + \cdots. \end{aligned}$$

Calculating the discriminant of the quadratic part gives

$$-16(b_1b_3 - b_1^2 - b_2^2 + b_2b_0)^2$$

which is always non positive and the previous lemma says that it is non zero if the umbilic is ordinary. □

Using results from [BT2] we can make some strong statements concerning the topological configuration of $\mathcal{C}_\alpha$ near an umbilic at $\alpha = \pi/2$. First we need to check the 'versality' criterion; see Subsection 7.3.1.

7.15 Lemma: *The versality condition from [BT2] is satisfied for the family $\mathcal{C}_{\pi/2+t}$ at an ordinary umbilic.*

Proof: By Lemma 7.9 the linear part of the coefficients of the BDE at an umbilic with principal curvature κ are,

$$\begin{aligned} a &= b_1 x + b_2 y + \kappa t \\ b &= (1/2)(b_0 - b_2)x + (1/2)(b_1 - b_3)y \\ c &= -b_1 x - b_2 y + \kappa t. \end{aligned}$$

The versality condition is then,

$$\begin{vmatrix} b_1 & b_2 & \kappa \\ \frac{b_0 - b_2}{2} & \frac{b_1 - b_3}{2} & 0 \\ -b_1 & -b_2 & \kappa \end{vmatrix} = \kappa(b_1^2 - b_1 b_3 - b_2 b_0 + b_2^2) \neq 0.$$

This is satisfied if the umbilic is ordinary by Lemma 7.13. □

We can now satisfy the hypotheses in Theorem 3.5 of [BT2], see Subsection 7.3.1. For $\mathcal{C}_{\pi/2}$ we have shown that the discriminant is Morse and an isolated point (note following Lemma 7.10 and Lemma 7.14). The previous lemma showed that the versality criterion is satisfied in this case, and we assume that the following cubic in p has no repeated roots,

$$b_2 p^3 + (2b_1 - b_3)p^2 + (b_0 - 2b_2)p - b_1.$$

We also assume that the zeros of the vector field ξ_0 in [BT2] are normal (a technical condition on the eigenvalues of the zeros of a vector field which holds for 'most' fields).

7.16 Proposition: *[BT2] Consider the family $\mathcal{C}_{\pi/2+t}$ Let $\Delta(\mathcal{C}_{\pi/2})$ be an isolated umbilic. Suppose that the discriminant $\Delta(\mathcal{C}_{\pi/2})$ is of Morse type (see note following Lemma 7.10), the following cubic in p,*

$$b_2 p^3 + (2b_1 - b_3)p^2 + (b_0 - 2b_2)p - b_1$$

has no repeated roots, the zeros of ξ_0 are normal and $\Delta(\mathcal{C}_{\pi/2})$ is an ordinary umbilic, then the family of BDEs is (fibre) topologically equivalent to one of the following normal forms,

(a)	*Lemon* $(1\,saddle)$	$(y+\alpha)dy^2 + 2xdxdy - ydx^2 = 0$
(b)	*Star* $(3\,saddles)$	$(y+\alpha)dy^2 - 2xdxdy - ydx^2 = 0$
(c)	*Monstar* $(2\,saddles + 1\,node)$	$(y+\alpha)dy^2 + (1/2)xdxdy - ydx^2 = 0.$

□

Figure 7.3 shows the normal forms for the three different types of ordinary umbilics and their deformation within the family.

7.4 The Spherical Image.

Whenever one is confronted with a particular curve congruence it is natural to examine the spherical image, where the unit directions on the surface get mapped to points on the standard unit sphere[1]. If we take one colour of a particular conjugate curve congruence and take its spherical image then this is locally a map from the plane to the plane. The singularities of this spherical image tell us much about the original geometry.

7.17 Definition: *The* **spherical image** *for a fixed angle α is the image of the vectors $\Theta^{-1}(\sin\alpha)$ on the unit sphere, where a vector v is mapped to the point on the sphere corresponding to the direction that v takes in* $\mathbf{R}^3$.

Notes on the definition. Recall that for some fixed angle α the conjugate curve congruence may have up to two directions at some points. We can take one colour of direction consistently (at least locally), say the light red direction, and then consider the 'light red spherical image for $\mathcal{C}_\alpha$'. Suppose that the light red directions on our surface M, locally parametrised by (s,t), are $v(s,t)$, then if $\mathcal{S}$ is the spherical map we have,

$$\begin{array}{ccc} & \mathcal{S} & \\ M & \to & S^2 \\ (s,t) & \mapsto & \frac{v(s,t)}{\|v(s,t)\|}. \end{array}$$

[1]Strictly we do not consider our congruences to have oriented curves and thus the sphere has antipodal points identified and we map to the projective plane.

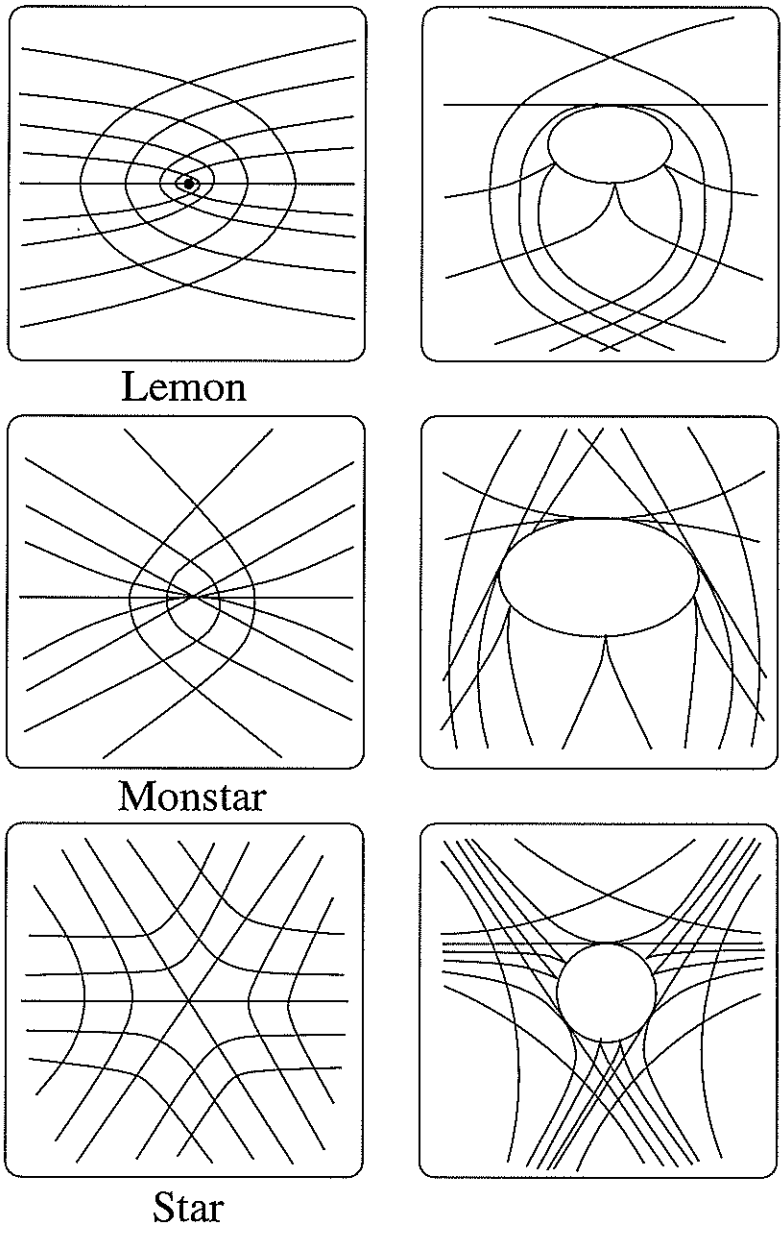

Figure 7.3: Schematic showing bifurcations of integral curves of BDEs of type Lemon, Star and Monstar.

We are thus drawn to the following definition.

7.18 Definition: *The* **fold curve** *(of a particular colour) for a fixed α is the set of critical points on the surface under the spherical map S. There are special points on the fold curve corresponding to cusps of the spherical image. The fold curves of $\mathcal{C}_\alpha$ are denoted $\mathcal{S}_\alpha$.*

In the following we make use of the **subparabolic curves** of a surface. Recall that the subparabolic curves are defined to be the set of points on the surface that gives rise to parabolic points on the focal set [BW]. However we make use of another characterisation of the subparabolic curve from [BW]; namely they are the folds of the principal spherical image. This is discussed below.

Examples.

1. Observe that the spherical image where $\alpha = \frac{\pi}{2}$ is the principal spherical image and it is known that this is the same as the Gauss map of the focal set [BW]. Thus the folds and cusps of this map correspond to parabolic curves and cusps of Gauss respectively on the focal set. Thus the subparabolic lines (two colours) are fold curves for the conjugate curve congruence corresponding to the angle $\pi/2$.

2. The spherical image for $\mathcal{C}_\alpha$ with $\alpha = 0$ gives the asymptotic spherical image whose folds correspond to the flecnodal curve, and cusps correspond to the biflecnodal points [KD, p.283]. The flecnodal curves (two colours) are fold curves for the conjugate curve congruence corresponding to the angle 0.

The fold curves are characterised in the following result by the loci of geodesic inflections of the curves of opposite shade. Recall that if we consider the light red curves of some $\mathcal{C}_\alpha$ then we can integrate the conjugate directions to get the dark red curves. We show that the light red fold curve is the locus of geodesic inflections of the dark red curves. Some examples are given below before the result to aid navigation in the result proper.

Examples.

1. It is known [RMO2], [RMO] that a subparabolic line is also the locus of geodesic inflections of lines of curvature of the opposite colour. In our present terminology the subparabolic line is a fold curve for the conjugate

curve congruence $\mathcal{C}_{\pi/2}$. The light red (resp. light blue) fold curve is the locus of geodesic inflections of the dark red (resp. dark blue) curve.

2. The flecnodal curve (of a particular colour) is characterised as the locus of points where the asymptotic curve of the same colour has a geodesic inflection [K, p.282]. In our terminology, the fold curve of $\mathcal{C}_0$ is the locus of points of geodesic inflection of the curve of the same colour, but different shade.

7.19 Proposition: *For some fixed angle α consider the congruence $\mathcal{C}_\alpha$. Provided the point p is not on the discriminant $\Delta(\mathcal{C}_\alpha)$ then p is on the light red fold curve iff the dark red curve has a geodesic inflection at p.*

Proof: We examine the condition for a point p to be on $\mathcal{S}_\alpha$ of a particular colour. Recall from the definition of a fold curve (7.18) that we have to find the condition for the spherical image to be singular. We proceed in local coordinates.

Writing our surface in Monge form $\mathbf{r}(x,y) = (x, y, h(x,y))$ we take

$$h = 1/2(a_0x^2 + 2a_1xy + a_2y^2) + 1/6(b_0x^3 + 3b_1x^2y + 3b_2xy^2 + b_3y^3) + \cdots.$$

We fix our x-axis as a member of $\mathcal{C}_\alpha$. The conjugate direction to (1,0) is $(-a_1, a_0)$ and setting α to be the angle between them, we find,

$$\sin\alpha = \frac{-a_0}{\sqrt{a_0^2 + a_1^2}}. \tag{7.5}$$

This has fixed the particular congruence we wish to examine; namely all those vectors whose sine of the angle between them and their conjugate is α. The x-axis is certainly a member of this congruence.

We label the conjugate direction $(1, -a_0/a_1)$ as 'light red' (so that $(1,0)$ is 'dark red') and we wish to examine all other light red directions near to $(1, -a_0/a_1)$, and take their spherical image. So consider vectors of the form $v(x,y) = (1, b(x,y))$, where we write b as,

$$b = -a_0/a_1 + b_{10}x + b_{01}y + \cdots.$$

We wish to calculate the jet of

$$\sin\alpha = \frac{-a_0}{a_0^2 + a_1^2} = \frac{S(v).v}{\|S(v)\|\|v\|}$$

to find the coefficients b_{10} and b_{01}.

With S denoting the shape operator and writing $E = \mathbf{r}_x.\mathbf{r}_x$, $F = \mathbf{r}_x.\mathbf{r}_y$, $G = \mathbf{r}_y.\mathbf{r}_y$, $l = S(\mathbf{r}_x).\mathbf{r}_x$, $m = S(\mathbf{r}_x).\mathbf{r}_y$ and $n = S(\mathbf{r}_y).\mathbf{r}_y$ a calculation shows that,

$$S(1,b) = \frac{1}{EG - F^2}((A_1G - A_2F)\mathbf{r}_x + (A_2E - A_1F)\mathbf{r}_y)$$

where A_1 and A_2 are,

$$\begin{aligned} A_1 &= S(v).\mathbf{r}_x &= l + bm \\ A_2 &= S(v).\mathbf{r}_y &= m + bn, \end{aligned}$$

More calculation gives the relatively simple result,

$$\begin{aligned} S(v).v &= A_1 + bA_2 \\ &= l + 2bm + b^2n. \end{aligned}$$

It is also straightforward to calculate,

$$\begin{aligned} v.v &= E + 2bF + b^2G \\ S(v).S(v) &= \frac{1}{EG - F^2}(GA_1^2 - 2FA_1A_2 + EA_2^2). \end{aligned}$$

We can express E, F, G, l, m, n in terms of the Monge form and calculate the jet of,

$$\|v\|^2\|S(v)\|^2 \sin^2\alpha = (S(v).v)^2.$$

Using MAPLE we find,

$$\begin{aligned} b_{10} &= \frac{a_1b_0 - a_0b_1}{a_0a_2 - 2a_1^2 - a_0^2} \\ b_{01} &= \frac{a_0b_2 - a_1b_1}{a_0a_2 - 2a_1^2 - a_0^2} \end{aligned}$$

and $a_0^2 + a_1^2 \neq 0$ since that would be an asymptotic direction at a parabolic point which is on the discriminant. The denominator is zero if the congruence we are considering is the principal one ($\alpha = \pi/2$) or the point is on the discriminant. In the case of $\alpha = \pi/2$ the statement of the result is known [RMO2], [RMO].

We are now ready to take the spherical image. Taking local coordinates makes this a map from $\mathbf{R^2}$ to $\mathbf{R^2}$. The vectors we are considering are, $(1,b) = r_x + br_y = (1, b, h_x + by_y)$. We project on to the yz plane and get the map,

$$\begin{aligned} \mathbf{R^2} &\rightarrow \mathbf{R^2} \\ x, y &\mapsto b, h_x + bh_y. \end{aligned}$$

The jacobian is singular precisely when the spherical image is singular. We evaluate the jacobian at the origin and using the derivatives b_{10} and b_{01} already calculated we get

$$\frac{1}{a_1}(a_1^2 - a_0 a_2)(a_0 b_1 - b_0 a_1) = 0. \tag{7.6}$$

The condition for the spherical image to have a singularity at the origin where the x-axis is a member of our congruence is equation 7.6.

We have found the condition for p to be on the light red fold curve. In these coordinates the dark red curve through p is tangent to the x-axis. We parametrise it as follows,

$$(x, \sigma x^2 + \cdots).$$

Thus $\sigma = 0$ is the condition for the dark red line to have a geodesic inflection. Along this curve the the tangent directions u must satisfy

$$\sin\alpha = \frac{-a_0}{\sqrt{a_0^2 + a_1^2}} = \frac{S(u).u}{\|S(u)\|\|u\|}$$

and so we simply expand the square of this (to eliminate the square roots in the denominator) to find the coefficient σ. Using MAPLE we find,

$$\sigma = \frac{a_0 b_1 - b_0 a_1}{a_0^2 - a_0 a_2 + 2a_1^2}.$$

The zero condition for this is the same as for (7.6), and the denominator vanishes only on the discriminant. This completes the proof. □

7.5 Cubic Forms.

In this section we study a cubic form defined on the tangent space of our surface. There is a cubic form for each point on the surface. Our cubic turns out to be a natural generalisation of the cubic defined at an umbilic that gives the limiting directions of lines of curvature. It is shown in a later section that the discriminant of the cubic form is connected to the envelope of fold curves $\mathcal{S}_\alpha$.

7.20 Definition: *The cubic form $\Gamma_p(u, v)$ is a function,*

$$\begin{array}{ccc} & \Gamma_p & \\ T_pM & \rightarrow & \boldsymbol{R} \\ (u,v) & \mapsto & \Gamma_p(u,v) \end{array}$$

defined at the point (0,0) for a surface in Monge form $(x, y, A(x,y)+B(x,y)+\cdots)$ *(with* A *quadratic and* B *cubic) as,*

$$\Gamma_{(0,0)}(u,v) = \left| \begin{array}{cc} \frac{\partial A}{\partial x} & \frac{\partial A}{\partial y} \\ \frac{\partial B}{\partial x} & \frac{\partial B}{\partial y} \end{array} \right|_{(x=u,y=v)}$$

7.21 Definition: *The cubic form* $ax^3 + 3bx^2y + 3cxy^2 + dy^3$ *is,*

Elliptic	*if there are*	*three distinct roots,*
Parabolic		*three real, two coincident roots,*
Hyperbolic		*one real, two complex conjugate roots,*
Cubical		*three real coincident roots.*

Note on Cubic Forms.

Taking our surface in Monge form with height function $h(x,y) = A(x,y) + B(x,y)+\ldots$ (with A quadratic and B cubic), we can form the following quadratic form,

$$\left| \begin{array}{cc} \frac{\partial A}{\partial x} & \frac{\partial A}{\partial y} \\ \frac{\partial (x^2+y^2)}{\partial x} & \frac{\partial (x^2+y^2)}{\partial y} \end{array} \right|$$

where $A(x,y)$ is essentially the second fundamental form, and $x^2 + y^2$ the first fundamental form. It is simple to deduce that the root directions of this quadratic form are the principal directions. At an umbilic this form is degenerate, and we create the following cubic form,

$$\left| \begin{array}{cc} \frac{\partial B}{\partial x} & \frac{\partial B}{\partial y} \\ \frac{\partial (x^2+y^2)}{\partial x} & \frac{\partial (x^2+y^2)}{\partial y} \end{array} \right|$$

whose roots at an umbilic are the limiting directions of the lines of curvature [W]. Indeed the limiting directions of the subparabolic lines at an ordinary umbilic are these root directions [WI], [BW]. We see that the cubic form Γ defined above is a natural generalisation.

We can divide our surface M into two disjoint subsets of points depending on the number of real solutions of Γ. Determining the discriminant of Γ is a complicated condition in local coordinates.

7.6 Geodesic Inflections of Σ—Part 1.

We now prove a result that connects the geodesic inflections of the critical set of a parallel projection, which we systematically denote by Σ, with the singularities of the spherical image of the congruence C_α. We set up some local coordinates in the next lemma which will be used in the main proposition. The following lemma says that the intuitive notion of a geodesic inflection, namely that projecting the curve into the tangent plane, gives the correct intuition.

7.22 Lemma: *The geodesic curvature of a curve on a surface M at a point p is zero iff the parallel projection along the normal at p of the curve into the tangent plane T_pM has an inflection.*

Proof: Take a curve γ on our surface (in Monge form) parametrised by y, without loss in generality. We write γ as $(x(y), y, h(x(y), y))$. The unit tangent to γ is,

$$T = \frac{(x', 1, h_x x' + h_y)}{\sqrt{1 + x'^2 + (h_x x' + h_y)^2}}$$

Calculation reveals that $T'(0)$, the derivative of T at the origin, is tangent to the vector $(x'', -x'x'', \cdots)$ where '$\cdots$' is some expression that will not concern us here. As in the usual frame we take the vector V to be $n \wedge T$ where n is the surface normal. In our case at the origin we have,

$$V(0) = n \wedge T = \frac{(-1, x', 0)}{\sqrt{1 + x'^2}}.$$

The geodesic curvature is defined to be $g = T'.V$ and so in our case $g = 0$ at the origin if and only if $x''(0) = 0$.

Observe that the projection of γ into the tangent plane at $(0, 0)$ is $(x(y), y))$ and this plane curve inflects at 0 iff $x''(0) = 0$. Hence result. □

The following lemma gives us the condition for Σ to have a geodesic inflection when the projection direction is $(1, 0, 0)$.

7.23 Lemma: *Given our surface in Monge form with the height function*

$$h(x, y) = \frac{1}{2}(a_0 x^2 + 2a_1 xy + a_2 y^2) + \frac{1}{6}(b_0 x^3 + 3b_1 x^2 y + 3b_2 xy^2 + b_3 y^3) + \ldots,$$

then projecting in the direction $(1, 0, 0)$ results in a geodesic inflection of Σ iff,

$$b_0 a_1^2 - 2b_1 a_1 a_0 + b_2 a_0^2 = 0.$$

Proof: Parametrise the line that is in the direction conjugate to $(1,0,0)$,

$$\begin{aligned} x(s) &= -a_1 s \\ y(s) &= a_0 s. \end{aligned}$$

The equation of Σ is $(1,0,0).(h_x, h_y, -1) = 0$, i.e. $h_x(x,y) = 0$. We examine the contact of Σ (given by an equation) with the conjugate direction (given as a parametrisation). Substituting the parametrisation in the equation we obtain,

$$\frac{1}{2}(b_0 a_1^2 - 2b_1 a_1 a_0 + b_2 a_0^2)s^2 + \ldots = 0.$$

We see that we have two point contact which is at it should be, and the vanishing of the coefficient of s^2 gives the condition for three point contact. □

Comment on the proof of lemma 7.23. The reason why this proof is valid is that the parameter space for a surface in Monge form is the same as the tangent plane to the surface at 0. The map from the parameter space to the surface is just the back-projection from the tangent plane. Therefore the projection of Σ onto the tangent plane at 0 is given by the equation of Σ, $h_x(x,y) = 0$.

The following result relates the geodesic inflections of Σ to the singularities of the spherical image. Suppose we have a projection direction v and the point p lies on the resulting critical set Σ. We wish to find out when Σ has a geodesic inflection at p. The following result tells us that we need to examine the particular congruence $\mathcal{C}_\alpha$ which has v as a member at p. Clearly $v \in T_pM$ is a member of *some* $\mathcal{C}_\alpha$ so we examine the spherical image of that $\mathcal{C}_\alpha$ around p. The following result says that if the spherical image is folded then Σ will have an inflection.

7.24 Proposition: *Let $v \in T_pM$ be the direction of a parallel projection, and v a light red direction of $\mathcal{C}_\alpha$. Provided p is not on the discriminant $\Delta(\mathcal{C}_\alpha)$, the resulting critical set Σ through p has a geodesic inflection iff p is on the light red fold curve of $\mathcal{C}_\alpha$. See Figure 7.4.*

Proof: We work in local coordinates and find the condition for a point p to be on the fold curve $\mathcal{S}_\alpha$. Recall from the definition of a fold curve that we have to find the condition for the spherical image to be singular.

Writing our surface in Monge form $\mathbf{r}(x,y) = (x, y, h(x,y))$ we take

$$h = 1/2(a_0 x^2 + 2a_1 xy + a_2 y^2) + 1/6(b_0 x^3 + 3b_1 x^2 y + 3b_2 xy^2 + b_3 y^3) + \cdots.$$

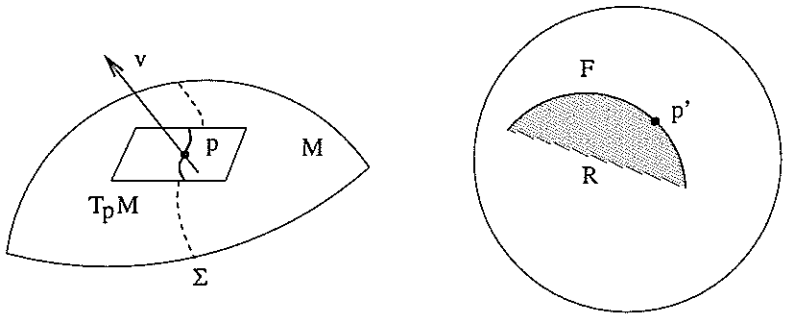

Figure 7.4: Left: surface M with projection direction v showing the critical set Σ (dotted) and projected along the normal into the tangent plane at p (solid). Right: the image of the spherical image on the unit sphere. The region R is the image of the spherical image of M of the vectors $\Theta^{-1}(\Theta(p,v))$. The curve F is the fold of the map and p' is the image of the point p under the spherical image map.

We fix the x-axis as a member of our congruence $\mathcal{C}_\alpha$. This will be the direction of projection v. The conjugate direction to (1,0) is $(-a_1, a_0)$ and setting α to be the angle between them, we find

$$\sin^2\alpha = \frac{a_0^2}{a_0^2 + a_1^2}.$$

This has fixed the particular congruence we wish to examine; namely all those vectors whose sine of the angle between them and their conjugate is α. The x-axis is certainly a member of the congruence.

We wish to examine all directions close to (1,0) in the congruence and take their spherical image. Consider vectors of the form $(1, b(x,y))$ with $b(0,0) = 0$ and write,

$$b = b_{10}x + b_{01}y + \cdots.$$

Using Lemma 7.2 we wish to calculate the jet of

$$\sin^2\alpha = \frac{a_0^2}{a_0^2 + a_1^2} = \frac{(S(v).v)^2}{\|S(v)\|^2\|v\|^2}$$

to find the coefficients b_{10} and b_{01}.

With S as the shape operator we write, $E = \mathbf{r}_x.\mathbf{r}_x$, $F = \mathbf{r}_x.\mathbf{r}_y$, $G = \mathbf{r}_y.\mathbf{r}_y$, $l = S(\mathbf{r}_x)\mathbf{r}_x$, $m = S(\mathbf{r}_x).\mathbf{r}_y$ and $n = S(\mathbf{r}_y).\mathbf{r}_y$ a calculation shows that

$$S(1,b) = \frac{1}{EG - F^2}((A_1G - A_2F)\mathbf{r}_x + (A_2E - A_1F)\mathbf{r}_y)$$

where A_1 and A_2 are,

$$\begin{aligned} A_1 &= S(v).\mathbf{r}_x = l + bm \\ A_2 &= S(v).\mathbf{r}_y = m + bn. \end{aligned}$$

More calculation gives the relatively simple result

$$\begin{aligned} S(v).v &= A_1 + bA_2 \\ &= l + 2bm + b^2 n. \end{aligned}$$

It is also straightforward to calculate,

$$\begin{aligned} v.v &= E + 2bF + b^2 G \\ S(v).S(v) &= \frac{1}{EG - F^2}(GA_1^2 - 2FA_1A_2 + EA_2^2). \end{aligned}$$

We can express E, F, G, l, m, n in terms of the Monge form and calculate the jet of

$$\|v\|^2 \|S(v)\| \sin^2 \alpha = (S(v).v)^2.$$

Using MAPLE we find,

$$\begin{aligned} b_{10} &= \frac{2a_0a_1^2b_0 - 2a_0^2a_1b_1}{2a_0^2a_1a_2 - 4a_0a_1^3 - 2a_0^3a_1} \\ b_{01} &= \frac{2a_0^2a_1b_2 - 2a_0a_1^2b_1}{2a_0^2a_1a_2 - 4a_0a_1^3 - 2a_0^3a_1}. \end{aligned}$$

We are now ready to take the spherical image of the vectors $(1, b)$. The vector $(1, b)$ in $\mathbf{R}^3$ is $(1, b, h_x + bh_y)$ and so we take local coordinates on the sphere by projecting in to the yz plane. The map is thus,

$$\begin{aligned} \mathbf{R}^2 &\to \mathbf{R}^2 \\ x, y &\mapsto b, h_x + bh_y. \end{aligned}$$

The jacobian is singular precisely when the spherical image is singular. We evaluate the jacobian at the origin and using the derivatives b_{10} and b_{01} already calculated above we get

$$\frac{b_0a_1^2 - 2a_1a_0b_1 + a_0^2b_2}{a_0a_2 - 2a_1^2 - a_0^2}. \tag{7.7}$$

The denominator is zero iff p is on the discriminant of the congruence. The numerator gives the condition for the spherical image to have a singularity at the origin when the x axis is a member of the congruence.

We now project in the direction (1,0,0) and find the condition for the critical set Σ to have an inflection. The equation of Σ in this case is $h_x = 0$. We know that Σ will be tangent to the conjugate direction $(-a_1, a_0)$, but we wish to find the condition for it to have extra contact when projected in to the tangent plane at the origin. We parametrise a line in the conjugate direction,

$$\begin{aligned} x &= -a_1 s \\ y &= a_0 s. \end{aligned}$$

We substitute this parametrisation into the equation for Σ and the condition for three point contact is

$$b_0 a_1^2 - 2b_1 a_1 a_0 + b_2 a_0^2 = 0$$

which is equivalent to (7.7), thus completing the proof. □

Notes on the Proposition. If the projection direction v is a *principal direction* then the resulting critical set will have an inflection iff the principal spherical image has a singularity, which by the examples in Definition 7.18 is a subparabolic point. This specific result was first noticed in [RMO]. Figure 7.5 gives a schematic for demonstrating the intuition behind this result. We first note that a 'near and far point' p is a point on the critical set Σ (for parallel projection) whose perpendicular distance to the viewplane is critical. This is equivalent to the view direction v being perpendicular to the tangent to Σ which is equivalent to v being a principal direction at p by the conjugacy of the view direction and tangent to Σ. An inflection arises when two near and far points come together and vanish in an inflection. Thus in Figure 7.5 v_1 is the view direction at a point on the view sphere where there are two principal directions resulting in two near/far points. The view direction v moves across the fold and in to a region of the view sphere where there are no principal view directions v_3 and thus the near/far points have come together through an inflection at v_2.

If v is an asymptotic direction then the critical set will have an inflection if the point is flecnodal and this is a singularity of the asymptotic spherical image.

7.7 Geodesic Inflections of Σ—Part 2.

In this section we characterise the condition for a geodesic inflection of Σ (the critical set for some parallel projection) in terms of the cubic form Γ, Definition 7.20. We prove that Σ has a geodesic inflection if Σ is tangent to to a root

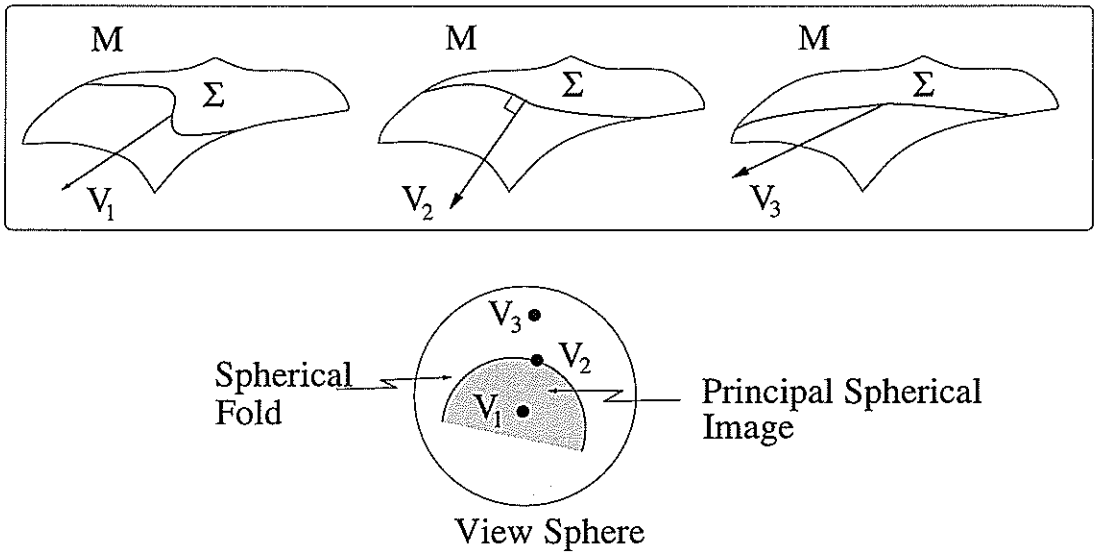

Figure 7.5:

line of Γ. Using this characterisation the root lines of Γ are investigated on the ellipsoid. Proposition 7.28 gives a new characterisation of the subparabolic lines and flecnodal curves of a surface. The red subparabolic line is the locus of tangency points between the roots of Γ and the blue principal curves. Proposition 7.29 proves the remarkable result that the envelope of $\mathcal{S}_\alpha$ is the discriminant of Γ.

The following lemma gives the condition for Σ at the origin to have a geodesic inflection. We find that there are one or three directions in the tangent plane where this phenomenon occurs.

7.25 Lemma: *If our surface is written in Monge form as* $(x, y, h(x, y))$ *where,*

$$h(x,y) = (1/2)(\kappa_1 x^2 + \kappa_2 y^2) + (1/6)(b_0 x^3 + 3b_1 x^2 y + 3b_2 x y^2 + b_3 y^3) + \ldots,$$

with $\kappa_1 \neq 0$ *and* $\kappa_2 \neq 0$ *and our parallel projection* Π *is in the direction* $(v_1, v_2, 0)$ *then* $\Sigma(\Pi)$ *has a geodesic inflection at* $(0,0)$ *iff*

$$b_1\kappa_2^2 v_2^3 + \left(b_0\kappa_2^2 - 2b_2\kappa_2\kappa_1\right) v_2^2 v_1 + \left(b_3\kappa_1^2 - 2b_1\kappa_2\kappa_1\right) v_2 v_1^2 + v_1^3 b_2 \kappa_1^2 = 0.$$

Proof: For the given surface and view direction the equation of the critical set $\Sigma(\Pi)$ is,

$$v_1\kappa_1 x + (1/2)v_1(b_0 x^2 + 2b_1 xy + b_2 y^2) + \ldots$$

$$+v_2\kappa_2 y + (1/2)v_2(b_1x^2 + 2b_2xy + b_3y^2) + \ldots = 0 \tag{7.8}$$

where ... signifies terms of order three. We now suppose that we can parametrise Σ by y. This will fail if the tangent to Σ is parallel to the x axis at 0. This will happen if $v_1 = 0$ in which case we can parametrise by x and the result is the same or $\theta = 0$ and $\kappa_1 = 0$, which are excluded. We thus write Σ as the curve $(x(y), y, h(x(y), y))$ with

$$x = a_1 y + (1/2)a_2 y^2 + \ldots$$

Therefore the condition we seek (by lemma 7.22) for the geodesic curvature at 0 to vanish is $a_2 = 0$.

Comparing the coefficients of y in equation 7.8 gives us,

$$a_1 = \frac{-v_2\kappa_2}{v_1\kappa_1} = \frac{-v_2}{v_1}\frac{\kappa_3}{\kappa_1}$$

Comparing coefficients of y^2 tells us that

$$a_2 = 0 \Leftrightarrow b_1\kappa_2^2 v_2^3 + \left(b_0\kappa_2^2 - 2b_2\kappa_2\kappa_1\right) v_2^2 v_1 + \left(b_3\kappa_1^2 - 2b_1\kappa_2\kappa_1\right) v_2 v_1^2 + v_1^3 b_2\kappa_1^2 = 0.$$

□

The following result gives a characterisation of the critical set having a geodesic inflection in terms of the cubic form Γ, (Definition 7.20) derived from the second fundamental form and cubic parts of the surface.

7.26 Proposition: *Given a parallel projection direction v the resulting critical set Σ will have a geodesic inflection iff Σ is tangent to a root direction of the cubic form Γ.*

Proof: We write

$$h(x, y) = \frac{1}{2}(\kappa_1 x^2 + \kappa_2 y^2) + \frac{1}{6}(b_0x^3 + 3b_1x^2y + 3b_2xy^2 + b_3y^3) + \ldots.$$

Recall that lemma 7.25 says that Σ will have a geodesic inflection at 0 under the projection $(v_1, v_2, 0)$ iff

$$b_1\kappa_2^2 v_2^3 + \left(b_0\kappa_2^2 - 2b_2\kappa_2\kappa_1\right) v_2^2 v_1 + \left(b_3\kappa_1^2 - 2b_1\kappa_2\kappa_1\right) v_2 v_1^2 + v_1^3 b_2\kappa_1^2 = 0. \tag{7.9}$$

Now the cubic form at the origin is,

$$\begin{aligned}\Gamma &= \begin{vmatrix} b_0x^2+2b_1xy+b_2y^2 & b_1x^2+2b_2xy+b_3y^2 \\ \kappa_1 x & \kappa_2 y \end{vmatrix} \\ &= -b_1\kappa_1x^3+(b_0\kappa_2-2b_2\kappa_1)x^2y+(2b_1\kappa_2-\kappa_1b_3)xy^2+\kappa_2b_2y^3. \quad (7.10)\end{aligned}$$

The conjugate direction to (v_1, v_2) is $(-\kappa_2 v_2, \kappa_1 v_1)$, and using the fact that the tangent to Σ is conjugate to the view direction we substitute in 7.10 giving 7.9. □

Definition 7.20 only describes the cubic form Γ for a surface at the origin in Monge form. We can use the previous proposition to calculate the root directions of Γ at a general point by doing a 'hands on' calculation of when the critical set of some projection has a geodesic inflection. We do this for the ellipsoid.

7.27 Example: Roots of Γ on the Ellipsoid.

We choose the ellipsoid because the critical sets under parallel projection are plane curves. The critical set Σ will thus have a geodesic inflection at a point p if and only if the normal at p lies in the plane of Σ. In that case the inflection will be extremely degenerate, in fact a straight line! We now work through the calculation.

Our surface is $\frac{x^2}{a^2}+\frac{y^2}{b^2}+\frac{z^2}{c^2}=1$ and has normal $(\frac{x}{a^2},\frac{y}{b^2},\frac{z}{c^2})$. We let the view direction be (v_1, v_2, v_3) and the two equations defining the critical set Σ are,

$$\begin{aligned}\frac{x^2}{a^2}+\frac{y^2}{b^2}+\frac{z^2}{c^2} &= 1 \\ \frac{v_1}{a^2}x+\frac{v_2}{b^2}y+\frac{v_3}{c^2}z &= 0.\end{aligned}$$

We see that the critical set is a plane curve on the ellipsoid. The normal to the plane is $(\frac{v_1}{a^2},\frac{v_2}{b^2},\frac{v_3}{c^2})$ and it passes through the origin. We now calculate the condition for the normal to the surface to lie in this plane. This is the extra condition, $\frac{v_1}{a^4}x+\frac{v_2}{b^4}y+\frac{v_3}{c^4}z=0$. We can now write a MAPLE routine that solves the three equations

$$\begin{aligned}\frac{v_1}{a^4}x+\frac{v_2}{b^4}y+\frac{v_3}{c^4}z &= 0 \\ \frac{v_1}{a^2}x+\frac{v_2}{b^2}y+\frac{v_3}{c^2}z &= 0 \\ v_1^2+v_2^2+v_3^2 &= 1\end{aligned}$$

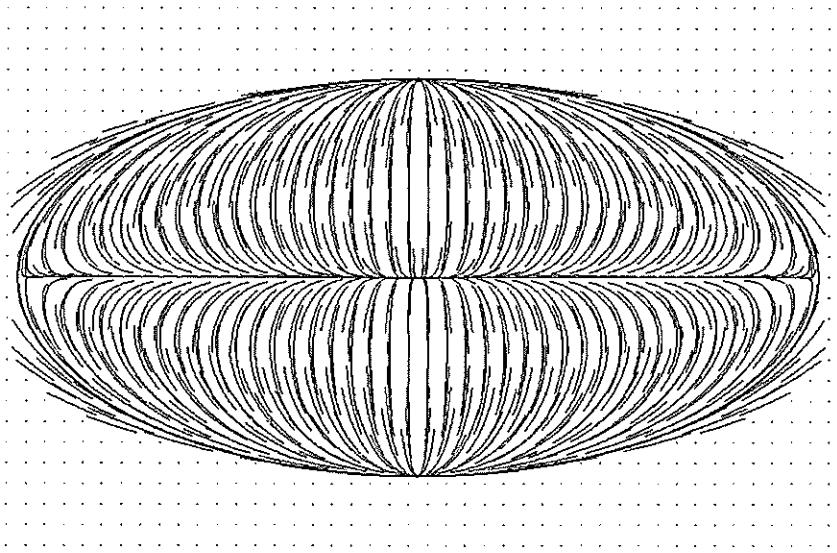

Figure 7.6: Root directions of Γ shown for an example ellipsoid looking down on the xy plane.

for v_1, v_2, v_3 if we supply a point x, y, z on the ellipsoid. We then wish to find the conjugate direction to v which we call $\overline{v}$. This is tangent to the critical set and is the root direction of Γ that we seek. So given x, y, z and v_1, v_2, v_3 we can find the direction $(\overline{v}_1, \overline{v}_2, \overline{v}_3)$. Now $\overline{v}$ is perpendicular to the normal $(\frac{x}{a^2}, \frac{y}{b^2}, \frac{z}{c^2})$ of the ellipsoid since it lies in the tangent plane, and it is perpendicular to the normal of the plane of Σ, $(\frac{v_1}{a^2}, \frac{v_2}{b^2}, \frac{v_3}{c^2})$, since this then makes it tangent to Σ. We can solve these to find the conjugate directions. These equations were solved symbolically in MAPLE and then the equations for the vector field were exported to the 'Liverpool Surface Modelling Package' (LSMP) which has a routine for numerically plotting the solutions to differential equations. For an example ellipsoid with $a = 1, b = 2, c = 3$ see Figure 7.6 where the xy plane is shown with the root directions of Γ. From Figure 7.6 we can see that at points where the ellipsoid cuts the axes Γ is degenerate. In fact a short calculation reveals that for any view direction at these points the normal is contained in the plane of the critical set Σ. In other words Σ *always* has a geodesic inflection at these points. The other major feature shown in Figure 7.6 is the discriminant of Γ which can be seen as the curve where there are three directions through a point. Two directions cusp at the discriminant. The ellipsoid is degenerate in the sense that the region where there are three directions has been compressed to a curve.

We now make some connections between the cubic Γ and the conjugate curve congruence family and its fold curves.

The key is to exploit the two characterisations of when Σ has a geodesic inflection. Namely,

- Iff the projection direction v is a singular point of the spherical image of the directions $\Theta^{-1}(\Theta(v))$. (Proposition 7.24.)
- Iff Σ is tangent to a root direction of Γ. (Proposition 7.26.)

The following proposition provides a new characterisation of the sub parabolic and flecnodal curves of a surface.

7.28 Proposition: *Away from the parabolic curve the fold curve $\mathcal{S}_\alpha$ for the dark red directions of a particular conjugate curve congruence $\mathcal{C}_\alpha$ is the locus of points where the root curves of Γ are tangent to the light red conjugate integral curves. See Figure 7.7.*

Proof: Given some α we have the congruence $\mathcal{C}_\alpha$ which away from Δ has two directions at each point called the dark red and blue directions. The conjugate directions, which we can integrate, give the light red and blue directions. We first prove that if p is a point on the dark red fold curve $\mathcal{S}_\alpha$ then this implies that a root direction of Γ is tangent to an integral curve of the light red directions. First we work away from the discriminant.

Let p be on the dark red fold curve for some given $\mathcal{C}_\alpha$ so by Definition 7.18 the spherical image for the dark red integral curves is singular at p. By Proposition 7.24 we know that by projecting along the dark red direction at p the resulting critical set Σ will have a geodesic inflection. The critical set is tangent to the light red (conjugate to dark red) direction, and by Proposition 7.26 Σ is tangent to a root direction of Γ. Therefore the root direction of Γ is tangent to the light red direction. See Figure 7.8.

Now we prove the converse. Suppose a root of Γ is tangent to the light red direction of some curve congruence. By (7.26) projecting in the dark red direction will give a critical set Σ with a geodesic inflection (since the tangent to Σ is along the root direction of Γ). But (7.24) says that the spherical image of the dark red directions for this congruence will be singular, and so p is a point on the dark red fold curve by Definition 7.18.

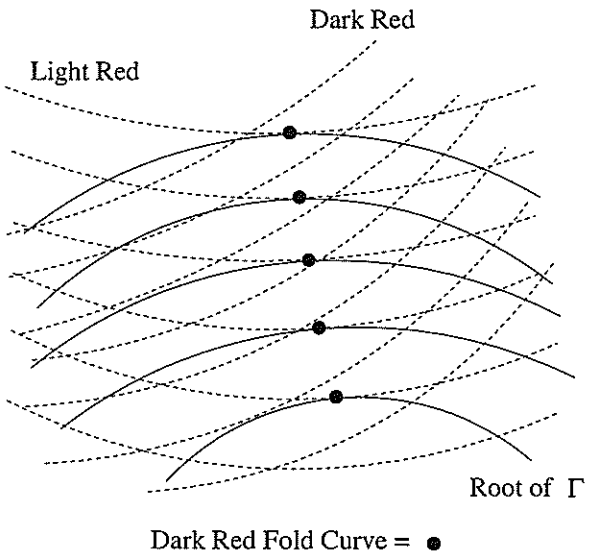

Figure 7.7: Half of the congruence $\mathcal{C}_\alpha$ is shown, namely the dark red directions (shown dotted). The conjugate curves (light red) are also shown dotted. The root curves of Γ are solid curves. In this schematic Γ has only one real root. Where Γ is tangent to the light red directions the point is a fold of the dark red spherical image.

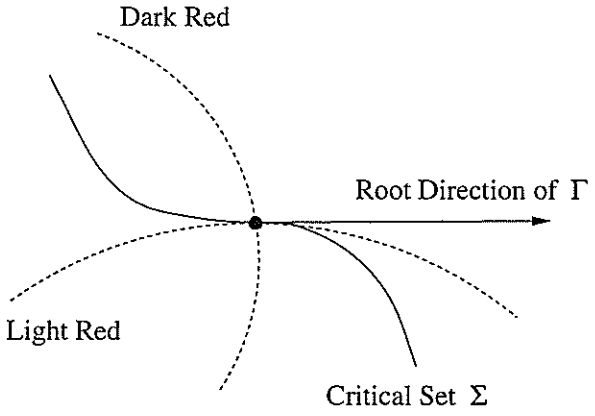

Figure 7.8: If we project in the dark red direction at a point of the dark red spherical image, then the resulting critical set Σ will have a geodesic inflection. It will be tangent to the light red direction since the tangent to Σ and the view direction are conjugate.

We now prove the result in the case when the point is on the discriminant. This is most easily accomplished with the surface in Monge form. Writing $p = \frac{\partial y}{\partial x}$ the BDE representing $\mathcal{C}_\alpha$ can be written $F = ap^2 + 2bp + c = 0$, which in the discriminant case is a surface folded over the xy plane. We can parametrise $F = 0$ by x and p in this case provided the BDE is not zero and we write $y = y(x, p)$. When the origin is a point on the discriminant and the x-axis is a member of the congruence, then MAPLE can be used to solve $F(x, y(x, p), p) = 0$ and thus obtain the derivative $\frac{\partial y}{\partial x} = \frac{b_0 a_1 - a_0 b_1}{a_0 b_2 - b_1 a_1}$ at zero. The directions of the congruence are $(1, p, h_x + ph_y)$ and we examine their spherical image. This is most easily obtained by taking local coordinates on the unit sphere, which we take as the yz plane. We then have a map,

$$\begin{aligned} \mathbf{R}^2 &\to \mathbf{R}^2 \\ x, p &\mapsto p, h_x + ph_y \end{aligned}$$

whose Jacobian determinant is

$$h_{xx} + h_{xy}\frac{\partial y}{\partial x} + ph_{xy} + ph_{yy}\frac{\partial y}{\partial x}.$$

Evaluated at zero and using the value of $\frac{\partial y}{\partial x}$ above we obtain the condition

$$a_0^2 b_2 - 2a_0 a_1 b_1 + a_1^2 b_0 = 0. \tag{7.11}$$

This is the condition for the congruence to have a singular spherical image at the discriminant where the x axis is a member.

Recall definition 7.20 for the cubic form Γ_p. In Monge form this becomes,

$$\begin{aligned} &(a_0 b_1 - a_1 b_0)x^3 + (2a_0 b_2 + a_1 b_1 - 2b_1 a_1 - a_2 b_0)x^2 y + \\ &(a_0 b_3 + 2b_2 a_1 - a_1 b_2 - 2b_1 a_2)xy^2 + (a_1 b_3 - a_2 b_2)y^3 = 0 \end{aligned}$$

and the condition for $(-a_1, a_0)$, the conjugate direction to $(1, 0)$, to be a solution is $(a_1^2 - a_0 a_2)(a_0^2 b_2 + a_1^2 b_0 - 2a_0 a_1 b_1) = 0$. Away from the parabolic curve this is equivalent to (7.11), hence the result. □

Notes on Proposition 7.28. As usual to make sense of the statement it is wise to specialise to a well known congruence like the principal curve congruence. Then the result says that the red subparabolic lines are the loci of points where the root directions of Γ are tangent to the blue principal directions.

Similarly the red flecnodal curves are the loci of points where the root directions are tangent to the red asymptotic curves.

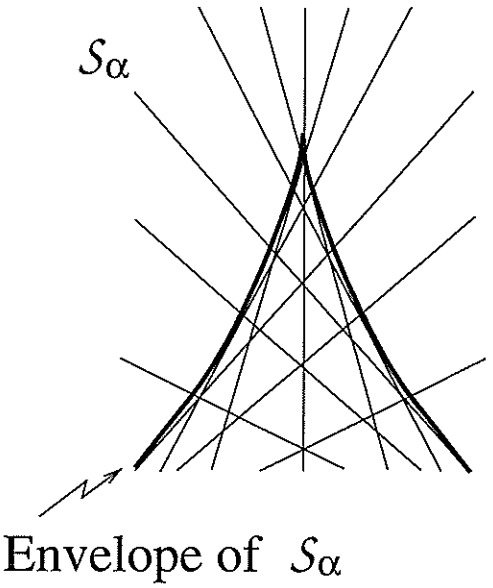

Figure 7.9: Hypothesised configuration of the fold curves forming an envelope on the surface.

We now dispel any final doubts over the interconnection between the cubic Γ and $\mathcal{C}_\alpha$. We show that the envelope of the family of fold curves $\mathcal{S}_\alpha$ is the discriminant of Γ. An intuitive grasp of this result can be obtained by considering the different characterisations of geodesic inflections on the critical set Σ. Recall that if Σ is tangent to a root of Γ then a geodesic inflection will result. Also the inflections are connected with the folds of the spherical image. So the number of roots of Γ at a point p must be connected to the number of fold curves $\mathcal{S}_\alpha$. Figure 7.9 gives a hypothesised configuration of the $\mathcal{S}_\alpha$ curves on a surface. We see that on one side of the envelope (which is also the discriminant of Γ) there are three directions through a point, and on the other side just one direction. It seems reasonable that the envelope could be singular at isolated points.

7.29 Proposition: *If p is on the envelope of fold curves $\mathcal{S}_\alpha$ away from $\Delta(\mathcal{C}_\alpha)$, then at p, Γ_p has at least two coincident real roots.*

Proof: We use a local Monge parametrisation. We fix α_0 and consider congruences $\mathcal{C}_{\alpha_0+\epsilon}$ 'near' to $\mathcal{C}_{\alpha_0}$. We calculate the family of fold curves and then the envelope. Consider directions $(1, b(x, y, \epsilon))$ with $b(0, 0, 0) = -a_0/a_1$. We let $\mathcal{C}_{\alpha_0}$

contain the directions $(1,0)$ and $(1,-a_0/a_1)$. Thus a straightforward calculation shows that

$$\sin\alpha_0 = \frac{-a_0}{\sqrt{a_0^2+a_1^2}}, \quad \cos\alpha_0 = \frac{a_1}{\sqrt{a_0^2+a_1^2}}.$$

We will also require the following,

$$\begin{aligned}\sin(\alpha_0+\epsilon) &= \frac{1}{\sqrt{a_0^2+a_1^2}}(-a_0\cos\epsilon + a_1\sin\epsilon)\\ &= \frac{1}{\sqrt{a_0^2+a_1^2}}(-a_0 + a_1\epsilon + a_0\epsilon^2/2 + \cdots).\end{aligned}$$

We expand $b(x,y,\epsilon)$ as a power series and use the identity

$$\|(1,b)\|^2\|S(1,b)\|^2\sin^2(\alpha_0+\epsilon) = (S(1,b).(1,b))^2 \tag{7.12}$$

to evaluate the coefficients in b.

Calculation gives the following, where E,F,G,l,m,n are the usual coefficients of the first and second fundamental forms,

$$\begin{aligned}S(1,b).(1,b) &= l+2bm+b^2n\\ (1,b).(1,b) &= E+2bF+b^2G\\ S(1,b).S(1,b) &= (1/EG-F^2)(G(l+bm)^2 -\\ &\quad 2F(l+bm)(m+bn)+E(m+bn)^2)\end{aligned}$$

and we can evaluate these in Monge form and substitute in (7.12).

We follow the proof of Proposition 7.19 and construct the spherical image in local coordinates. Recall that the vector $(1,b)$ is $(1,b,h_x+bh_y)$ and we project on to the yz plane for local coordinates of the spherical image to get the map,

$$\begin{aligned}\mathbf{R^2} &\to \mathbf{R^2}\\ x,y &\mapsto b, h_x+bh_y.\end{aligned}$$

This is actually a family of maps since b is a function of x,y and ϵ is the parameter. The condition for the jacobian to be singular is,

$$\frac{\partial b}{\partial x}(h_xy+bh_yy) - \frac{\partial b}{\partial y}(h_xx+bh_xy) = 0. \tag{7.13}$$

For some ϵ this gives the equation for $\mathcal{S}_\alpha$ where b satisfies (7.12). Evaluated at $(x,y,\epsilon)=(0,0,0)$ we have $\frac{\partial b}{\partial x}=0$ and MAPLE gives,

$$\frac{\partial b}{\partial x} = \frac{(a_0^2+a_1^2)(a_0b_1-a_1b_0)}{a_1^2(2a_1^2+a_0^2-a_0a_2)}.$$

Recall that the condition $2a_1^2 + a_0^2 - a_0a_2 = 0$ is the condition for the point p to be on the discriminant of the congruence $\Delta\, C_\alpha$. So the condition (in this setup) for p to be on the fold curve $\mathcal{S}_\alpha$ is $a_0b_1 - a_1b_0 = 0$.

Equation 7.13 actually gives a *family* of curves since b is a function of ϵ. To find the envelope we differentiate by ϵ and evaluate at $\epsilon = 0$. This gives the envelope condition,

$$\frac{\partial^2 b}{\partial x \partial \epsilon}(a_1^2 - a_0a_2) - a_1^2 \frac{\partial b}{\partial y}\frac{\partial b}{\partial \epsilon} = 0$$

where everything is to be evaluated at the origin. Using MAPLE to calculate derivatives of b from (7.12) and enforcing the above condition for $\mathcal{S}_\alpha$, $a_0b_1 - a_1b_0 = 0$ we obtain $2a_0^2b_2 - a_0a_2b_0 - a_1^2b_0 = 0$. Using $a_0b_1 - a_1b_0 = 0$ we can make a substitution so that the envelope condition becomes $a_0(2a_0b_2 - a_1b_1 - a_2b_0) = 0$.

In this coordinate system the cubic Γ is,

$$\begin{aligned}\Gamma_0(x,y) &= x^3(a_0b_1 - a_1b_0) + x^2y(2a_0b_2 - a_1b_1 - a_2b_0) \\ &\quad xy^2(a_0b_3 + a_1b_2 - 2a_2b_1) + y^3(a_1b_3 - a_2b_2).\end{aligned}$$

We see that the condition for p to be on the light red fold curve ($a_0b_1 - a_1b_0 = 0$) is that a root direction of Γ_0 is tangent to the dark red direction—in this case along the x-axis and y is a solution of Γ_0. The condition for p to be on the envelope of $\mathcal{S}_\alpha$ ($2a_0b_2 - a_1b_1 - a_2b_0 = 0$) is that Γ_0 has a double root, and the x^3 and x^2y terms of Γ_0 vanish. This completes the proof. □

7.8 Zeros Of C_α.

We now turn our attention to zeros of the BDE C_α. Recall (e.g. [D]) that along the discriminant the integral curves of the BDE cusp, and at special isolated points the unique direction is tangent to the discriminant. It can be shown that when the BDE is lifted on to a double cover to make a single valued vector field, the zeros of this lifted field occur precisely on the lifted discriminant, which is sometimes called the *criminant*. These are the standard planar vector field singularities such as a saddle, node, focus etc. When projected down they become the 'well-folded' saddle, node focus, shown in Figure 7.10.

We investigate the behaviour of the integral curves of C_α at the discriminant. Consider C_α with $\alpha \neq 0$ or $\alpha \neq \pi/2$. The congruence C_α away from $\Delta(C_\alpha)$ consists of two directions at each point, call these light red and light blue. Their

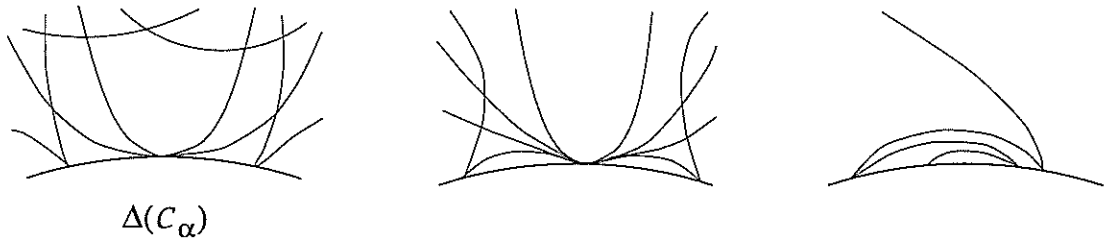

Figure 7.10: Schematic showing the integral curves of $\mathcal{C}_\alpha$ at $\Delta(\mathcal{C}_\alpha)$ around zeros of the lifted field.

respective conjugates are the dark red and dark blue directions. At the discriminant $\Delta(\mathcal{C}_\alpha)$ the light red and blue directions coalesce in to a unique direction. The integral curves of the light red and light blue directions typically cusp at $\Delta(\mathcal{C}_\alpha)$ but there are isolated points on the discriminant where they are tangent to Δ, as in Figure 7.10.

7.8.1 Saddle Node Bifurcation

Since we are working in a family, phenomena that were previously non generic become generic. It is not generic for the zero of a single vector field to be degenerate, or non–hyperbolic (in the language of [AP, p.68]). In a family we expect vector field bifurcations, and the codimension one bifurcation for vector fields in the plane is the saddle–node bifurcation, see Figure 7.11. This bifurcation is versally unfolded by one parameter. We expect $\mathcal{C}_\alpha$ to undergo saddle–node bifurcations and this is now investigated.

We set up some local coordinates and make some preliminary calculations.

7.30 Lemma: *If we write our surface in Monge form,* $(x, y, h(x, y))$ *with*

$$\begin{aligned} h(x,y) \;=\; & \frac{1}{2}(a_0x^2 + 2a_1xy + a_2y^2) + \\ & \frac{1}{6}(b_0x^3 + 3b_1x^2y + 3b_2xy^2 + b_3y^3) + \\ & \frac{1}{24}(c_0x^4 + 4c_1x^3y + 6c_2x^2y^2 + 4c_3xy^3 + c_4y^4) + \cdots \end{aligned}$$

and fix the x*-axis as a member of our congruence* $\mathcal{C}_\alpha$ *with* $(0,0)$ *a point on the non singular discriminant then,*

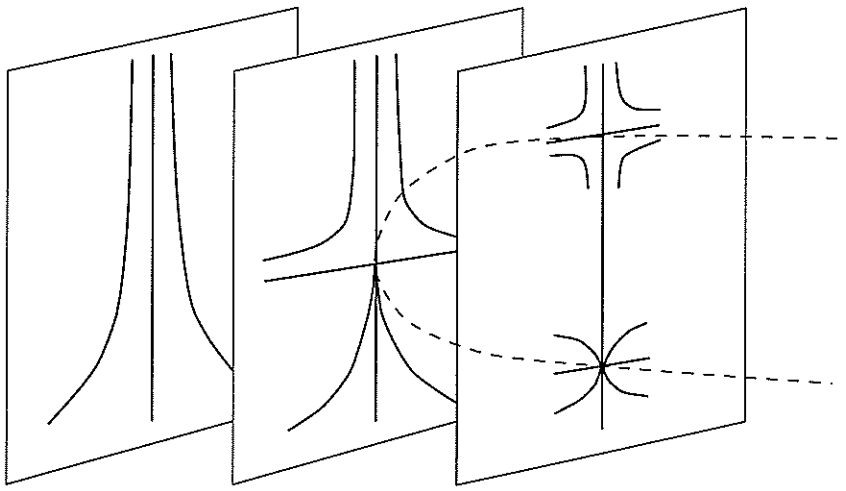

Figure 7.11: Saddle node bifurcation.

1. $\sin\alpha = \frac{a_0}{\sqrt{a_0^2+a_1^2}}$, $\cos\alpha = \frac{-a_1}{\sqrt{a_0^2+a_1^2}}$, *and* $a_0^2 - a_0a_2 + 2a_1^2 = 0$.

2. $\mathcal{C}_\alpha$ *has a zero at* $(0,0)$ *iff the previous conditions in part 1 hold and*

$$b_0a_1 - b_1a_0 = 0,$$

and a degenerate zero if in addition $-(-3b_0a_0^4b_2+b_0^2a_0^4+5b_0^2a_0^2a_1^2-7b_0a_1^2a_0^2b_2+6b_0^2a_1^4+2a_0^4b_2^2-8a_1^4a_0^4-4a_1^2a_0^3c_0-4a_1^2a_0^6-4a_1^6a_0^2-4a_1^4a_0c_0) = c_1(4a_0^4a_1+4a_0^2a_1^3)$

3. *The origin is a fold point of the spherical image if and only if,* $a_0^2b_2 - 2a_0a_1b_1 + a_1^2b_0 = 0$.

Proof: (1) We require $(1,0,0)$ to be a member of our congruence. The conjugate direction to $(1,0)$ in the xy plane is easily calculated as $(-a_1,a_0)$. As usual α denotes the angle between a direction and its conjugate and in this case the dot product gives, $\cos\alpha = \frac{-a_1}{\sqrt{a_1^2+a_0^2}}$, and thus we find that $\sin\alpha = \frac{a_0}{\sqrt{a_1^2+a_0^2}}$. Now by Corollary 7.8 we equate $\sin\alpha$ just given with $\frac{\sqrt{K}}{H}$ at the origin to get the condition $a_0^2 - a_0a_2 + 2a_1^2 = 0$.

(2) Using Lemma 7.9 we can expand $b^2 - ac$, and imposing the results from part (1) above we find that the normal to the discriminant is

$$[b_0a_1 - b_1a_0, b_1a_1 - b_2a_0]. \tag{7.14}$$

(Observe that the normal given in Lemma 7.10 is for a surface written as a different graph.)

Since we have set up things so that $(1,0)$ is a member of $\mathcal{C}_\alpha$ then the condition for a zero of the BDE is that the normal to the discriminant is along the y-axis and the unique direction is tangent to the discriminant, hence the result.

The calculation required for the degenerate zero is more involved. We follow [BT1] and construct a lift of the BDE. If we write $p = \frac{dy}{dx}$ then the BDE can be written $F = ap^2 + 2bp + c = 0$, and this can be viewed as a surface in xyp space. It is shown in [BT] that at the discriminant the projection map onto the first two components is equivalent to a fold map, see Figure 7.12. As described in [BT] a suitable lift is the vector field,

$$\xi = F_p \frac{\partial}{\partial x} + pF_p \frac{\partial}{\partial y} - (F_x + pF_y)\frac{\partial}{\partial p},$$

and at a smooth point on the discriminant we have $F = F_p = 0$, $F_{pp} \neq 0$ and the surface $F = 0$ is folded over the xy plane. We wish to take local coordinates on $F = 0$ and provided $F_y \neq 0$ we can use x and p as local coordinates. A short calculation shows that the condition $F_y \neq 0$ is equivalent to $b_1 a_1 - b_2 a_0 \neq 0$ and we see from (7.14) that this can not be zero otherwise the discriminant would be singular. Therefore in practical terms we may write y as a power series in x and p and solve the equation $F(x, y(x,p), p) = 0$ with MAPLE to find successive coefficients of y. This will give us the first few terms of the planar vector field $F_p \frac{\partial}{\partial x} - (F_x + pF_y)\frac{\partial}{\partial p}$. By imposing the condition $b_1 a_0 - b_0 a_1 = 0$ found above, the vector field will be singular. The condition for a transition singularity of the bifurcation of vector fields requires that the Jacobian has zero eigen-values [AP]. The Jacobian is the following,

$$\begin{bmatrix} F_{px} + F_{py}\frac{\partial y}{\partial x} & F_{pp} + F_{py}\frac{\partial y}{\partial p} \\ -F_{xx} - F_{xy}\frac{\partial y}{\partial x} - pF_{yx} - pF_{yy}\frac{\partial y}{\partial x} & -F_{xp} - F_{xy}\frac{\partial y}{\partial p} - F_y - pF_{yp} - pF_{yy}\frac{\partial y}{\partial p} \end{bmatrix}$$

The determinant gives the required condition.

(3) The spherical image has been discussed in an earlier section but only away from the discriminant. At the discriminant we can not parametrise the directions of $\mathcal{C}_\alpha$ by x and y, and it is necessary to introduce another variable $p = \frac{dy}{dx}$. We closely follow the proof of part (2) and use the surface $F = 0$, and parametrise by y. A point (x, y, p) on F corresponds to the direction $\mathbf{r}_x + p\mathbf{r}_y = (1, p, h_x + ph_y)$ in xyz space. Since $(1,0,0)$ is a point in our congruence things are set up so that $x = y = p = 0$ is a solution of F. Now the direction $(1, p, h_x + ph_y)$ gets mapped

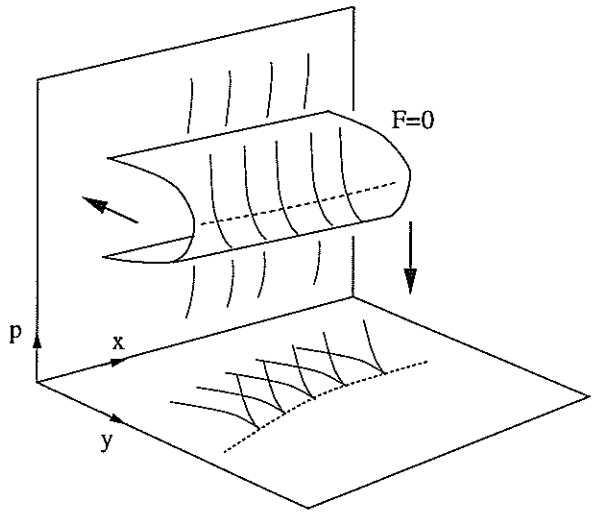

Figure 7.12: Schematic showing the lifted surface F folded over the xy plane at the discriminant. The dotted curve in the xy plane is the discriminant and the integral curves cusp here. The dotted line on the surface is the lifted curve called the *criminant*. The solid curves in the xy plane are the integral curves of the BDE, and on the surface F are the lifted integral curves forming a single valued vector field. The solid curves in the xp plane are the projections of the lifted integral curves on to this local coordinate system.

to the unit sphere, and we can introduce simple local coordinates (that do not change the singularities of the spherical image) by taking the y and z components. So we have a series of mappings: (x,p) are local coordinates of $F=0$ and map to $(x,y(x,p),p)$, then this maps to the direction $\frac{1}{\sqrt{1+p^2+(h_x+ph_y)^2}}(1,p,h_x+ph_y)$, and local coordinates on the unit sphere gives us a map to (p,h_x+ph_y). The composite is a map,

$$\begin{aligned} \mathbf{R}^2 &\to \mathbf{R}^2 \\ x,p &\mapsto p,h_x+ph_y, \end{aligned}$$

whose Jacobian is,

$$h_{xx}+h_{xy}\frac{\partial y}{\partial x}+ph_{xy}+ph_{yy}\frac{\partial y}{\partial x},$$

which is the equation of the fold curve. The derivative $\frac{\partial y}{\partial x}$ can be calculated by solving $F(x,y(x,p),p)=0$ as described in the proof of part (2) and we obtain the condition

$$a_0^2b_2-2a_0a_1b_1+a_1^2b_0=0.$$

□

Note On the Lemma.

- The condition in part 2 of the statement of the lemma is the condition for a degenerate zero, i.e. a bifurcating zero where a saddle and node meet. Recall the discriminant of $\mathcal{C}_\alpha$ is defined by $\sin^2\alpha=\frac{K}{H^2}$ and so for any elliptic point p we find that there is some α solving this equation, and so there is a discriminant of some congruence passing through p. It is then two conditions for p to be a zero of $\mathcal{C}_\alpha$, and one further condition to be a degenerate zero, making a total of three conditions. In a one parameter family of BDEs on a surface we have three variables, so we expect saddle–nodes to be generic in our family. For the bifurcation to *not* be versally unfolded requires the satisfaction of a further two conditions, see [AP, p.203]. We thus conclude, from a naive counting of conditions, that our bifurcations are versally unfolded generically in $\mathcal{C}_\alpha$.

  It is in fact straightforward, though tedious and ultimately unilluminating at this stage, to calculate the versal unfolding conditions (see [AP, p.203]). On observing the complexity of the condition for a degenerate zero in the statement of the lemma, one holds little hope at this stage of interpreting the versality conditions geometrically.

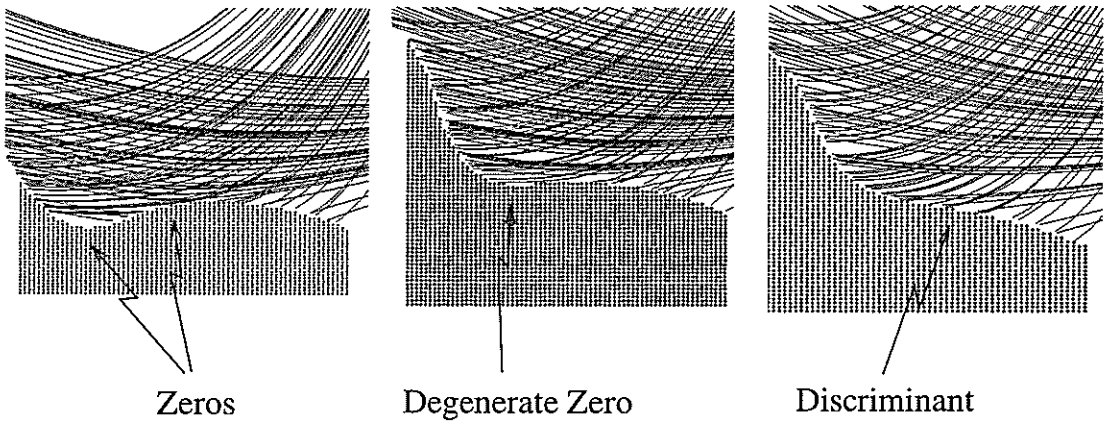

Figure 7.13: Bifurcating saddle node zero on $\mathcal{C}_\alpha$.

Figure 7.13 shows an example of $\mathcal{C}_\alpha$ bifurcating through a saddle node. On the left we see two zeros, the centre picture one zero, and the right hand side has no zeros. The discriminant in each case is marked as the boundary of the shaded region. As far as we know this is the first picture of the saddle node bifurcation in a one parameter family of BDEs.

This concludes our discussion of the saddle node bifurcation of $\mathcal{C}_\alpha$.

7.8.2 Singular Discriminant

We have already discussed some results concerning the singular instances of the discriminant. Lemma 7.14 tells us that the discriminant of $\mathcal{C}_{\pi/2}$ at an ordinary umbilic is a point. As discussed in the note following Lemma 7.10 our discriminants arise as the level sets of some smooth surface, and we therefore expect there to be Morse transitions through a point or a crossing.

The following result characterises the singularities of the discriminant as the points where the tangency points of the fold curves with the discriminant meet the singular points of $\mathcal{C}_\alpha$.

7.31 Proposition: *With $\alpha \neq 0$ and $\alpha \neq \pi/2$ the following are equivalent,*

1. *A point p is a singular point of $\Delta(\mathcal{C}_\alpha)$*
2. *The lifted surface $F = ap^2 + 2bp + c = 0$ is singular.*

3. *The point p is a zero of $\mathcal{C}_\alpha$ (so consequently on the discriminant) and the fold curve $\mathcal{S}_\alpha$ of $\mathcal{C}_\alpha$ passes through p.*

Proof: (1)⇔(2). We take our surface in Monge form identical to the previous lemma. Writing $F = ap^2 + 2bp + c = 0$ for the lifted surface it is straightforward to calculate the derivatives and we make use of lemma 7.9,

$$\begin{aligned} F_x(\mathbf{0}) &= -b_1 \sin\alpha - b_0 \cos\alpha \\ F_y(\mathbf{0}) &= -b_2 \sin\alpha - b_1 \cos\alpha \\ F_p(\mathbf{0}) &= \sin\alpha(a_0 - a_2) - 2a_1 \cos\alpha. \end{aligned}$$

If we set $\sin\alpha = \frac{a_0}{\sqrt{a_0^2+a_1^2}}$ and $\cos\alpha = \frac{-a_1}{\sqrt{a_0^2+a_1^2}}$ then the x axis will be a member of the congruence and the derivatives of F will be zero if and only if,

$$\begin{aligned} F_x &= b_0a_1 - b_1a_0 = 0 \\ F_y &= b_1a_1 - b_2a_0 = 0 \\ F_p &= a_0^2 - a_0a_2 + 2a_1^2 = 0. \end{aligned}$$

Now from Lemma 7.30 part 1 F_p vanishes iff the point is on the discriminant, and in fact this is the condition for $F = 0$ to be folded. One can use Lemma 7.9 to expand $b^2 - ac$ as described in the proof of Lemma 7.30 to get

$$b^2 - ac = (b_0a_1 - b_1a_0)x + (b_1a_1 - b_2a_0)y + \cdots.$$

Thus we see that the discriminant is singular iff $F = 0$ is a singular surface.

(3) ⇔ (2). Recall from lemma 7.30 part 2 that the condition for a zero of $\mathcal{C}_\alpha$ in this coordinate system is

$$b_0a_1 - b_1a_0 = 0. \tag{7.15}$$

In the proof of Lemma 7.30 the condition for a fold of the spherical image at the discriminant is calculated and found to be (equation 7.11)

$$a_0^2b_2 - 2a_0a_1b_1 + a_1^2b_0 = 0.$$

Solving (7.15) for b_0 and substituting in the above we obtain the condition $a_0(a_0b_2 - a_1b_1) = 0$ which is what we seek. □

Figure 7.14 shows the bifurcation of the discriminant through a Morse crossing.

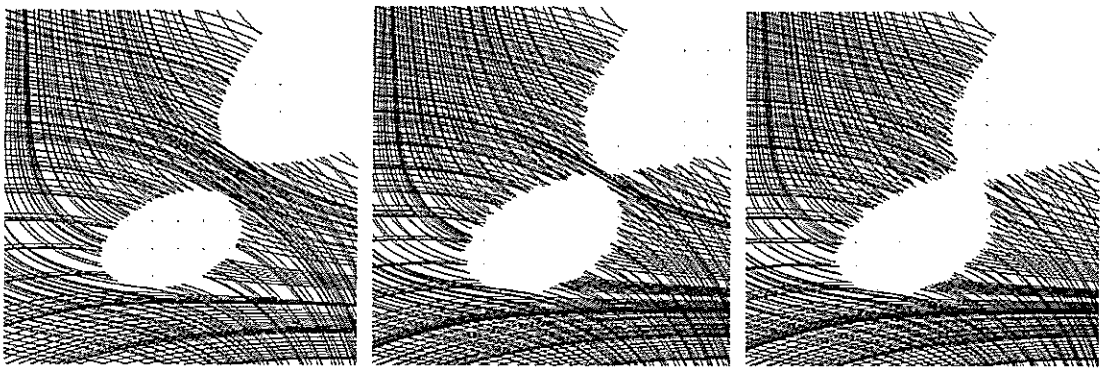

Figure 7.14: Bifurcation of discriminant through a Morse crossing.

Consider the lifted surface $F = 0$. The BDE lifts to a single valued field on the lifted surface and at the discriminant the surface is folded over. Technical proofs are outside the scope of this thesis but we present a plausible pictorial argument to describe the annihilation of the zeros in Figure 7.14.

Reading from left to right in Figure 7.14 we can consider this as the breaking of a handle on the lifted surface through a singularity. Figure 7.15 shows this with the solid area representing the region shown in Figure 7.14 and the dotted lines extend to give more of a global view of the topology.

We now use the Poincaré-Hopf Theorem, which states that for a compact manifold M and w a smooth vector field on M with isolated zeros, the sum of the indices of w is equal to the Euler number of M [MI]. Passing from left to right we can see that the Euler characteristic has increased by two. From 7.14 we see that we have also lost two singularities and so we conclude that we have lost two of index -1. In other words two saddles have come together in this transition. Projected on to the surface they become well folded saddles. Figure 7.16 shows the lifted field and the lifted discriminant, the criminant.

7.9 A Global View

In this section we examine the evolution of the zeros of $\mathcal{C}_\alpha$ on the discriminants, with a view to making global statements connecting the cusps of Gauss and the umbilics on a surface. At this stage we are lacking some technical results, including a complete classification of the generic bifurcations of $\mathcal{C}_\alpha$, but the

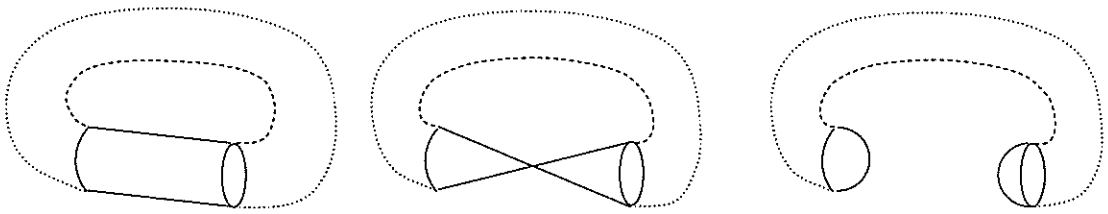

Figure 7.15: Lifted surface showing the destruction of a handle as the discriminant (not shown) passes through a Morse transition on the surface.

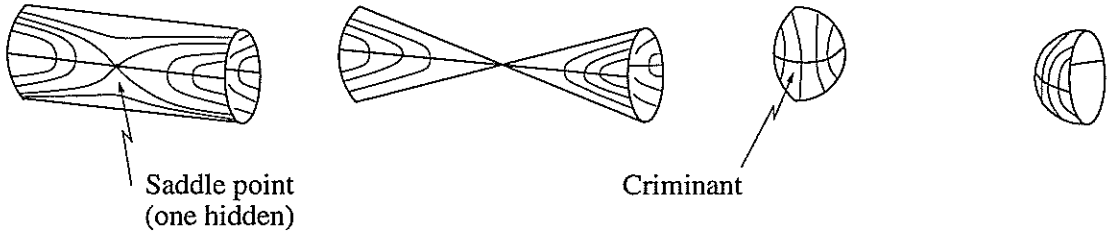

Figure 7.16: Lifted field and criminant shown for this Morse transition.

general idea is by far the most important.

Consider an isolated zero on the discriminant of $\mathcal{C}_{\alpha_0}$. This is the zero of a vector field and will persist if we perturb the family, so that $\mathcal{C}_{\alpha_0+\epsilon}$ will have a zero as well. It will also be the same type, i.e. saddle, node or focus. We call the path that the zeros make as we evolve the family, the **umbilical cord**. (Later when we consider umbilics we think of these curves as extending from them.) Figure 7.17 shows a smooth discriminant evolving with a zero on. The locus of the zero points gives an umbilical cord. Observe that since the discriminants of $\mathcal{C}_\alpha$ occur only in the elliptic region the umbilical cords only occur here, and moreover they end at the cusps of Gauss.

Umbilical cords are not arbitrary curves on the surface; they are severely constrained by their definition. It is only possible for two different umbilical cords to meet if that then defines a legitimate bifurcation of lifted vector fields. Thus it is not possible for two different focus umbilical cords to meet since this indicates two foci on the lifted surface coming together which in general is not a legal bifurcation of plane curves.

We now proceed by presenting pictorial examples that increase in complexity.

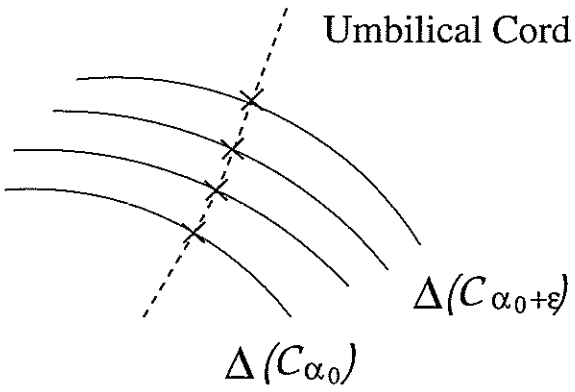

Figure 7.17: Crosses on the discriminant indicate zeros of C_α, and the umbilical cord is the locus of zeros.

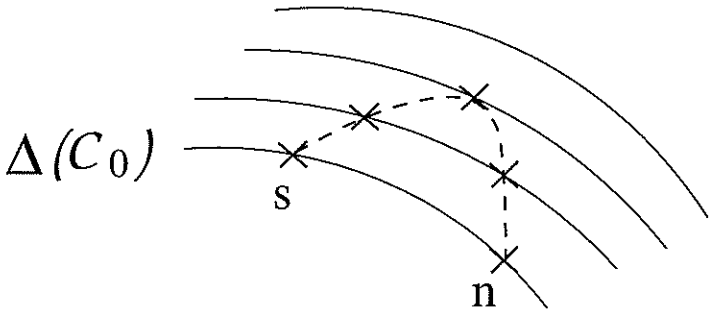

Figure 7.18: Saddle (s) and node (n) cusp of Gauss on the parabolic set $\Delta(C_0)$. The zero curve is tangent to the discriminant at the saddle node bifurcation.

As indicated earlier these are hypothesised results and we lack the technical proofs. Our first example illustrates a configuration of umbilical cords at the saddle node bifurcation.

Example: Consider two cusps of Gauss on the parabolic curve, one a node, and the other a saddle. We have written earlier on the saddle node bifurcation of C_α and Figure 7.18 shows a schematic for what we expect the zero curves to be in this case.

Recall Proposition 7.16 where we established the bifurcations of C_α at an umbilic. For a Lemon we have a saddle appearing, a Star 3 saddles, and a Monstar 2 saddles and a node. Thus a saddle umbilical cord is born at a Lemon, three saddle umbilical cords are born at a Star, and at a Monstar a node umbilical

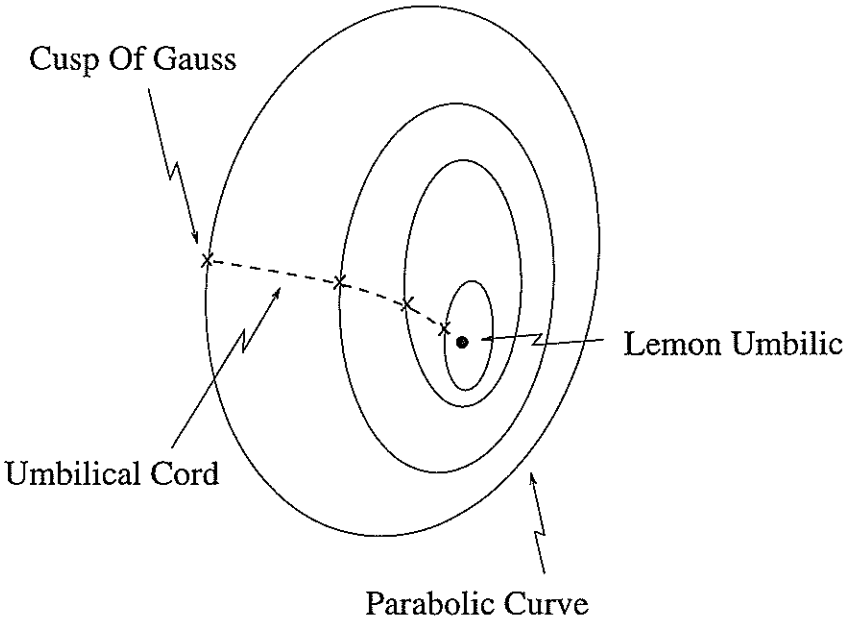

Figure 7.19:

cord and two saddle umbilical cords are born. The following example considers this umbilic situation.

Example: Consider a very simple surface patch consisting of a simple closed parabolic curve enclosing a Lemon umbilic. Consider perturbing the discriminant $\Delta(\mathcal{C}_{\pi/2})$, we know from above that a saddle is born. Figure 7.3 shows the configuration. The discriminant close to the umbilic is a closed curve encircling it. We assume that there are no other Morse transitions on the discriminants, so the discriminant expands as a series of concentric curves from the umbilic to the parabolic curve. The umbilical cord also evolves until it meets the parabolic curve, and that then indicates a saddle cusp of Gauss. See Figure 7.19.

Example: Now consider a simple closed parabolic curve enclosing a Monstar and no other Morse transitions of the discriminants. There are two possible configurations. Either when the umbilical cords (2s+1n) are born they progress unimpeded to the parabolic curve, or a saddle and node bifurcate and disappear. Figure 7.20(left) shows the first of these and the right hand side shows the second option. We thus either have a saddle cusp of Gauss or two saddles and a node cusp of Gauss.

Observe that if we now introduce two or more umbilics in the closed parabolic

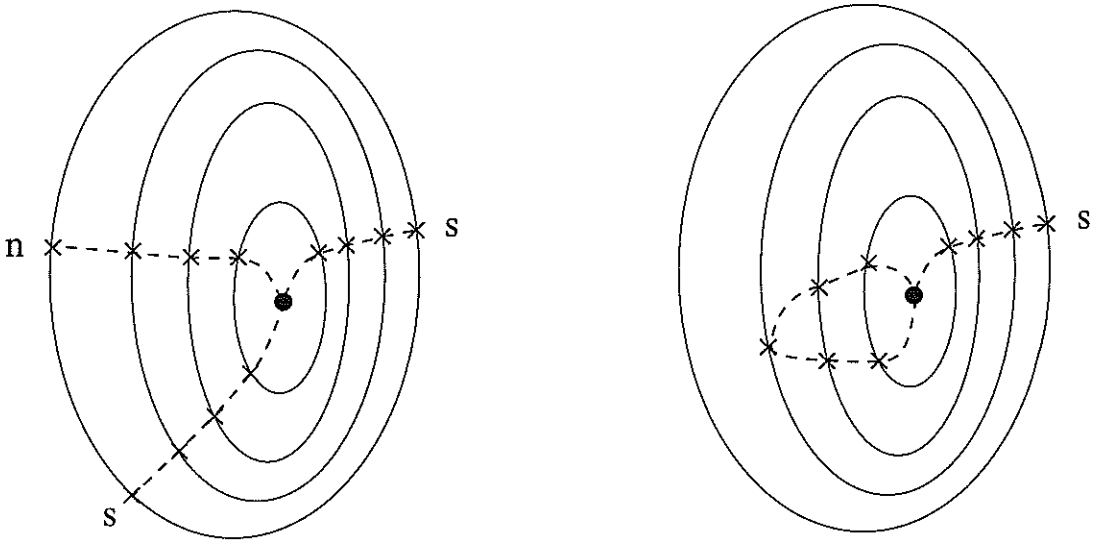

Figure 7.20: (Left) Three cusps of Gauss surrounding a Monstar. (Right) One saddle cusp of Gauss and a saddle node bifurcation.

curve the discriminant will have to undergo a Morse crossing. These were investigated in Section 7.8.2. Recall that in evolving $\mathcal{C}_\alpha$ from 0 two saddles are born in the Morse crossing situation. The next example considers three umbilics in a closed elliptic region.

Example: Consider a closed parabolic curve enclosing a Lemon, Star and Monstar. There will be at least two Morse crossings of the discriminant and we assume that there are no more. In other words we assume that there are no isolated Morse points of the discriminant other than the three umbilics. Consider evolving $\mathcal{C}_\alpha$ from the umbilics at $\pi/2$. The Lemon gives birth to one saddle, the Star three saddles and the Monstar a saddle and a node. As we evolve towards the parabolic curve the Morse crossings each eat two saddles. A possible configuration is shown in Figure 7.21 where we have 3 cusps of Gauss. It is also possible (not illustrated) for one saddle and a node to bifurcate and disappear leaving just one cusp of Gauss.

We now show how a simple index theorem could be derived. Consider generalising the last example, with n umbilics of various varieties enclosed by a parabolic curve, $n-1$ Morse crossings and no other singular discriminants. Let the number of lemons be l, the number of stars s and monstars m and therefore $l+s+m-1$ is the number of Morse crossings. Let S be the number of saddle

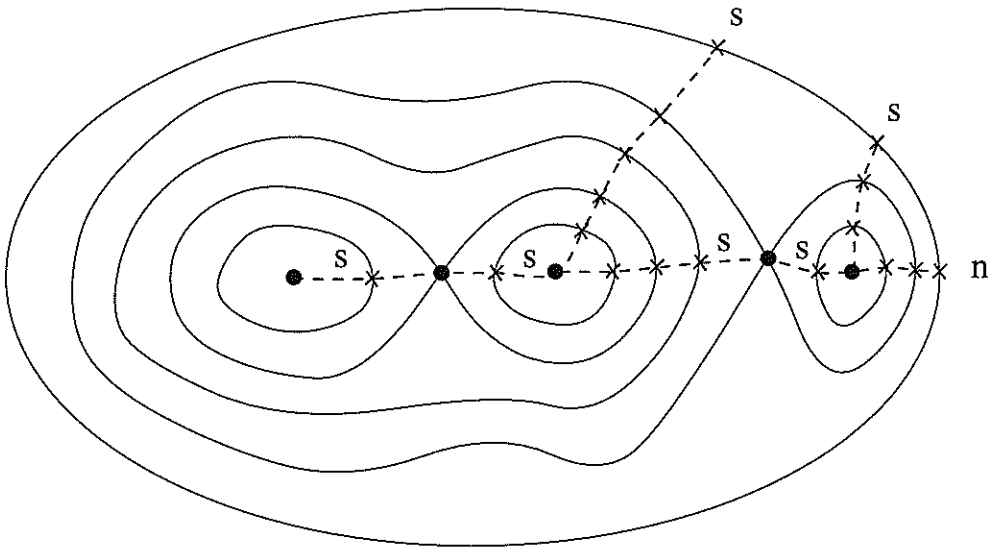

Figure 7.21: Three umbilics, Lemon, Star, Monstar left to right, with two saddles and a node cusp of Gauss on the parabolic curve.

cusps of Gauss and N the number of node cusps of Gauss. The number of saddles born in the umbilics is $l+3s+2m$. i.e. one for every lemon, 3 for every star and 2 for each monstar. For the nodes we have m nodes born, since only monstars give birth to nodes. The Morse crossings eat 2 saddles each. So examining the quantity of saddles and equating with S the number of saddle cusps of Gauss we have,

$$\begin{aligned} l+3s+2m-2(l+s+m-1) &= S \\ \text{i.e. } s-l+2 &= S, \end{aligned}$$

and the nodes,

$$m = N.$$

Unfortunately things are further complicated by the appearance of saddle node bifurcations. As we evolve from the umbilics we either have a saddle and node being eaten which we call sn^- or a spontaneous birth of a saddle node, which we denote sn^+. Figure 7.18 shows a sn^+ because as we evolve from the umbilic (i.e. decreasing α) a saddle and node are born. Figure 7.20(right) shows a sn^-. So a sn^+ increases the saddle and node count by one each, and sn^- decreases by one. We therefore have the following formulae for the saddles and

nodes,

$$\begin{aligned} s - l + 2 + sn^+ - sn^- &= S \\ m + sn^+ - sn^- &= N. \end{aligned}$$

Obviously we do not intend for this to be a general statement since only special cases have been considered, but with a better understanding of the generic behaviour of $\mathcal{C}_\alpha$, theorems of this nature could be proved.

Comment: We recall from [BGM] that cusps of Gauss can occur as foci. What happens here? The short answer is that we do not know! We assume everything is compact, so the surface is compact, and the family $\mathcal{C}_\alpha$ is compact in the sense that $\mathcal{C}_{\pi/2} = \mathcal{C}_{-\pi/2}$. Thus if we have a focus cusp of Gauss on the parabolic curve it must evolve and trace out an umbilical cord. Where does this curve terminate? As yet we have found no bifurcations involving foci, and this problem requires further investigation.

7.10 Conclusion

We have introduced the conjugate curve congruence $\mathcal{C}_\alpha$ which is a smooth family of curve congruences connecting the asymptotic curves with the principal curves. We have found that it is most naturally written as a one parameter family of binary differential equations.

The discriminants of the $\mathcal{C}_\alpha$ were investigated and these included both the parabolic curves and the umbilics. Other Morse transitions of the discriminant were found to occur. Results of Bruce and Tari were applied to the case of $\mathcal{C}_{\pi/2}$ and topological pictures were found. In the case of the more general Morse transition we lacked the formal results, but were able to provide some pictures and a topological argument for the zeros that we expect.

The family of spherical images was investigated and the notion of a fold curve was introduced. It was found that the fold curves were the loci of geodesic inflections of the conjugate integral curves. This naturally generalised the result that the red subparabolic lines are the loci of geodesic inflections of the blue lines of curvature, and the red flecnodal curves are the loci of geodesic inflections of the red asymptotic curves. It was also proved that the critical set of a parallel projection has a geodesic inflection if the point is on a fold curve and the view direction is along the direction corresponding to that.

We introduced the cubic form Γ which naturally generalised the classifying cubic defined at umbilics, for the whole surface. It was found that the critical set Σ of a parallel projection has a geodesic inflection if and only if it is tangent to a root of Γ. This immediately connected $\mathcal{C}_\alpha$ with Γ through the geodesic inflections of Σ. Indeed it was found that the dark red fold curve is the locus of intersections between the roots of Γ and the light red curves. This provided a new characterisation of the subparabolic and flecnodal curves. The intimacy between Γ and $\mathcal{C}_\alpha$ was further revealed by the result that showed that the discriminant of Γ is the envelope of fold curves.

The zeros of $\mathcal{C}_\alpha$ were investigated, in particular the saddle node bifurcations and singular discriminant bifurcations. Conditions were found in each case and pictures provided. There are no published results concerning the singular discriminant case and the technical results are outside the scope of this thesis, so a more discursive analysis was presented. The surprising result was found that in general the fold curve is not tangent to the discriminant at a zero. This *is* the case at a parabolic curve, where the flecnodal curve is tangent to the parabolic curve at a cusp of Gauss.

The chapter finished with a discussion on the global consequences of $\mathcal{C}_\alpha$. In particular it seems that the zeros of $\mathcal{C}_\alpha$ may provide a link between the umbilics and the cusps of Gauss of a smooth surface.

There is much further work to be done. Some possible items include,

- Condition for geodesic inflection of the critical Σ set under perspective projection. The fold curves in this case may well become ruled surfaces. c.f. the CAD and FS.
- Generic degeneracy of the geodesic inflections of Σ. Is it the case that Σ has a degenerate inflection at point of the envelope of fold curves, and even more degenerate at a cusp of the envelope?
- Satisfactory pictures of the root lines of the cubic Γ. A coordinate free description of Γ.
- Pictures of the envelope of fold curves.
- Clearer pictures for the generic configuration of $\mathcal{C}_\alpha$ at a saddle node bifurcation.

- Possible generalisation of the focal set. Is it possible to construct a caustic surface for each $\mathcal{C}_\alpha$?
- Results extending the work of Bruce and Tari to include all Morse transitions of the discriminant.
- A full catalogue of the generic bifurcations that $\mathcal{C}_\alpha$ undergoes, with a view towards an index theorem.
- A geometrical understanding of the singular discriminant case, and the saddle node bifurcation. A more geometrical understanding of the connection between the fold curves and the zeros of $\mathcal{C}_\alpha$.
- Pictures of how the subparabolic curves deform in the family of fold curves at an umbilic.

Appendix A

```
> # Example of finding the double point space
> # in the case when the frontier and the singular curve cross.
> # We find the functions a_i and b_i and then calculate the
> cubic terms of the double point space.
>
> # These values of x avoid logs and trig functions in Y and c_3.
> # Give values to the coefficients of p.
> # Integers here seem to mean mostly rational coefficients
> later apart from the odd root 2.
>
>  x01:=2: x20:=-1: x11:=0: x02:=3: x30:=-2: x21:=-3:
> x12:=0: x03:=-4: z01:=-2: z10:=-4: z20:=-2: z11:=-3: z02:=1:
> # Give values to the coeff's of c.
> c10:=1: c11:=2:c12:=2: c20:=1: c21:=-4:
> # Work out c22 in the case where we want
> to make the surface singular
> c22:= (-3*c21*z01^2*z20-4*c21*z01*z10^2*x11+
> 6*c21*z01*z10*z11-8*c21*z10^2*z02+16*c21*z10^3*x02+
> 3*z01^2*c11*z10-14*z01*x01*z10^2*c11+16*z10^3*c11*x01^2)/
>  (8*z10^2*(2*z10*x01-z01)):
>
>
> # Give a value to the "constant of integration" c30 = c3(t=0).
> Probably make this < 0.
> c30:=-6:
> #with(plots):
> X:= s+x01*t+x20*s^2+x11*s*t+x02*t^2+x30*s^3+
> x21*s^2*t+x12*s*t^2+x03*t^3:
> Y3:=   z10*s+z01*t+z20*s^2+z11*s*t+z02*t^2:
> c1:= c10+c11*t+c12*t^2: c2:=c20+c21*t+c22*t^2:
> c1t:=diff(c1,t): c2t:=diff(c2,t):
```

```
>
> Y3t:=diff(Y3,t): Y3s:=diff(Y3,s):
> Y30:=subs({s=0},Y3):
> Y1:=s*Y3:
> X0:=subs({s=0},X):
> Y1s0:=subs( {s=0},Y3 ):
> Xt0:=diff( subs({s=0},X), t ):
> Xs0:=subs({s=0}, diff(X,s) ):
> Xs:=diff(X,s):
> Xt:=diff(X,t):
> Y2t:=simplify( Xt0*Y1s0/Xs0 ):
>
> integrand:= subs( {t=u}, simplify( Xt0*Y1s0/Xs0) ):
> g:=Xs*Y3t-Xt*Y3s+ simplify((Xs*Y2t-Xt*Y3)/s ):
> g:=simplify(g):
> Y2:=int( integrand, u=0...t):
> Y:=s*Y3+Y2:
> Y:=simplify(Y):
> Y0:=subs( {s=0},Y):
>
> c3t:=( c2t*Y1s0-c1t*(X0*Y1s0-Xs0*Y2 ) )/Xs0 :
> f:= -c2t*Y3s+c1t*( X*Y3s-Xs*Y3)+
> simplify( ((Xs*Y30-Xs0*Y3)*c2t+
> c1t*(X*Y3*Xs0-X0*Y30*Xs))/(s*Xs0) ) :
> f:=simplify(f):
>
> lambda:=simplify(-f/g):
> f01:=subs({t=t1},f):
> f11:=subs({s=s1},{t=t1},f):
> g01:=subs({t=t1},g):
> g11:=subs({s=s1},{t=t1},g):
> X01:=subs({t=t1},X):
> X11:=subs({s=s1},{t=t1},X):
>
> Y01:=subs({t=t1},Y):
> Y11:=subs({s=s1},{t=t1},Y):
> # ********************** Now calculate the a's
> a1:=(f11*g01-f01*g11)/(g11*g01*(s-s1)):
> a1:=simplify(a1):
```

```
> subs({s=s1},a1): # Should not give an error division by zero.
>
> a2:=(f11*g01*X11-f01*g11*X01)/(g11*g01*(s-s1)):
> a2:=simplify(a2):
> subs({s=s1},a2): # Should not give an error division by zero.
>
> a3:=(f11*g01*Y11-f01*g11*Y01)/(g11*g01*(s-s1)):
>
> a3:=simplify(a3):
> subs({s=s1},a3): # Should not give an error division by zero.
> # ***************************** finished calculating the a's
> # Now evaluate c3 by splitting up c3t and integrating each part.
> c3t_a:= simplify( c2t*Y1s0/Xs0 ):
> c3t_b:= simplify(c1t*(X0*Y1s0) /Xs0):
> c3t_c:=expand(simplify( c1t*Y2 )):
> c3_a:=int(c3t_a,t=0...u):
> c3_b:=-int(c3t_b,t=0...u):
> c3_c:= int(c3t_c,t=0...u):
> c3:=c3_a+c3_b+c3_c:
>
> c3:=c30+subs( {u=t},simplify(c3)):
> # ************************ Now start calculating the b's
> c1_1:=subs({t=t1},c1):
> c2_1:=subs({t=t1},c2):
> c3_1:=subs({t=t1},c3):
> b1_1:=simplify((c1-c1_1)/(t-t1)):
> b2_1:=simplify((c2-c2_1)/(t-t1)):
> b3_1:=simplify((c3-c3_1)/(t-t1)):
> b1_2:=simplify((f01*g-f*g01)/(g*g01*(t-t1))):
> subs({t=t1},b1_2): # Should not give a divide-by-zero error.
> b2_2:=simplify((f01*g*X01-f*g01*X)/(g*g01*(t-t1))):
> subs({t=t1},b2_2):  # Should not give a divide-by-zero error.
>
> b3_2:=simplify((f01*g*Y01-f*g01*Y)/(g*g01*(t-t1))):
> subs({t=t1},b3_2):
> b1:=b1_1+b1_2:
> b2:=b2_1+b2_2:
> b3:=b3_1+b3_2:
>
```

```
> # ************************* finished calculating the b's
> r1:= c1+lambda:
> r2:=c2+lambda*X:
> r3:=c3+lambda*Y :
> # Check that r1, r2, r3 really are of the form
> ri = (s-s1)ai + (t-t1)bi
>
> a1:=simplify(a1):
> a2:=simplify(a2):
> a3:=simplify(a3):
> b1:=simplify(b1):
> b2:=simplify(b2):
> b3:=simplify(b3):
>
> r1:=simplify(r1):
> r111:=subs({s=s1,t=t1},r1):
> diff_1:=simplify(r111-r1):
>
> r2:=simplify(r2):
> r211:=subs({s=s1,t=t1},r2):
> diff_2:=simplify(r211-r2):
>
> r3:=simplify(r3):
> r311:=subs({s=s1,t=t1},r3):
> diff_3:=simplify(r311-r3):
> numer_1:=numer(diff_1):
> numer_2:=numer(diff_2):
> numer_3:=numer(diff_3):
> numer_4:=numer(a1*b3-a3*b1):
> numer_4:=simplify(numer_4):
> numer_5:=numer(a1*b2-a2*b1):
> numer_5:=simplify(numer_5):
> # Work out the Jacobian matrix of the map
> from R^4 to R^3 defining D^2(r)
> readlib(coeftayl):
> m_14:=coeftayl(numer_3,[s,t,s1,t1]=[0,0,0,0],[0,0,0,1]):
> m_13:=coeftayl(numer_3,[s,t,s1,t1]=[0,0,0,0],[0,0,1,0]):
> m_12:=coeftayl(numer_3,[s,t,s1,t1]=[0,0,0,0],[0,1,0,0]):
> m_11:=coeftayl(numer_3,[s,t,s1,t1]=[0,0,0,0],[1,0,0,0]):
```

```
> m_24:=coeftayl(numer_4,[s,t,s1,t1]=[0,0,0,0],[0,0,0,1]):
> m_23:=coeftayl(numer_4,[s,t,s1,t1]=[0,0,0,0],[0,0,1,0]):
> m_22:=coeftayl(numer_4,[s,t,s1,t1]=[0,0,0,0],[0,1,0,0]):
> m_21:=coeftayl(numer_4,[s,t,s1,t1]=[0,0,0,0],[1,0,0,0]):
> m_34:=coeftayl(numer_5,[s,t,s1,t1]=[0,0,0,0],[0,0,0,1]):
> m_33:=coeftayl(numer_5,[s,t,s1,t1]=[0,0,0,0],[0,0,1,0]):
> m_32:=coeftayl(numer_5,[s,t,s1,t1]=[0,0,0,0],[0,1,0,0]):
> m_31:=coeftayl(numer_5,[s,t,s1,t1]=[0,0,0,0],[1,0,0,0]):
> # Truncate the LARGE expressions for numer_4 and numer_5
> to make the computations faster.
> readlib(mtaylor):
> trunc_numer_5:=mtaylor( numer_5, [s,t,s1,t1], 4 ):
> trunc_numer_4:=mtaylor( numer_4, [s,t,s1,t1], 4 ):
> trunc_numer_3:=mtaylor( numer_3, [s,t,s1,t1], 4 ):
> trunc_numer_1:=mtaylor( numer_1, [s,t,s1,t1], 4 ):
> trunc_numer_2:=mtaylor( numer_2, [s,t,s1,t1], 4 ):
>
> # Substitute in polynomial in s and t in the
> two 'nice' surfaces to get s1 and t1
> # as functions of s and t.
> s1_poly:=u10*s+u01*t+u20*s^2+u11*s*t+u02*t^2+
> u30*s^3+u21*s^2*t+u12*s*t^2+u03*t^3:
> t1_poly:=v10*s+v01*t+v20*s^2+v11*s*t+v02*t^2+
> v30*s^3+v21*s^2*t+v12*s*t^2+v03*t^3:
> T4:=expand( subs( {s1=s1_poly, t1=t1_poly}, trunc_numer_4 )):
> T5:=expand( subs( {s1=s1_poly, t1=t1_poly}, trunc_numer_5 )):
> # Now expand and solve the coeff's u and v.
> solve( {coeff( coeff(T4,s,1),t,0),
> coeff( coeff(T5,s,1),t,0)},{v10,u10} ):
> assign(");
> solve( {coeff( coeff(T4,s,0),t,1),
> coeff( coeff(T5,s,0),t,1)},{v01,u01} ):
> assign(");
> solve( {coeff( coeff(T4,s,2),t,0),
> coeff( coeff(T5,s,2),t,0)},{u20,v20}) :
> assign(");
> solve( {coeff( coeff(T4,s,1),t,1),
> coeff( coeff(T5,s,1),t,1)},{v11,u11} ):
> assign(");
> solve( {coeff( coeff(T4,s,0),t,2),
> coeff( coeff(T5,s,0),t,2)},{v02,u02} ):
> assign(");
```

```
> solve( {coeff( coeff(T4,s,3),t,0),
> coeff( coeff(T5,s,3),t,0)},{v30,u30} ):
> assign(");
> solve( {coeff( coeff(T4,s,2),t,1),
> coeff( coeff(T5,s,2),t,1)},{v21,u21} ):
> assign(");
> solve( {coeff( coeff(T4,s,1),t,2),
> coeff( coeff(T5,s,1),t,2)},{v12,u12} ):
> assign(");
> solve( {coeff( coeff(T4,s,0),t,3),
> coeff( coeff(T5,s,0),t,3)},{v03,u03} ):
> assign(");
>
> # Now that we have calculated s1 and t1
> in terms of s and t we can substitute these expansions
> # in the third equation -
> which is the singular surface in  D^2 space.
> expand( subs( {s1=s1_poly,t1=t1_poly}, trunc_numer_3 ) ):
> mtaylor( ",[s,t],5):
> expand( subs( {s1=s1_poly,t1=t1_poly}, trunc_numer_1 ) ):
> soln1:=mtaylor( ",[s,t],4):
> factor(");
```

$$-\frac{22937}{1572817827}\,(t+4\,s)\,(22937\,t+160\,s)^2$$

```
> expand( subs( {s1=s1_poly,t1=t1_poly}, trunc_numer_2 ) ):
> soln2:=mtaylor( ",[s,t],4):
> factor(");
```

$$-\frac{91748}{224688261}\,(t+4\,s)\,(22937\,t+160\,s)^2$$

```
>
```

Bibliography

[A] Arnold, V.I., *Catastrophe Theory*, Springer-Verlag 1984.

[AP] Arrowsmith, A.P., Place, C.M., *An Introduction to Dynamical Systems*, CUP 1991.

[ACG95] Astrom, K., Cipolla, R., Giblin, P., Motion from the Frontier of Surfaces. *Proc. Fifth Int. Conf. Comp. Vision.*, Cambridge, Mass. June 1995 pp269-275.

[ACG96] Astrom, K., Cipolla, R., Giblin, P., Generalised Epipolar Constraints. *Proc. European Conf. Computer Vision* Cambridge U.K. 1996.

[BGM] Banchoff, T., Gaffney, T., McCrory, C., Cusps of Gauss Mappings, Research Notes in Mathematics 55, Pitman Publishing Program, 1982.

[BT] Barrow, H.G., Tenenbaum, J.M., Recovering Intrinsic Scene Characterisitics from Images, Computer Vision Systems, Editors: A. Hanson and E. Riseman, Academic Press, New York, 1978.

[BC89] Blake, A., Cipolla, R., Robust Estimation of Surface Curvature from Deformation of Apparent Contours, *Technical Report* OEUL 1278/89, University of Oxford, 1989.

[BB] Boyer, E., Berger, M.O., 3d Surface Reconstruction Using Occluded Contours. *Technical Report* 95-R-013, Crin/Inria Loraine, 1995.

[BF] Bruce, J.W., Fidal, D.L., On Binary Differential Equations and Umbilics, *Proc. Royal Society of Edinburgh*, **111A** (1989), 147-168.

[BG85] Buce, J.W., Giblin, P.J., Outlines and their Duals, *Proc. of LMS* Vol.50 (1985) 552-570.

[BG] Bruce, J.W., Giblin, P.J., *Curves and Singularities (2ed)*, Cambridge University Press, 1992.

[BGT] Bruce, J.W., Giblin, P.J., Tari, F., Ridges, Crests and Sub-parabolic Lines of Evolving Surfaces, *Int. J. Computer Vision*, 18(3), 195-210 (1996).

[BGT2] Bruce, J.W., Giblin, P.J., Tari, F., Special Surfaces and their Duals; Preliminary Version, *Liverpool University Preprint* (1995).

[BT1] Bruce, J.W., Tari, F., On Binary Differential Equations. *Nonlinearity* **8** (1995) 255-271.

[BT2] Bruce, J.W., Tari, F., Generic 1-Parameter Families of Binary Differential Equations of Morse Type, to appear in *Discrete and Continuous Dynamical Systems*, 1996.

[BW] Bruce, J.W., Wilkinson, T.C., Folding Maps and Focal Sets, *Proc. of Warwick Symposium on Singularities* (1988), Lecture notes in math. 1462, Springer, Berlin, pp 63-72.

[C] Carlsson, S., Sufficient Image Structure for 3d Motion and Shape Estimation. *Proc. 2rd ECCV* Vol.1 pp.83-91, Springer-Verlag, 1994.

[CI] Cipolla, R., Active Visual Inference of Surface Shape, *Ph.D. Thesis, University of Oxford, 1991.*

[CB] Cipolla R, Blake, A., Surface Shape from the Deformation of Apparent Contours. *Int. J.Comp.Vision.* **9**(2) 1992.

[CFG] Cipolla, R., Fletcher, G.J., Giblin, P.J., Singular Profiles. *Proc. Fifth Int. Conf. Comp. Vision.*, Cambridge, Mass. June 1995

[CFG2] Cipolla, R., Fletcher, G.J., Giblin, P.J., Singular Profiles, to appear in *IJCV.*

[D] Davydov, A.A., Normal forms of differential equations unresolved with respect to derivatives in a neighbourhood of its singular point. *Funct. Anal. Appl.* **19** 1-10 (1985).

[DU] J.P.Dufour, Familles De Courbes Planes Differentiables, *Topology* Vol.22 No.4 (1983).

[E] Eisenhart, L.P., *A Treatise on the Differential Geometry of Curves and Surfaces.* The Athenaum Press, 1909.

[FG] Fletcher, G.J., Giblin, P.J., Class Based Reconstruction Techniques Using Singular Apparent Contours. *Proc. European Conf. Computer Vision,* Cambridge U.K. 1996.

[FG2] Fletcher, G.J., Giblin, P.J., Apparent Contour, Surfaces and Motion, *Int. Workshop on Computer Vision and Applied Geometry,* Nordfjordeid, Norway Aug. 1995.

[FMZR] Forsyth, D.A., Mundy, J.L., Zisserman, A., Rothwell, C.A., Recognising Rotationally Symmetric Surfaces from their Outlines, *Proc. Second European Conference on Computer Vision*, Santa Margherita Ligure (Italy), pp.639-647 May 1992.

[G] Gaffney, T., The Structure of $T\mathcal{R}(f)$, Classification and an Application to Differential Geometry, *Proceedings of the Symposia in Pure Mathematics*, **40** Part 1 (1983),409-427.

[GDL] Glachet, R., Dhome, M., Lapreste, J.T., Finding the Pose of an Object of Revolution, *Proc. Second European Conference on Computer Vision*, Santa Margherita Ligure (Italy), pp.681-686, May 1992.

[GPR] Giblin, P.J., Pollick, F.E., Rycroft, J.E., Recovery of an Unknown Axis of Rotation from the Profiles of a Rotating Surface. *J.Opt. Soc. Am.* , Vol.11 No.7 (1994) pp.1976-1984.

[GS] Giblin, P.J., Soares, M.G., On the Geometry of a Surface and its Singular Profiles, *Image and Vision Comp.* **6**(1988), 225-234.

[GW] Giblin, P.J., Weiss, R., Reconstruction of Surfaces from Profiles. *Proc. Int. Conf. Comp. Vision.* 1987.

[GO] Goursat, E., *A Course In Mathematical Analysis,* Ginn and Company, 1904.

[JAP] Joshi, T., Ahuja, N., Ponce, J., Structure and Motion Estimation from Dynamic Silhouettes Under Perspective Projection. *Int. Conf. Comp. Vision.* 1995.

[Ke] Kergosien, Y.L., La Famille des Projections d'une Surface et ses Singularites, *C.R. Acad. Sci. Paris,* **292** (1981), 1929-1932.

[KK] Kleppner, D., Kolenkow, R.J., *An Introduction to Mechanics*, Mc Graw-Hill 1973.

[K84] Koenderink, J.J., What Does the Occluding Contour Tell Us About Solid Shape? *Perception,* **13** (1984), 321-330.

[K] Koenderink, J., *Solid Shape*, MIT press 1990.

[KD] Koenderink, J.J., van Doorn, A.J., Photometric Invariants Related to Solid Shape, *Optica Acta*, 1980, vol.27, No.7, 981-996.

[KvD76] Koenderink, J.J., van Doorn, A.J., The Singularities of the Visual Mapping, *Biological Cybernetics*, **24** (1976), 51-59.

[KvD82] Koenderink, J.J., van Doorn, A.J., The Shape Of Smooth Objects and the Way Contours End. *Perception,* **11** (1982), 129-137.

[KvD91] Koenderink, J.J., van Doorn, A.J., Affine Structure from Motion, *Biological Cybernetics*, **8** (1991), 321-330.

[KD] Kutulakos, K., Dyer, C., Global Surface Reconstruction By Purposive Control of Observer Motion. *Proc. IEEE Conf. Comp. Vision Patt. Recog.* , 1993.

[LU] Lu, Y.C., *Singularity Theory/Catastrophe theory*, Springer-Verlag 1976.

[JD] MacDonnel S.J., J., *Jesuit Geometers* , Vatican Observatory 1989.

[M] Martinet, J., *Singularities of Smooth Functions and Maps*, London Mathematical Society Lecture Note Series 58, Cambridge University Press, 1982.

[MI] Milnor, J.W., *Topology From the Differentiable Viewpoint*, The University Press of Virginia Charlottesville, 1969.

[MO] Mond, D.M.Q., *The Classification of Germs of Maps from Surfaces to 3-space With Applications to the Differential Geometry of Immersions*, PhD thesis, University of Liverpool.

[MO1] Mond, D., Some Remarks on the Geometry and Classification of Germs of Maps from Surfaces to 3-Space. *Topology* Vol.26, No.3, pp.361-383, 1987.

[MO2] Mond, D., Singularities of the Exponential Map of the Tangent Bundle Associated with an Immersion. *Proc. London Math. Soc.*, **53** (1986), pp.357-384.

[MO3] Mond, D., Private Communication, Sept. 1996.

[RMO] Morris, R., The Sub-Parabolic Lines of a Surface, *Mathematics of Surfaces VI*, Ed. Glen Mullineux, IMA new series 58, Clarendon Press, Oxford, 1996.

[RMO2] Morris, R., *Symmetry of Curves and the Geometry of Surfaces: Two Explorations with the aid of Computer Graphics*, PhD Thesis, University of Liverpool 1990.

[ON] O'Neill, B., *Elementary Differential Geometry* Academic Press 1966.

[P] Ponce, J., Invariant Properties of Straight Homogeneous Generalized Cylinders. *IEEE PAMI*, vol.11, no.9, pp.951-965, 1989.

[PC] Ponce, J., Chelberg, D., Finding the Limbs and Cusps of Generalized Cylinders, *Int. J. Comp. Vision 1*, (1987) pp.195-210.

[PP] Porrill, J., Pollard, S.B., Curve Matching and Stereo Calibration. *Im. and Vision Comp.* **9**(1): 45-50, 1991.

[Poz] Pozzo, A., *Rules and examples of perspective proper for painters and architects, etc*, Benj. Motte, Lond., 1707.

[PTVF] Press, W.H., Teukolsky, S.A., Vetterling, W.T., Flannery, B.P., *Numerical Recipes in C*, 2.ed. Cambridge University Press, 1992.

[R86] Rieger, J.H., Three Dimensional Motion from Fixed Points of a Deforming Profile Curve. *Opt. Lett.* Vol.11 (1986) pp.123-125.

[R87] Rieger, J.H., Families of Maps from the Plane to the Plane, *Journal of the London Mathematical Society 2*, **36**(1987),351-369.

[R88] Rieger, J.H., Apparent Contours and their Singularities, *Ph.D. Thesis, University of London, Queen Mary College, 1988.*

[R92] Rieger, J.H., Projections of Generic Surfaces of Revolution, *Geometriae Dedicata*, 1993, Vol.48, No.20, pp.211-230.

[RY] Rycroft, J.E., *A Geometrical Investigation into the Projections of Surfaces and Space Curves* PhD Thesis, University of Liverpool 1992.

[SW] Szeliski, R., Weiss, R., Robust Shape Recovery From Occluding Contours Using a Linear Smoother. *Proc. IEEE Conf. Comp. Vision Patt. Recog.*, 1993.

[VF] Vaillant, R., Faugeras, O., Using Extremal Boundaries for 3d Object Modelling. *IEEE Trans. Patt. Anal. Mach. Intell.* **14**(2), 1992.

[VKP] Vijagakumar, B., Kriegman, D., Ponce, J., Structure and Motion of Curved 3d Objects from Monocular Silhouettes. *IEEE Conf. on Comp. Vision and Patt. Recog.* 1996.

[WE] Weatherburn *Differential Geometry Vol.1*, Cambridge University Press, 1939.

[Wh] Whitney, H., On the Singularities of Euclidean Space 1: Mappings of the Plane to the Plane, *Annals of Mathematics*, **62** (1955),374-410.

[WI] Wilkinson, T.C., The Geometry of Folding Maps, *PhD Thesis*, University of Newcastle 1991.

[W] Willmore, T.J., An Introduction To Differential Geometry. Oxford University Press, 1959.

[Z] Zheng, J.Y., Acquiring 3d Models from Sequences of Contours. *IEEE Trans. Patt. Anal. Mach. Intell.* **16**(2), 1994.

[ZM] Zisserman, A., Mundy, J., Forsyth, D., Liu, J., Pillow, N., Rothwell, C., Utcke, S., Class–Based Groupings in Perspective Images, *Proc. Fifth Int. Conf. on Computer Vision*, Cambridge, Mass. June 1995.

[ZN] Zerroug, M., Nevatia, R., Segmentation and Recovery of SHGCs from a Real Intesity Image, *Proc. Third European Conference on Computer Vision* , Stockholm, Sweden Vol.I, pp.319-330, May 1994.